Retina regeneration:

new strategies to treat inherited retinal dystrophies

Doctoral thesis by Marina Pavlou

Munich 2021

Dissertation zur Erlangung des Doktorgrades
der Fakultät für Chemie und Pharmazie
der Ludwig-Maximilians-Universität München

Retina regeneration:

new strategies to treat inherited retinal dystrophies

Marina Pavlou

aus

Stuttgart, Deutschland

2021

Erklärung

Diese Dissertation wurde im Sinne von §7 der Promotionsordnung vom 28. November 2011 von Herrn Prof. Dr. Stylianos Michalakis betreut.

Eidesstattliche Versicherung

Diese Dissertation wurde eigenständig und ohne unerlaubte Hilfe erarbeitet.
München, 25/02/2021

Marina Pavlou

Dissertation eingereicht am:	25/02/2021
1. Gutachterin/ 1. Gutachter:	Prof. Dr. Stylianos Michalakis
2. Gutachterin/ 2. Gutachter:	Prof. Dr. Martin Biel
Mündliche Prüfung am:	13/04/2021

Acknowledgements

My doctorate degree has been a long journey through which I evolved as a scientist and as an individual. I set high goals for myself when I started my doctorate and was able to achieve them with help both on the professional and personal level.

On the professional level, this work was made possible by the collective effort of colleagues and collaborators, as well as the support of supervisors and scientific advisors. First, I wish to thank my supervisor Prof. Dr. Stylianos Michalakis for giving me the opportunity to pursue my doctorate in his team. I would also like to thank all the members of my thesis advisory committee, Prof. Dr. Stylianos Michalakis, Prof. Dr. Martin Biel, Prof. Dr. Dirk Grimm and Dr. Sergio Gascón, for their guidance and scientific input throughout my doctorate. Thank you also to all the members of the LMU Department of Pharmacology for Natural Sciences for their cooperative spirit and readiness to share expertise or troubleshooting tips.

On the personal level, I wish to speak from the heart and therefore in my mother language. Ενα μεγάλο ευχαριστώ στις συνεργάτιδες και φίλες μου, Ελίζα και Γκράτσια, για την αλληλεγγύη και εκτίμησή σας. Με βοηθήσατε να έχω εμπιστοσύνη στις ικανότητές μου και χάρη σε εσάς οι πιο δύσκολες στιγμές μετατράπηκαν σε ζήλο για ένα καλύτερο αύριο. Στους ανθρώπους μου, ένα τεράστιο ευχαριστώ. Γεωργία μου είσαι μια σταθερή αξία στη ζωή μου, παρέχοντας μου ηρεμία και αισιοδοξία σε κάθε φάση. Βίκτωρ μου ήσουν, είσαι και θα είσαι ένα αναπόσπαστο κομμάτι μου και είμαι απέραντα ευγνόμων για την αγάπη και υποστήριξή σου σε κάθε μου βήμα. Τέλος το μεγαλύτερο ευχαριστώ πάει στους γονείς μου, που είναι πάντα μια απύθμενη πηγή αγάπης και συμπαράστασης. Μάμα, παπά, είσαστεν οι βράχοι μου. Με μεγαλώσατε με αξίες και μου δώσατε αρετές χάρη στις οποίες σήμερα στέκω περήφανη για το έργο μου.

Το διδακτορικό μου είναι αφιερωμένο στους αγαπημένους μου γονείς, Παύλο & Στέλλα Παύλου.

Contents

Abbreviations

AAP	assembly-activating protein
AAV	adeno-associated virus
ANOVA	analysis of variance
Anti/Anti	Antimycotic/Antimyotic
Ascl1	achaete-scute family BHLH transcription factor 1
Atf6a	activating transcription factor 6-α
BHLH	basic helix-loop-helix
bp	base pairs
BRB	blood-retina-barrier
Brn2	POU Domain Class 3, Transcription Factor 2
BSA	bovine serum albumin
Cabp5	calcium binding protein 5
$CaCl_2$	calcium chloride
Cacna1s	calcium voltage-gated channel subunit alpha 1 S
CAG	CMV enhancer, chicken beta-actin promoter and rabbit beta-globin splice acceptor site
Calb1	Calbindin 1
cDNA	complementary DNA
cGMP	cyclic guanosine monophosphate
CMV	cytomegalovirus
c-Myc	MYC proto-oncogene, BHLH transcription factor
CNS	central nervous system
CNG	cyclic nucleotide-gated channel
Cnga3	cyclic nucleotide-gated channel subunit α-3
Cngb3	cyclic nucleotide-gated channel subunit β-3
CO_2	carbon dioxide
Crx	cone-rod homeobox protein
CSF2	colony stimulating factor 2
cSLO	confocal scanning laser ophthalmoscopy
Cx3cr1	C-X3-C motif chemokine receptor 1
DAPI	4,6-diamidino-2-phenylindole
DGCR8	DiGeorge Syndrome Critical Region 8
Dhcr24	24-dehydrocholesterol reductase

Dkk3	dickkopf-related protein 3
DMEM	Dulbecco's Modified Eagle Medium
DMSO	dimethyl sulfoxide
DNA	deoxyribonucleic acid
DPI	days post infection
DPBS	Dulbecco's phosphate-buffered saline
ds	double-stranded
E	embryonic day
eGFP	enhanced green fluorescent protein
ERG	electroretinography
F12	nutrient mixture F12
FACS	fluorescence activated cell sorting
FBS	fetal bovine serum
Fcho2	F-BAR domain only protein 2
FMO	fluorescence-minus-one
FW	forward
Gad1	glutamate decarboxylase 1
gDNA	genomic DNA
GCL	ganglion cell layer
GECI	genetically encoded calcium indicator
GFAP	glial fibrillary acidic protein
Glu1	glucoamylase GLU1
Gnat2	cone-transducin α-subunit
Goα	G protein subunit alpha o1
Grm6	metabotropic glutamate receptor 6
GS	glutamine synthetase
HEPES	4-(2-hydroxyethyl)-1-piperazineethanesulfonic acid
HSPG	heparan sulphate proteoglycan
HBSS	Hank's balanced salt solution
Iba1	ionised calcium-binding adapter molecule 1
IHC	immunohistochemistry
ILM	inner limiting membrane
INL	inner nuclear layer

IPL	inner plexiform layer
IRDs	inherited retinal dystrophies
ITRs	inverted terminal repeats
kb	kilobase
KCl	potassium chloride
Kcnip3	potassium voltage-gated channel interacting protein 3
Klf4	Kruppel like factor 4
MACS	magnetic-activated cell sorting
MOI	multiplicity of infection
mRNA	messenger RNA
Myt1l	myelin transcription factor 1-like protein
NeuroD1	neurogenic differentiation 1
Ngn2	neurogenin 2
NFL	nerve fibre layer
NHP	non-human primate
nm	nanometres
ONL	outer nuclear layer
OPL	outer plexiform layer
OCT	optimal cutting temperature compound
Oct3/4	octamer-binding transcription factor 3/4
P	postnatal day
Pax6	paired box protein Pax-6
PBS	phosphate-buffered saline
PCR	polymerase chain reaction
Pcp2	purkinje cell protein 2
PDB	protein database
PDE	phosphodiesterase
Pde6c	phosphodiesterase 6C
Pde6h	phosphodiesterase 6H
PDL	poly-D-lysine
pen/strep	penicillin/streptomycin
PFA	paraformaldehyde
PNA	peanut agglutinin

Prkca	protein kinase C alpha
Prdm1	PR-SET domain zinc-finger transcription factor Blimp1
Q	quadrants
rAAV	recombinant AAV
Rax	retinal homeobox protein
Rep	replication proteins
Rho	rhodopsin
RhGC	rhodopsin guanylyl cyclase
Rlbp1	retinaldehyde-binding protein 1
RNA	ribonucleic acid
RNAseq	RNA sequencing
Rpe65	retinoid isomerohydrolase
rpm	rounds per minute
RT	room temperature
RV	reverse
sc	self-complementary
ss	single-stranded
SD	standard deviation
Slc6a6	sodium- and chloride-dependent taurine transporter
SEM	standard error of mean
Sox2	SRY-Box transcription factor 2
Tacc1	transforming acidic coiled-coil-containing protein 1
Tacr3	tachykinin receptor 3
Th	tyrosine hydroxylase
Trbp2	TAR RNA-binding protein 2
Tuj1	neuron-specific class III beta-tubulin
vg	viral genomes
VP	viral proteins
WPI	weeks post injection
Zic1	Zinc finger protein of the cerebellum 1
λ	wavelength

Abstract

Our sense of vision largely defines who we are as individuals and as a society, by shaping our perception and allowing us to communicate beyond language barriers. Blinding diseases such as inherited retinal dystrophies therefore have severe mental and socio-economic consequences, which sparked multiple efforts to halt and reverse degeneration in these patients. This thesis set out to advance different therapeutic strategies that are both clinically established or under investigation, for patients at all disease stages. To address the needs of patients with early- to mid-stage retinal degeneration, two potent AAV capsids were engineered to deliver genetic cargo via a less invasive administration route, namely intravitreal injection. The properties of these novel vectors were verified in mouse, dog, non-human primate and human retina, showing a widespread transduction of photoreceptors across species. To demonstrate the potential of these vectors in gene supplementation therapy, a mouse model of achromatopsia was treated, resulting in the rescue of cone photoreceptor function and showing signs of tissue rejuvenation. For patients with late-stage retinal degeneration, two therapeutic approaches were explored that would either confer light-sensing abilities to the remaining retinal network or replenish the missing neuronal population by reprogramming retinal glia. Regarding the former, a universal method for isolating ON bipolar cells was established that would enable the development of novel vectors for delivering optogenetic tools in a cell-specific manner. Regarding the latter, a series of exploratory experiments were performed showing the potential of pioneering factors to directly reprogram retinal microglia into neurons, highlighting the potential of regenerating the retina from within. This body of work was able to optimise existing strategies to treat inherited retinal dystrophies and offered new solutions for patients with so far limited therapeutic options.

Introduction

3.1 Vision in mammals

3.1.1 Eyes: the windows to our world

Of all our senses, vision is the most valuable. Our eyes are the main means of perceiving ourselves and our surroundings, as we collect images and motions that build our consciousness from the moment we open our eyes to the moment we close them. Vision has an intricate value to humanity not only on a singular but also a global level, as it remains a timeless and universal means of communication; no matter who, no matter when, everyone can interpret what they see. The phrase Arthur Brisbane (1864-1936) coined is as valid then as it is now: "Use an image. It's worth 1000 words." With this in mind, our interest in understanding how our eyes detect and process visual stimuli is undeniably natural.

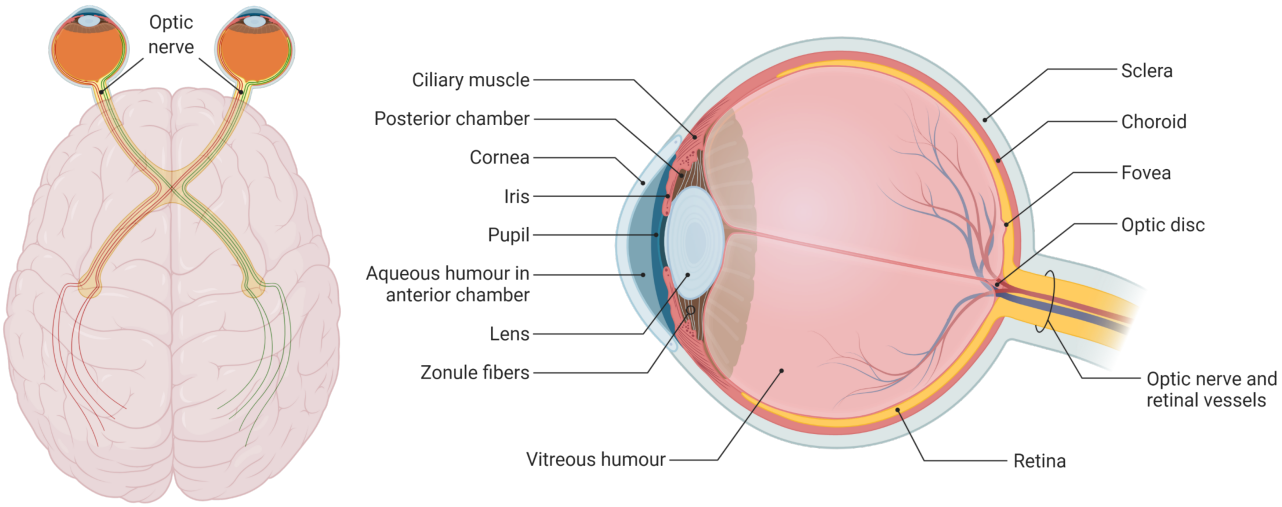

Figure 3.1: Schematic of human CNS and sagittal section of human eye

The eyes are an extension of our central nervous system (CNS) and have a globular structure that connects to the brain via the optic nerve (Fig.3.1). Anatomically, the *bulbus oculi* is divided into three liquid-filled compartments; the anterior chamber, posterior chamber and vitreous humour. The two chambers are filled with aqueous humour, a blood serum derivative that is constantly recycled to nourish the surrounding tissue and help maintain a constant intraocular pressure. The vitreous humour is a gelatinous mass that maintains the shape of the ocular globe and glues the interior structures in position. Functionally, the eyeball is divided into two apparatuses; the refractive and sensory. The former is comprised of the cornea, anteroposterior chambers and lens, which are responsible for collecting and focusing the incoming light-rays onto the latter. With regard to light-sensitivity, the anterior eyeball is termed *pars caeca*

retinae where no light-sensation occurs, whereas the posterior is termed *pars optica retinae*; the junction between them is termed *ora serrata*. Looking from the outside in, the posterior part of the eye is comprised of three overlapping tissue layers; the outermost sclera, the middle choroid and the innermost retina. The sclera is a hard tissue that defines the shape of the ocular globe, whereas the choroid is a soft layer of vascular capillaries that nourish the retina with oxygen and metabolites. The retina is the sensory tissue where light is converted into electrical impulses and it is further divided into cellular layers, each with their own purpose. In the human retina, as well as in some non-human primates (NHP), there a specialised locus termed *macula lutea* and at its centre the tissue forms a small pit called the *fovea centralis*, which is responsible for our sharp central vision in daylight [1].

Human eyes share many anatomical and functional features with mouse eyes, which are widely used in basic and translational research to investigate vision and its pathologies. Unlike humans, mice are nocturnal mammals and their eyes have evolved accordingly, such that they lack a fovea and their lenses have a more spherical shape that occupy a larger proportion of the vitreous cavity, enabling them to focus light-rays from a wider field of view [2]. Nevertheless, the lamination of the retina and the major cell groups comprising each lamina are identical between human and mouse.

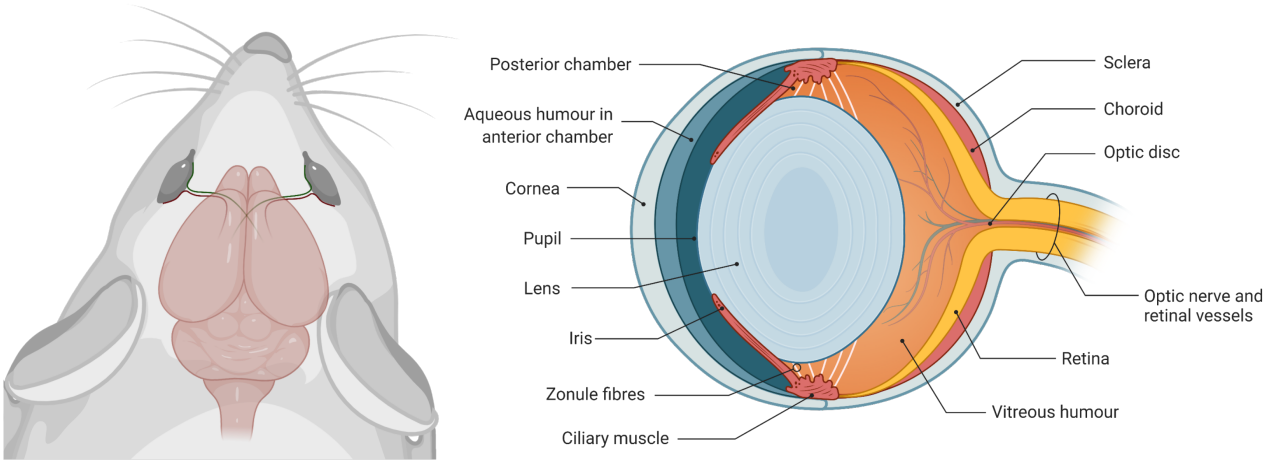

Figure 3.2: Schematic of mouse CNS and sagittal section of mouse eye

3.1.2 Retina: the sensory epithelium

As light crosses the refractive apparatus and hits the retina, it crosses an organised network of semi-transparent laminae that contain the somata of seven main cell groups and their synapses (Fig.3.3) [3, 4]. The light-facing surface of the retina is the inner limiting membrane (ILM), comprised of the end feet of Müller glia that serve as a diffusion barrier between the retina

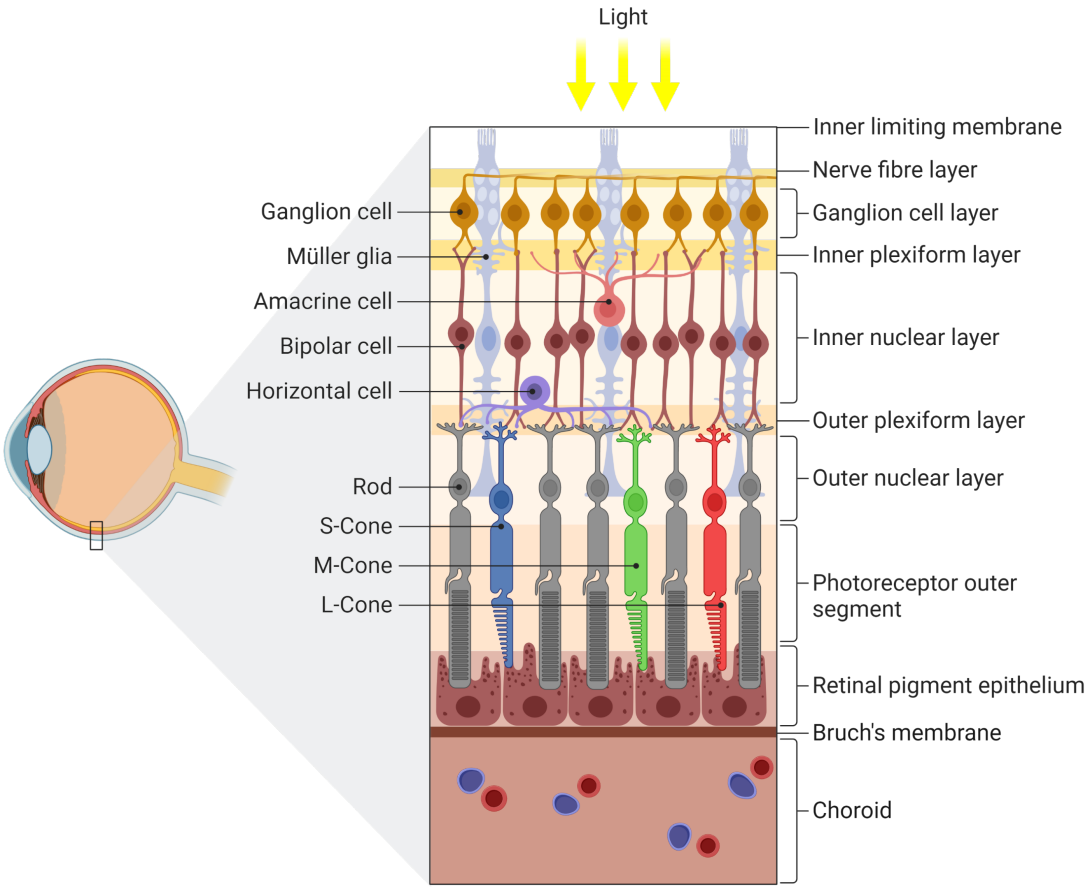

Figure 3.3: Schematic of light path within retina

and the vitreous humour. Müller glia are large cells that span all retinal laminae and serve many functions with regard to structural integrity, response to pathogens, nutrient diffusion and photopigment recycling. Beyond the ILM is the nerve fibre layer (NFL), which is made of the ganglion cell axons that merge to form the optic nerve, through which the ganglion cell layer (GCL) projects electrical impulses in the form of action potentials to thalamic nuclei of the brain, where they are processed and sent to the visual cortex [5]. Certain types of ganglion cells have non-visual responses to light, which are integral for regulating the circadian rhythm and pupillary reflex, as they express the photopigment melanopsin [6]. The dendrites of ganglion cells are found in the inner plexiform layer (IPL) where they receive input from a group of interneurons, namely amacrine, bipolar and horizontal cells, whose somata are in the inner nuclear layer (INL). Bipolar cells synapse with gangion cells in the IPL and transmit excitatory or inhibitory signals after processing the input received from photoreceptors; this is the main stream of vertical signal flow within the retina that is either active in the presence of light (ON-circuit) or the absence of light (OFF-circuit)[3]. Amacrine and horizontal cells connect laterally and provide feedback or feedforward signals; the former between bipolar and ganglion cells and the latter between photoreceptor and bipolar cells [7, 4]. Bipolar and horizontal cells synapse

with photoreceptor cells in the outer plexiform layer (OPL). Depending on their partner, there are either rod bipolar or cone bipolar cells, and they are further divided into ON bipolar if they depolarise or OFF bipolar if they hyperpolarise in response to photoreceptor-mediate light stimuli [8]. The somata of photoreceptors form the outer nuclear layer (ONL), with their inner and outer segments extending towards and contacting the retinal pigment epithelium (RPE), respectively. There are two types of photoreceptors, rods and cones, which are slightly different with regard to morphology and function, as they detect different wavelengths of incoming light (Fig.3.4). The outermost retinal layer is the RPE, which is an impermeable epithelial monolayer that forms the outer blood-retina-barrier (BRB) and helps maintain the immune privilege of the retina. Due to their pigment, RPE cells absorb scattered photons that were not captured by photoreceptors, to avoid interferences caused by light reflection. Moreover, RPE and photoreceptors exchange signalling molecules, nutrients (glucose, vitamin A) and metabolic end products provided by the choroid [9]. RPE cells are also crucial for the lifelong maintenance of photoreceptors, as they phagocyte their distal outer segments to enable their renewal [10] and recycle the light-capturing chromophore *all-trans* retinal back to *11-cis* retinal.

3.1.3 Photoreceptors and phototransduction

Photoreceptors are the light-sensing cells in the retina and have a unique design that allows them to capture photons and convert that energy into an electrochemical signal that gets passed along to the subsequent neural network. Structurally they are comprised of an outer and inner segment, linked by a connecting cilium, a small soma and a synaptic terminal. The connecting cilium functions as a gatekeeper of proteins involved in phototransduction [11]. The apical outer segments are made of consecutive membranous folds (discs), where phototransduction takes place. In rods, the discs are discrete compartments within the plasma membrane, whereas in cones they are a continuation of the plasma membrane. The mitochondria-rich inner segments are the cell's powerhouse and the synaptic terminal is where the neurotransmitter glutamate is released in response to changes in membrane potential.

Rods have an absorption maximum at 498 nanometres (nm) and are predominantly used for scotopic (light-dark) vision, as they are activated by only a few photons and have a slow response time. In humans and other trichromatic mammals, cones are either short-wavelength (S), middle-wavelength (M) or long-wavelength (L) based on the light spectrum their photopigment (opsin) responds to; their absorption maxima peak at 420 nm, 534 nm or 564 nm, respectively. Cones are also less sensitive to incoming light and they have fast response kinetics. As such they

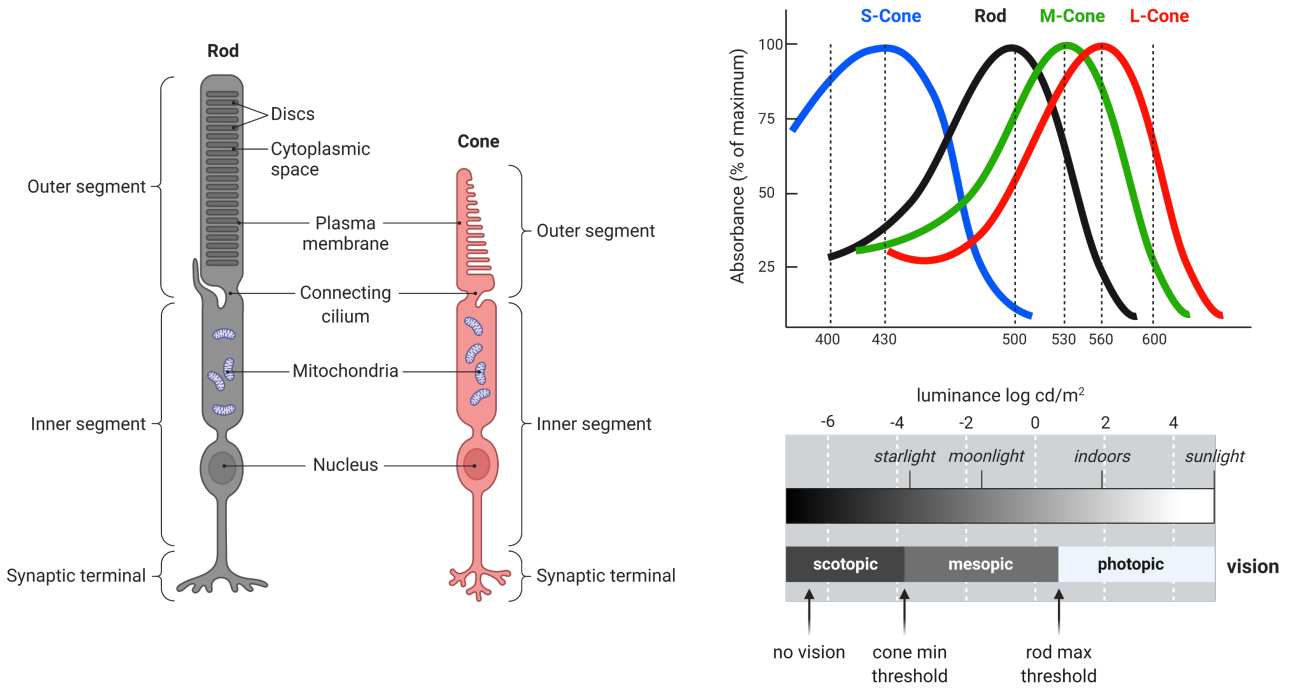

Figure 3.4: Schematic of photoreceptor morphology, absorption spectra and visual function (adapted from Neuroscience 2nd Edition, Sinauer Associates)

are used for photopic vision, which includes colour/contrast discrimination and visual acuity [3, 12]. Unlike the trichromatic vision that humans have, mice have dichromatic vision as their retinas only contain S-cones, M-cones or S/M-chimeras that form a distribution gradient on the dorsoventral axis, with true S-cones predominantly in the ventral compared to dorsal retina (Fig.3.5)[13].

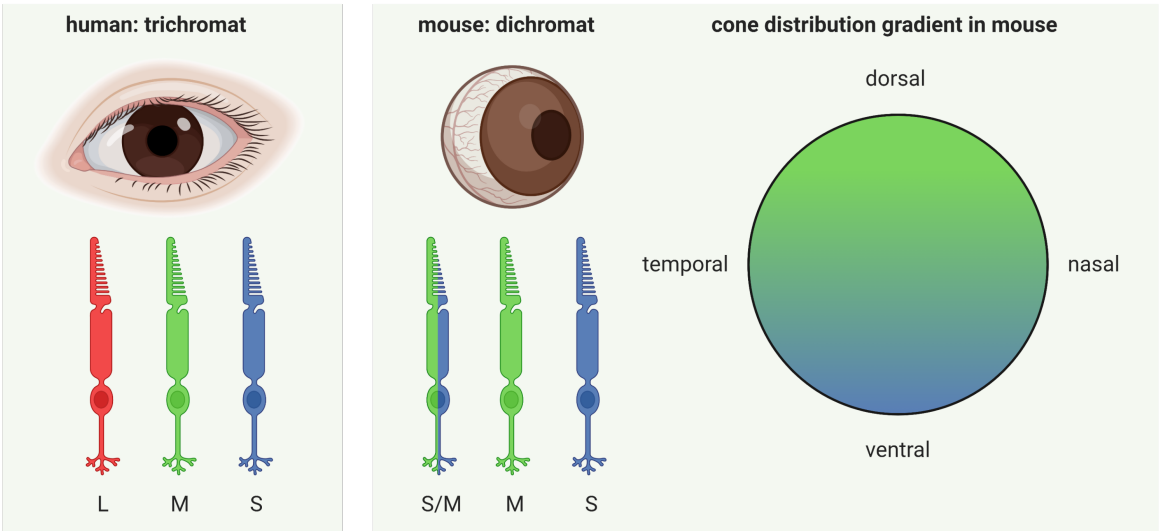

Figure 3.5: Schematic of distinct cone types in human and mouse, illustrating the distribution of cones in the mouse retina (adapted from [14])

The process of phototransduction takes place in the outer segments of photoreceptors (Fig3.6). The cascade is comprised of a photopigment (opsin), a G-protein (transducin), a phosphodiesterase (PDE) and a cyclic nucleotide-gated (CNG) ion channel. In the dark, the cell is depolarised and releases glutamate, as the cation influx through the open CNG channels keeps the membrane potential more positive (-30 mV) than the resting potential. Once illuminated, the chromophore *11-cis* retinal that resides within the photopigment becomes isomerised to *all-trans* retinal and causes a conformational change. This active photopigment causes the release of the transducin α-subunit, which triggers PDE to hydrolyse cyclic guanosine monophosphate (cGMP). The cGMP levels decrease and the molecules dissociate from the CNG channel leading to its closure. As such, the membrane potential of the cell becomes more negative (-70 mV) and hyperpolarises, causing less glutamate release at the synaptic terminal. Mutations in any of the constituents of the phototransduction cascade leads to photoreceptor degeneration and vision loss.

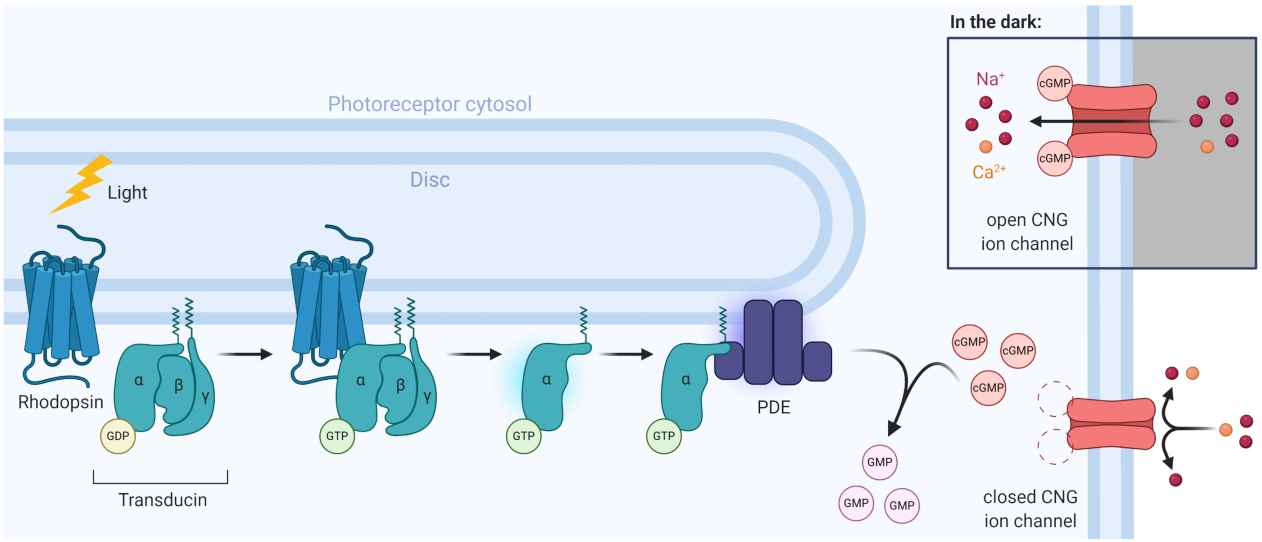

Figure 3.6: Schematic of phototransduction in rod outer segments

3.2 Cone degeneration and therapeutic strategies

Achromatopsia is a devastating inherited retinal dystrophy (IRD), defined by loss of cone function, colour blindness, visual acuity loss, pendular nystagmus and extreme light sensitivity (photophobia)[15]. In human, this autosomal recessive disease is caused by mutations in genes cyclic nucleotide-gated channel subunit α- and β-3 (*CNGA3*,*CNGB3*), cone-transducin α-subunit (*GNAT2*), phosphodiesterase 6C and 6H (*PDE6C*, *PDE6H*) and the activating transcription factor 6-α (*ATF6A*)[16]. The majority of patients have mutations in *CNGB3* (40-50%)

or *CNGA3* (25%)[17], leading to non-functional or absent proteins. This in turn leads to defective CNG channels, which are normally made of three α-subunits and one β-subunit [18], thereby interfering with the cGMP-regulated cation influx and ultimately cone integrity. In humans, the manifestation of the disease has been staged by spectral-domain optical coherence tomography to 5 stages: *(1)* intact outer retina, *(2)* inner segment ellipsoid line disruption, *(3)* presence of an optically empty space, *(4)* optically empty space with partial RPE disruption and *(5)* complete RPE disruption and/or loss of the ONL [19]. In the *Cnga3*$^{-/-}$ mouse model of achromatopsia, cones exhibit delayed migration within the ONL during development, defective development or retraction of outer segments already by postnatal week 3 and extensive cell death with only 10-20 % of cones left after postnatal month 2 [20, 14]. The gradual degeneration of cones offers a window of opportunity for therapeutic interventions, designed to delay or halt cell death.

Depending on the stage of retinal degeneration, different strategies hold therapeutic potential (Fig.3.7), some of which have been advanced in this work to deliver optimised therapies. At the early disease stages, dormant cones can be targeted to regenerate their outer segments using developmental cues [21] or to restore their function by supplementing the missing/mutated gene [22, 23] (see:5.3). At the later disease stages, when no viable cones remain, approaches such as cell-transplantation [24], retinal implants [25], reprogramming [26, 27] and optogenetic tool delivery [28] hold promise in recovering the missing cell population (see:5.4.2) or inducing photo-sensitivity in the remaining retinal network (see:5.4.1).

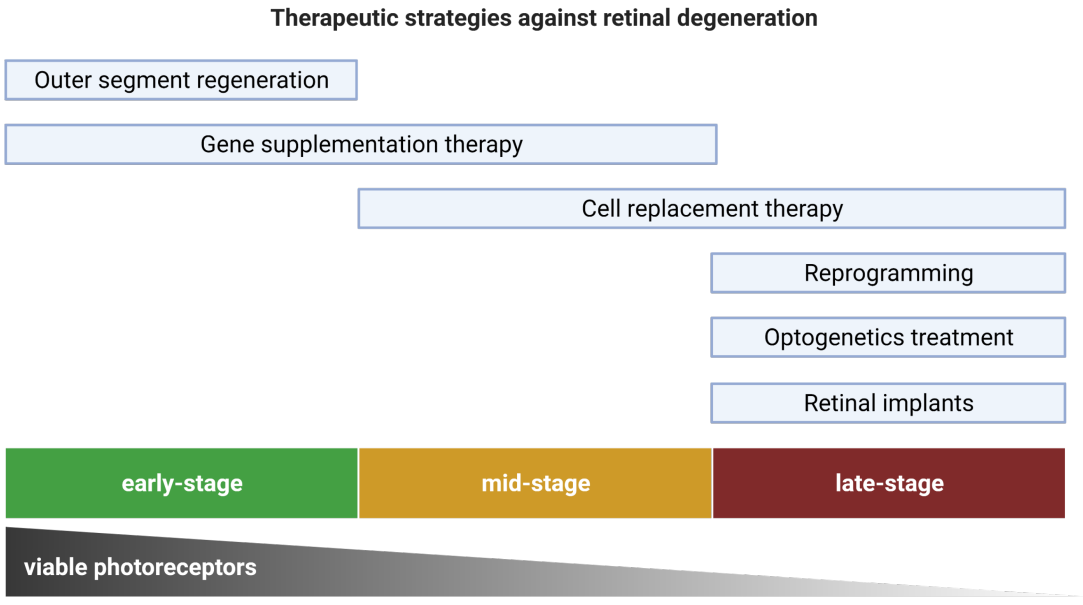

Figure 3.7: Schematic of therapeutic strategies according to degeneration timeline

The presence of outer segments, even if not fully formed [29], is a prerequisite for early therapeutic strategies aimed to restore cone function, as ectopic protein expression after gene supplementation therapy can stress the endoplasmic reticulum and further burden cone health. Though cone cell fate is already determined from embryonic day 10 (E10) to E18 [30], cone outer segments only appear on postnatal day 5-6 in mice [31] and seem to require the expression of microRNA (miRNA) cluster 96/182/183 during development [21]. MiRNAs are small RNA species that serve as temporal post-transcriptional repressors that are coded in introns, exons or both (Fig.3.8)[32].

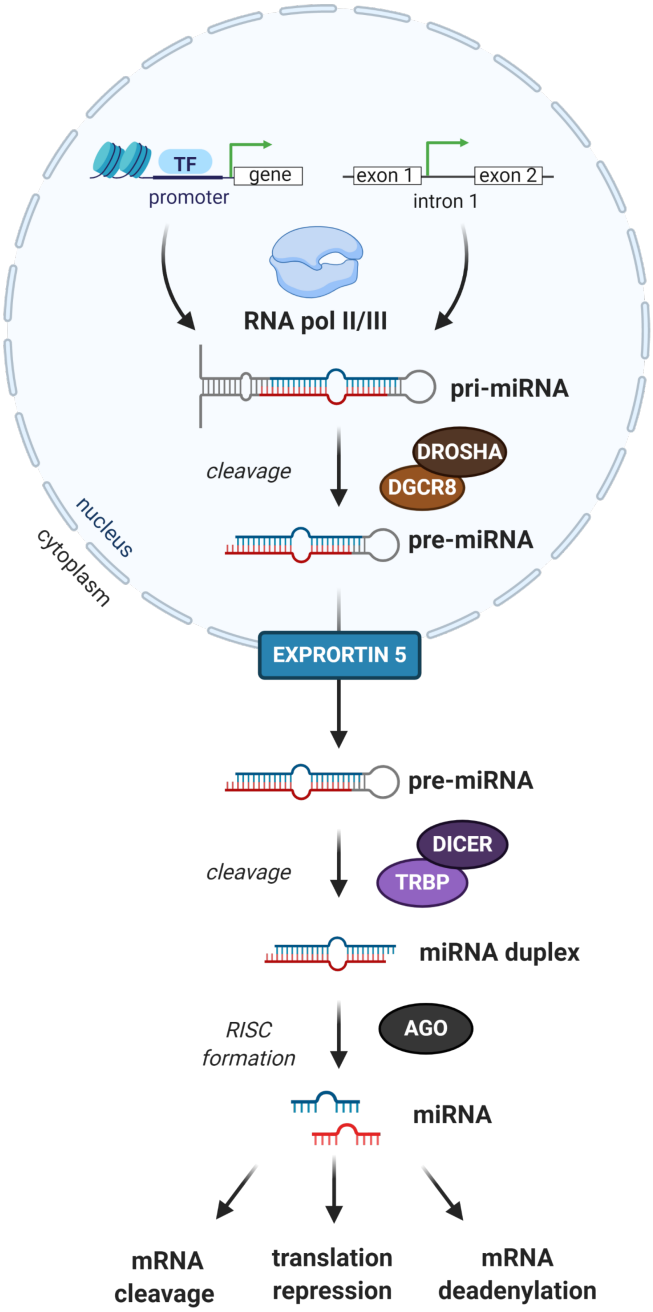

Figure 3.8: Schematic of miRNA processing cycle

They are predominantly transcribed by RNA polymerase II, but also III [33], into primary-miRNA (pri-miRNA) transcripts that are cleaved by the Drosha/DGCR8 complex to give precursor-miRNAs (pre-miRNA). These are transported out of the nucleus and further cleaved to their mature forms (5p or 3p) by the Dicer/TRBP2 complex. The forward (5p) or reverse (3p) mature miRNA strands bind to the 3' UTR of mRNA transcripts, leading to their degradation [32]. Depletion of miRNA-96/182/183 during retinal development or in adult retinas leads to photoreceptor degeneration [21, 34]. As such, these miRNAs and their targets could be exploited for the regeneration of outer segments in various cone dystrophies, including achromatopsia.

The most promising therapeutic strategy thus far, in halting degeneration and restoring vision in recessive IRDs, is gene supplementation therapy [35]. This entails the delivery of the intact coding sequence of the mutated or missing genes in the affected cells, so that they produce functional proteins that can counteract the disease phenotype. With the advancement of viral vector technology, this approach has yielded the first clinically approved gene therapy, voretigene neparvovec, to treat a form of IRD that affects RPE cells. Preclinical studies in mouse models of achromatopsia have shown that gene supplementation is able to partially recover cone function [22, 23], albeit with limitations relating to the administration route and therapeutic vector spreading. To address this, advanced tools capable of targeting all or most cones with minimal collateral damage to the deteriorating retina are needed. Furthermore, understanding the molecular mechanisms triggered after gene supplementation in cones could help improve all future therapeutic strategies.

At the late stages of retinal degeneration, when photoreceptors are depleted, all interventions are redirected to the remaining retinal network. Promising approaches focus on the delivery of optogenetic tools, i.e. light-sensing proteins to ganglion cells, bipolar cells or dormant (non-functional) cones, with the aim of making them photosensitive [36, 28]. In order to choose an appropriate target cell population, it is important to first consider the functional output of the mammalian retina, which is dictated by two overarching signalling circuits; the ON- and OFF-circuit. Each circuit is made of specific neuronal subtypes that form distinct synaptic connections and interrelations. For the purpose of restoring vision in diurnal mammals, targeting the ON circuit is in line with its natural capacity to respond to increasing brightness, whilst the OFF circuit responds predominantly to darkness [37, 38]. Although ganglion cells could be suitable candidates due to their accessible location, their position at the end of the retinal circuitry does not allow for any signal amplification or fine-tuning that is required for daylight vision. In this regard, ON bipolar cells are better suited targets for optogenetic therapies, as any light-induced signals they generate would be processed in the IPL [37] before they are

relayed by ganglion cells to the thalamus. To this end, the efficient targeting of ON bipolar cells across species is paramount.

Another phenomenon with therapeutic implications is that in all contexts of neuronal damage in the CNS, whether intrinsic or extrinsic, the first response comes from glia and microglia cells [39]. As resident immune cells, microglia span all areas of the CNS and have diverse roles in neuronal development, connectivity and homeostasis; from pruning neuronal synapses and regulating extracellular cues to eliminating pathogens or defective cells [40, 41]. During retinal development at E11.5 [40], resident microglia in the optic nerve or macrophages in the ciliary body/iris serve as sources of microglia [42] that populate the healthy retina, predominantly in the synaptic layers with a ramified morphology (Fig.5.29.A). However in degenerative diseases, such as IRDs, microglia are strongly activated by the cell death in the ONL; they adopt an amoeboid morphology and rapidly infiltrate the affected area to dispose of the defective cells (Fig.5.29.A). This phagocytosis frenzy triggered by dying photoreceptors often causes microglia to attack cells that are healthy yet "at the wrong place in the wrong time". It was hypothesised that an effective way to overcome two undesired effects at once is to directly reprogram microglia into neurons, which would stop excess microglia from damaging residual healthy tissue and at the same time repopulate the missing photoreceptors (Fig.5.36).

Irrespective of the therapeutic approach, whether at the early or later disease stages, the common denominator across all aforementioned strategies is the need for an effective vector that is potent in the retina. The most promising vectors for ocular delivery are based on adeno-associated viruses (AAVs).

3.3 Gene therapy using recombinant AAV vectors

AAVs are small non-enveloped viruses that belong to the genus Dependoparvovirus of the family *Parvoviridae*, first discovered in 1965 by Bob Atchison, David Hoggan and Wallace Rowe in adenovirus preparations. They contain a ~4.7 kilobase (kb) single-stranded (ss) DNA genome flanked by inverted terminal repeats (ITRs) that serve as origins of replication and enable low levels of integration into the host genome. After discovering that AAVs require the presence of adenovirus genes to replicate, they started being investigated as therapeutic vectors due to their latent presence in infected cells and non-pathogenic nature [43]. Once the wildtype AAV genome was cloned into a plasmid in 1982 by Samulski *et al* [44], a journey of more than 30 years began where AAVs turned into vectors and used to deliver generic cargo in cells or tissues.

The viral genome contains a *rep* gene that encodes for replication proteins (Rep78, Rep68,

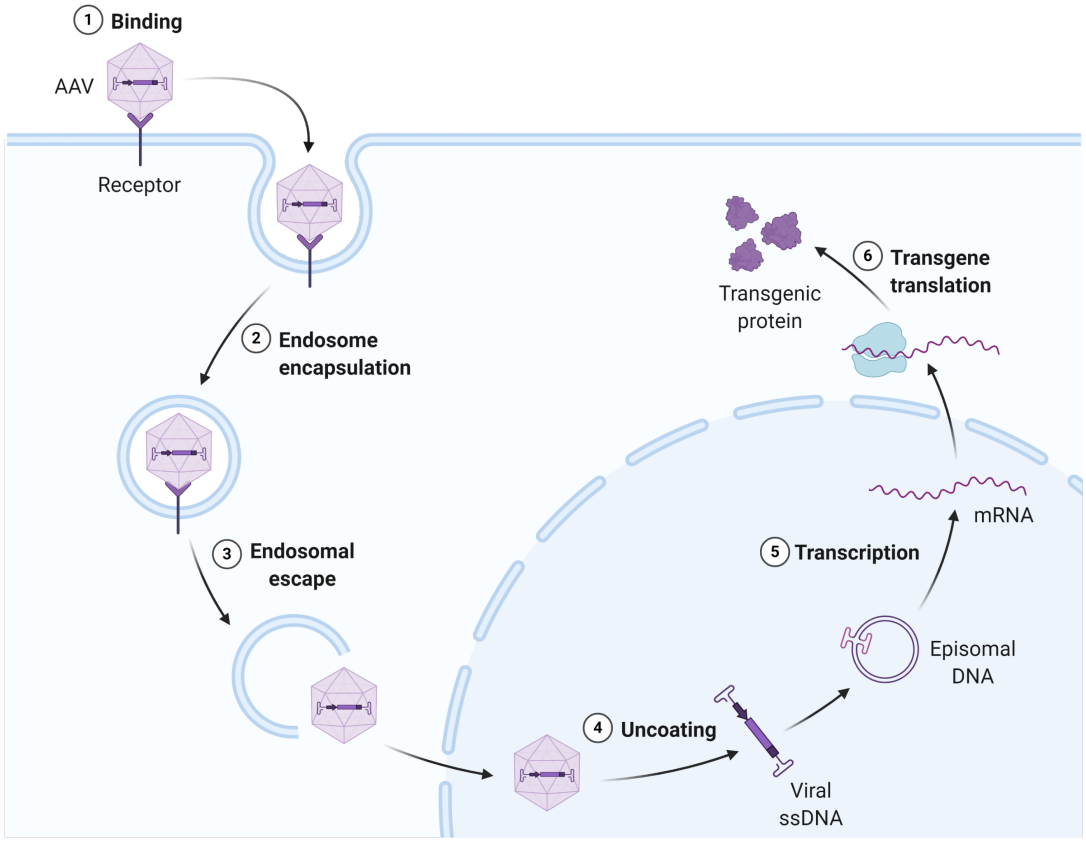

Figure 3.9: Schematic of AAV infection cycle

Rep52, Rep40), a *cap* gene that encodes for viral proteins 1, 2 and 3 (VP1, VP2, VP3) and an *aap* gene that encodes the assembly-activating protein (AAP). Once expressed, the genome is packed inside an icosahedral capsid comprised of 60 units with a 1:1:10 ratio of VP1, 2 and 3, respectively [43]. AAV capsids interact with glycan moieties on the cell surface that help them dock and bind to surface receptors. The AAV-receptor complex then becomes internalised via clathrin-mediated endocytosis [43]. AAVs are trafficked in endosomes using the microtubule network [45] and exit late endosomes [46] after acidification to enter the nucleus [47]. Once inside the nucleus, the AAV is uncoated and its ssDNA genome becomes polymerised to double-stranded (ds) ahead of transcription [48]. This dsDNA remains episomally in the nucleus of post-mitotic cells and can be transcribed over the host cell lifetime [49].

An increasing number of natural AAV serotypes has been identified, AAV1-13 [50], and some have been characterised for their tissue tropism, i.e. preferential uptake by cells of certain organs. Though the transduction efficiency of each serotype varies, Figure 3.10 summarises the main tissues infected by natural AAVs [51]. By replacing the viral genome with a transgene cassette of choice, virtually any 4.7 kb sequence can be delivered *in vivo* using recombinant AAVs (rAAVs).

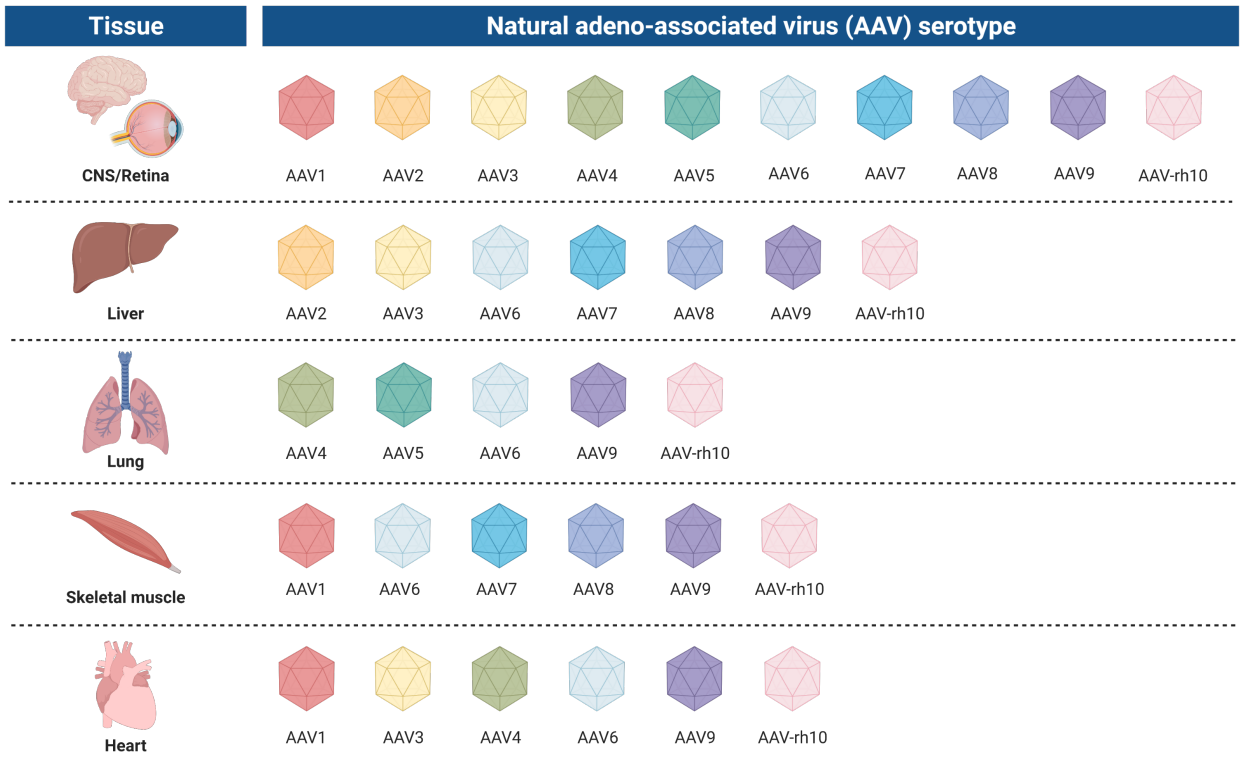

Figure 3.10: Schematic of natural AAV serotype tropism

As the field of AAV biology advanced, it became apparent that its capsid is malleable and tolerates a variety of changes while still producing infectious particles. This led to an outpouring of approaches to engineer AAV capsids either via rational design or directed evolution, so as to generate novel vectors with pre-determined features [52]. These approaches include, but are not limited to, the replacement of key residues to avoid proteosomal degradation of the capsid during intracellular trafficking (e.g. AAV6.2 [53]) and the modification of key loci that determine the strong capsid affinity for specific glycan moieties or receptors (e.g. AAV2-QuadYF [54]). Though rational design may have its moments, nature can do it better. As such, capsid diversification strategies that produce large mutant libraries, which are then screened for desired properties, became more popular. Such strategies include: *(1)* error-prone PCR of *cap*, *(2)* peptide-display on protruding capsid loci (AAV2.7m8 [55]), *(3)* capsid domain shuffling (AAV-DJ [56, 57]), *(4)* Cre recombinase-based targeted evolution (AAV-PHP.eB and AAV-PHP.S [58]), or a combination of them (AAV-DJ8 [56], AAV2-retro [59]).

While natural AAV serotypes have been widely used in preclinical and first-in-human trials to treat monogenic diseases, the emergence of next generation vectors broadens the potential for therapeutic success. Focusing on IRDs, natural AAV serotypes 2, 5 and 8 have been predominantly used [35], with the first approved gene therapy drug against Leber's congenital amaurosis, voretigene neparvovec, using AAV2 to deliver a therapeutic *Rpe65*-encoding

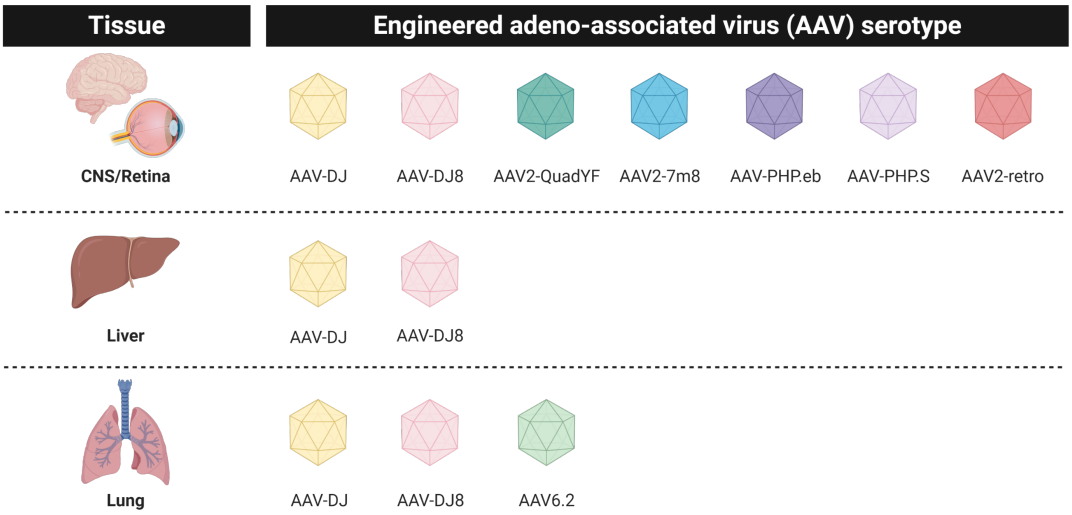

Figure 3.11: Schematic of engineered AAV serotype tropism

transgene after subretinal injection [60]. Despite its efficacy in targeting photoreceptors, the subretinal injection procedure can be deleterious to an already compromised retina. With the exception of certain engineered capsids [61, 62], conventional AAV serotypes are unable to spread laterally and achieve only local transduction. As such, there is an urgent clinical need for potent rAAV vectors that can target larger areas of the retina and be applicable via a less invasive route, such as intravitreal injection.

Materials and methods

Summary tables of primers and antibodies used in each project are included at the end of their respective section. All schematics were generated using biorender.com and the figures were generated in Inkscape or Adobe Illustrator 2021.

4.1 Generic methods

4.1.1 Molecular Biology

Gibson Assembly

All primers were designed using the NEBuilder Assembly tool (nebuilder.neb.com) and manufactured as cloning oligos by Eurofins Genomics. The lyophilised primers were reconstituted to 100 mM concentration with molecular grade water (MFCD00011332, VWR) and further diluted to a 10 mM working concentration; solutions mixed thoroughly in each step. All primer solutions were kept at -20 °C and thawed to room temperature (RT) before use. One-step isothermal assembly at 50 °C was performed with equimolar components at a 1:1 or 1:3 ratio of backbone to insert using the published protocol (Fig.4.1)[63].

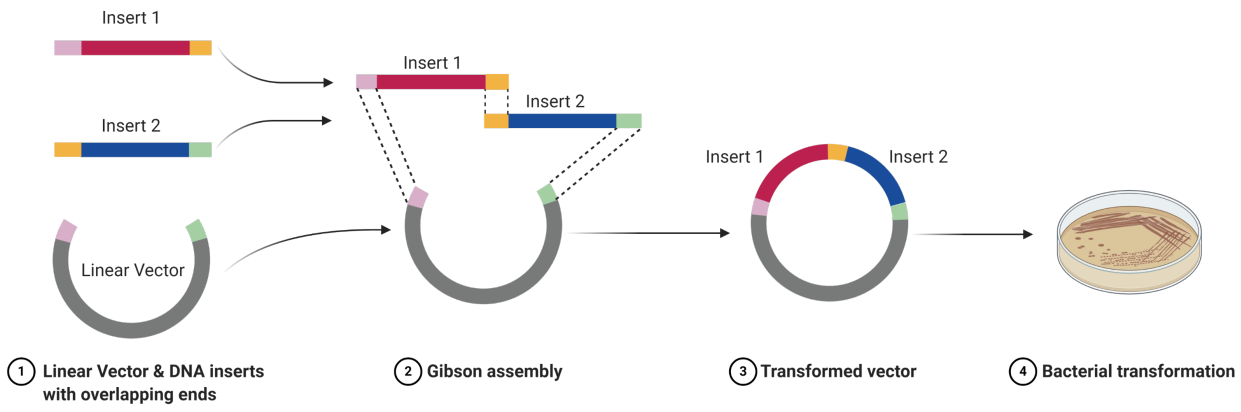

Figure 4.1: Schematic of Gibson Assembly

Nucleic acid extraction from cells and tissues

DNA was extracted from cells according to the manufacturer instructions using the PureLink HiPure Plasmid Maxiprep Kit (K210007, Thermo Fisher) and PureLink HiPure Expi Plasmid Megaprep Kit (K210008XP, Thermo Fisher). Bands after DNA electrophoresis were extracted using the QIAquick Gel Extraction Kit (28115, Qiagen). For simultaneous RNA and miRNA isolation from retinal tissue the mirVana miRNA Isolation Kit was used with phenol (AM1560,

Thermo Fisher). RNA was isolated from fresh retinal tissue using the RNeasy Plus Mini Kit (74136, Qiagen). For gDNA extraction from *in vitro* cultures, cells were washed with DPBS$^{-CaCl_2}$ and harvested with 1% β-mercaptoethanol (Sigma Aldrich) in RLT buffer (Qiagen). The lysate was homogenised in safe-lock 2 ml Eppendorf tubes using a steel ball and the mixer mill MM400 (Retsch) at 30 Hz for 1'. Subsequently, the tubes were centrifuged at max speed for 5' and up to 800 μl supernatant was loaded on a Zymo-Spin IIC-XL column (Zymo Research) for gDNA isolation following an in house protocol. RNA and gDNA were simultaneously extracted from fixed cells using the Allprep DNA/RNA FFPE kit (80234, Qiagen) and the protocol was adapted to isolate RNA from fixed tissue slices (Fig.4.2). Briefly, tissue slices (10-14 μm) were scraped with a sterile scalpel from 2 glass slides and collected in an Eppendorf tube. For mouse, dog and NHP material 10, 6 and 6 tissue slices were pooled, respectively. Subsequently the material was deparaffinised by dissolving the scrapings in PKD buffer followed by a proteinase K digestion at 56 °C for 15' and then at 80 °C for 15'. The solution was finally chilled for 3' on ice and centrifuged at ≥12000 rpm. The supernatant was then used for RNA extraction following the manufacturer instructions. RNA/DNA amounts were determined using a NanoDrop 2000 spectrophotometer (Thermo Fisher).

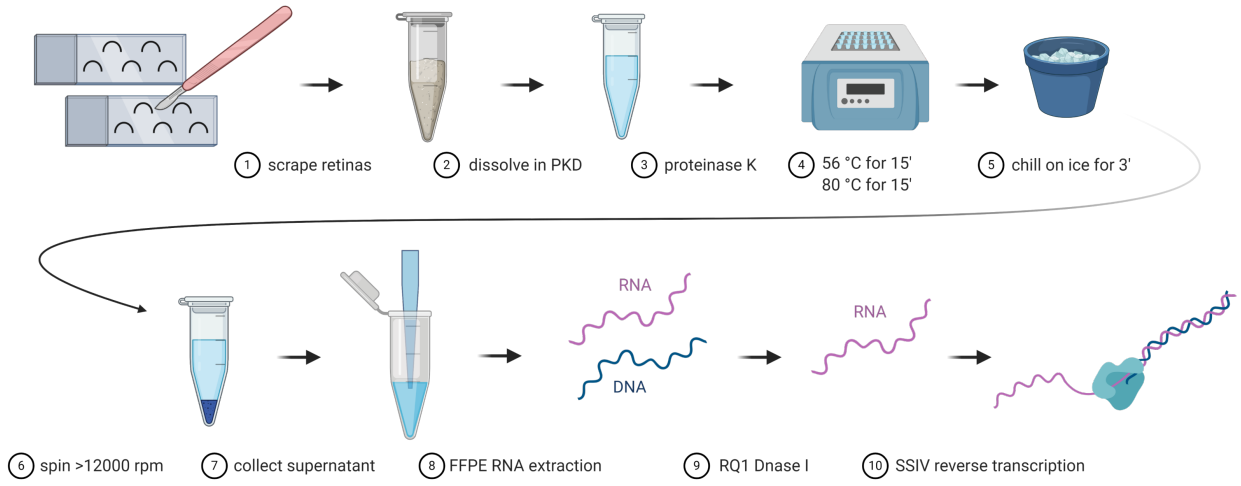

Figure 4.2: Schematic of RNA extraction from sectioned retinal tissue

Gene expression analysis

Extracted RNA from AAV-transduced cells or tissues was digested with RQ1 RNase-free DNase (M6101, Promega) to eliminate DNA contaminants. Fifty-200 ng of RNA were reverse-transcribed to cDNA using SuperScript IV Reverse Transcriptase (18090050, Thermo Fisher) or RevertAid First Strand cDNA Synthesis Kit (K1621, Thermo Fisher). For all types of ex-

	Target	Forward primer	Reverse primer	Annealing T °C
general	*eGFP*	CGACCACTACCAGCAGAACAC	TTCTCGTTGGGGTCTTTGCTCAG	62
	ITR2	GGAACCCCTAGTGATGGAGTT	CGGCCTCAGTGAGCGA	58
	GCaMP6s	CCCGACAACCACTACCTGAG	GTCCATGCCGAGAGTGATCC	60
	jRCaMP1a	AAGACAGGTCACGCAGTCAG	GAGTGTAACCACGCAGACCA	60
	jRCaMP1b	GGAATAAGTGGGGTCACGCA	GAGTGTAACCACGCAGACCA	60
mouse	*Alas1*	GGATGGCGTCATGCCAAAAA	GTCGATCAGCAAACTCGTGC	60
	Gapdh	AATGGTGAAGGTCGGTGTGAA	GCAACAATCTCCACTTTGCCA	60
	Slc6a6	CTCCGGGACCTGGTTGCT	GCACTGGTTCTGCACCTGG	61
	Fcho2	TGGCGCATTTCGTGGAGAAT	GCCTCTTCTATTGTAGCTCTTTCT	60
	Celf6	TGTGCTTACCCAAGGTGCTT	CACCACCATTGACCAGCTTTA	60
	Zfyve26	TCCAGATACGCAGGGAAAGC	GGTGAATCATGGAATCTGATCGT	60
	Snap23	GCACCCTGTCCGATCTTCTA	TACGGATACTCTGTCCCGCT	60
	Tacc1	CAAATCCCTGAGTTTCAGCTCG	GATTCTTGGGGTTTGGCCTC	60
	Dhcr24	TCTCCCTCCTGAAGCTGACC	TGGGGTAGACGTGGATGTCA	60
	Arr3	GGTGTCCTATGGGGGCATTC	CGATGACTATGTCCTCCGAGC	60
	Cngb3	TCCTGCACATTAACGCCTGT	GCATCGCAGATACTTGTTGCC	60
	Cnga3	GTGAAACAGCCTCACAGCAGG	TGGAAGATGTCTCCTCACATGG	61
	Cnga1	AACGAGCCATTTGTGCTGC	TGGTTAGTTTAATATCTGCGCTTGT	60
	Grm6	TGCACTACATCCGAGCAGTC	TGGAAGATGTCATAGCGCCC	60
	Pcp2	CAGAACCCAGAAAGCCAGGGT	GGGTGTTGACCAGCATATCCA	60
	Vsx2	CAAGAAGCGTAAGAAGCGGC	AGACATCTGGGTAGTGGGCT	60
	Cabp5	GCTTGGTGAACACTACCTGCT	TCCTGTCCCAGTGGTCTCTC	60
	Rho	AGGGCTTCTTTGCCACACTT	GGAAGTTGCTCATCGGCTTG	60
	Nrl	CTATTCAGGGAGCCCGGGAG	GTTCAACTCGCGCACAGACA	60
	Pde6c	CCAAAGACTCCAGATGGCAGG	GGCAATCCACTAACAAGCGTCC	62
	s-Opsin	TTTTGGCTGGAGCAGGTTCA	TCGCTTCGATACTTGGTGCC	60
	Kcnip3	GGCTCAGACAGCAGTGACAGT	GGTCTGAGCTTGTAGCTGGTC	60
	Prkca	GACAAGCCGCCATTTCTGAC	TCCATGACGAAGTACAGCCG	60
	Tacr3	GTGACAAGTACCATGAGCAGC	CATGGTAGGGTAGCCAGCAG	60
dog	*Sdha*	CGGTCCATGACTCTGGAAAT	GCAACTGCAGGTACACATGG	60
human/NHP	*HPRT1*	TTCTTTGCTGACCTGCTGGA	GTCCCCTGTTGACTGGTCATT	60
	GRM6	TTCGAGCTGTCCGCTTCAAT	ACTGGAAGATGTCGTACCGC	60
	PCP2	GGAGTCCAGGGACATGATGG	ACGTGGCTCAGCAGATTGAA	60
	CABP5	TTTGTGGAGCTGATGACCCC	GATCTCCCCATCTCCGTTCG	60
	RHO	ACCCTCTACACCTCTCTGCAT	GACCACCAAGGACCACAGG	60
	PRKCA	CACGAGGTGAAGGACCACAA	CAAACTTGGCACTGGAAGCC	60
	TACR3	TTTGTGCAATGGCCAGAAGG	CCATGATGAGCAATGGGAAACA	60
	KCNIP3	CCACCTATGCACACTTCCTCT	TGAGCTTCTCGTGGACTGTG	60

Table 4.1: List of primer pairs

pression analyses, primer pairs were designed for eGFP, ITR2, GECIs, mouse, dog and NHP samples, with an annealing temperature between 58-62°C (Table4.1). For quantification of ma-

ture miRNAs, the TaqMan MicroRNA Reverse Transcription Kit (4366596, Thermo Fisher) was used together with TaqMan MicroRNA Assays (IDs: 002334, 002269, 000186, 001973, Thermo Fisher) and the TaqMan Fast Advanced Master Mix (4444556, Thermo Fisher) according to the manufacturer instructions. Quantitative PCR was done using the PowerUp SYBR Green Master Mix (A25742, Thermo Fisher) and QuantStudio 5 Real-Time PCR platform.

4.1.2 Tissue processing and imaging

Immunohistochemistry

After cervical dislocation, mouse eyes were enucleated, fixed in 4% PFA/PBS for 1 hour at RT followed by overnight incubation in 30% sucrose/PBS and embedded in optimal cutting temperature (OCT) compound (Fig.4.3). For dog and NHP, after humane euthanasia (overdose of pentobarbitone), eyes were enucleated, slits made into the vitreal cavity at the pars plana region and the entire globe were immersed in 4% PFA at 4 °C for 3.5 hours for the dogs and 3.25 hours for the NHP. The globes were then processed as previously described [54]. For human explants, the tissues were fixed in 4% PFA for 2 hours at room temperature (RT) followed by overnight incubation in 30% sucrose/PBS and subsequent embedding in OCT. Extra care was taken to prevent detachment of the explant from the underlying filter. Coronal cryo-sections (14 to 20 μm) were collected serially using cryostat Leica CM1950 and stored at -80°C unless used immediately.

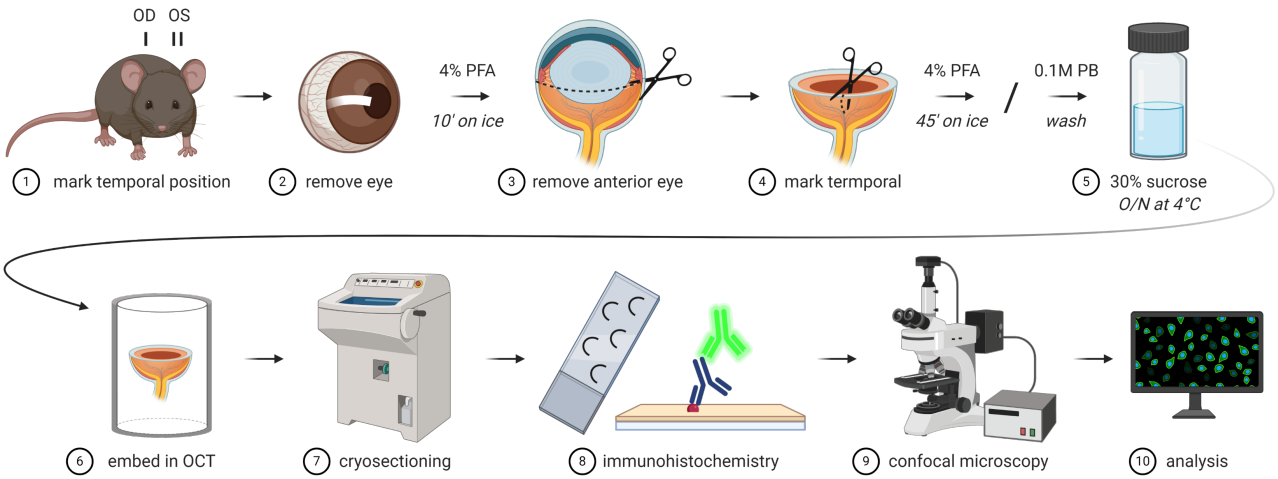

Figure 4.3: Schematic of mouse eye preparation and histological processing

Cryosections were thawed and marked with a pap-pen, then incubated at RT for 60' with a blocking solution of 2% BSA/0.3% Triton X-100 in PBS. Samples were incubated with primary antibodies diluted in blocking solution overnight at 4°C. On the next day, samples were washed

Ab I	Clone	Host	Isotype	Supplier	Catalog No	ICC	IHC
Arrestin, visual	E-12	Goat		Santa Cruz	sc-34547		1:250
Cacna1s (Gpr179)		Mouse	IgG1	Millipore	MAB427		1:250
Calbindin-D-28K	CB-955	Mouse	IgG1	Sigma Aldrich	C9848		1:500
CD11b	M1/70	Rat	IgG2b	Biolegend	101202	1:500	1:500
cGMP		Sheep		Abcam	AB836	1:3000	
ChAT		Goat		Millipore	AB144P		1:100
Chx10/Vsx2		Sheep		Exalpha	X1179P	1:500	1:500
CNGA3		Rabbit		Custom made	Biel *et al* . 1999		1:1000
Goα		Mouse	IgG1	Millipore	MAB3073		1:500
GFAP		Rabbit		Agilent	Z033429-2		1:500
GFAP	2E1.E9	Mouse	IgG2b	Biolegend	644701		1:500
GFP		Chicken		Aves Labs	GFP-1020		1:1000
GFP		Rabbit		Chromotek	PABG1		1:500
Glutamine Synthetase		Rabbit		Abcam	ab49873	1:1000	1:500
Iba1		Guinea pig		Synaptic Systems	234004		1:100
Iba1		Rabbit		Wako	019-19741	1:500	
Iba1		Rabbit		Synaptic Systems	234 013		1:500
Ki67	SP6	Rabbit		Thermo Fisher	MA5-14520	1:500	
NG2		Rabbit		Merck	AB5320		1:250-1:500
Olig2	211F1.1	Mouse	IgG2a	Merck	MABN50	1:500	
Opsin, red/green		Rabbit		Merck	AB5405		1:500
Otx2	OTI3G9	Mouse	IgG1	Origene	CF809627	1:1000	
P2RY12	S16007D	Rat	IgG2b	Biolegend	848001		1:500
Pcp2		Mouse	IgG2b	Santa Cruz	137064		1:500
PKC-biotin	MC5	Mouse	IgG2a	Leinco Technologies	P108		1:500
Recoverin		Rabbit		Millipore	AB5585	1:500	1:500
RFP		Rat	IgG2a	Chromotek	5F8	1:500	1:500
Rhodopsin	1D4	Mouse	IgG1	Merck	MAB5356		1:2000
RPE65	401.8B11.3D9	Mouse	IgG1	Invitrogen	MA1-16578	1:10-1:500	1:250
Sox2		Rabbit		Abcam	ab97959		1:500
βIII-tubulin	TUJ1	Mouse	IgG2a	Covance (Biolegends)	MMS-435P	1:500	1:500

Table 4.2: List of primary antibodies

Anti-	Ab II	Isotype	Host	Colour	Catalog No	Supplier	Working dilution
GFAP	Cy3	IgG1	mouse		C9205	Sigma Aldrich	1:1000
goat	Cy3	IgG (H+L)	bovine		805-165-180	Jackson	1:300
goat	Alexa 633	IgG (H+L)	donkey		A-21082	Thermo Fisher	1:400
guinea pig	Alexa 488	IgG (H+L)	goat		A-11073	Thermo Fisher	1:500
mouse	Alexa 488	IgG (H+L)	goat		A-11001	Invitrogen	1:800
mouse	Alexa 488	IgG1	goat		A-21121	Thermo Fisher	1:500
mouse	Alexa 488	IgG2a	goat		A-21131	Thermo Fisher	1:500
mouse	Cy3	IgG (H+L)	donkey		715-165-150	Jackson	1:400
mouse	Alexa 555	IgG1	goat		A-21127	Thermo Fisher	1:500
mouse	Alexa 555	IgG2b	goat		A-21147	Thermo Fisher	1:500
mouse	Alexa 594	IgG2a	goat		A-21135	Thermo Fisher	1:500
mouse	Alexa 647	IgG (H+L)	goat		A-21236	Thermo Fisher	1:400
rabbit	Cy2	IgG (H+L)	goat		111-225-144	Jackson	1:200
rabbit	Alexa 555	IgG (H+L)	donkey		A-31572	Thermo Fisher	1:500
rabbit	Cy3	IgG (H+L)	donkey		711-165-152	Jackson	1:400
rabbit	Cy3	IgG (H+L)	donkey		AP182C	Millipore	1:400
rabbit	Alexa 633	IgG (H+L)	goat		A-21071	Thermo Fisher	1:400
rabbit	Alexa 647	IgG (H+L)	chicken		A-21443	Thermo Fisher	1:400
rabbit	Alexa Plus 647	IgG (H+L)	goat		A-32733	Thermo Fisher	1:500
rabbit	Cy5	IgG (H+L)	donkey		711-175-152	Jackson	1:1000
rabbit	Alexa 405	IgG (H+L)	goat		A-31556	Thermo Fisher	1:500
rat	Alexa 488	IgG (H+L)	donkey		A-21208	Thermo Fisher	1:500
rat	Cy3	IgG (H+L)	goat		112-165-143	Jackson	1:200
rat	Cy3	IgG (H+L)	donkey		712-165-153	Jackson	1:500
rat	Alexa 647	IgG (H+L)	goat		A-21247	Thermo Fisher	1:500
sheep	Alexa 488	IgG (H+L)	donkey		A-11015	Thermo Fisher	1:500
sheep	Alexa 594	IgG (H+L)	donkey		A-11016	Thermo Fisher	1:500
PNA	Alexa 594		*Arachis hypogaea*		L32459	Invitrogen	1:300

Table 4.3: List of secondary antibodies

several times with PBS and incubated for 2 hours at RT with secondary antibodies diluted in blocking solution. The sections were then washed in PBS and counterstained with Hoechst-33342 or DAPI (1:2000; D1306, Thermo Fisher) prior to mounting with a glass slide (18606-5, Aqua-Poly/Mount).

Image acquisition and visualisation

Images were acquired with an inverted or upright Leica SP8 confocal microscope equipped with lasers emitting at the wavelengths (λ) 405, 488, 552 and 638, using an objective magnification of 10x, 20x, 40x or 63x. The original images, consisting of multiple z-stacks, were further processed with the open-source software Fiji [64].

4.1.3 *in vivo* animal experiments

Animals

All animal experiments were performed according to the ARVO statement for the use of animals in ophthalmic and vision research and were approved by the local authorities (Regierung von Oberbayern, Michigan State University and Charles River Laboratories Institutional Animal Care and Use Committees). The use of human tissue samples was approved by the institutional review board of the Ludwig-Maximilians-University Munich (Project number 17-531) and conformed to the principles set out in the WMA Declaration of Helsinki and the Department of Health and Human Services Belmont Report. Written informed consent was obtained from patients before the tissue samples were collected and used for investigational purposes. Male and female adult (2-3 month-old) C57BL6/J, C57BL6/J x 129/sv, $Pde6b^{wt}$ (*Rd1 wt*), $Pde6b^{rd1}$ (*Rd1 mut*), *RG-eGFP* mice expressing eGFP under control of the cone-specific RG promoter [65] and 2-week-old $Cnga3^{-/-}$ mice [20] were used. The *RG-eGFP* mice were kindly provided by Drs. Y. Fei and T.E. Hughes (Yale University School of Medicine). The day of birth was counted as postnatal (P) day 0. For the large animal studies, male and female 10-month-old beagles and two approximately 3-year old male cynomolgus macaques were used. Mice, dogs, and NHP were housed under standard white cyclic lighting conditions and were used irrespective of gender.

Intraocular injections

In mice, subretinal injections were performed as previously described [66] and intravitreal injections were done with slight modifications. In brief, mice were anaesthetized by intraperitoneal

injections of ketamine (0.1 mg/g) and xylazine (0.02 mg/g). Tropicamide eye drops were applied to dilate the pupils (Mydriadicum Stulln). Injections were performed either free hand or with the UMP3T-1 Microinjection Syringe Pump using the Nanofil Sub-Microliter Injection System (World Precision Instruments) equipped with a 34-gauge bevelled needle under an Opmi 1 FR pro surgical microscope (Carl Zeiss). For intravitreal injections, the needle bevel was turned down while penetrating the sclera, choroid and retina. Intravitreal positioning of the needle was confirmed using the surgical stereomicroscope. One μl of rAAV vector solution was injected into the vitreous of the animals and held for $\geq$20" to avoid backflow. Special care was taken to avoid damage of the lens.

For dog injections, animals were pre-medicated with subcutaneous or intramuscular acepromazine (0.02-0.025 mg/kg, Henry Schein Animal Health). Then anaesthesia was induced with intravenous propofol (4 to 6 mg/kg, PropoFol, Abbott Animal Health), the dogs were intubated, and anaesthesia maintained with isoflurane (Isoflo, Abbott Laboratories, between 2-3.5% in a 1-2 L/min oxygen flow) via a re-breathing circle system. They received topical tropicamide solution (UPS 1%, Falcon Pharmaceuticals Ltd.) to induce mydriasis. Injections were performed under direct visualization using a microscope and a Machemer irrigating vitrectomy lens after routine aseptic preparation of the eye with betadine. All dogs received 200 μL of vector solution containing a total of 2E11 vg. The injection technique was performed as previously described [67]. Post-operatively, dogs received a subconjunctival injection of 2mg methylprednisolone acetate, 0.1mg dexamethasone and 1mg gentamicin. Prednisone was given for 1 month at decreasing doses post-surgery starting at 1 mg/kg once daily.

For non-human primate (NHP) injections, animals were sedated to effect by intramuscular injection of ketamine (10 mg/kg) and dexmedetomidine (0.02 mg/kg) and placed in dorsal recumbence. Tropicamide solution and phenylephrine were administered for mydriasis. After topical proparacaine for local anaesthesia, the eyelid margins were swabbed with undiluted 5% betadine solution and conjunctival fornixes were flushed with 0.5% betadine solution. A calliper was used to mark a spot 3.0 mm posterior to the limbus on the supratemporal bulbar conjunctiva, and the spot was swabbed with 5% betadine solution. A transparent adhesive drape was placed over the palpebral fissure and an eyelid speculum was inserted. A 50 μl aqueous paracentesis was performed. A 31-gauge needle on an insulin syringe was inserted at the marked spot, through the sclera and advanced into the vitreous humour. The needle bevel was positioned to face the posterior axis of the globe and the contents delivered into the mid-vitreous by slowly depressing the syringe plunger. The needle was held in place for at least 2' to lessen reflux of the injected material. When total injection volume exceeded 50 μl, they

were split into two injections of equal volume to prevent elevated intraocular pressure.

Fluorescent confocal scanning laser ophthalmoscopy

cSLO imaging of the retina was performed in anaesthetized animals. Animals were anaesthetised and their pupils dilated as described above. Mouse retinas were examined using a modified Spectralis HRA + OCT system (Heidelberg Engineering) at 488 nm excitation and BP 550/49 emission as previously described [68]. Unless otherwise stated, images were taken weekly for the study duration, at the maximum detector sensitivity (107) in high resolution mode with the scanner set to 30° field of view.

Dogs received topical tropicamide for mydriasis for ophthalmic examinations and retinal imaging. Regular ophthalmic examination and regular colour fundus images (RetCam II, Clarity Medical Systems) were captured post-injection; either awake (using topical proparacaine for corneal anaesthesia) or after cSLO examination (under general anaesthesia) as previously described [67]. Wide-field blue-laser (488 nm) cSLO images were acquired using a Spectralis HRA + OCT at a sensitivity setting of 60-107 and images were recorded at increments of 10: from 60 to 100 and 107; maximum setting to monitor eGFP expression. cSLO images were collected weekly from 4 weeks following intravitreal vector administration.

NHPs were sedated to effect, as above, and placed in sternal recumbence. Topical tropicamide and phenylephrine were administered for mydriasis. Wide-field blue-laser cSLO images were acquired from the central and peripheral retina using a Spectralis HRA + OCT to document distribution of eGFP expression at a sensitivity setting of 100. Images were collected weekly following vector administration for the 8-week study duration. Wide field colour fundus images were also collected using a RetCam Shuttle (Natus Medical Incorporated), following instillation of topical proparacaine, during weeks 4, 6, and 8 following vector administration.

Electroretinography

Mice were anaesthetized and tropicamide eye drops were applied for pupil dilation (Mydriadicum Stulln). Full-field electroretinography (ERG) responses were recorded using a Celeris apparatus (Diagnosys LLC). Light guide electrodes which are embedded in the stimulators were placed on each eye. After a 5-minute light adaptation step with 9 cd/m^2, sequential photopic responses were recorded for Single Flash steps 1, 3 and 10 cd.s/m^2 with constant 9 cd/m^2 background illumination. Flicker recordings were performed for 1, 5, 10, 20 and 30 Hz at 3 cd.s/m^2 with constant 9 cd/m^2 background illumination.

Statistical analysis

Data were collected from biological repeats n≥3; where technical repeats are shown instead of biological repeats this is clearly stated. Graphs and statistical analyses were performed using Prism 9 (Graph-Pad, San Diego). The results are presented as mean±SEM. Paired Student's t test was used to compare two conditions of the same sample population. For more than two populations, a one-way ANOVA and Holm-Sidak multiple comparisons test was performed. For grouped datasets ordinary two-way ANOVA followed by Dunnetts post hoc test or multiple t-tests using the Holm-Sidak method was used, assuming sample populations have the same scatter (SD). The significance $\alpha = 0.05$ was accepted. (p≤0.05 *, ≤0.01 **, ≤0.001 ***).

4.2 Generation of new cell lines

Cell culture

Immortalised cells were cultured according to standard practices. Briefly, cells were cryopreserved in low glucose DMEM (11885084, Thermo Fisher) or high glucose DMEM (61965026, Thermo Fisher) supplemented with 20% FBS (S0615-500ML, Sigma Aldrich) and 10% DMSO (C6295, Sigma Aldrich) in liquid N_2. To bring them in culture, cryovials were thawed and resuspended in warmed complete medium made of DMEM supplemented with 10% FBS and 1% Anti/Anti (15240062, Thermo Fisher). The cell suspension was centrifuged at 0.5 rcf for 5' to remove the DMSO, the cell pellet was resuspended in complete medium and transferred to a sterile T-75 flask. Cells were maintained in an incubator at 37 °C, 5% CO_2, 85-95% humidity and passaged once 90% confluent. For passaging, the medium was aspirated, the cells washed once with DPBS$^{-CaCl_2}$ and then detached from the flask using 0.05% Trypsin-EDTA (5' incubation at 37 °C, 5% CO_2). Cells were counted using 0.4% Trypan Blue Stain (T10282, Thermo Fisher) and the Countess 3 FL Automated Cell Counter (Thermo Fisher) before seeding in a new recipient.

Generation of new HeLa cell lines

The piggyBac vector was cloned using the backbone: pB09-TRE-MCS-Ef1a-rtTA(TetO)-PuroR-SV40pA (kindly provided by Prof. Dr. Volker Busskamp, University of Bonn). The backbone was linearised via enzymatic digestion using Fast Digest (FD) BamHI (FD0054, Thermo Fisher) followed by FastAP Thermosensitive Alkaline Phosphatase (1 U/ţL) treatment (EF0654, Thermo Fisher). The RhGC and GECI genes were PCR amplified using Gibson Assembly primers. The

RhGC and GECI genes were linked by a T2A element, leading to a bicistronic transcript for simultaneous expression of both proteins in the presence of doxycycline. The resulting plasmids were: pB09-TRE-MCS-RhGC(BE)-T2A-GCaMP6s-SV40pA-Tet.O-T2A-PuroR (11 kb), pB09-TRE-MCS-RhGC(BE)-T2A-jRCaMP1a-SV40pA-Tet.O-T2A-PuroR (11.033 kb), pB09-TRE-MCS-RhGC(BE)-T2A-jRCaMP1b-SV40pA-Tet.O-T2A-PuroR (11.033 kb). The piggyBac vector also encoded a puromycin resistance gene that was required to select for HeLa cells in which successful genome integration had occurred. After transposition and a 7-day puromycin (1 mg/ml) selection period, single HeLa cells were picked, following a serial dilution step, and grown to separate colonies. Using 200 ng gDNA from the single colonies as template, quantitative PCR (qPCR) revealed which colonies had the highest number of inserts, and these were taken forward for all *in vitro* experiments.

4.3 Directed evolution of AAV libraries and novel vector assessment

AAV libraries and vector production

24 hours after intravenous injections of rAAV libraries, mice were euthanized by cervical dislocation and their retinas were harvested. Nuclei were isolated from whole retina using the Subcellular Protein Fractionation Kit for Tissues (87790, Thermo Fischer). DNA was isolated using the DNeasy Blood & Tissue Kit (69504, Qiagen) and assayed by qPCR using cap specific primers [69]. In addition, total DNA was isolated from retina using the DNeasy Blood & Tissue Kit (69504, Qiagen), amplified by PCR with primers 5'-GTATCTACCAACCTCCAGAGAG-3' and 5'-GTGTTGACATCTGCGGTAGC-3' and cloned into the plasmids pWt.oen or pLG to generate a plasmid pool for sub-library production. NGS analysis was performed on a 454-pyrosequencing platform (GS Junior, Roche). For the generation of helper plasmids for rAAV vector production, sense and antisense oligonucleotides with corresponding peptide insert sequences including linkers were synthesized (Eurofins Genomics GmbH). Oligos were hybridised to form double stranded DNA oligos and then cloned into pRC99 [70, 71] encoding AAV2 *rep* and *cap* genes resulting in the generation of AAV2 *cap* open reading frame with the intended peptide insertions at I-587 of VP1. The insertion of the sequence destroys the MluI / AscI sites and generates a novel EagI site, which can be used for screening correct clones. Vector production was performed as previously described [72]. A self-complementary (sc) rAAV plasmid containing a CMV-eGFP expression cassette [73] and single strand rAAV plasmids containing a hRho-eGFP or mSWS-mCnga3 expression cassette [22] were used as *cis* plasmids.

Retinal harvesting and photoreceptor isolation

For retinal isolation from euthanized mice, each eye was protruded by placing Dumont 7 curved forceps (Fine Science Tools) around the rear part close to the optic nerve and applying gentle pressure. The cornea was cut along the equator with a sharp blade. Subsequently, the retina was detached from the retinal pigment epithelium and removed from remaining eye tissue, together with the lens and the vitreous body, by gently pulling the forceps upwards. After rinsing the tissue in ice cold 0.1 M phosphate buffer (PB) and removing the lens and any remaining RPE cells with the forceps, the two retinas per mouse were pooled and transferred into an Eppendorf tube, snap frozen in liquid nitrogen and stored at -80°C. For isolation of rods and cones, retinas were dissociated as previously described [74]. eGFP$^+$ cones were isolated from *RG-eGFP* retinas by fluorescence activated cell sorting (FACS) using a FACSAria II system (BD Biosciences). Rods were enriched by magnetic-activated cell sorting (MACS) using the Dynabeads Protein G Immunoprecipitation Kit (10007D, Thermo Fisher) in combination with a rat anti-mouse CD73 antibody (1:50, 550738, BD Biosciences) [75]. Whole cell DNA from isolated cones and rods were analysed by next generation sequencing (NGS).

Human retinal explant culture

Eyes from human donors were transferred into CO_2-independent medium (18045-054, Thermo Fisher) after surgical removal. 2-3 hours after surgery, the retinas were cut into 6 pieces and transferred to cell culture inserts with 30 mm diameter and 0.40 μm pore size (PICMORG50, Millipore). The photoreceptor side of the retina was faced to the membrane. The retinal explants were cultured in Neurobasal A medium (10888022, Thermo Fisher) supplemented with 2mM L-Glutamine (25030024, Thermo Fisher), B27 supplement (17504044, Thermo Fisher) and Anti/Anti (15240062, Thermo Fisher) at 37 °C, 5% CO_2, 85-95% humidity. 70% of cell culture medium was replaced every day. 40 μl of AAV suspension was applied at the first day of culture to the vitreal side of the tissue. eGFP fluorescence was recorded using an EVOS FL cell imaging system (Thermo Fisher) at 2x and 10x magnification. After an incubation period of 9-10 days, until which no severe tissue compromise was detected, cultures were fixed with 4% PFA.

Image analysis and cell quantification

Confocal images were collected using a Leica SP8 confocal laser scanning microscope. The quantification of eGFP$^+$ photoreceptors in the ONL of NHP sections was done using ImageJ

[64]. A rectangle with fixed 5 mm^2 area was drawn over the ONL of xy images and nuclei which co-localised with eGFP signal were manually counted. Due to the absence of biological replicates for NHP, technical replicates were performed from different sections ($n \geq 3$).

Subcellular fractionation

HeLa cells, cultured in low glucose DMEM (10% FBS 1% Pen/Strep), were plated in 6 well plates. 24 hours later, cells were counted and transduced with vector particles at a particle per cell ratio of 1000. 24 hours later, cells were harvested by extensive trypsin treatment and PBS washing steps to remove any membrane bound vector particles. Cells were counted and 3-5x10^5 cells were used for subcellular fractionation, while 10^5 cells were analysed by flow cytometry (CytoFlex S platform, Beckman Coulter) to determine transduction efficiency. Subcellular fractionation was performed as previously described [69]. Membrane, cytosolic and nuclear fractions were collected. Purity of fractions was confirmed by Western Blot using anti-Rab 5 (1:100, sc46692, Santa Cruz), anti-Tubulin (1:5000, T5198, Sigma Aldrich), anti-Lamin B1 (1:5000, 16048, Abcam), and anti-Calreticulin (1:100, PA3-900, Affinity BioReagents) antibodies. Fractions were subjected to DNA isolation (Qiagen, DNeasy Tissue kit) followed by qPCR analysis (FastStart essential DNA green master reagent, Roche) using CMV promoter specific primers on the Light-Cycler 96 real-time PCR system (Roche). The specificity of target DNA amplification was confirmed by melting-curve analysis. All samples were run in technical duplicates.

Heparin affinity assay

A 1 ml HiTrap heparin affinity column (Amersham) was equilibrated with PBS/1 mM $MgCl_2$/2.5 mM KCl. Vector preparations of AAV2, AAV2.NN and AAV2.GL purified by iodixanol gradient were diluted in PBS/1 mM $MgCl_2$/2.5 mM KCl and loaded on the column. Flow-through as well as 4 x 5 ml wash fractions were collected. In order to determine the affinity, elution was performed in 5 ml-steps using increasing ionic strength (PBS/1 mM $MgCl_2$/2.5 mM KCl plus 100 mM NaCl up to PBS/1 mM $MgCl_2$/2.5 mM KCl plus 1 M NaCl). DNA of samples was isolated (DNeasy Tissue kit, Qiagen) and analysed by qPCR on a LightCylcer 96 real-time PCR system (Roche) using transgene-specific primers. The specificity of target DNA amplification was confirmed by melting-curve analysis. As a second independent measure, a native dot blot was performed using the capsid antibody A20 (1:50) [76] for probing (kindly provided by Martin Müller, DKFZ, Heidelberg, Germany).

Neutralisation assay

HeLa cells were seeded in a 12 well plate one day prior to the neutralisation assay. Human serum was diluted in DMEM medium containing 10% FBS and 1% Pen/Strep. Vector preparations of AAV2, AAV2.NN and AAV2.GL were added to the serum dilution. As negative control, vector preparations were diluted in medium without human serum. Following incubation for 1 hour at RT, medium in the 12 well plate was exchanged by the rAAV vector-serum dilutions. The number of transgene-expressing cells was determined by flow cytometry 48 hours post transduction.

Thermal stability assay

A 96 well qPCR plate was loaded with 2E9 vector particles/well diluted in PBS and subjected to a temperature gradient using the LightCycler 96 System (Roche Life Science) as previously described [69]. Subsequently, samples were diluted in PBS and transferred to a nitrocellulose membrane using a vacuum blotter. Membrane was probed with B1 (1:5000, 16048, Abcam) antibody recognising the C'-terminus of all AAV2 capsid proteins and with A20 (1:50) antibody [76] binding to intact capsids. B1 and A20 were kindly provided by Martin Muller (DKFZ, Heidelberg, Germany). As secondary antibody, a horseradish peroxidase-conjugated anti-mouse antibody (1:10000, Sigma Aldrich) was applied. Finally, the membranes were treated with an enhanced chemiluminescence reagent (West Dura, Pierce) and analysed by FusionFX device (Peqlab).

4.4 ON bipolar cell isolation method

NHP retinal explant culture

Eyes from NHPs were transferred into CO_2-independent medium (18045-054, Thermo Fisher) after surgical removal. Upon arrival (4-5 hours after surgery), the eyes were sectioned to expose the posterior eye cup, which was subsequently cut into quadrants. The retina was then gently peeled off the underlying retinal pigmented epithelium and further sectioned to separate 4 peripheral quadrants, which were later transferred to hydrophilic PTFE cell culture inserts with 30 mm diameter and 0.4 μm pore size (PICMORG50, Millipore) with the ONL of the retina placed facing the membrane. Retinal explants were cultured in Neurobasal A medium (10888022, Thermo Fisher) supplemented with 2 mM L-Glutamine (25030024, Thermo Fisher), B27 supplement (17504044, Thermo Fisher) and Anti/Anti (15240062, Thermo Fisher). Retinal

explants were kept overnight at 37°C, 5% CO_2, 85-95% humidity and processed for cell sorting the next day.

Dissociation of retinas

Acutely isolated mouse retinas were pooled from one animal for dissociation. The Papain Dissociation System (Worthington Biochemical Corporation link) was used as previously described [77]. Briefly, retinas were minced into smaller pieces and incubated in a mixture of papain and DNase at 37°C for 45-60', in the presence of mild agitation (600 rpm). A solution containing DNase/BSA/Ovomucoid in EBSS was then added, followed by BSA/Ovomucoid and more pipetting, until no more retinal pieces were visible. The cell suspension was then centrifuged at 0.4 rcf for 5' at 4°C and the supernatant discarded. For NHP retinas, after the night in culture the explant quadrants were processed as a whole or punctured with a 6 mm biopsy punch (270038, Stiefel Einweg-Biopsy-Punch, Stiefel Laboratorium) to excise a sample for subsequent dissociation. The same protocol followed for mouse retinas was used with up-scaled (2-4 times) reagent volumes.

Staining protocol for cell sorting

All incubation steps were performed on ice and all centrifugation steps were done at 0.4 rcf for 5' at 4°C. The reagent dilutions were prepared fresh before use and all antibodies diluted 1:250. The cell pellet obtained from the dissociation was first stained with eBioscience Fixable Viability Dye eFluor 780 (65-0865-14, Thermo Fisher) 1:1000 in PBS for 20'. The suspension was then centrifuged and the supernatant discarded. Cells were fixed in BD Phosflow Fix Buffer I (557870, BD Biosciences) for 20', followed by centrifugation and supernatant removal. The cell pellet was then resuspended in BD Phosflow Perm/Wash Buffer I (557885, BD Biosciences) according to the manufacturer instructions. Ten μl aliquots of the cell suspension were used as controls for the viability dye and the secondary antibody as well as for a fluorescence-minus-one (FMO) control. The remaining cell suspension was incubated with the primary antibody for Goα (MAB3073, Merck/Millipore) for 20'. After spinning down to remove the solution and washing once with BD Phosflow Perm/Wash Buffer I, the conjugated antibody for Pcp2•Alexa Fluor 647 (sc-137064 AF647, Santa Cruz) and the secondary antibody Alexa Fluor 488 (A-21121, Thermo Fisher) were added to the cells and incubated for 20'. The suspension was ready for cell sorting after a last centrifugation and wash step (Fig.4.4).

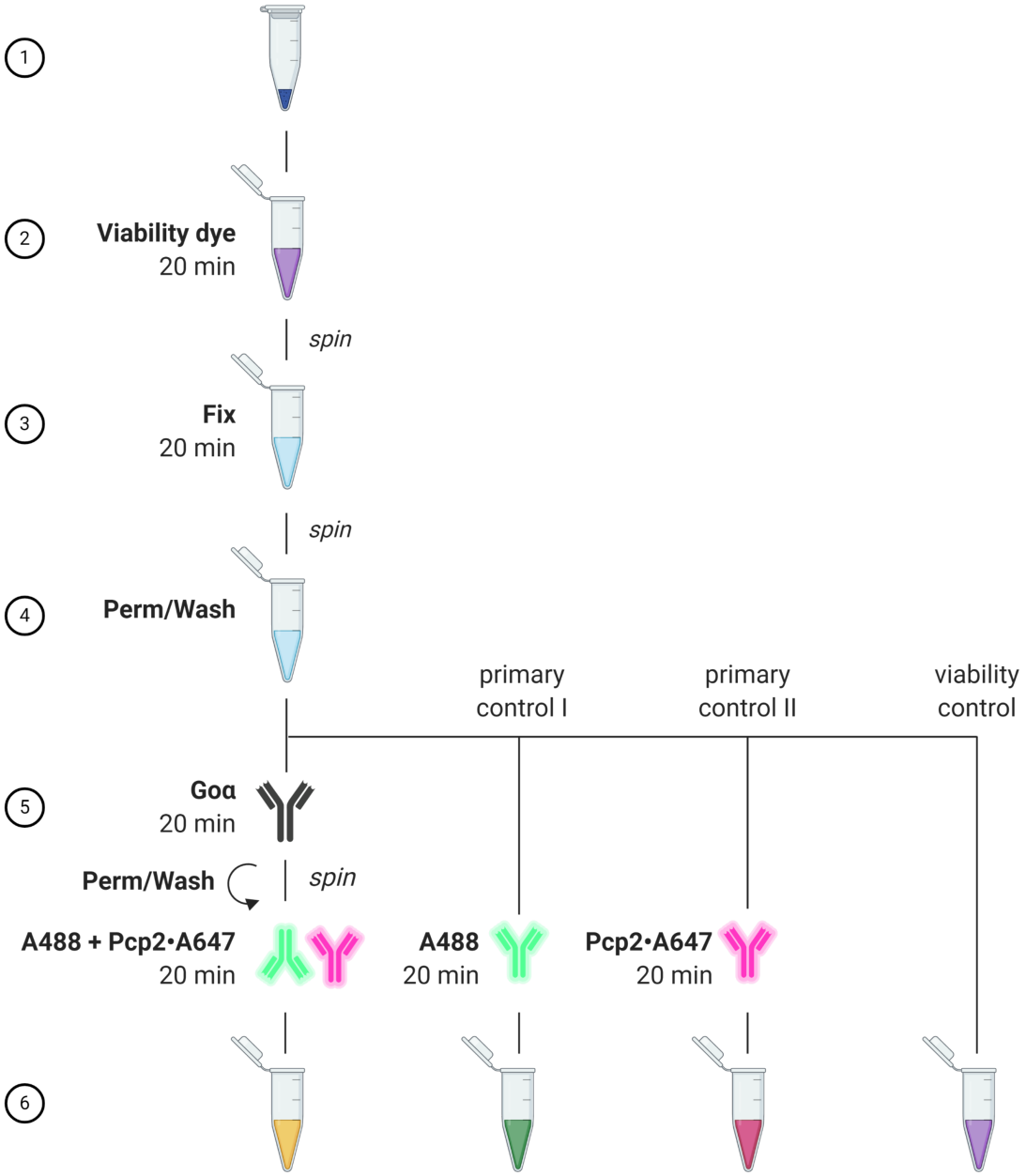

Figure 4.4: Schematic figure of stepwise staining protocol before FACS

Cell sorting

Cell sorting was performed using a FACS AriaFusion (Becton Dickinson) on BD FACSDiva software v8.0 using a 100 μm Nozzle at 20 psi. To this end, cells were filtered through a PluriStrainer Mini 40 μm (43-10040-60, PluriSelect) right before sorting. For downstream RNA/genomic DNA extraction, single, eFluor780$^-$ cells were sorted into PBS, according to their expression levels of Pcp2 and Goα as indicated. Data was analysed with FlowJo 10.6.1 for Mac OS X. FMO controls or controls without primary antibody were used as gating controls.

RNA sequencing

Total RNA was submitted to the Genomic Technologies Core Facility (GTCF) in the Faculty of Biology, Medicine and Health at the University of Manchester. Quality and integrity of the RNA samples were assessed using a 2200 TapeStation (Agilent Technologies) and then libraries generated using the TruSeq Stranded mRNA assay (Illumina, Inc.) according to the manufacturer instructions. Briefly, the total RNA was used as input material from which polyadenylated mRNA was purified using poly-T, oligo-attached, magnetic beads. The mRNA was then fragmented using divalent cations under elevated temperature and next reverse-transcribed into first strand cDNA using random primers. Second-strand cDNA was then synthesized using DNA Polymerase I and RNase H. Following a single 'A' base addition, adapters were ligated to the cDNA fragments, and the products were purified and enriched by PCR to create the final cDNA library. Adapter indices were used to multiplex libraries, which were pooled prior to cluster generation using a cBot instrument. The loaded flow-cell was then paired-end sequenced (76 + 76 cycles, plus indices) on an Illumina HiSeq4000 instrument. Finally, the output data was demultiplexed (allowing one mismatch) and BCL-to-Fastq conversion performed using Illumina's bcl2fastq software, version 2.20.0.422. The data have been deposited in the ArrayExpress database at EMBL-EBI (link) under accession number E-MTAB-9685.

Visualisation of RNAseq data

Data were sorted according to the number of reads and the first 50 genes in each sorted population were used as query for the Single Cell Portal of the Broad Institute (for mouse: link, for NHP: link) and the resulting heat map was sorted descending. Only the genes that found a match were also visualised, therefore for some query a number $\leq$50 is shown in the figures. For NHP data, the database specific for peripheral bipolar cells was selected prior to the analysis.

Detection of AAV genomes from sorted cells

AAV genomes were detected from gDNA extracted from sorted populations. To quantify viral concentration in the libraries and the cellular uptake of AAVs, DNA extracts were quantified using a ddPCR. Virus genome copy numbers were quantified using a TaqMan probe against the AAV2 *rep2* gene (FW: AAGTCCTCGGCCCAGATAGAC, RV: CAATCACGGCGCACATGT, TaqMan probe: FAMTATCGTCACCTCCAACA-BHQ1), and the mouse and NHP genome copies were quantified using a commercially available TaqMan Probe (ddPCR Gene Expression Assay: Rpp30, Mouse, Cat. No:10031255, BioRad) for mouse samples and one de-

signed against albumin for NHPs (FW: ATCTCTCCCTGGCATTGTTG, RV: ATCCAAACT-CATGGGAGCTG, TaqMan probe: HEX-TTGCAGATGTCAATGAAAGAGAACCGG-BHQ1). Reactions were processed according to the manufacturer instructions and were read in a QX200 Droplet Digital PCR System (BioRad).

4.5 Direct reprogramming *in vitro*

Primary retinal culture

Five P5-7 C57BL6/J pups were decapitated and their eyes enucleated into cold HBSS$^{-CaCl_2}$ with 1M HEPES. After sectioning the anterior part of the eye, the retina was carefully isolated from the posterior eye cup. All non-retinal tissue was removed and then retinas were pooled together in a new petri dish with fresh HBSS$^{-CaCl_2}$/HEPES. Each retina was sectioned into 8 smaller pieces and then mechanically triturated using a P1000 pipette followed by a P200 pipette until no more pieces were visible. The cell suspension was transferred into a T-75 flask or 24-well plate with warmed DMEM/F12 without L-glutamine (21331020, Thermo Fisher) medium supplemented with 1% Anti/Anti and 10% heat-inactivated FBS (56 °C). Medium was changed 7 days later and every 2 days after that.

Primary microglia culture from mouse cortex or retina

For both cortical or retinal microglia culture, the Papain Dissociation System was used as previously described (see:4.4). The microglia culturing medium consisted of DMEM/F12 without L-glutamine, 1% Pen/Strep, GlutaMAX supplement (35050038, Thermo Fisher), 1.5 μg/ml cholesterol (stock: 15 mg/ml in ethanol at RT)(C3045, Sigma Aldrich), 0.45% glucose (A2494001, Thermo Fisher), 10% heat-inactivated FBS and 1 ng/ml CSF2 (stock: 0.5 mg/ml in PBS/0.1% BSA)(315-03-50UG, Peprotech) added fresh each time. For the purpose of *in vitro* reprogramming after transduction, the FBS was omitted from the culture medium.

To obtain a retinal microglia culture, the retinas of 5 P10-11 pups were collected in HBSS$^{-CaCl_2}$ with 1M HEPES and dissociated according to [77] with small modification. The tissue was digested for only 10' at 37 °C without agitation and once the digestion was quenched, the cell suspension was mixed with warmed microglia medium (10 ml for T-75) and sieved through a 40 μm nylon cell strainer. The filtered cell suspension was then transferred to a T-75 and 50% of the media was changed after 7 days and twice a week after that. For pups younger than P7, the papain dissociation is not necessary and retinas can be processed via mechanical trituration

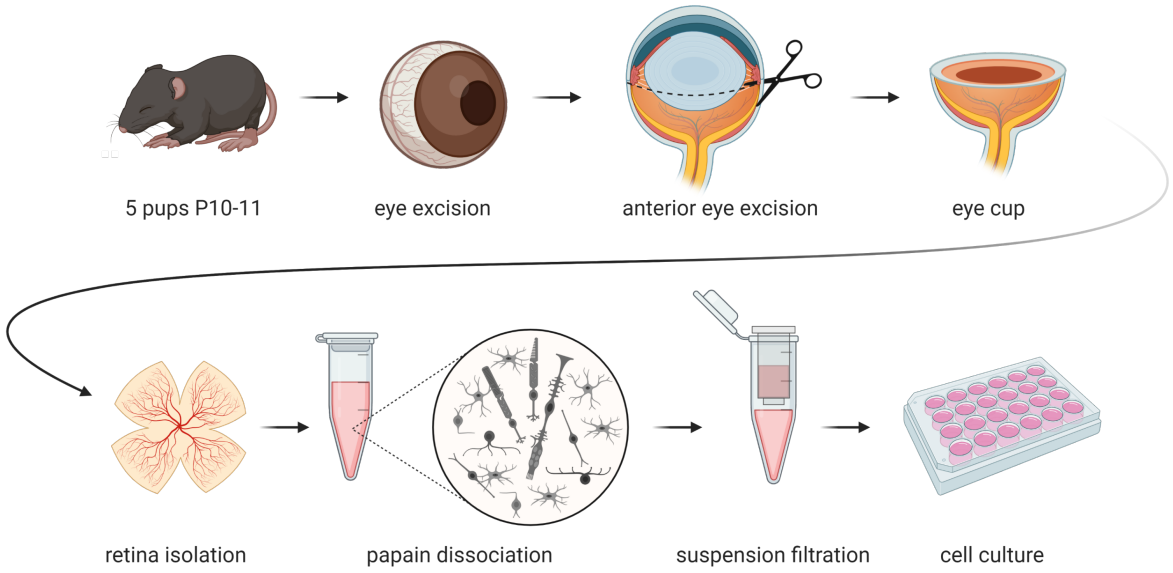

Figure 4.5: Schematic of retinal microglia culture preparation

as described above. To obtain a cortical microglia culture, the brains of pups aged P3-5 were collected in HBSS$^{-CaCl_2}$ with 1M HEPES and dissected so that the olfactory bulbs, hindbrain and cerebellum were removed. Subsequently the meninges (dura mater) were carefully removed and the cortex was isolated. The cortex was then dissected into smaller pieces and dissociated as described above, following the same culturing steps (Fig.5.39.A). Where cells were intended for imaging, pre-treated glass slides as in [78] were coated with poly-D-lysine (P6407, Sigma Aldrich) according to the manufacturer instructions and then used as substrate for the cell suspension.

Lentivirus vector production

HEK293T cells, cultured in high glucose DMEM (61965026, Thermo Fisher) supplemented with 10% FBS, 1% Anti/Anti, were plated on 6 x 15 cm plates and cultured until ≤80% confluence in 37 °C, 10% CO_2, 85-95% humidity. All subsequent steps were done in accordance with biosafetly level 2 regulations. To transfect 6 plates, the following reagents/volumes were used: 108 μg transgene plasmid DNA, 70 μg pMDL DNA, 32 μg pRSVRev DNA, 29 μg pMD2.G DNA, 6 μg 8 mg/ml Polybrene (107689, Sigma Aldrich), 600 μl 10mg/ml Dextran (95771, Fluka), 600 μl 2.5M $CaCl^2$, 6 ml 2xBBS and H_2O up to 6 ml.

The reagents were added in the following order: *(1)* H_2O, *(2)* plasmid DNA (transgene construct with 3rd generation lenti backbone 34999 from Addgene, lentivirus packaging plasmids: pMDL, mRSVRev, pMD2.G), *(3)* Polybrene, *(4)* Dextran, *(5)* dropwise $CaCl^2$ with frequent vortexing and *(6)* 2xBBS with vigorous vortexing. Two ml of the transfection solution were

added dropwise over each plate and the plates were incubated in 37 °C, 5% CO_2, 85-95% humidity. Media was changed after 24 hours and the plates were returned to 37 °C, 10% CO_2, 85-95% humidity. The lentivirus-containing media was harvested 24 and 48 hours later.

In the first harvest, the media was collected, filtered (0.45 μm, Nalgene 115 ml, 734-5002 VWR) and 30 ml/tube was transferred into open-top tubes (358126 Beckman & Coulter) inside metal ultracentrifugation screw-cap tubes fitting an SW28 rotor. The media was replenished over the culture plates and cells were further incubated. After balancing, the tubes were centrifuged at 19400 rpm for 2 hours at 17 °C. After discarding the supernatant and drying the tubes, the pellets were dissolved in 250 μl HBSS$^{-CaCl_2}$, collected in screw-cap 1.5 ml Eppendorf tubes and kept overnight at 4 °C.

In the second harvest, the same process as above was repeated. The collected supernatants were added over 2 ml 20% sucrose/H_2O in plastic open-top tubes (326819 Beckman & Coulter) inside metal ultracentrifugation screw-cap tubes fitting an SW55 rotor. After balancing with HBSS$^{-CaCl_2}$, the tubes were centrifuged at 21000 rpm for 2 hours at 17 °C. The supernatant was removed, tubes were dried and the pellets were dissolved in 70 μl HBSS$^{-CaCl_2}$ in a screw-cap 1.5 ml Eppendorf. The solution was vigorously shaken for 45' at 1400 rpm, aliquoted and stored in -80 °C until use.

Results

5.1 *in vitro* model for assessing novel vectors

An immortalised cell line, with high susceptibility to AAV transduction, i.e. HeLa [79], was used to generate an *in vitro* model that would indicate the potency of novel vectors aimed to treat monogenic retinal dystrophies. Specifically, this cell-based system should help discriminate between different capsid variants and elements of the transgene cassette, in order to facilitate the design of optimal vectors ahead of experiments *in vivo*. To assess whether the delivered transgene can be translated into a functional protein that alters cell behaviour, HeLa cells were genetically engineered to express proteins that assemble a binary reporter, using the piggyBac transposon system [80].

Concept overview

HeLa cells were transfected with the piggyBac transposon system, leading to the integration of two transgenes into the host cell genome, under the control of a tetracycline ON (TetON) system [81, 82]. As such, cells exposed to the tetracycline analogue doxycycline would express a fungal rhodopsin guanylyl cyclase (RhGC) from *Blastocladiella emersonii* [83] and an ultra-sensitive genetically encoded calcium indicator (GECI); either GCaMP6s [84], jRCaMP1a or jRCaMP1b [85]. It was hypothesised that these cells could be used as a test-bed for novel AAV vectors carrying a CNG channel subunit transgene, e.g. *Cnga3*, as the GECI would function as a binary reporter that indirectly indicates whether or not a functional CNG channel was formed. If transduced efficiently, the cells would express the proteins RhGC, CNG and GECI in their inactive states. In order to trigger the reporter cascade, the cells would be illuminated at the excitation wavelength (λex) of RhGC, i.e. 500-560 nm [83], that would lead to the formation of cGMP. The cGMP molecules would bind the closed CNG channel and open it, leading to the influx of cations, including Ca^{2+}. The incoming Ca^{2+} would then bind the GECI and when illuminated with its λex the GECI would emit a detectable fluorescent signal (λem), which would indirectly confirm the presence of a functional vector-borne CNG channel (Fig.5.1).

Validation of basic functions

In order to test whether the GECIs would detect Ca^{2+} under physiological conditions, the three stable cell lines were exposed to increasing concentrations of doxycycline, namely 0.25 μg/ml, 0.5 μg/ml, 1 μg/ml. After 48 hours incubation, the medium was replaced with $HBSS^{+CaCl_2}$ and the cells were imaged using the EVOS fluorescence microscope with filters for GFP (λex

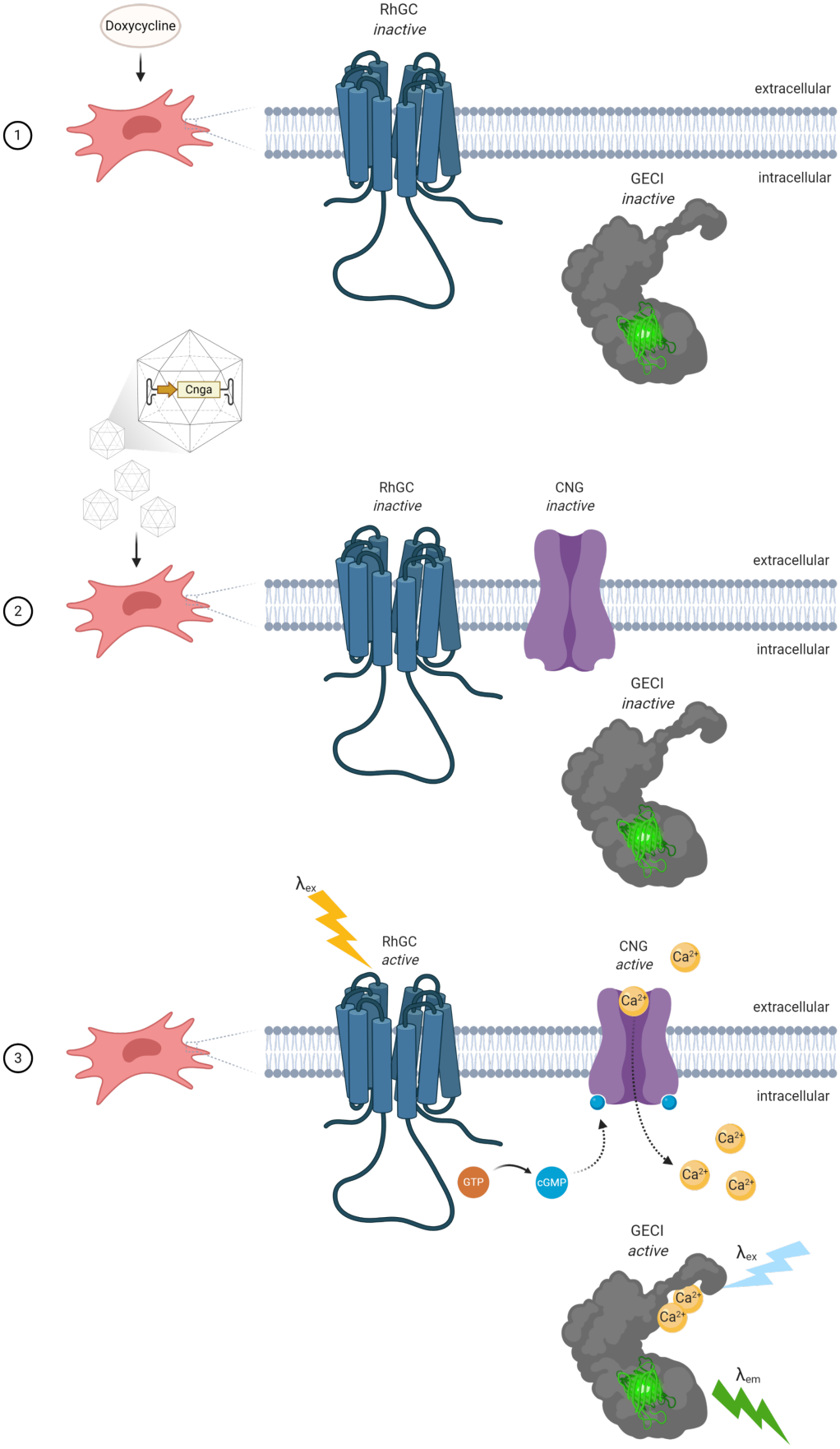

Figure 5.1: schematic overview of the *in vitro* system

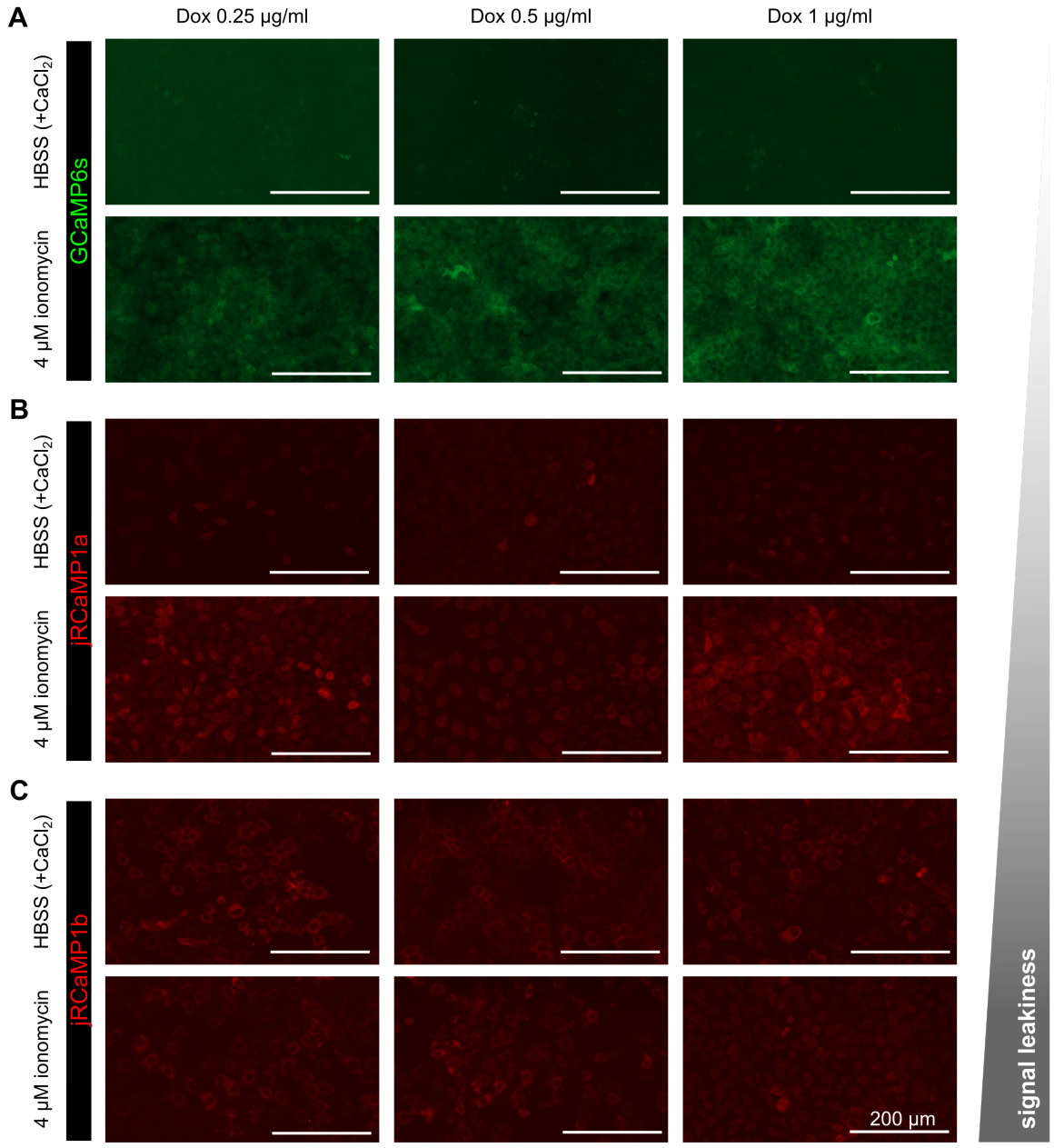

Figure 5.2: controls of doxycycline (Dox) treatment

488, λem 510) and Texas Red (λex 596, λem 615). The signal obtained was comparable for all doxycycline concentrations and it was therefore decided to treat cells with 0.5 μg/ml for all subsequent experiments. As a positive control of the maximum signal achieved when the GECIs are bound to Ca^{2+}, the cells were treated with 4 μM ionomycin for 5', which allowed the free influx of Ca^{2+} into the cell by disrupting their cell membrane. By comparing the fluorescent images before and after ionomycin treatment, it was evident that the signal from GCaMP6s (Fig.5.2.A) and jRCaMP1a (Fig.5.2.B) differed the most between conditions whereas that from jRCaMP1b (Fig.5.2.C) did not. As such, the GECI jRCaMP1b was deemed too leaky to use for AAV vector testing, as it would not be possible to distinguish between the background signal

and that obtained as a result of a vector-borne CNG channel.

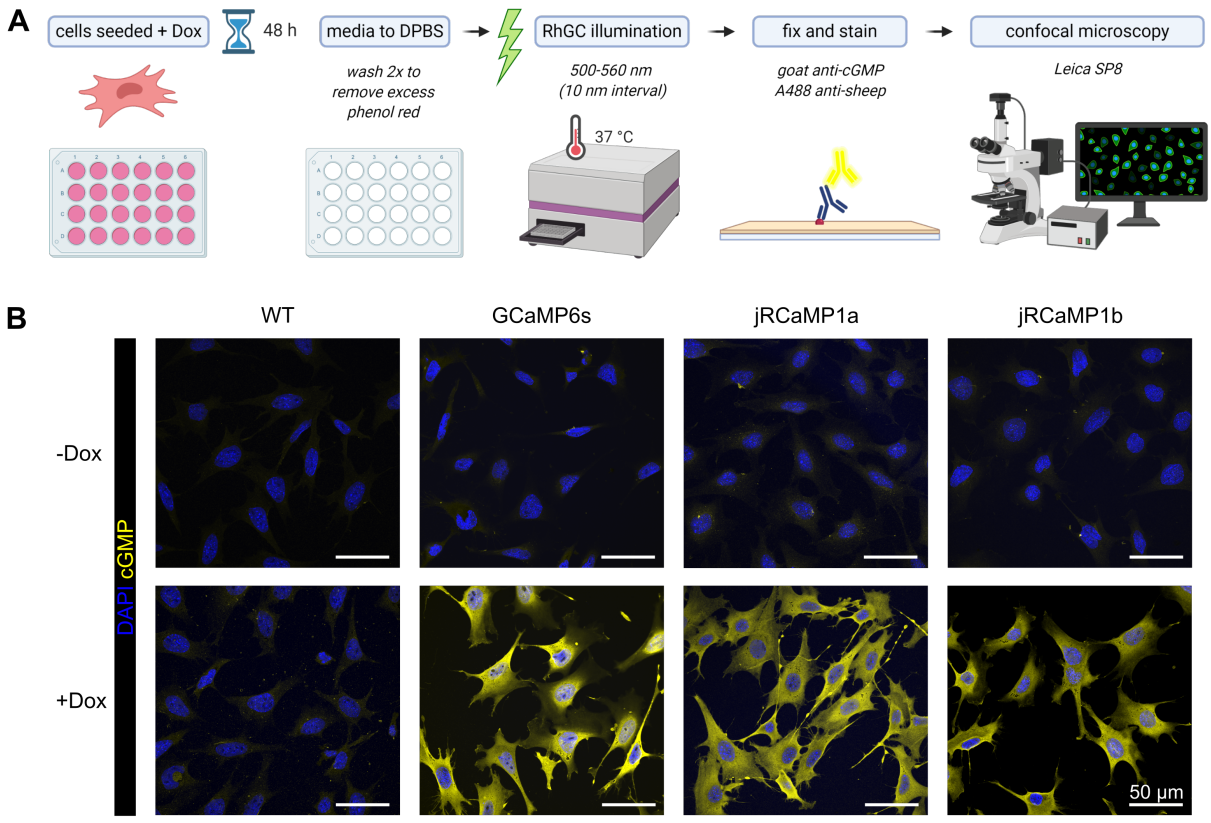

Figure 5.3: controls of RhGC activity

To validate the function of RhGC, all three stable cell lines were seeded in 24-well plates and incubated with 0.5 μg/ml doxycycline for 48 hours. Subsequently, the media was replaced with DPBS$^{-CaCl_2}$ and the cells were illuminated in a warmed (37°C) iD3 plate-reader at 500-560 nm in 10 nm intervals. The cells were then immediately fixed and stained for cGMP, and imaged using a confocal microscope (Fig.5.3.A). Imaging showed that only the engineered cells stained strongly for cGMP in the presence of doxycycline, whereas WT cells did not. Furthermore, none of the cell lines generated a detectable cGMP signal in the absence of doxycycline (Fig.5.3.B), thereby confirming that the TetON-dependent RhGC produces cGMP after illumination. The final validation was to test whether the individual constituents would work together in the presence of a CNG channel. Using a new piggyBac vector, the engineered HeLa cells containing RhGC-GCaMP6s or -jRCaMP1a were further modified to express the *Cnga1* gene under the same TetON system. This means that all three proteins would be expressed after exposing the cells to doxycycline and the cascade of functions after RhGC illumination could be tested (Fig.5.4). Newly engineered cells were seeded in a 24-well plate and after 48 hours of incubation with 0.5 μg/ml doxycycline the media was replaced with

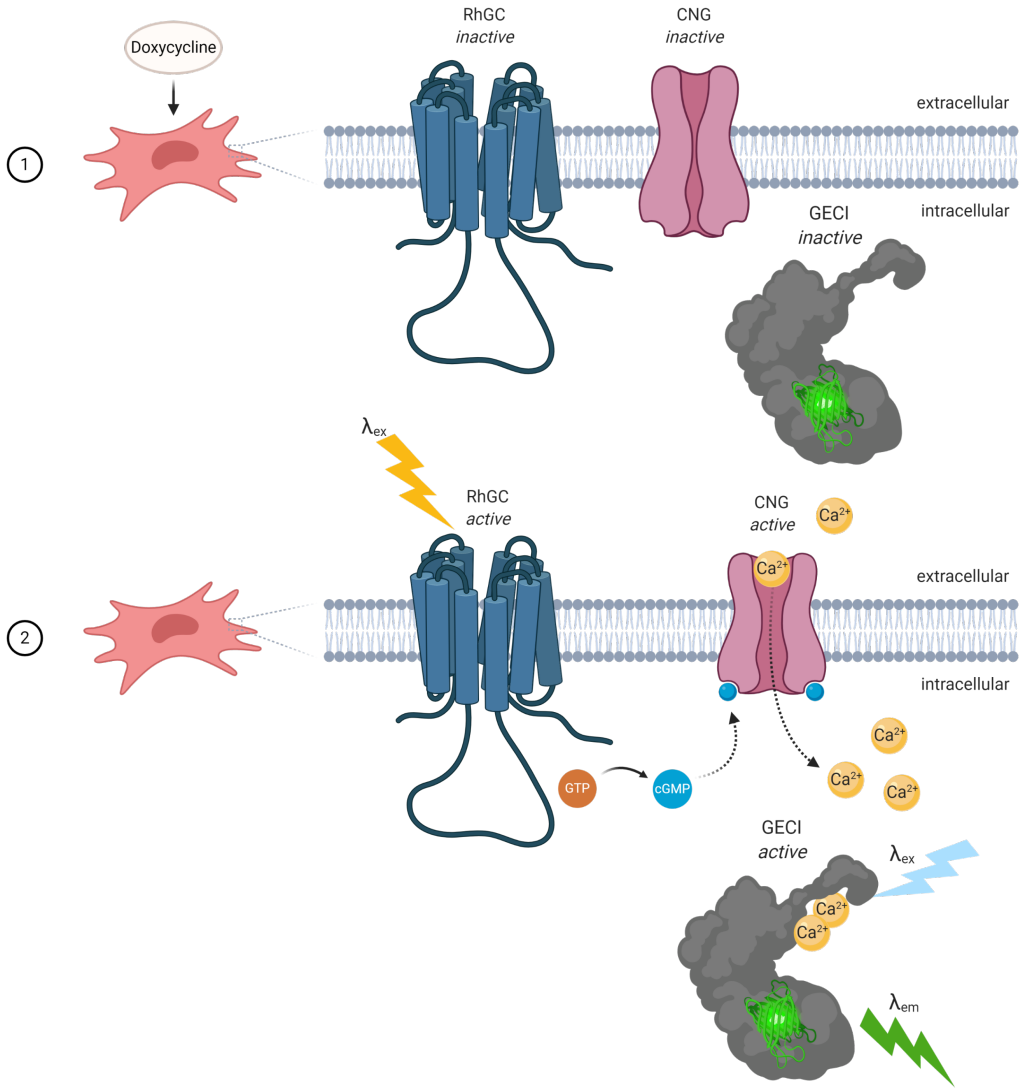

Figure 5.4: schematic of CNG control

DPBS$^{-CaCl_2}$. The cells were then illuminated in a warmed (37°C) iD3 plate-reader at 500-560 nm in 10 nm intervals to trigger cGMP formation. The baseline signal for GCaMP6s and jRCaMP1a was measured in the iD3 using the maximum sensitivity settings. Subsequently, the extracellular Ca^{2+} level was increased by replacing DPBS with HBSS$^{+CaCl_2}$ and the test signal for both GECIs was again measured in the iD3. Finally using the iD3 microinjector, ionomycin was added to the cells to a final 4 μM concentration and the maximum GECI signal was recorded in iD3 (Fig.5.5.A). Fluorescence imaging alongside the plate-reader experiment revealed that the cells expressing RhGC-GECI-Cnga1 gave a strong signal in the presence of extracellular Ca^{2+}, as oppose to RhGC-GECI alone (Fig.5.5.B). This was reflected in the iD3 signal quantification, where both GCaMP6s and jRCaMP1a signal significantly increased as a result of Cnga1-dependent Ca^{2+} influx (Fig.5.5.C).

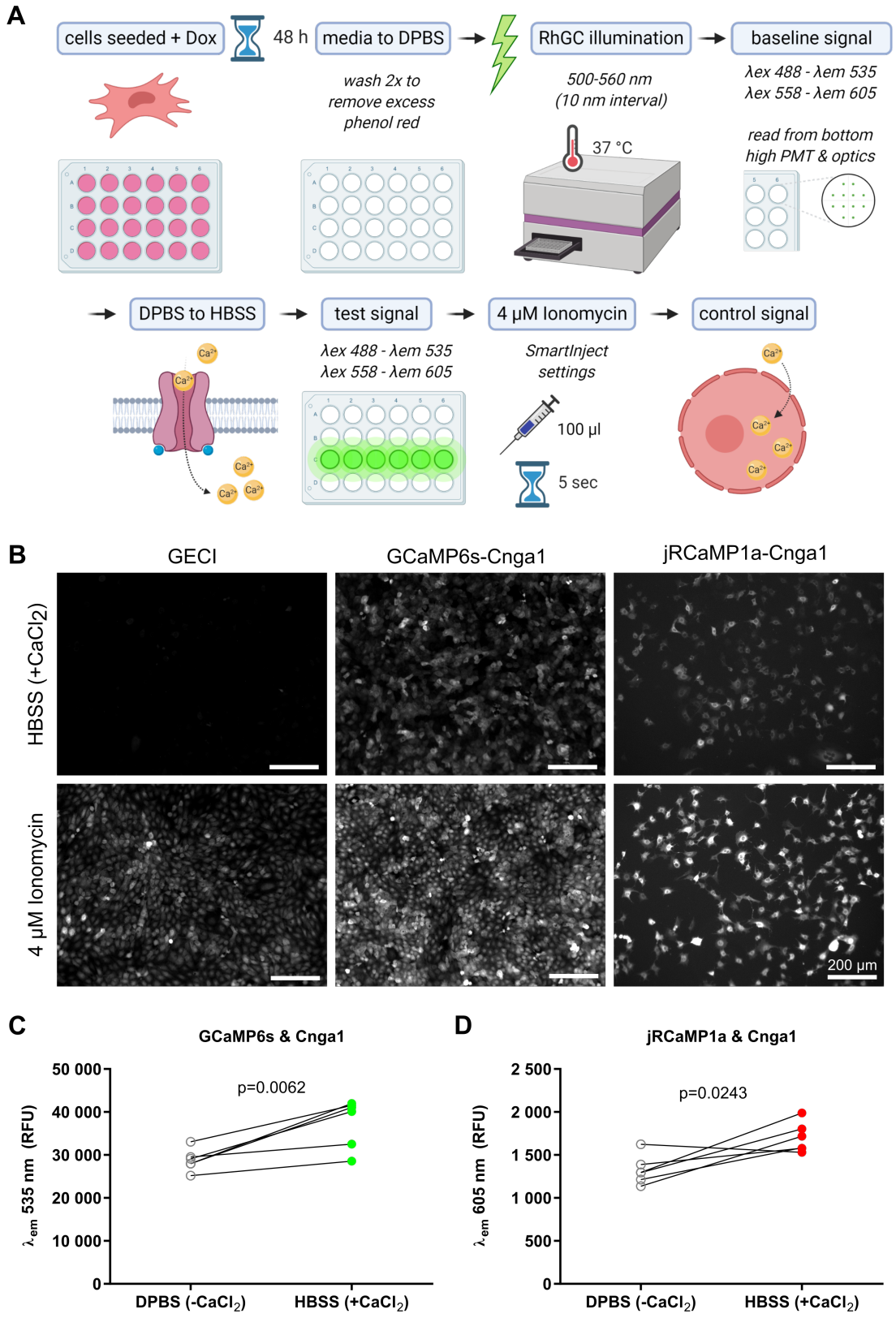

Figure 5.5: controls of CNG activity

Testing novel vectors with CNG subunit cargo

Once the *in vitro* system was validated, a novel rAAV vector was tested on both the RhGC-GCaMP6s and RhGC-jRCaMP1a HeLa cells. Four hours after seeding the cells in a 24-well plate with doxycycline, the cells were infected with AAVs (with DMSO catalyst) at an MOI 10^4 and 10^5 and incubated for 48 hours. As before, the media was replaced with DPBS$^{-CaCl_2}$ and the cells were illuminated in a warmed (37°C) iD3 plate-reader at 500-560 nm in 10 nm intervals to trigger cGMP formation. The baseline signal for GCaMP6s and jRCaMP1a was measured and then DPBS$^{-CaCl_2}$ was replaced with HBSS$^{+CaCl_2}$. The test signal for both GECIs was measured in the iD3 and finally ionomycin was added to the cells in order to record the maximum signal as positive control (Fig.5.6.A). The fluorescence images acquired alongside the plate-reader experiment showed there was detectable jRCaMP1a signal already in the untreated cells (Fig.5.6.B), which was somewhat anticipated from the results in Fig.5.2.B, and the signal remained the same for both MOIs (Fig.5.6.B). Instead, the GCaMP6s signal was restricted to the treated cells, showing no qualitative difference between the two MOIs (Fig.5.6.B). The quantification of jRCaMP1a revealed that although there was a higher signal in HBSS$^{+CaCl_2}$ compared to DPBS$^{-CaCl_2}$, this was not different than the positive control (Fig.5.6.C). This was in disagreement with the fluorescence imaging in the left panel of Fig.5.6.B, raising the question of inconsistency among signal detection methods. However, this was not the case for the GCaMP6s signal as the plate-reader quantification reflected the imaging. The signal gradually increased from baseline DPBS$^{-CaCl_2}$ to test HBSS$^{+CaCl_2}$ and then to the positive control (Fig.5.6.D), as seen in the right panel of Fig.5.6.B. With this, it was confirmed that the AAV vector had successfully delivered the *Cnga3* gene into the cells, which in turn produced a functional protein that lead to cGMP-dependent channel opening and Ca^{2+} influx.

After concluding that the RhGC-GCaMP6s HeLa cells were the most reliable across different methods, three Cnga3-carrying vectors were tested using the same experimental set-up as above. Vectors were either packaged with a hArr3-hCnga3 or mSWS-mCnga3 cassette and packaged in either AAV2.GL or AAV2.8 capsids. All vectors were used at an MOI of 10^5, which was sufficient to evoke the desired change in GCaMP6s signal intensity after changing the level of extracellular Ca^{2+} (Fig.5.7.A). The quantitative results confirmed the presence of a functional vector-borne CNG channel after cells were transduced with AAV2.GL/mSWS-mCnga3 (Fig.5.7.B) and AAV2.GL/hArr3-hCnga3 (Fig.5.7.C). This was not the case for AAV2.8/hArr3-hCnga3 (Fig.5.7.D), which more likely reflects the limitations of the capsid rather than the cargo.

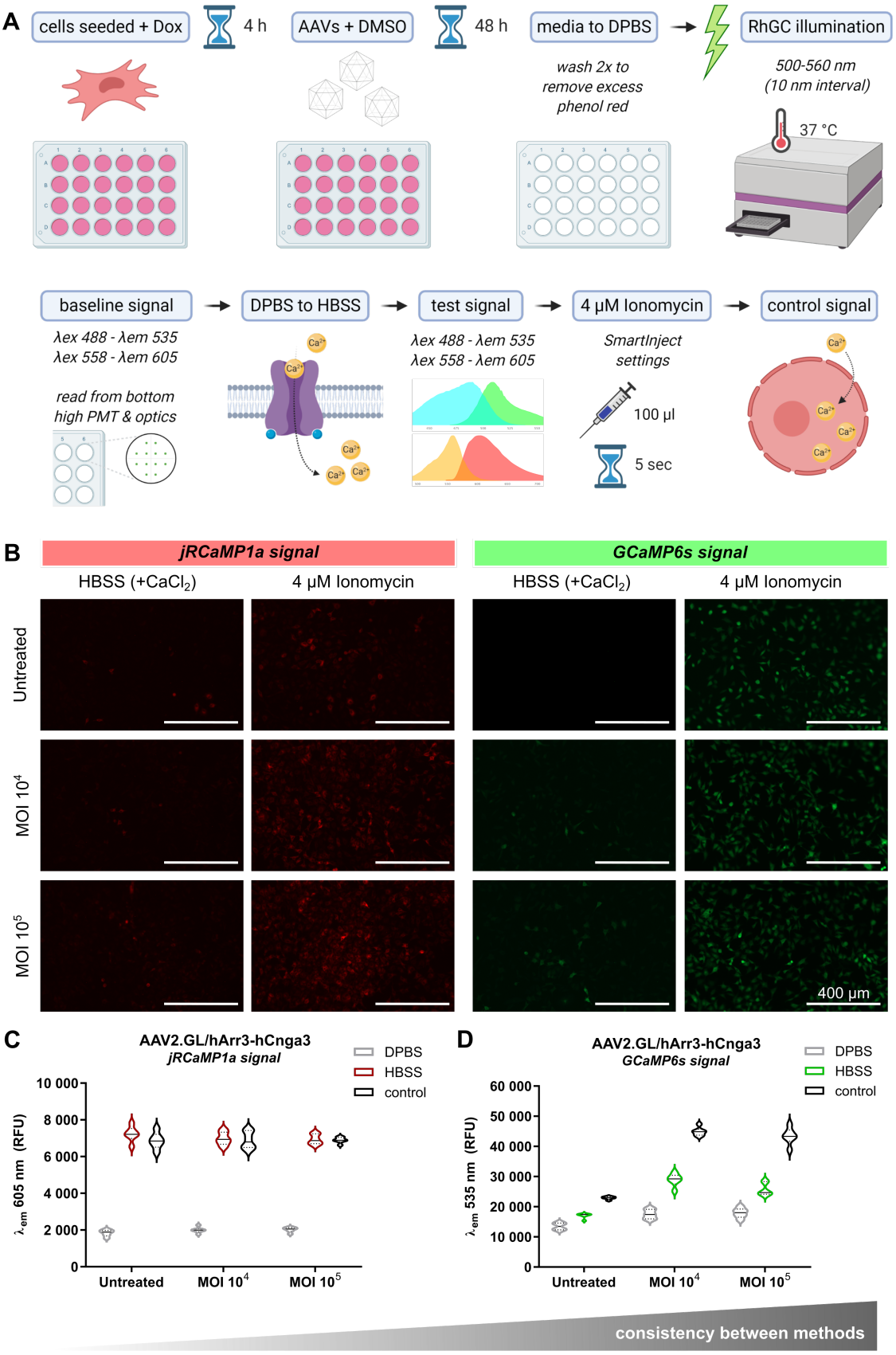

Figure 5.6: testing a novel Cnga3 vector

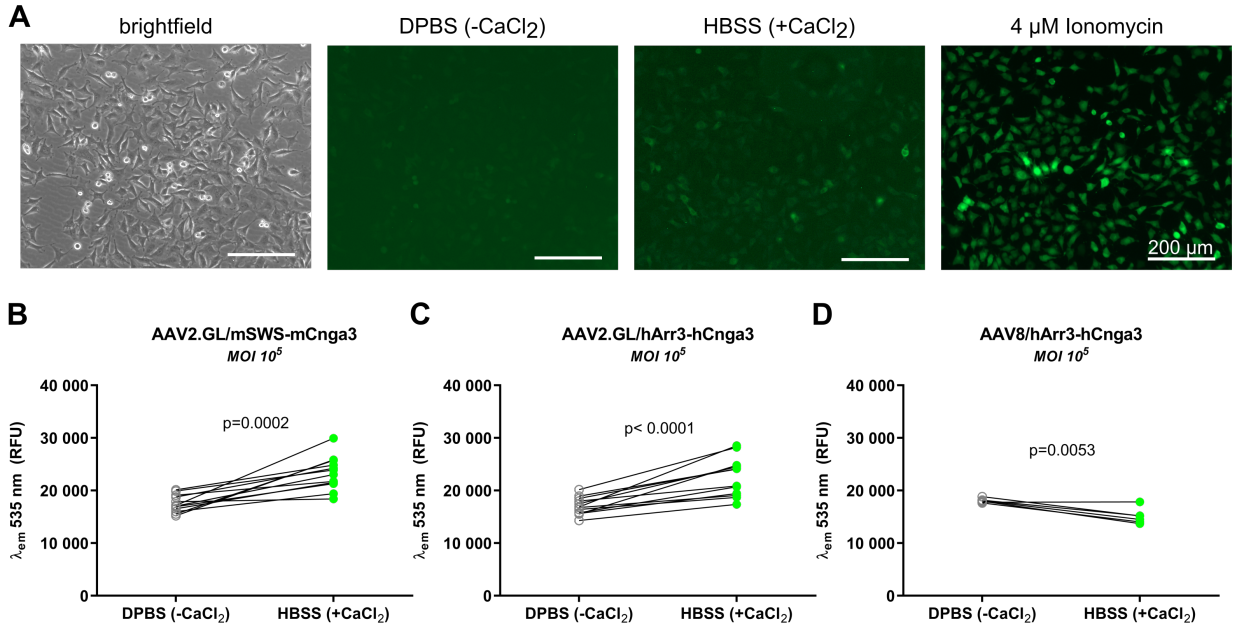

Figure 5.7: testing different Cnga3 vectors

Testing novel vectors with PDE subunit cargo

To further challenge the usability of this *in vitro* model, the co-delivery of two AAV vectors with antagonising properties was tested using the RhGC-GCaMP6s HeLa cells. Vectors carrying the *Cnga3* or *Pde6a* genes were applied simultaneously and it was hypothesised that if both proteins were expressed, the cGMP required for CNG-dependent Ca^{2+} influx would become hydrolysed by the PDE, leading to an absent or decreased GCaMP6s signal (Fig.5.8.A). Indeed, representative fluorescent images showed that the minimal baseline GCaMP6s signal was diminished after increasing the extracellular Ca^{2+} levels (Fig.5.8.B), although this is more likely to be a function of time and the gradual cGMP hydrolysis by PDE, rather than the change in extracellular solution. This phenomenon was reflected also in the iD3 signal quantification showing that all three vector combinations of simultaneous *Cnga3* and *Pde6a* delivery resulted in significantly decreased GCaMP6s signal (Fig.5.8.C-E).

With this it was established that novel vectors with both CNG- and PDE-subunit cargo could be assessed using this non-ratiometric *in vitro* system.

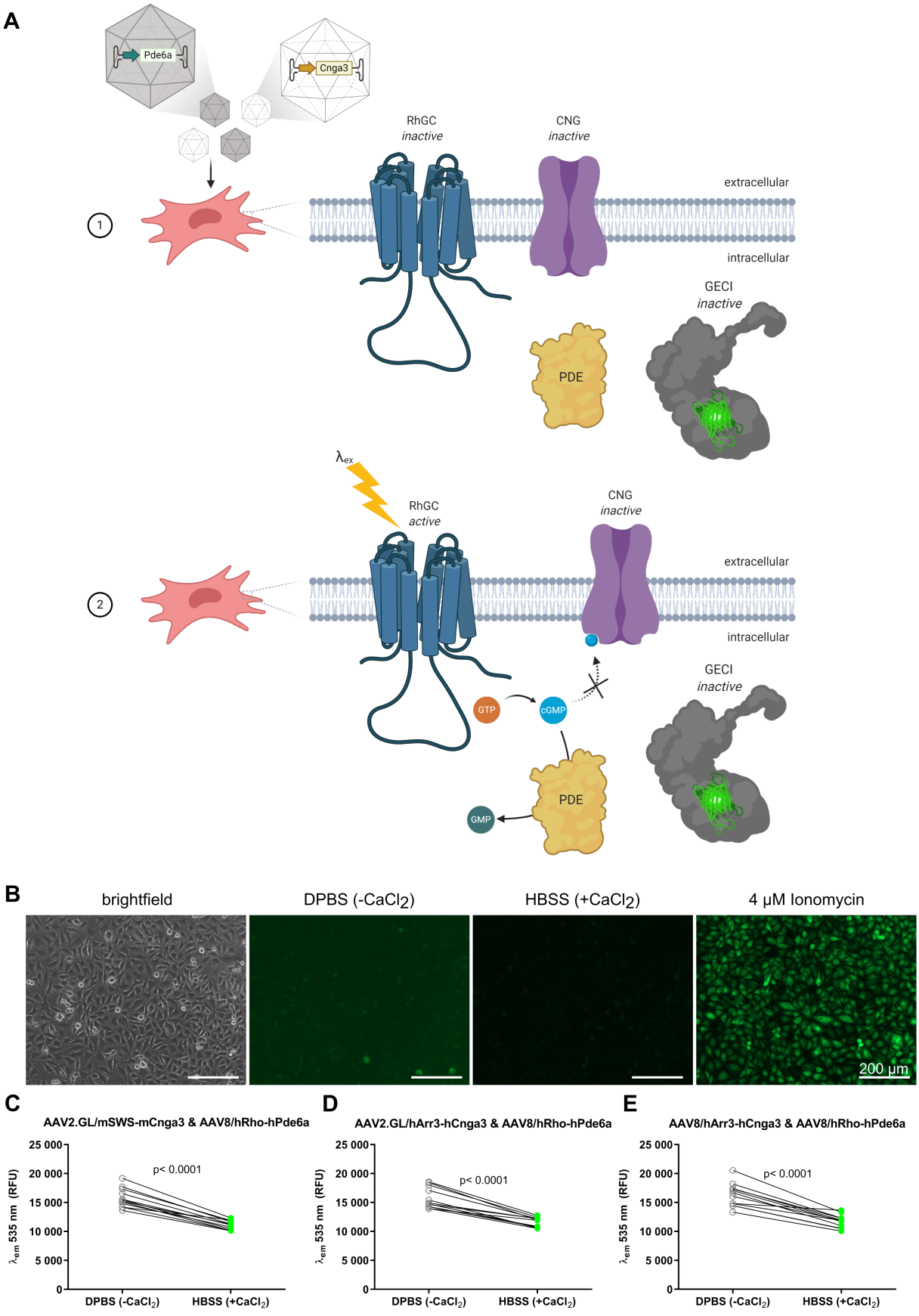

Figure 5.8: testing Pde6a vector

5.2 Directed evolution of novel vectors for intravitreal delivery

Gene therapy using recombinant adeno-associated virus (rAAV) vectors to treat blinding retinal dystrophies has become clinical reality. Therapeutically impactful targeting of photoreceptors still relies on subretinal vector delivery, which detaches the retina and harbours substantial risks of collateral damage, often without achieving widespread photoreceptor transduction. As such, the development of novel engineered rAAV vectors that enable efficient targeting of photoreceptors via less invasive intravitreal administration remains an unmet clinical need. To address this, novel AAVs were engineered using directed evolution [86].

Library screening in mice

A peptide-display library using the AAV2 capsid as scaffold was generated (Fig.5.9.A), where a random 7-mer amino acid sequence was inserted between N587 and R588 (Fig.5.9.B). The resulting library with approximately 5 million unique variants [87, 88] was counter-selected for wildtype or enhanced heparan sulphate proteoglycan (HSPG) binding using heparin affinity chromatography and then injected intravenously into adult C57BL6/J mice (2-months old) with $>$ 8E10 total viral genomes (vg) of the initial library (library 1) per mouse. At only 24 hours after injection, animals were sacrificed, their retinas harvested, and DNA was isolated. The presence of viral genomes in retinal cells was assessed via qPCR using isolated gDNA, and thus confirmed the successful crossing of extracellular barriers. Subsequently, AAV genomes were amplified and served as template for sub-library production (library 2).

This procedure was repeated in the second selection round with intravenous injection of $>$ 5E11 vg of the first sub-library (library 2). In the second round, DNA from whole retina and retinal cell nuclei was analysed, revealing that capsid variants not only reached the target cells and were internalised, but that they were also transported into the nucleus. The second sub-library (library 3) was generated as before, and in the third selection round 5E11 vg of library 3 were injected intravenously in both adult C57BL6/J and *RG-eGFP* mice (2-months old). 24 hours after injection, rod photoreceptors were isolated by magnetic-activated cell sorting (MACS) and cone photoreceptors by fluorescence-activated cell sorting (FACS). DNA from AAV variants that reached rods and/or cones was extracted and NGS was performed to identify the capsid variants that targeted rods and cones most efficiently (Fig.5.9.C).

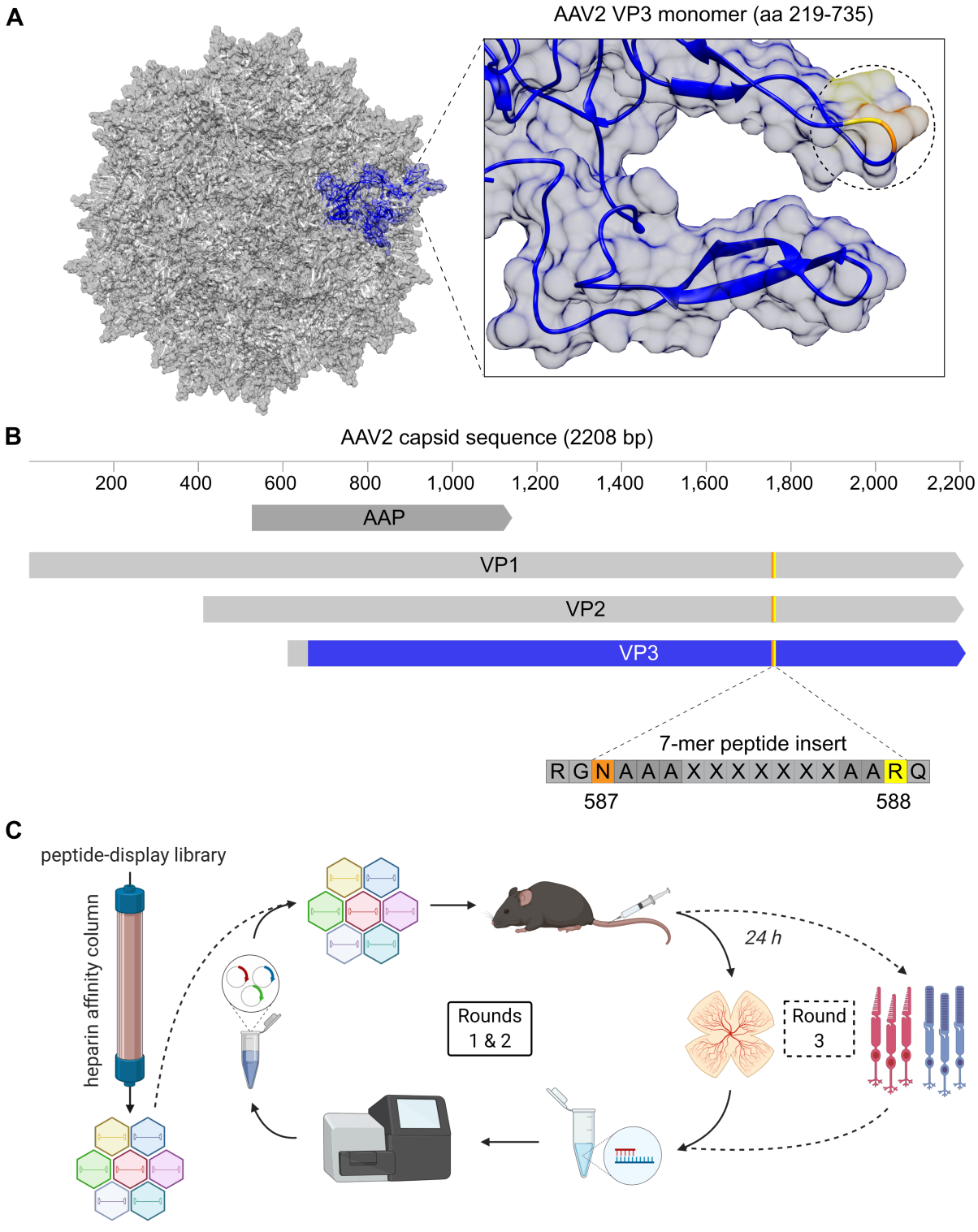

Figure 5.9: Schematic of capsid evolution strategy

Side-by-side comparison of AAV candidates

Valid NGS reads from whole retina, rods and cones were compared, where valid means only those containing the sequence encoding for AAA $X_1X_2X_3X_4X_5X_6X_7$ AA, where X indicates

random amino acids (Fig.5.10.A). Sequences detected in rods and cones but not in the whole retina, were excluded. Furthermore, the ratio of valid reads in cones or rods over the whole retina was calculated, to select for those enriched in photoreceptors, favouring the cones. The top five most frequent capsid variants were AAV2.GL, AAV2.NN, AAV2.GA, AAV2.NS and AAV2.SS (Fig.5.10.A), which were then vectorised and tested *in vivo* in mice (Fig.5.10.B).

A

Abbreviation	*Capsid variant peptide insert*	*Enrichment factor rods/whole retina*	*Enrichment factor cones/whole retina*
AAV2.GL	AAA GLSPPTR AA	n/d	36
AAV2.NN	AAA NNPTPSR AA	137	n/d
AAV2.GA	AAA GAHRSDS AA	n/d	28
AAV2.NS	AAA NSRPAAA AA	n/d	4
AAV2.SS	AAA SSPGLPR AA	n/d	36

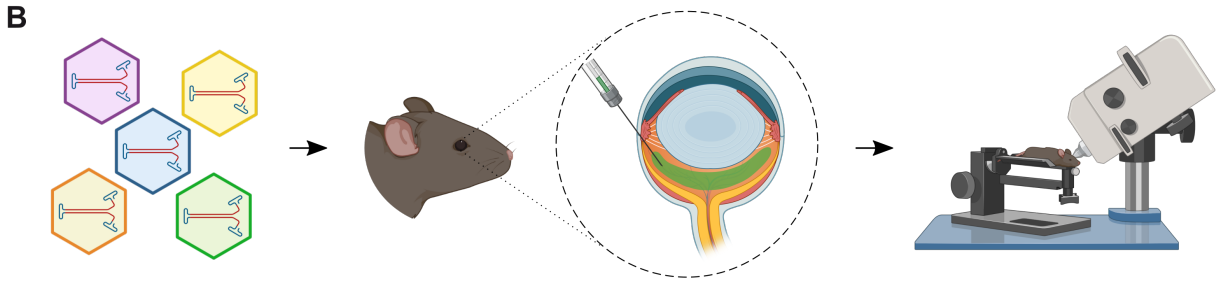

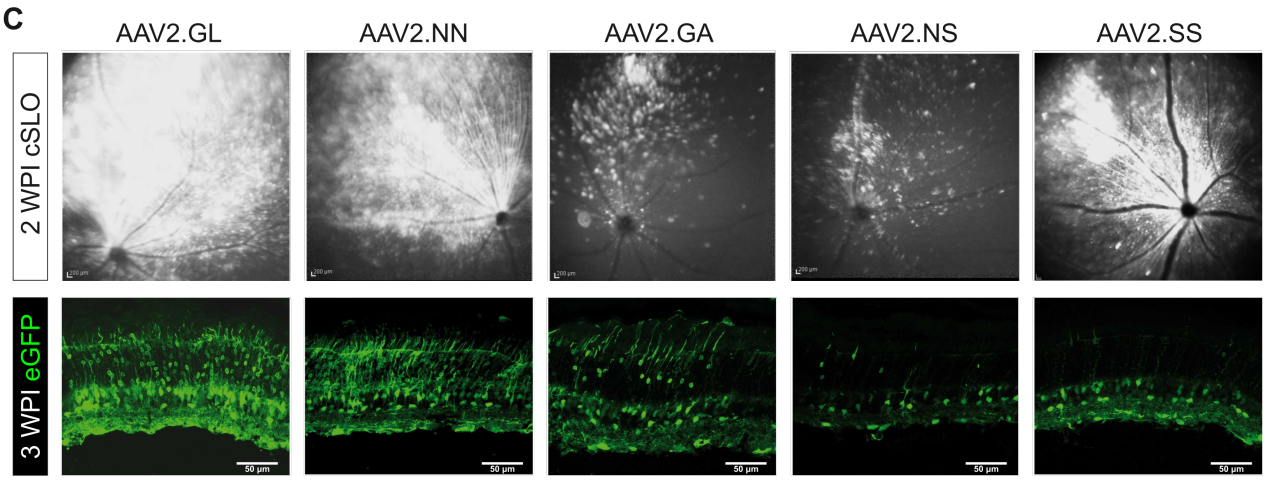

Figure 5.10: Candidate selection and evaluation (images courtesy of Dr. Christian Schön)

The vectors displayed the selected peptides and encoded a self-complementary (sc) AAV vector genome encoding for enhanced green fluorescent protein (eGFP) as marker gene controlled by the ubiquitous cytomegalovirus (CMV) promoter. To interrogate their transduction capacity in the retina, 2E9 vg of the 5 vectorised candidates were injected intravitreally in 2-month old C57BL6/J mice (n = 2-4). At 2 weeks post injection (WPI), *in vivo* cSLO imaging was performed to document eGFP expression (Fig.5.10.C upper panel), which revealed success-

ful transduction by all five capsid variants in the mouse retina. Using constant detector gain to observe comparable levels of fluorescence in the cSLO it was shown that AAV2.GL, AAV2.NN and AAV2.SS achieved the brightest eGFP fluorescence by 2 WPI. The subsequent histological analysis of retinal cryosections at 3 WPI (Fig.5.10.C lower panel) determined AAV2.GL and AAV2.NN as the top candidates for further analysis. Note that in all subsequent figures AAV2.GL will be abbreviated to GL and AAV2.NN to NN.

in silico modelling and *in vitro* characterisation of novel capsids

To obtain some insight into the possible structural changes induced by the peptide insertions, AAV2.GL and AAV2.NN were modelled *in silico* based on the structure of AAV2 (PDB 6IH9) (Fig.5.11.A,C) using Robetta [89, 90].The resulting models were then aligned to the reported structure of parental AAV2 (PDB 6IH9) (Fig.5.11.B,D). This revealed striking similarities between AAV2.GL and AAV2.NN, as well as clear differences of both novel capsids when compared to AAV2. Specifically, this modelling data suggest that the loop extension caused by the peptide insertion in AAV2.GL and AAV2.NN is oriented towards the opposite hypervariable loop.

The novel capsids were also evaluated with respect to yield, physical properties and host-vector interactions. Multiple independent production cycles showed that both AAV2.GL and AAV2.NN are produced to the same titre as parental AAV2 and state-of-art AAV2.7m8 [55], whether harvested from cell supernatant (Fig.5.12.A) or cell pellet (Fig.5.12.B). As previously mentioned, the library was counter-selected for variants with wildtype or strong heparin affinity (analogue for HSPG) using standard heparin affinity chromatography. Interestingly however, position 7 of the unique peptide insert for both AAV2.GL and AAV2.NN has an arginine residue. This arginine residue, together with the two alanine linker residues and with R588 of the parental AAV2 sequence, forms a potential HSPG binding motif [88, 91]. To determine the HSPG binding ability of the novel capsids, a heparin affinity chromatography with gradient elution was performed. As suggested by the sequence, both AAV2.GL and AAV2.NN bind to heparin but with lower affinity than AAV2 as they elute at a lower salt concentration, i.e. earlier from the column (Fig.5.12.C). In addition to virion capturing by surface proteoglycans, inefficient uncoating i.e. the release of vector genomes into the nucleus has been proposed as a transduction barrier [92, 69]. As an indirect measure of uncoating, a thermal stability assay was performed [92, 69] showing that most AAV2 particles are still intact at 63°C (step 7), while AAV2.GL and AAV2.NN particles were already disassembled at this temperature (Fig.5.12.D) suggesting their genome is released under less harsh conditions. Finally, the nuclear transport

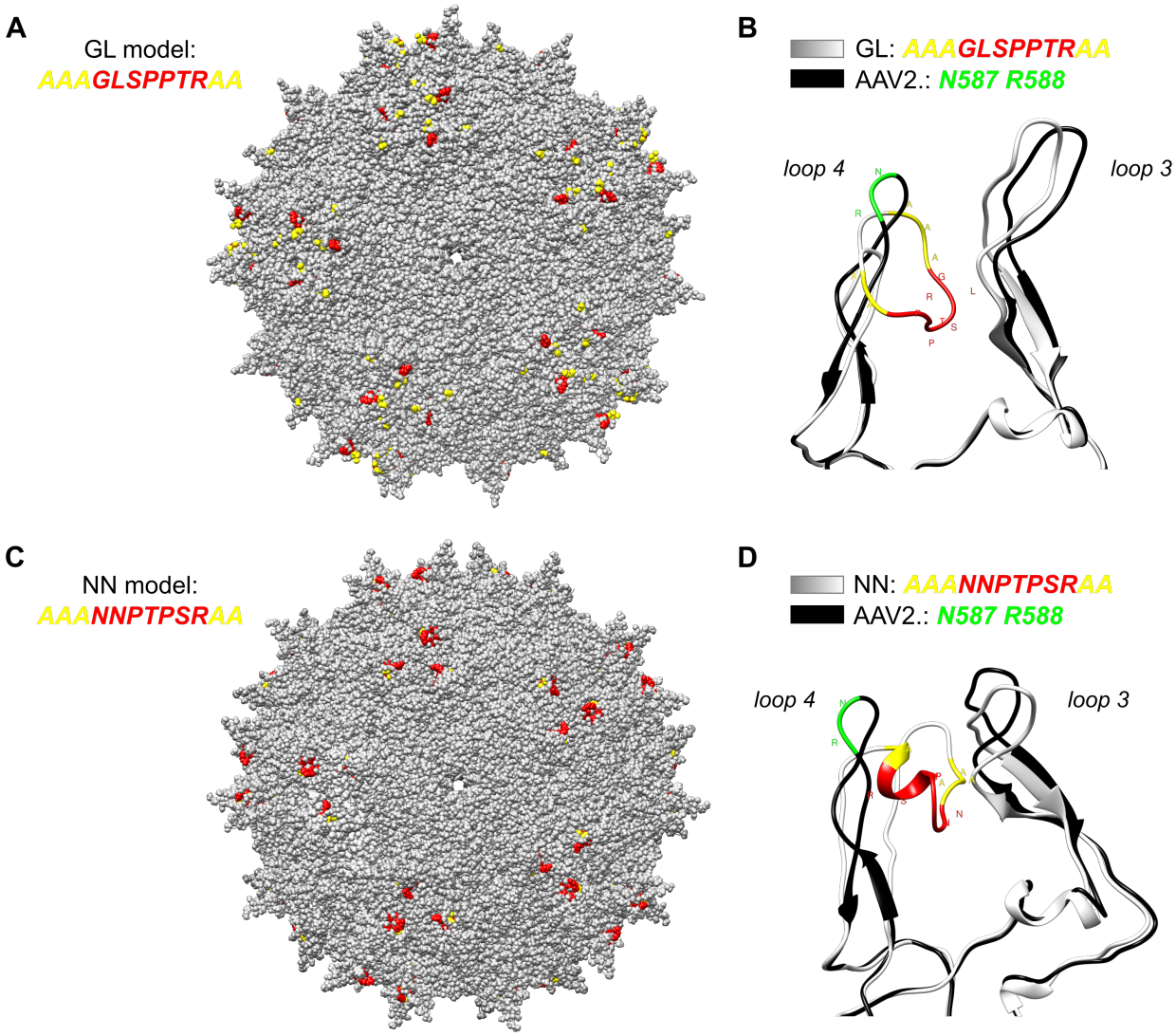

Figure 5.11: *in silico* models of novel capsids

efficiency of the novel capsids was evaluated. Both localised within the nucleus with 2-fold (AAV2.NN) and 4-fold (AAV2.GL) higher efficiency compared to AAV2 (Fig.5.12.E). The peptide insertions not only mediate cell transduction but also impact the structure of the second highest peak (Fig.5.11.B,D), thereby affecting recognition by pre-existing neutralising antibodies. To test this, a neutralisation assay with human serum was performed (Fig.5.12.F). Both novel capsids, particularly AAV2.GL, were less sensitive to neutralisation compared to AAV2; a promising feature in light of the neutralising antibody prevalence in the human population.

Novel capsids compared to AAV2 and AAV2.7m8 in mice

To evaluate the performance of AAV2.GL and AAV2.NN in the retina, they were compared to the parental AAV2 and state-of-art AAV2.7m8 [93]. A sc/CMV-eGFP cassette was packaged and a total of 2E9 vg of each vector were injected intravitreally in 2-month-old wildtype mice

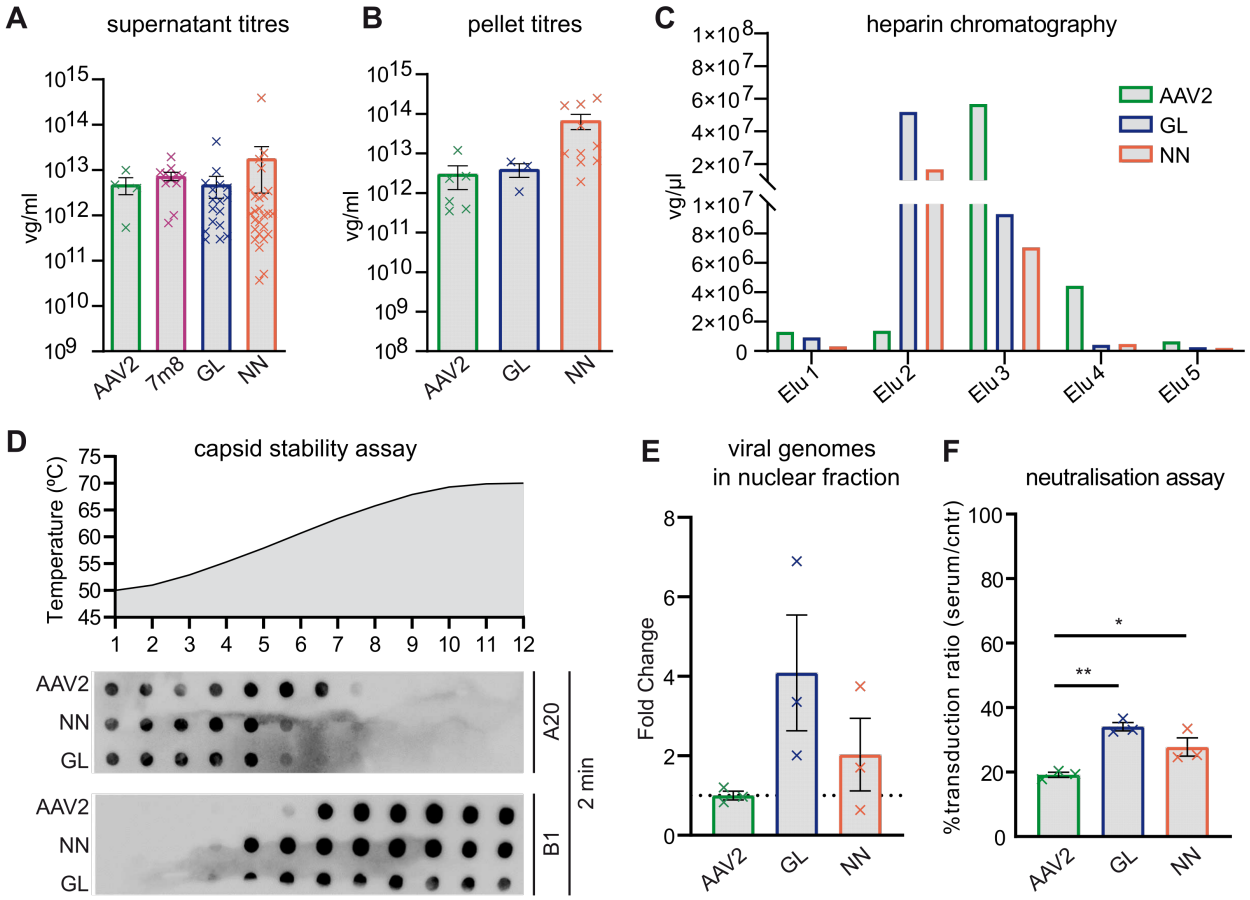

Figure 5.12: *in vitro* evaluation of novel capsids; mean±SEM (data courtesy of Dr. Axel Rossi and Dr. Nadja Meumann)

(n = 3-4)(Fig.5.13.A). Their fundus fluorescence was monitored weekly via cSLO imaging, which showed that animals treated with AAV2 had a scattered and weak eGFP expression by 1 WPI that became gradually more intense. In contrast, AAV2.7m8, AAV2.GL and AAV2.NN treated eyes had a strong eGFP signal already by 1 WPI, which expanded to most of the mouse fundus by 2 WPI (Fig.5.13.B). At 3 WPI all mice were euthanized and retinas were processed for IHC. Confocal scans of retinal cross-sections revealed that AAV2-treated eyes had only limited eGFP signal mainly at the GCL, with only sparse eGFP-positive cells in the INL or ONL. Engineered capsids AAV2.7m8, AAV2.GL and AAV2.NN, however, achieved a strong eGFP signal that spanned throughout all retinal layers (Fig.5.13.C). Notably, eGFP expression from AAV2.GL and AAV2.NN was stronger in a larger portion of the mouse retina compared to AAV2.7m8 (Fig.5.13.D) and co-localised with the photoreceptor-specific marker recoverin (Fig.5.13.E). Furthermore, qPCR analysis of eGFP expression from mouse retinal samples (n≥3) revealed a 13.4-fold increase (p=0.0086) in transcript levels for AAV2.GL and 12.1-fold increase (p=0.0211) for AAV2.NN compared to AAV2. While AAV2.7m8 had a 5.5-

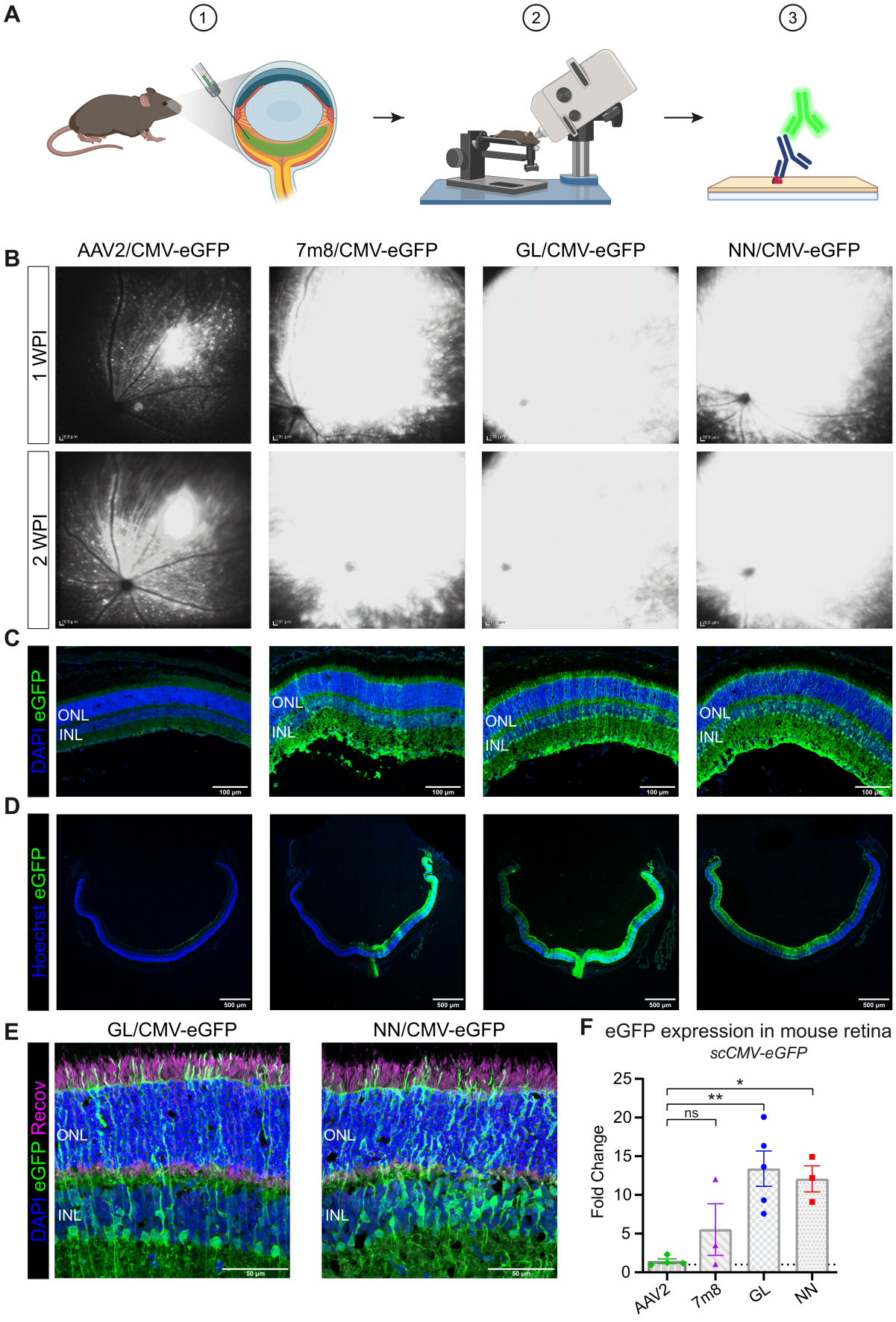

Figure 5.13: Intravitreal mouse study with ubiquitous promoter; mean±SEM

fold increase in eGFP transcripts, this was not significantly different from AAV2 (p=0.2295) (Fig.5.13.F). To compare the photoreceptor-specific transduction efficiency among capsids, the previous study was repeated and 8E9 vg of AAV vectors carrying a single stranded (ss) eGFP cassette under the control of a human rhodopsin (hRho) promoter were intravitreally injected.

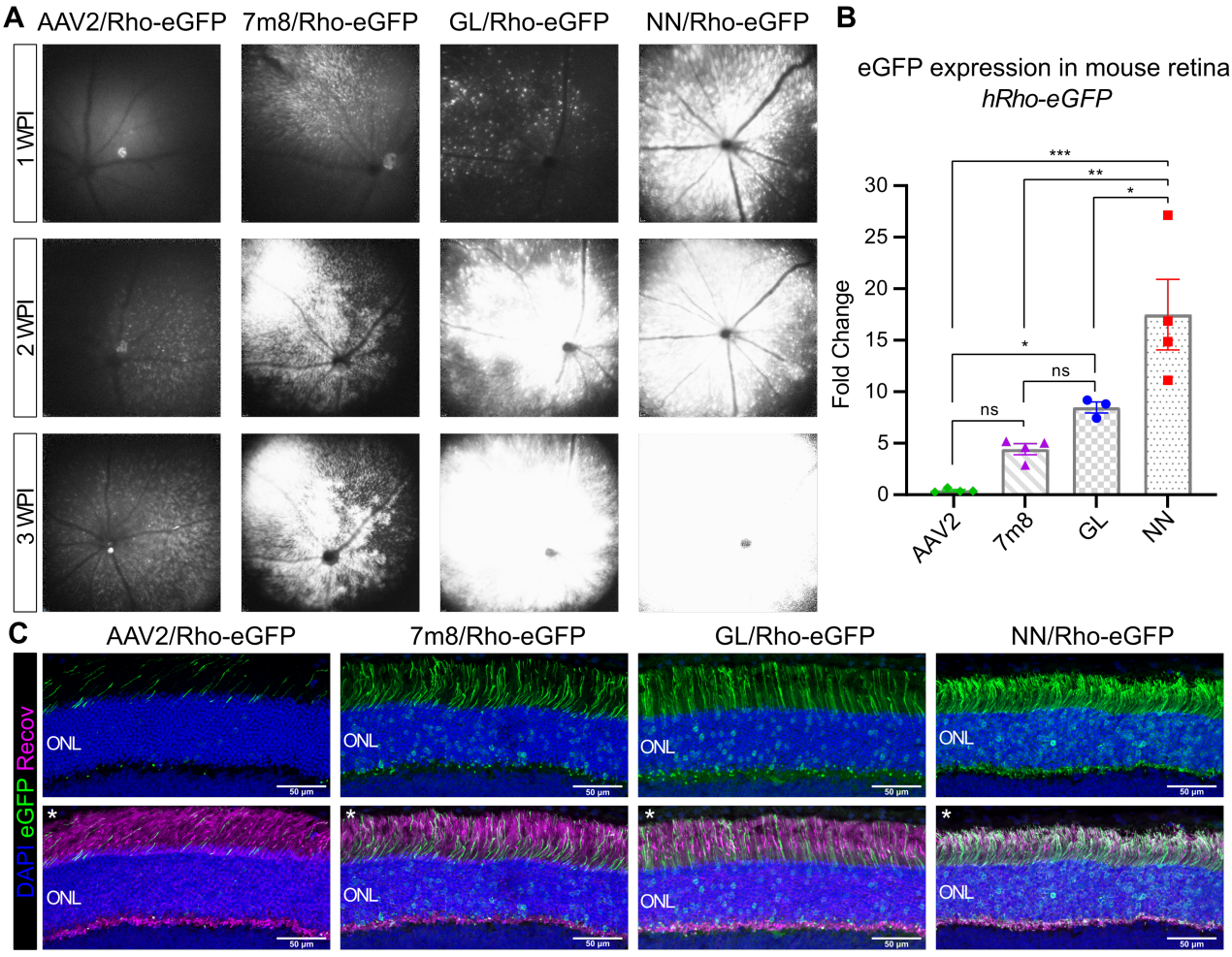

Figure 5.14: Intravitreal mouse study with photoreceptor-specific promoter; mean±SEM

The fundus eGFP signal was again monitored via in life cSLO over a 3 week period (Fig.5.14.A). All three engineered AAV variants outperformed AAV2, with AAV2.NN showing the strongest signal. Specifically, AAV2.NN produced a faster and brighter eGFP signal that was already present at 1 WPI, in line with the rod-favouring nature of this novel capsid (Fig.5.10.A). qPCR quantification at 3 WPI confirmed this finding and showed a significantly higher level of eGFP transcripts in retinas injected with AAV2.NN compared to AAV2 (p=0.0002), AAV2.7m8 (p=0.0018) and AAV2.GL (p=0.0313). AAV2.GL also achieved significantly higher transcript levels than AAV2 (p=0.0427) but only a trending increase compared to AAV2.7m8 (p=0.2725). A trending increase in eGFP transcripts was also recorded in AAV2.7m8-treated retinas compared to AAV2 (p=0.2725) (Fig.5.14.B). Confocal scans of reti-

nal cross-sections further confirmed the superiority of AAV2.NN over AAV2 and AAV2.7m8 in targeting photoreceptors in the ONL, while AAV2.GL performed at least as well as AAV2.7m8 (Fig.5.14.C).

Novel vectors achieve widespread transduction in dog retina

To test whether the novel variants are functional in species which better approximate human eye size and physiology, five 10-month-old beagles received a single intravitreal injection containing 2E11 total vg of sc/CMV-eGFP packaged with AAV2, AAV2.GL or AAV2.NN capsids and monitored over a 6-week period. As in the mouse study, the treated dogs were followed up using cSLO fundus fluorescence imaging. Intraocular inflammation developed at 2 and 3 WPI in two animals. The inflammation was independent of the vector capsid used, as the affected eyes had been treated with AAV2, AAV2.GL or AAV2.NN. The two affected dogs were euthanized at 4 WPI and the remaining three animals that showed no evidence of inflammation were euthanized at 6 WPI. AAV2 resulted only in weak and sparse eGFP fluorescence primarily across the nerve fibres, while both novel capsids produced very strong and broadly distributed eGFP signal in the dog retina (Fig.5.15.A). This signal was stronger in the central/nasal regions of the fundus compared to temporal, as seen previously [94]. Confocal scans of retinal cross sections revealed widespread eGFP signal (Fig.5.15.B) and penetrance throughout all retinal layers, as well as retinal pigmented epithelium (RPE), for both AAV2.GL and AAV2.NN. In contrast, dog eyes injected with AAV2 had only a few $eGFP^{+}$ cells in the retina ONL (Fig.5.15.C). For both novel variants, the eGFP signal co-localised with both rhodopsin and M-opsin expression in the ONL (Fig.5.15.D-E), confirming photoreceptor transduction. The results from this first large animal study highlighted the importance of preclinical testing in multiple organisms for multifaceted evaluation of novel therapeutic agents.

Novel vectors transduce non-human primate fovea and retinal periphery

The evaluation of AAV2.GL and AAV2.NN capsids was further expanded using non-human primate (NHP) eyes since their retinal anatomy and physiology are the closest to human. The first of the two animals was intravitreally injected with 1E12 total vg of sc/CMV-eGFP packaged with AAV2.NN to the right eye and 1E12 total vg of AAV2.GL to the left eye. To avoid axial bias and assess low-volume delivery, the second animal received in both eyes 39 μl 1E12 total vg of AAV2.GL. The animals were monitored weekly and at 8 WPI revealed a strong eGFP signal for both novel capsids in the fovea, around major blood vessels throughout the retina and

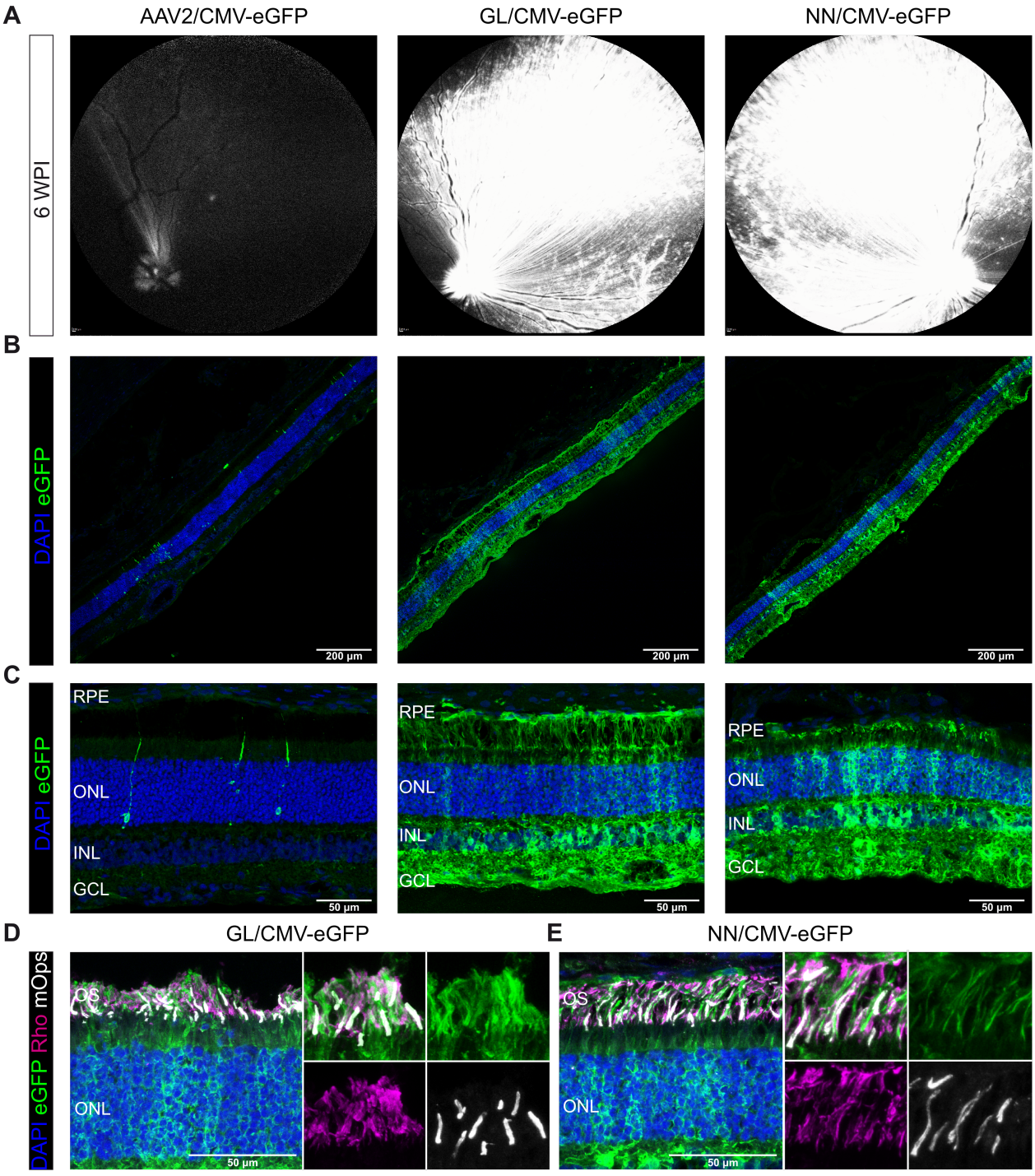

Figure 5.15: Intravitreal dog study with ubiquitous promoter (cSLO images courtesy of Dr. Laurence Occelli)

towards the periphery (Fig.5.16.A-B). After euthanasia at 8 WPI, the NHP eyes were extracted and processed for histological analyses. Staining and confocal microscopy for eGFP revealed an excellent penetrance profile of both novel capsid variants into all retinal layers, particularly at the fovea centralis (Fig.5.16.C-D) where a mean 54.5% and 54.3% of photoreceptors were eGFP$^+$ in the AAV2.GL and AAV2.NN treated retina, respectively (AAV2.GL technical n=4,

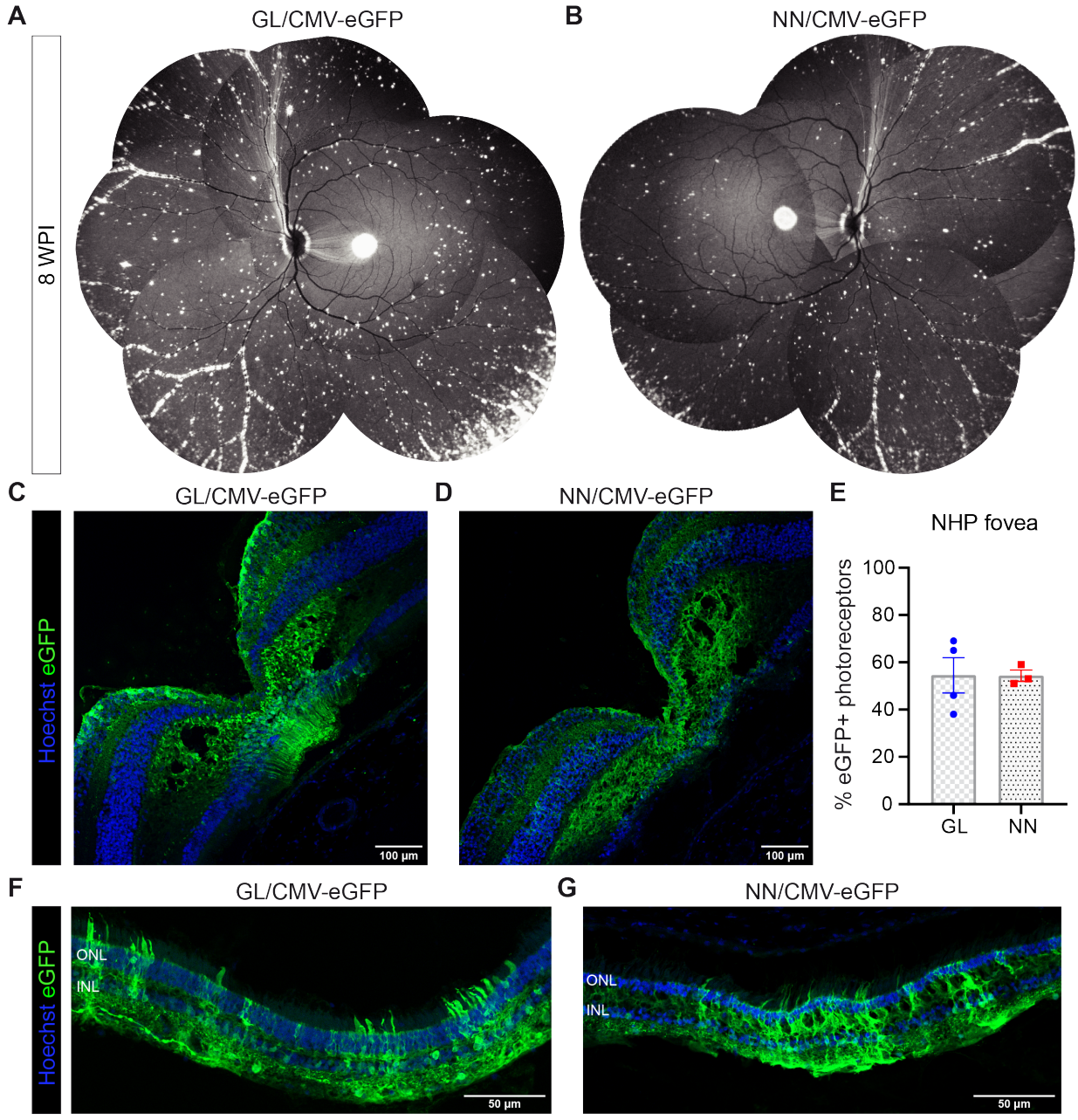

Figure 5.16: Intravitreal non-human primate study with ubiquitous promoter (cSLO images courtesy of Dr. Joshua Bartoe and Dr. Ryan Boyd, overlapped and merged using Adobe Photoshop 2021); mean±SEM

AAV2.NN technical n=3) (Fig.5.16.E). The punctate signal recorded via cSLO was observed also in the peripheral retina (Fig.5.16.F-G) and co-staining with PNA revealed multiple loci with eGFP$^+$ photoreceptors in the centre and periphery (Fig.5.17).

Novel vectors transduce human photoreceptors

As a final evaluation step, AAV2.GL and AAV2.NN were tested in an *ex vivo* model of the human retina. To this end, 1E11 vg of the novel vectors packaged with sc/CMV-eGFP were

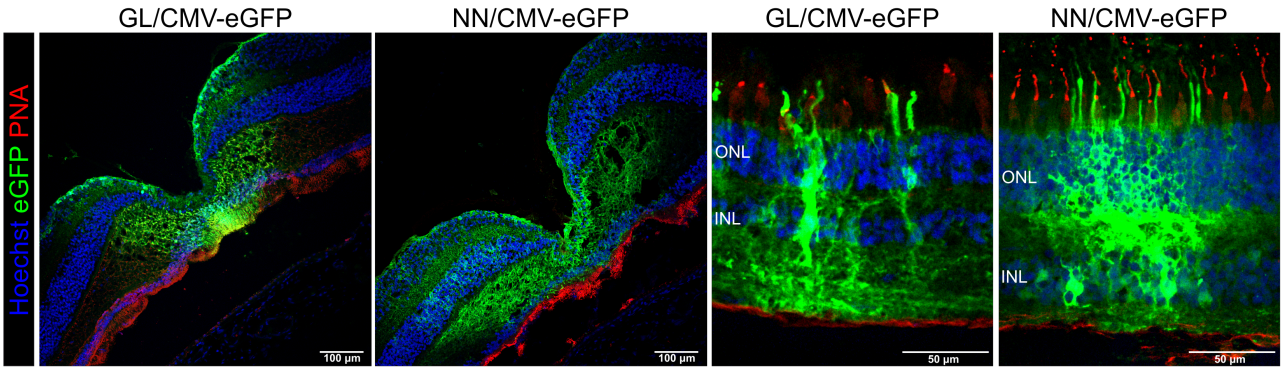

Figure 5.17: Transduction of non-human primate photoreceptors

locally applied to the vitreal side (ILM side) of freshly isolated and cultivated human retinal explants (n = 3) (Fig.5.18.A). Human retinal explants were kept in culture for 10 days after transduction and eGFP was tracked with the EVOS fluorescence microscope. The *en face* view images at 3, 6 and 9 days post infection (DPI) revealed a broad eGFP signal across the entire retinal explant that gradually increased over time for both capsid variants (Fig.5.18.B). IHC at 10 DPI revealed robust expression of eGFP that was most prominent in the photoreceptors of the human retinas for both AAV2.GL and AAV2.NN (Fig.5.18.C).

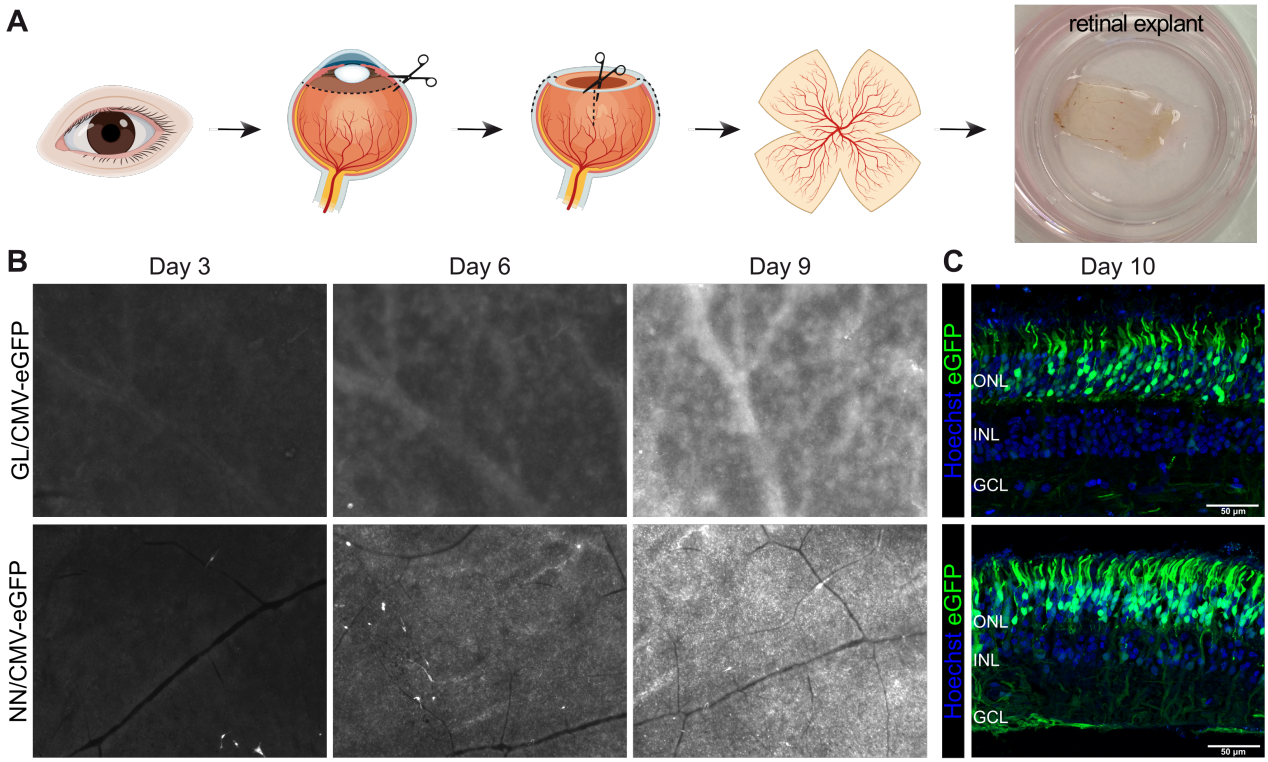

Figure 5.18: Transduction of human retina explant (images courtesy of Dr. Christian Schön)

A second set of experiments with peripheral human retina was performed and explant cultures were transduced with 1E10 vg of AAV2.GL and AAV2.NN on the vitreal side. Imaging

at 10 DPI showed a more widespread eGFP signal, particularly in the synaptic layers. Staining for eGFP and photoreceptor markers recoverin (Fig.5.19.A) or calbindin (Fig.5.19.B) revealed limited marker co-localisation, mostly for AAV2.NN. Note that there are some differences in the thickness of the human retina, reflecting the variable tissue quality caused by the *ex vivo* culturing conditions.

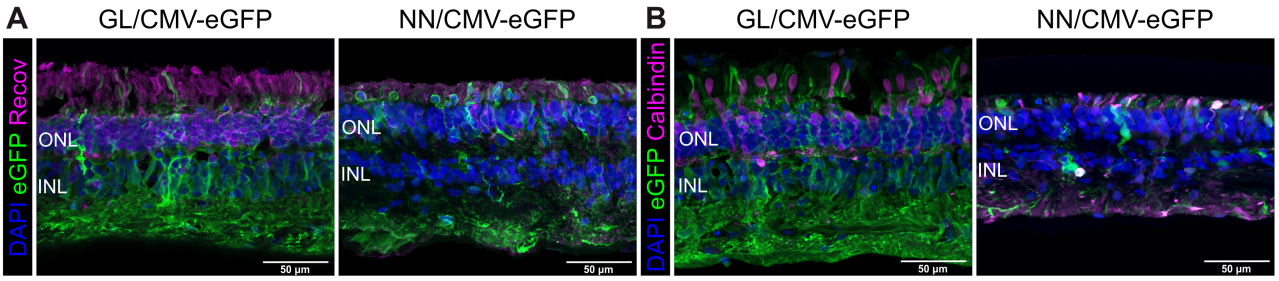

Figure 5.19: Transduction of photoreceptors in the human retina explant

Assessment of inflammation in treated retinas across species

Considering the detrimental impact of vector-induced inflammation during gene therapies in the clinic, it was important to assess the presence of any markers that would indicate inflammation at the time of analysis. To this end, retinal sections from the mouse and dog studies were stained for glial fibrillary acidic protein (GFAP), known to coincide with Müller glia activation, as animals in these studies were injected with both wildtype and engineered capsid variants.

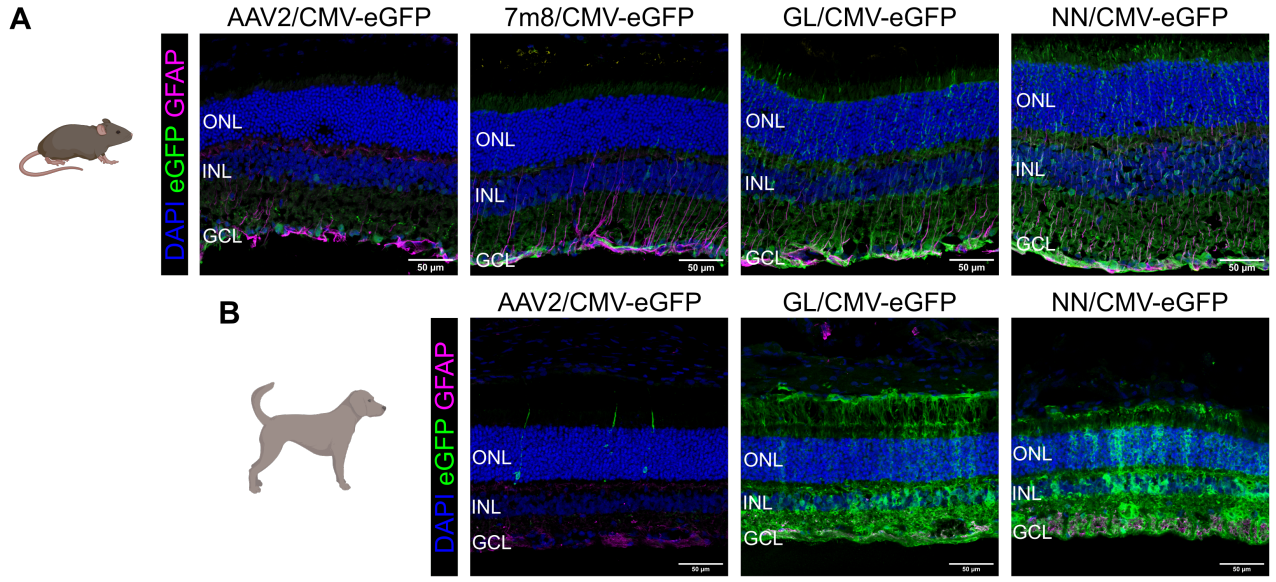

Figure 5.20: Assessment of inflammatory markers in treated retinas across species

From the mouse study, animals treated with AAV2.7m8 showed the strongest GFAP expression coming from Müller glia end-feet and processes, as well as astrocytes below the GCL.

Those treated with AAV2, AAV2.GL and AAV2.NN had comparable levels of GFAP, which was most prominent at the nerve fibre layer (Fig.5.20.A). In the dog retina, the eyes treated with all three vectors that did not show any signs of inflammation via cSLO also had minimal GFAP, indicative of none or low glia activation (Fig.5.20.B). While this does not exclude transient inflammation after vector delivery, it indicates that there was no adverse tissue inflammation in neither mice or dogs at the time of transduction evaluation.

5.3 *Cnga3* gene supplementation therapy using novel vectors

To evaluate the efficiency of the newly engineered capsids in a relevant preclinical disease model, a series of proof-of-concept gene supplementation studies were performed in the *Cnga3*$^{-/-}$ mouse model of achromatopsia [20] using the cone-favouring AAV2.GL capsid (Fig.5.10.A). The objective was to investigate the recovery of cone function after either subretinal or intravitreal administration of a therapeutic vector (Fig.5.21).

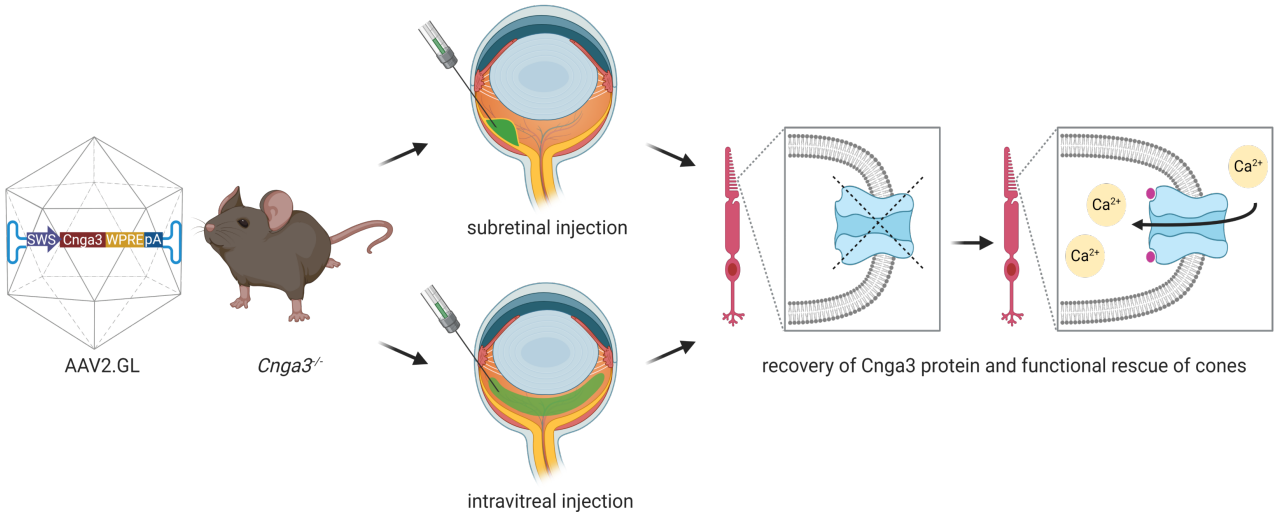

Figure 5.21: Schematic of *Cnga3* gene supplementation strategies

As a first experiment to confirm vector efficacy, 2-week old *Cnga3*$^{-/-}$ mice were injected subretinally with 5E9 vg (1 μl) of either the therapeutic vector AAV2.GL/mSWS-mCnga3, with the murine *Cnga3* gene under the control of a murine short-wavelength opsin promoter (mSWS) [22], or control vector AAV2.GL/mSWS-eGFP. The animals were monitored via fundus fluorescence imaging and electroretinography at time points 6, 10, 14 and 18 WPI (Fig.5.22.A). The control vector induced a widespread eGFP signal that spanned more than half the mouse fundus already by 6 WPI, however the signal gradually faded after 10 WPI (Fig.5.22.B), reflecting the slow cone degeneration in *Cnga3*$^{-/-}$. Photopic ERG traces showed a therapeutic effect of

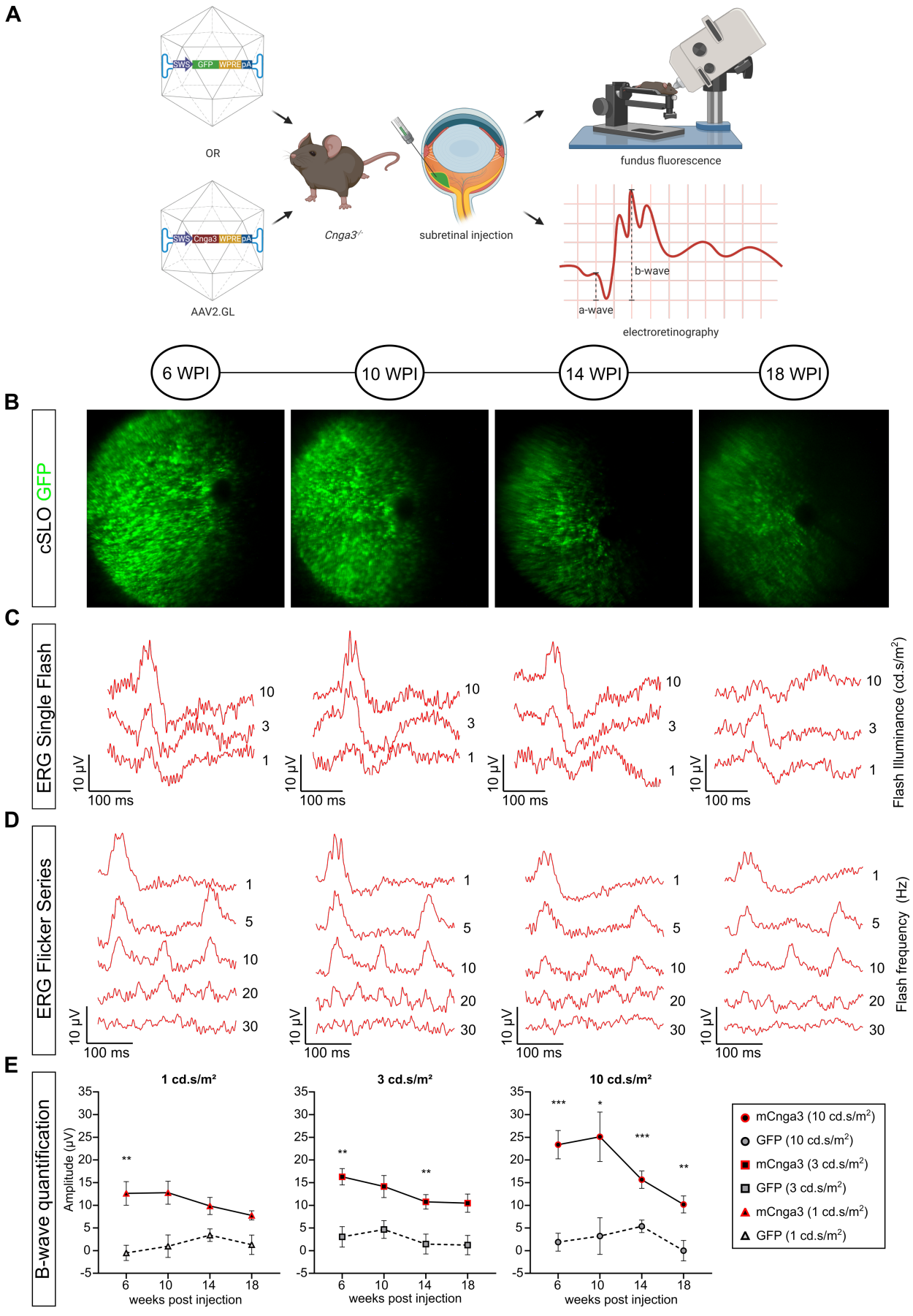

Figure 5.22: Subretinal *Cnga3* gene supplementation therapy; mean±SEM

the AAV2.GL/mSWS-mCnga3 vector, both using single flashes at increasing illuminations 1, 3 and 10 cd.s/m^2 (Fig.5.22.C) or flicker series at 3 cd.s/m^2 with increasing frequencies 1-30 Hz (Fig.5.22.D). Comparing the B-wave amplitudes of photopic responses between the therapeutic and control vector highlighted the ability of subretinal gene supplementation to recover cone function. Specifically at 10 cd.s/m^2, the B-waves were significantly different from the control at all time points (Fig.5.22.E). Notably, the amplitude gradually decreased after the 10 WPI, indicating that the therapeutic effects decelerated but could not halt degeneration in *Cnga3*$^{-/-}$, potentially as a result of the vector administration route. Mice were euthanized at 18 WPI and retinas were stained for Cnga3 and cone outer segment marker peanut agglutinin (PNA) to assess protein expression and localisation in cones. By dividing the mouse retina into quadrants (Q), it was evident that the highest density of Cnga3$^+$PNA$^+$ cones were found in the injected Q2 and proximal Q3 of the same hemisphere. Images from Q1 and Q4 showed no Cnga3 staining and sparse PNA$^+$ cones (Fig.5.23).

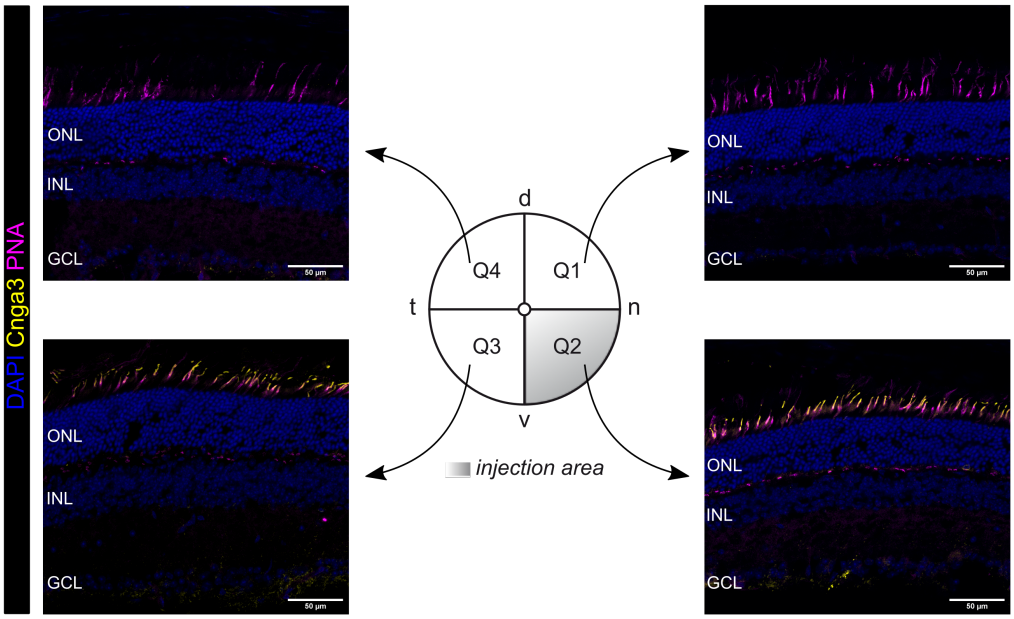

Figure 5.23: Cnga3 protein expression after subretinal gene supplementation therapy

In a subsequent experiment, 1E10 vg (1 μl) of AAV2.GL/mSWS-mCnga3 vector were delivered intravitreally in 2-week old *Cnga3*$^{-/-}$ mice (Fig.5.24.A). The animals were followed-up as before. Both photopic single flash (Fig.5.24.B) and flicker responses (Fig.5.24.C) showed a clear restoration of cone function that persisted across time points 6-18 WPI.

At 10 WPI the B-wave amplitudes in treated eyes were significantly different than age-matched untreated *Cnga3*$^{-/-}$for all three illuminances, namely 1 cd.s/m^2 (p=0.005284), 3 cd.s/m^2 (p=0.000029) and 10 cd.s/m^2 (p=0.000006), although these were still approximately 1 order

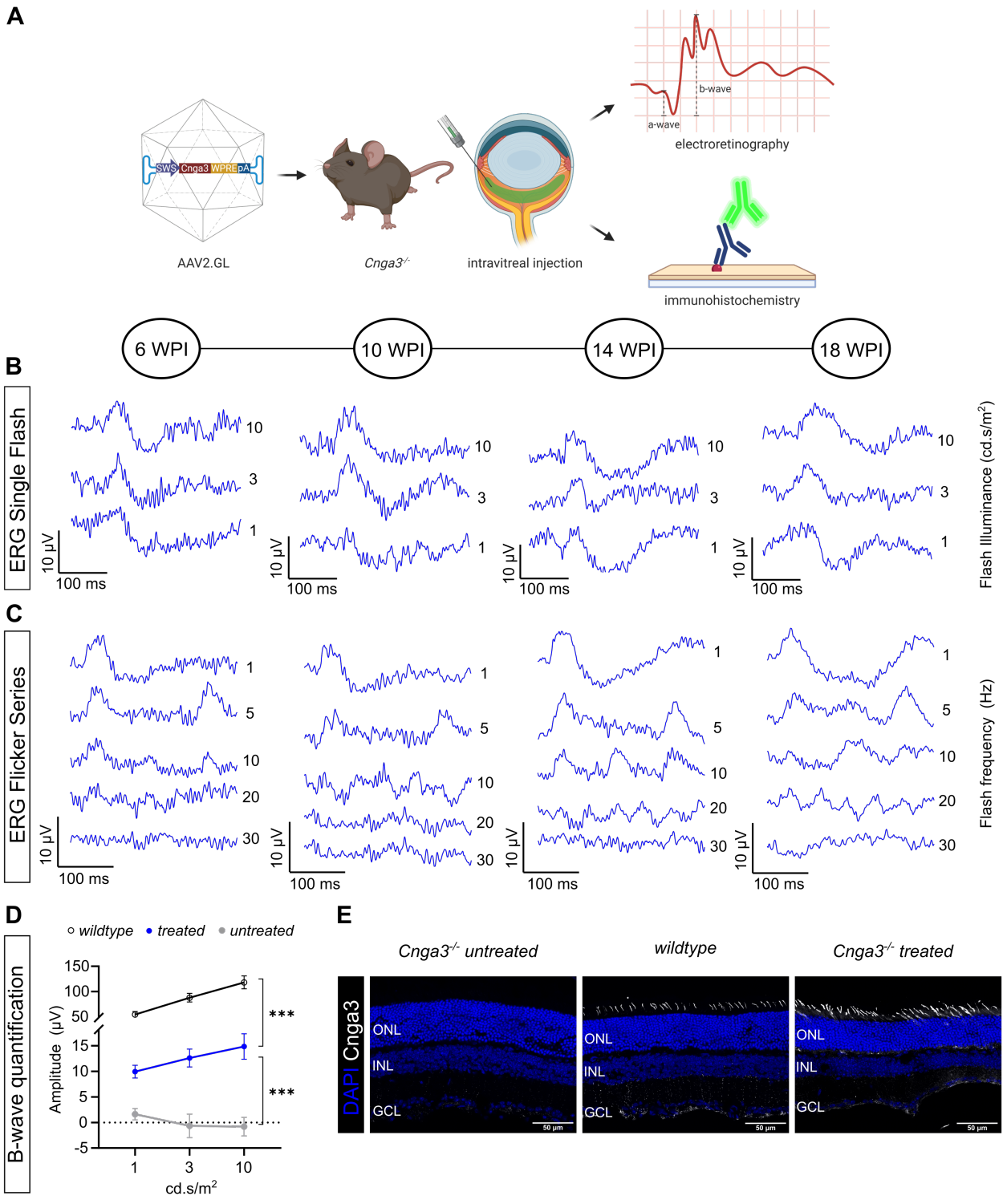

Figure 5.24: Intravitreal *Cnga3* gene supplementation therapy; mean±SEM

of magnitude lower than wildtype responses (Fig.5.24.D). After euthanasia, Cnga3 expression was compared among treated, untreated and wildtype retinas, showing a strong wildtype-like expression and correct protein localisation in treated retinas (Fig.5.24.E). Confocal microscopy of retinal flatmounts further confirmed the widespread transduction and wildtype-like expression of the Cnga3 protein in PNA$^+$ cones (Fig.5.25). This highlights the potential of AAV2.GL

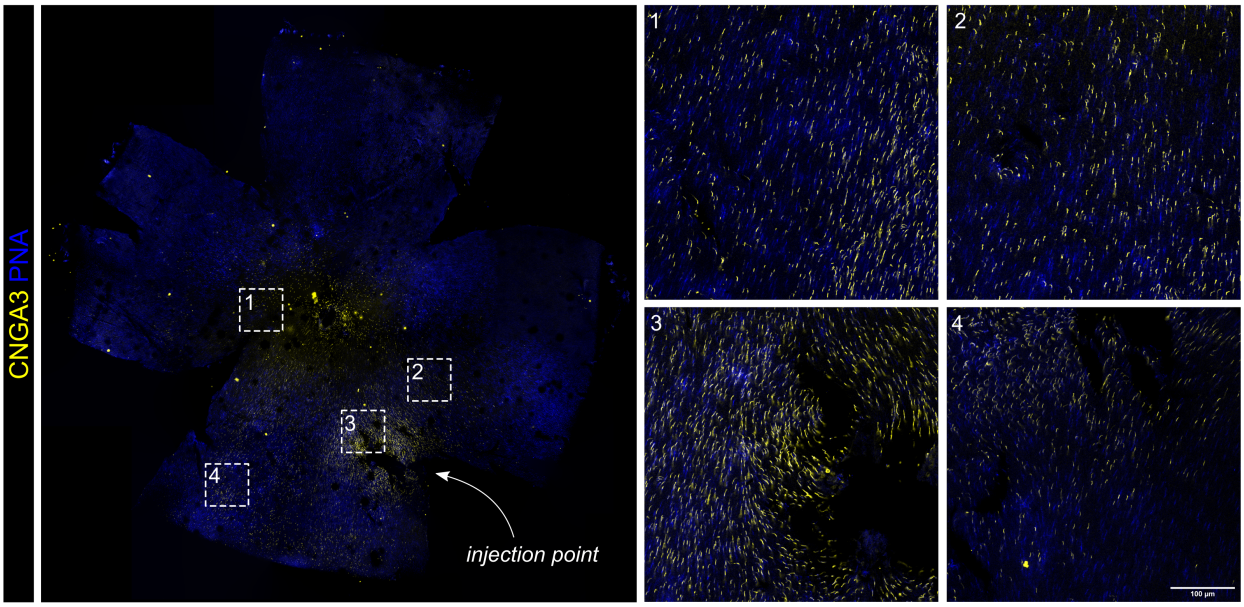

Figure 5.25: Flatmount of treated *Cnga3*$^{-/-}$ retina after intravitreal gene supplementation

as a vector for effective gene delivery using an administration route with less collateral damage.

Comparing AAV2.GL to AAV2.7m8 for intravitreal *Cnga3* delivery

In order to assess how the novel capsid compares to the state-of-art AAV2.7m8 with regard to *Cnga3* gene supplementation, 2-week old *Cnga3*$^{-/-}$ mice were injected intravitreally with either capsid delivering the same cargo (Fig.5.26.A). Both photopic single flash (Fig.5.26.B) and flicker (Fig.5.26.C) responses were comparable between the two capsids. The B-wave quantification also showed that at all illuminances and time points there was no significant difference between the two vectors in successfully delivering *Cnga3* (Fig.5.26.D).

The effects of *Cnga3* supplementation on gene and miRNA expression

The broad impact of supplementing the missing *Cnga3* gene in *Cnga3*$^{-/-}$ was clearly demonstrated by ERG and IHC. In order to begin understanding what changes occur molecularly after treatment, it was necessary to first establish the expression levels of selected genes (Fig.5.27.A) and miRNA species (Fig.5.27.B) in wildtype and *Cnga3*$^{-/-}$ retinas. The genes chosen were either relevant phototransduction cascade members or targets of a miRNA cluster known to be required for cone development and maintenance, namely miRNA-96/182/183 [21, 95, 96, 97].

As expected, the transcript levels of *Cnga3*, *Cngb3* and *Arr3* were significantly lower in adult *Cnga3*$^{-/-}$ compared to wildtype retinas; all other transcript levels were similar between the two genotypes (Fig.5.27.A). With regard to the miRNA levels, these were highly variable

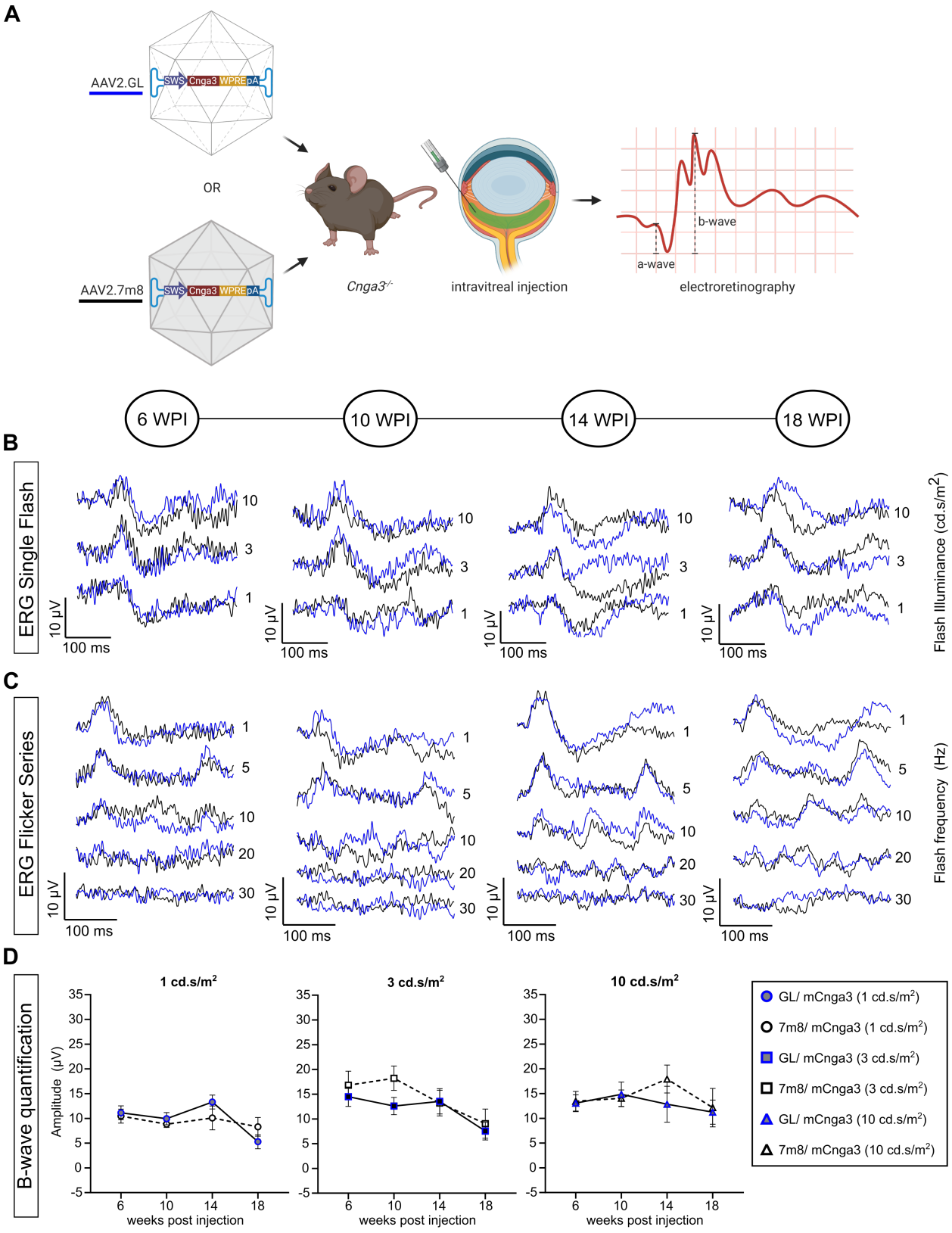

Figure 5.26: Intravitreal *Cnga3* gene supplementation using AAV2.GL or AAV2.7m8; mean±SEM

and not different between retinas from age-matched (2-3 months old) mice: C57BL6/J x 129/sv mixed wildtype, *Cnga3*$^{-/-}$ (C57BL6/J x 129/sv mixed) and C57BL6/J. As a sample, one piece

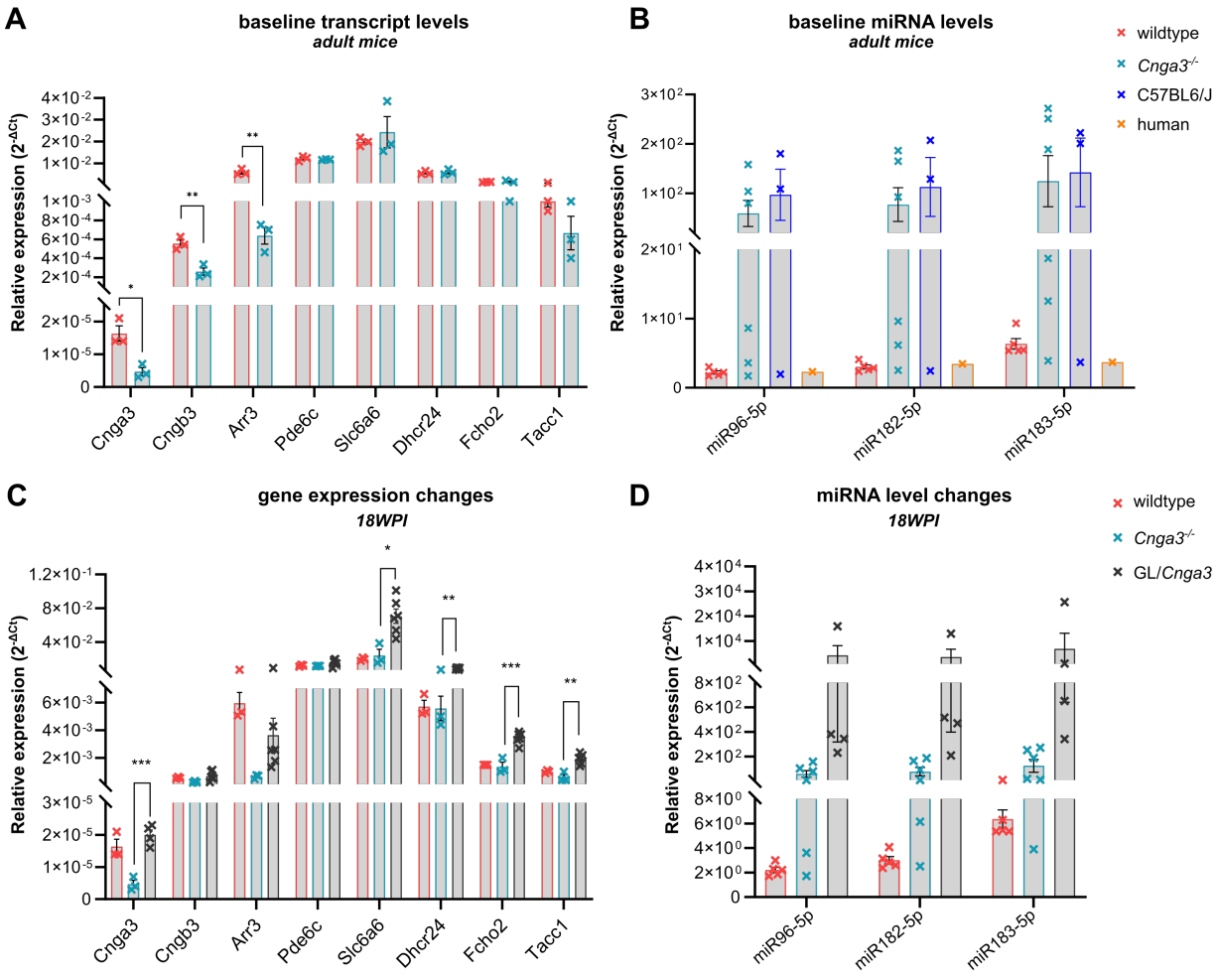

Figure 5.27: Changes in gene or miRNA expression after *Cnga3* supplementation in *Cnga3*$^{-/-}$; mean±SEM

of human retina was also processed, showing low levels of all three miRNAs (Fig.5.27.B). After vector delivery, treated retinas had a recovered *Cnga3* expression that equalled wildtype levels (Fig.5.27.C), in line with the Cnga3 protein pattern (Fig.5.24.E). Furthermore, treated retinas showed a significant increase in transcript levels of the sodium- and chloride-dependent taurine transporter (*Slc6a6*), 24-dehydrocholesterol reductase (*Dhcr24*), F-BAR domain only protein 2 (*Fcho2*) and transforming acidic coiled-coil-containing protein 1 (*Tacc1*) (Fig.5.27.C). This was accompanied by a trending increase of miRNA-96/182/183 cluster levels compared to untreated (Fig.5.27.D), which could be due to the increasing levels of some of the miRNA target transcripts *Slc6a6*, *Dhcr24*, *Fcho2* and *Tacc1* [21, 95]. These results led to the hypothesis, that during cone photoreceptor recovery due to *Cnga3* supplementation, the cells trigger multiple pathways to facilitate their survival. A model of how each upregulated gene plays a role in this hypothesis, is shown in Fig.(6.1) and elaborated in the discussion.

5.4 Alternative approaches at late stages of retinal degeneration

Gene supplementation therapy using viral vectors requires the presence of viable photoreceptors at the time of intervention. At later disease stages, photoreceptors are lost and can no longer be rescued with this approach. For these patients, conferring light-sensing abilities to the remaining interneurons of the ON circuit (i.e. ON bipolar cells) using optogenetic tools poses a promising treatment strategy (Fig.5.28). Alternatively, direct reprogramming of retinal glia into neurons could regenerate the tissue and replenish the missing cell populations. Primary results in both of these research avenues are covered in the following sections.

5.4.1 A universal protocol for isolating ON bipolar cells

Alternative treatments targeting ON bipolar cells are hampered by the lack of efficient gene delivery tools, which in turn rely on the effective isolation of these cells to facilitate tool development. To this end, a universal method to selectively isolate ON bipolar cells via fluorescence-activated cell sorting (FACS) was established [98].

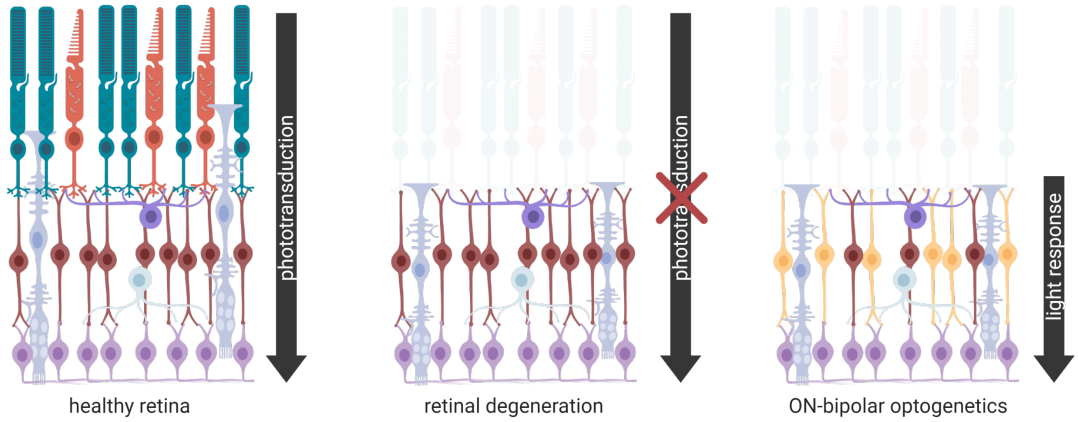

Figure 5.28: Schematic overview of therapeutic strategy targeting ON bipolar cells

ON bipolar cell markers in healthy and diseased retina.

In order to develop a protocol for sorting ON bipolar cells, cytoplasmic markers were assessed for their specific and stable expression in these cells, as there are currently no reliable cell surface markers. The method was intended for both healthy and disease contexts, therefore *Pde6b*^{wt} (herein *Rd1* wt) and *Pde6b*^{rd1} mutant (*Rd1* mut) mice were used. The latter served as a model of early-onset and fast-progressing retinal dystrophy [99, 100, 101] with degeneration peaking at P14 and reaching full photoreceptor ablation by P60 (Fig.5.29.A). Conventional ON

bipolar markers targeting the dendritic spines, such as Cacna1s [102, 103], was present in wt but absent in mut tissue already at the early stage of degeneration (P14) (Fig.5.29.B).

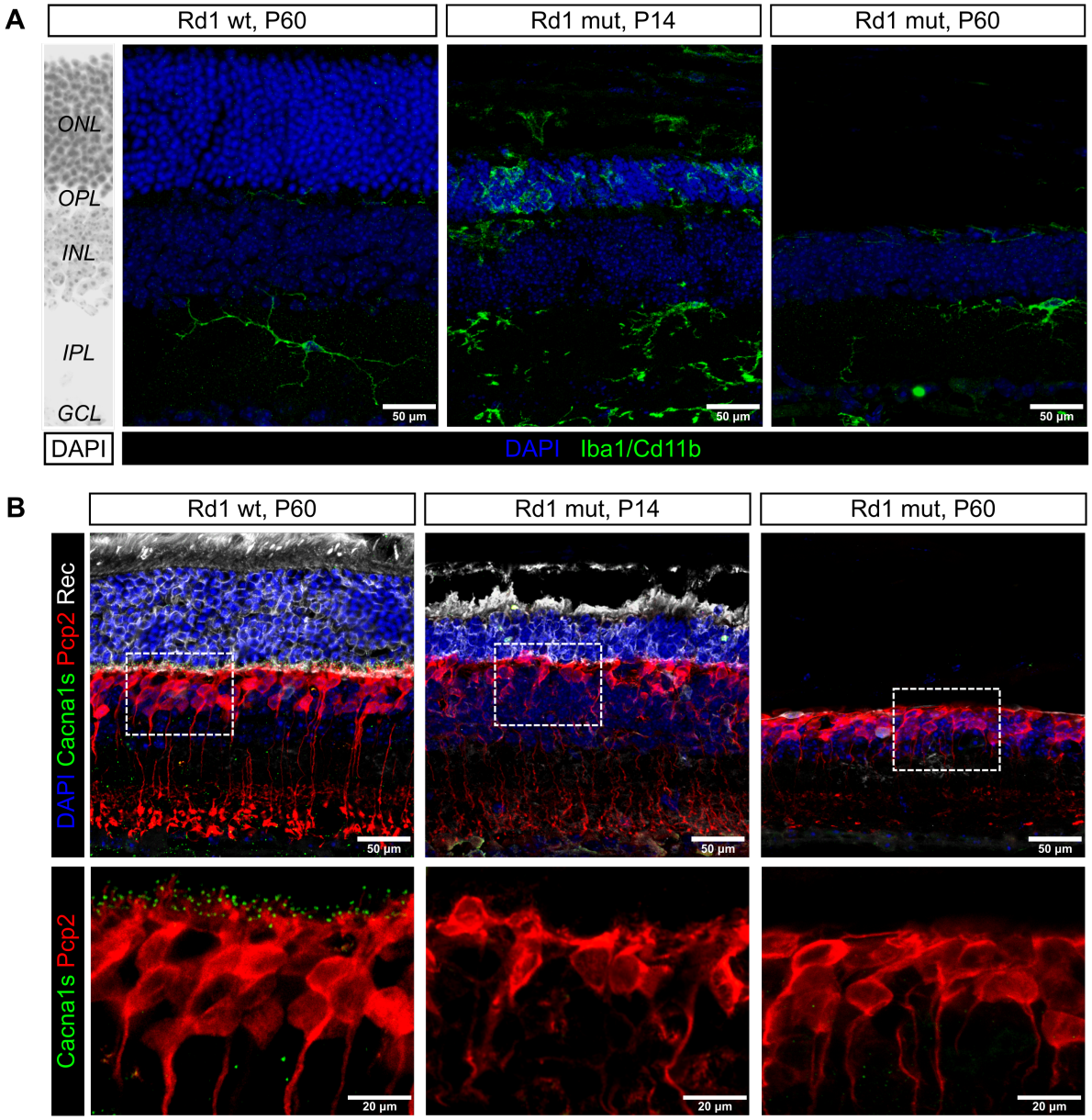

Figure 5.29: Late-stage retinal degeneration and marker testing

As such, non-conventional but known cytoplasmic markers Goα[104, 103] and Pcp2 [105, 103] were tested. They showed a clear cytoplasmic signal in the INL of *Rd1* wt and mut retinas both at early- (P14) and late-stage (P60) degeneration, when most photoreceptors were already lost (Fig.5.30.A), and were therefore used for FACS. Retinas from 2-month-old *Rd1* wt and mut animals were acutely isolated and each animal had their two retinas pooled before proceeding with papain dissociation; a process that preserves neuronal viability and has been shown to allow good separation of retinal cells [77]. Dissociated cells were first stained with a viability dye to discriminate live from dead cells while sorting, followed by a mild fixation/permeabilisation

step. The cells were then stained for Goα and Pcp2 (Fig.4.4) and the cooled cell suspensions were processed via FACS. Baseline gates were first set to discriminate viable single cells from debris and cell aggregates (Fig.5.30.B). A mean viability of about 95% of sorted cells was obtained (Fig.5.30.B), indicating that the dissociation process was well tolerated.

As observed in Fig.5.30.A, Goα expression was leaky in the synaptic IPL, whereas Pcp2 was confined to the cytoplasm of the ON bipolar cells. Accordingly, viable single cells were first gated with respect to Goα expression and subsequently with respect to Pcp2 (Fig.5.30.C-D). In order to characterise the entire Pcp2^{+} population, two sub-populations were identified and sorted: Goα^{+}/Pcp2$^{+\text{high}}$ and Goα^{+}/Pcp2$^{+\text{low}}$, while Goα^{-}/Pcp2^{-} cells were collected as a negative control. Notably, the mean number of sorted events for each population was different between the two mouse lines, with approximately one order of magnitude difference in the Goα^{-}/Pcp2^{-} population (Fig.5.30.E), reflecting the loss of photoreceptors in the *Rd1* mut retina at P60 (Fig.5.29.A).

The Goα^{+}/Pcp2$^{+\text{high}}$ population is exclusive for ON bipolar cells in mice.

After FACS, RNA was isolated from the three populations, using a formalin-fixed and paraffin-embedded (FFPE) kit to revert formaldehyde modifications of nucleic acids, to determine the identity of the sorted cells. The extracted RNA (Table5.1) was analysed via RNAseq to obtain the gene expression profiles of the Goα^{+}/Pcp2$^{+\text{high}}$ and Goα^{+}/Pcp2$^{+\text{low}}$ populations.

	RNA Mean ± StDev (ng)		
Population	**Rd1 wt**	**Rd1 mut**	**NHP quadrants**
Goα⁺Pcp2⁺ʰⁱᵍʰ	443 ± 160	270 ± 146	1100 ± 354
Goα⁺Pcp2⁺ˡᵒʷ	421 ± 205	383 ± 261	812 ± 300
Goα⁻Pcp2⁻	246 ± 88	221 ± 140	961 ± 409
Goα⁻Pcp2⁺ˡᵒʷ	n/a	n/a	753 ± 550

Table 5.1: Total RNA extracted from sorted mouse and NHP retina populations

The top 50 genes in the Goα^{+}/Pcp2$^{+\text{high}}$ population were selected and compared to a published single-cell RNAseq database from mouse retina [103]. The dot plots generated show only the genes that match the database, with the individual bipolar subtype clusters for either ON or OFF indicated. The size of the circle represents the percentage of cells expressing a gene in the corresponding single-cell RNAseq cluster, while the colour indicates its mean level of expression. For both *Rd1* wt and mut samples, genes with high expression in ON bipolar cells, including

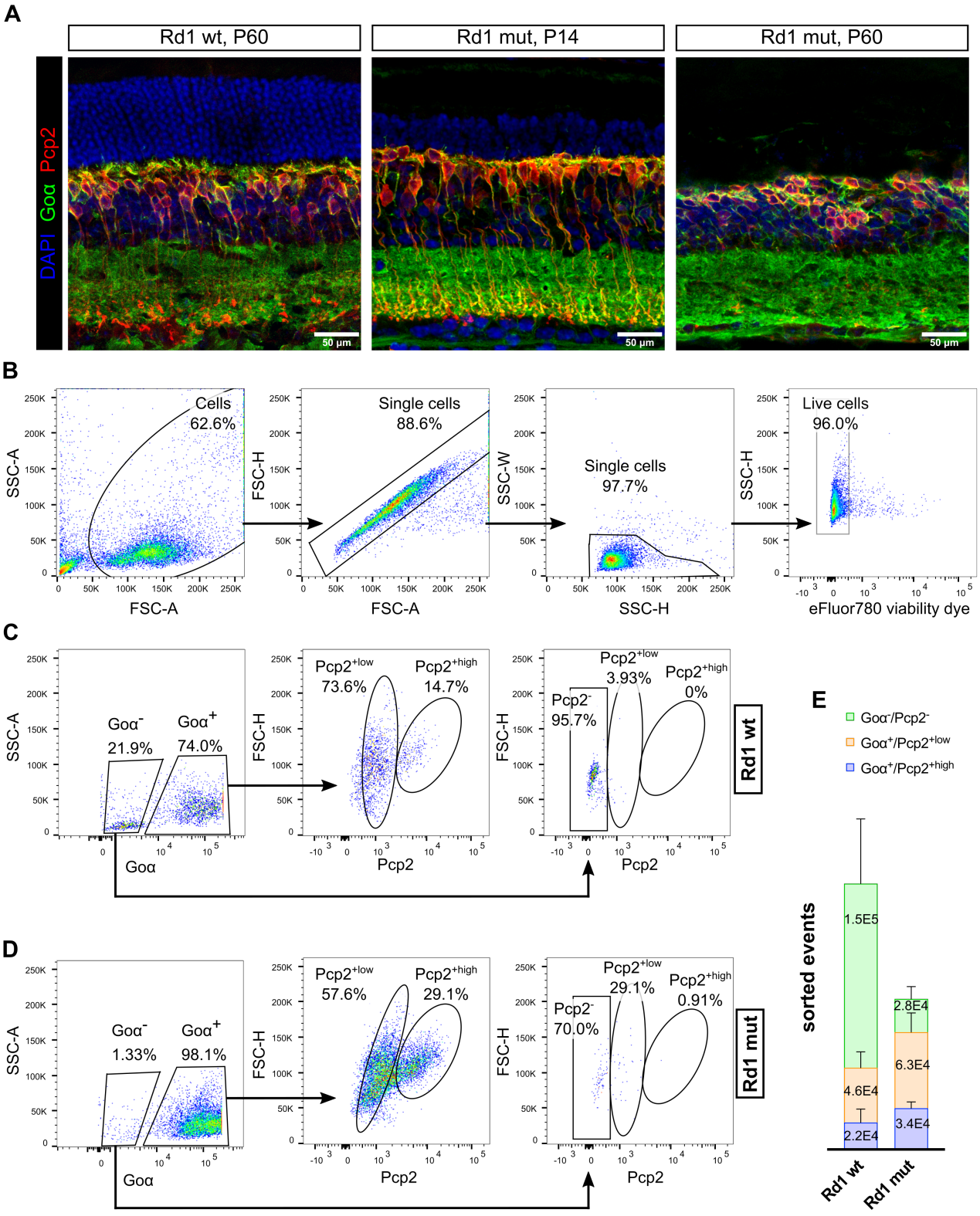

Figure 5.30: Goα and Pcp2 labelled *Rd1* wt and mut retinas used to sort ON bipolar cells

those with specific enrichment in ON but not OFF bipolar cells, were strongly represented in the Goα^{+}/Pcp2^{+high} population (Fig.5.31.A-B;cyan). This result was further confirmed by the

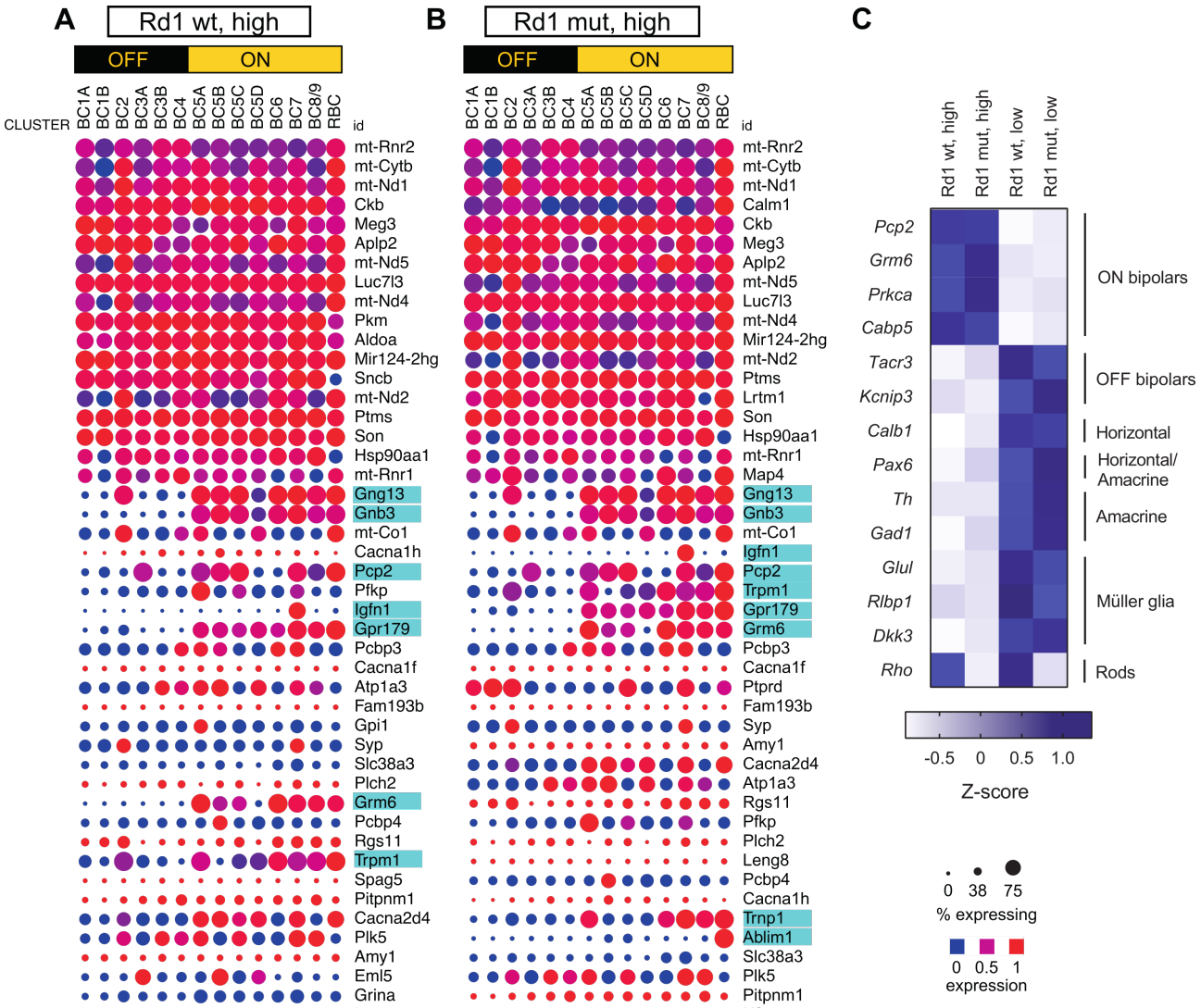

Figure 5.31: RNAseq analysis of mouse Goα^{+}/Pcp2^{+high} populations (plots courtesy of Dr. Elisa Murenu); ON bipolar genes = cyan

enrichment i.e. Z-score of ON bipolar genes (*Pcp2*, *Grm6*, *Prkca* and *Cabp5*) and the absence of OFF bipolar (*Kcnip3* and *Tacr3*) [106], horizontal (*Calb1*, *Pax6*), amacrine (*Pax6*, *Th*, *Gad1*), Müller glia (*Glu1*, *Rlbp1*, *Dkk3*) and rod photoreceptor (*Rho*) genes (Fig.5.31.C). *Rho* was the only exception, as its expression was detected in the Goα^{+}/Pcp2^{+high} population of *Rd1* wt animals, although at lower levels than in the Goα^{+}/Pcp2^{+low} population (Fig.5.31.C). However, this is apportioned to the >1 log unit greater number of rod photoreceptors compared to bipolar cells in the wt mouse retina [107]. In the analogous analysis of the RNAseq data from the Goα^{+}/Pcp2^{+low} population, there was no match with any ON bipolar genes from the single-cell RNAseq database (Fig.5.32.A-B). The patterns of enriched genes was random, as oppose to that from Goα^{+}/Pcp2^{+high}.

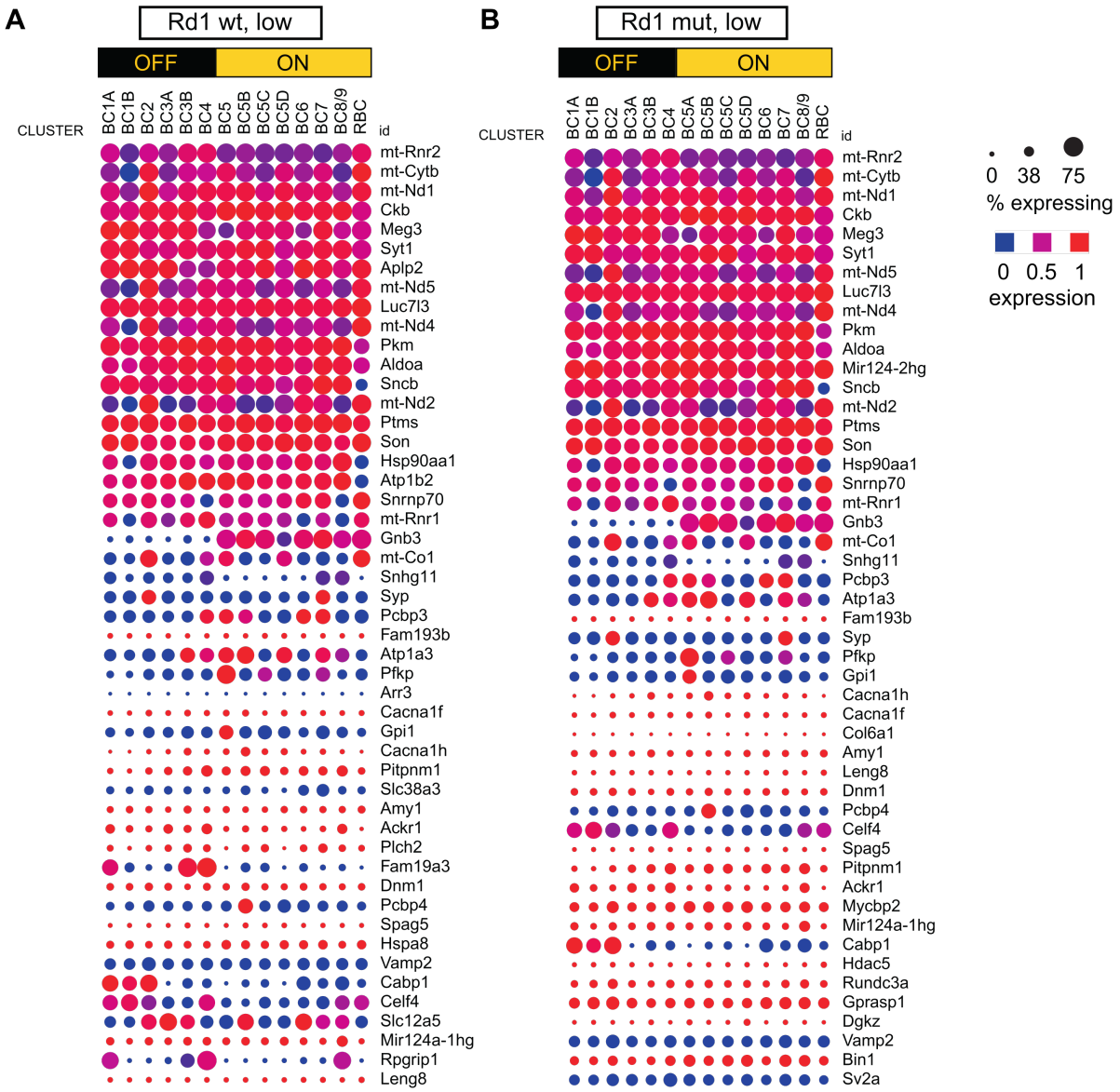

Figure 5.32: RNAseq analysis of mouse Goα^{+}/Pcp2^{+low} populations (plots courtesy of Dr. Elisa Murenu)

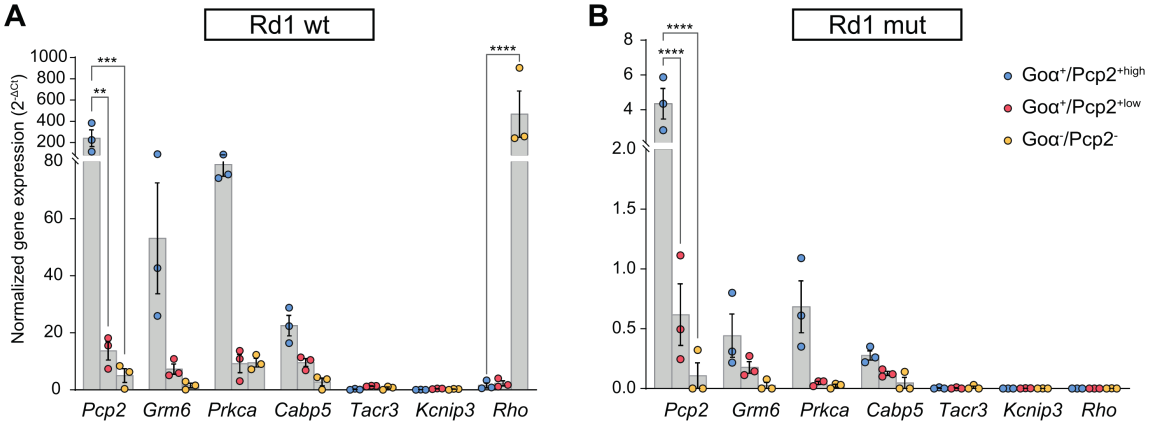

Figure 5.33: qPCR analysis of sorted mouse populations; mean±SEM

To further validate these findings, the expression of selected marker genes was assessed via qPCR. This confirmed the enrichment of ON bipolar genes *Pcp2*, *Grm6*, *Prkca* and *Cabp5* in the Goα^{+}/Pcp2^{+high} population from both *Rd1* wt and mut animals, with either none or minimal detection of OFF bipolar genes *Kcnip3* and *Tacr3* or the rod photoreceptor marker *Rho* (Fig.5.33.A-B). The same ON bipolar genes were also detected in the Goα^{+}/Pcp2^{+low} population, albeit at lower expression levels than Goα^{+}/Pcp2^{+high}, thus corroborating the distinction of two Pcp2^{+} populations with this sorting protocol. As expected, *Rho* was highly enriched in the Goα^{-}/Pcp2^{-} control population of *Rd1* wt samples (Fig.5.33.A), but absent from *Rd1* mut samples (Fig.5.33.B), well in agreement with the lack of rod photoreceptors in adult *Rd1* mice.

Goα and Pcp2 selectively label ON bipolar cells in NHP

Given the high efficiency and specificity of ON bipolar isolation in mice, the method was transposed to the NHP retina, as it better approximates human physiology. To this end, retinas from naïve NHP eyes were removed and carefully dissected into quadrants (Fig.5.34.A). For logistical reasons and to allow for *ex vivo* manipulation, the tissue was maintained overnight in the form of retinal explant cultures, with the ONL facing down on hydrophilic methyl-cellulose culture inserts(Fig.5.34.A). Subsequent IHC analysis showed that Goα and Pcp2 antibodies efficiently labelled ON bipolar cells, as inferred by their intra-layer localisation and distribution in the INL (Fig.5.34.B). After the overnight culture, NHP retinal explants were harvested and dissociated either as a whole or as small pieces of 6 mm diameter. The papain dissociation and staining protocol were adapted with respect to reagent quantities, to compensate for the larger tissue amount, thickness and composition. Contrary to the mouse samples, FACS showed a lower cell viability (mean 56%; Fig.5.34.C). This is apportioned to lengthier process of isolating fresh retina from NHP eyes, as well as the over-night culturing step as explants. Nevertheless, the viable cell fraction had a distinct Goα^{+} population that was further discriminated into Pcp2^{+high} and Pcp2^{+low}. Interestingly, the Goα^{-} population was also further divided into Goα^{-}Pcp2^{+low} and Goα^{-}Pcp2^{-}, although the former accounted for only a small fraction of the entire Goα^{-} population (Fig.5.34.D).

RNA was extracted from all sorted populations as described above (Table5.1) and used to perform RNAseq. The top 50 genes with the highest reads were then compared to a published single-cell RNAseq database from NHP retina [108]. Among those genes, several of the Goα^{+}/Pcp2^{+high} population were specific for ON bipolar cells (cyan highlight;Fig.5.35.A), while only *GNB3* was found in both Goα^{+}/Pcp2^{+high} and Goα^{+}/Pcp2^{+low} (cyan highlight;Fig.5.35.B).

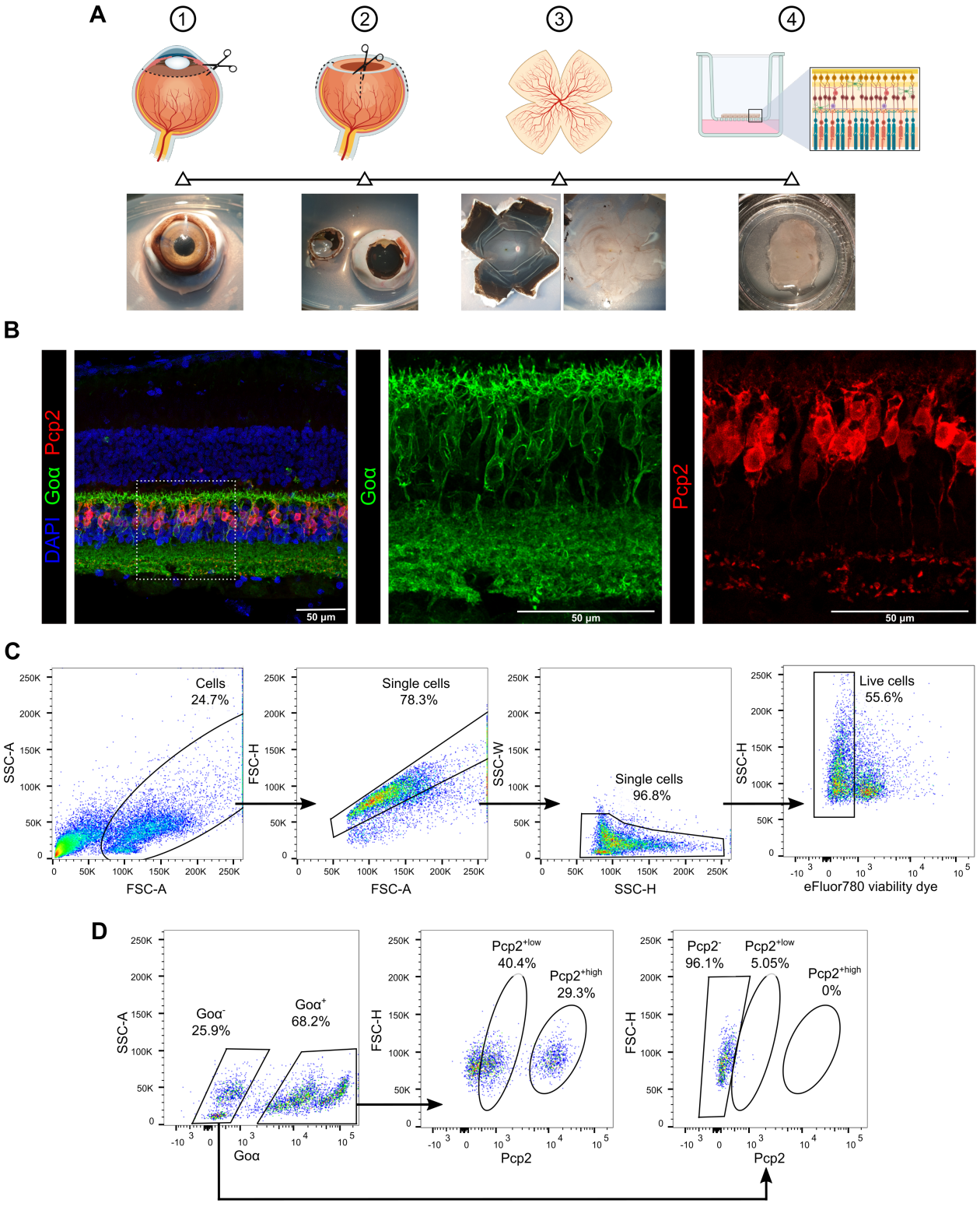

Figure 5.34: Goα- and Pcp2-labelled NHP retinal explants used to sort ON bipolar cells

Previous data reported *GNB3* expression also in the OFF bipolar subtype DB1 [108], potentially explaining the detection of this gene in both sorted populations. The same markers analysed in the mouse RNAseq also showed high expression levels in the NHP Goα^{+}/Pcp2^{+high} population, further confirming ON bipolar cell enrichment (Fig.5.35.C). Specifically, *PCP2*,

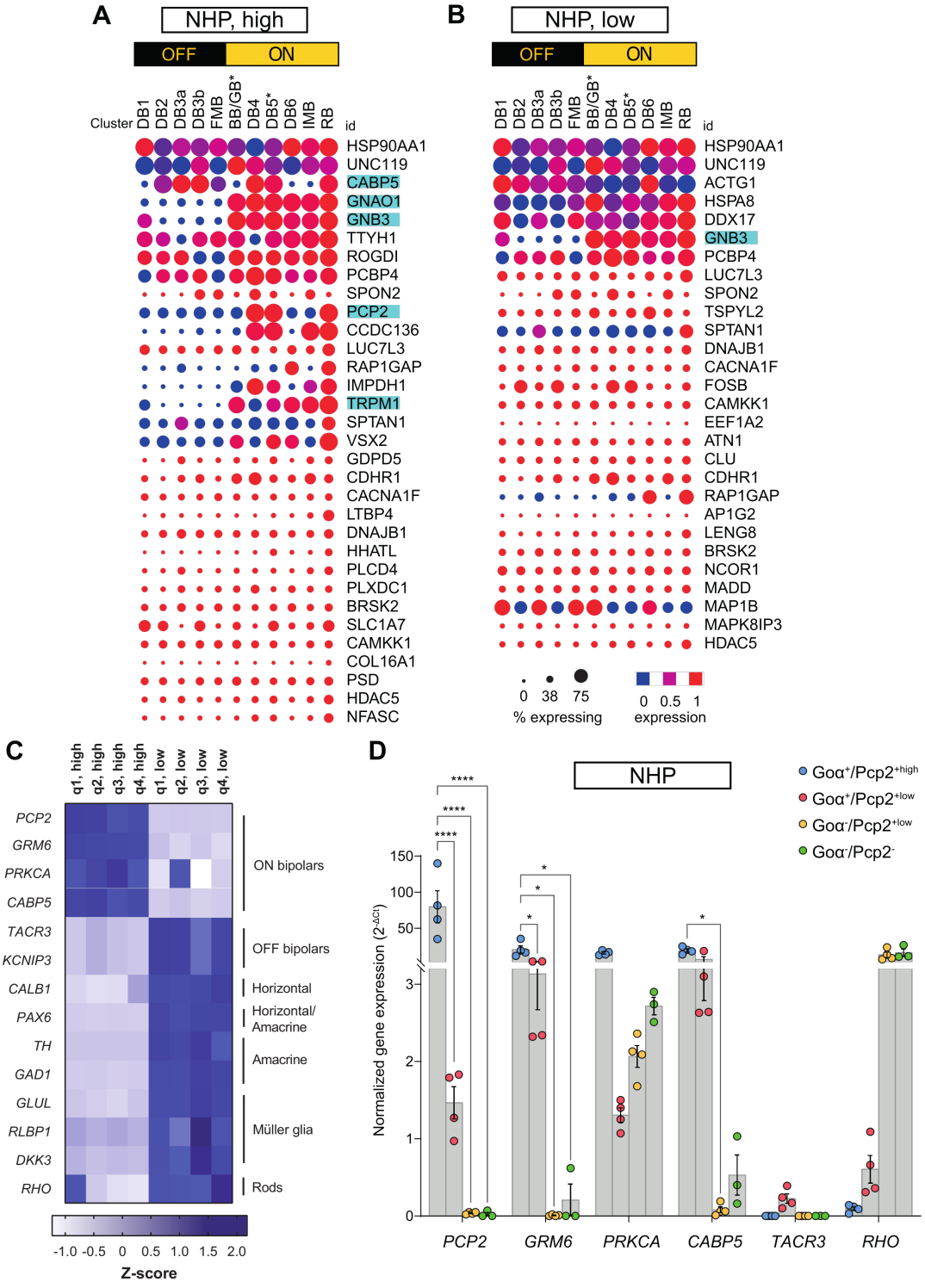

Figure 5.35: RNAseq and qPCR analysis of sorted NHP populations; ON bipolar genes = cyan; mean±SEM

GRM6, *PRKCA*, and *CABP5* showed an almost exclusive expression in the Goα^{+}/Pcp2^{+high}, while genes of all other cell types i.e. *KCNIP3*, *TACR3*, *CALB1*, *PAX6*, *TH*, *GAD1*, *GLUL*, *RLBP1*, *DKK3* and *RHO* had the highest reads in the Goα^{+}/Pcp2^{+low} population for all processed quadrants (Fig.5.35.C). Only one quadrant had detectable *RHO* expression in the Goα^{+}/Pcp2^{+high}, possibly as a result of photoreceptor contamination in this specific sample. To

further validate the RNAseq data, selected markers were assessed via qPCR for all four sorted cell populations, namely Goα^{+}/Pcp2^{+high}, Goα^{+}/Pcp2^{+low}, Goα^{-}/Pcp2^{+low} and Goα^{-}/Pcp2^{-}. As observed in mice, the Goα^{+}/Pcp2^{+high} population displayed the highest levels of ON bipolar genes *PCP2*, *GRM6*, *PRKCA*, and *CABP5*, whose expression was instead reduced in the Goα^{+}/Pcp2^{+low} and Goα^{-} pool (Fig.5.35.D). Strikingly, there were few to none detectable transcripts for OFF bipolar gene *TACR3* and rod gene *RHO* in the Goα^{+}/Pcp2^{+high}, thereby sustaining the high bias of this sorting method for pure ON bipolar cells. Conversely, *TACR3* was detectable in the Goα^{+}/Pcp2^{+low} population, as seen in both mouse specimens (Fig.5.33). Overall, with this universal FACS protocol it is possible to isolate a Goα^{+}/Pcp2^{+high} population from both mouse and NHP retinas, which is highly exclusive for ON bipolar cells. Furthermore, downstream molecular analyses can be efficiently performed regardless of the extensive sample manipulation.

AAV genomes are detected and retrieved from sorted cells after subretinal delivery

After assessing the impact of fixation on downstream analyses focusing on RNA, a proof-of-concept study was performed to demonstrate that sorted Goα^{+}/Pcp2^{+high}, Goα^{+}/Pcp2^{+low} and Goα^{-}/Pcp2^{-} populations could be used for screening viral vector libraries. For this purpose, *Rd1* mut mice and NHPs were subretinally injected with 1E9 vg of AAV libraries [69, 109], with virions containing the AAV *rep* and modified *cap* genes. Retinas were harvested after an in-life period of 24 hours and 1 week, for mice and NHPs respectively. All retina samples were then processed for sorting with the previously established method, followed by isolation of gDNA using the FFPE kit. The ddPCR-based analysis confirmed the expression of viral gene *rep2*, thus verifying the presence of AAV library genomes in the isolated cell populations (Table5.2).

	gDNA Mean ± StDev (ng)		***viral genomes Mean ± StDev (vg)***	
Population	**Mouse**	**NHP**	**Mouse**	**NHP**
Goα^{+}Pcp2^{+high}	203 ± 129	273 ± 172	7271 ± 5092	11916 ± 7968
Goα^{+}Pcp2^{+low}	234 ± 230	236 ± 178	22397 ± 29370	90804 ± 93082
Goα^{-}Pcp2^{-}	214 ± 204	408 ± 118	22746 ± 17717	2625000 ± 1965003

Table 5.2: Total gDNA extracted and total AAV viral genomes detected in sorted populations (ddPCR data courtesy of Dr. Kleopatra Rapti)

Interestingly, although the total gDNA yield was comparable between sorted populations originating from mouse and NHP retinas, the number of total viral genomes detected in NHP

samples was two orders of magnitude greater, specifically in the Goα^-/Pcp2$^-$ population (Table5.2). The quantity and quality of the detected viral genomes were deemed sufficient for the production of AAV sub-libraries, thus demonstrating the applicability of this sorting method as part of a wider vector-library screening pipeline.

5.4.2 Direct reprogramming of microglia into neurons

Different strategies are being explored to trigger retina regeneration from within, in order to replenish various cell populations. The most successful approaches so far have made use of chromatin modifiers, also known as pioneering factors, together with developmental cues of cell differentiation [110]. Initial steps were taken to test the potential of retinal glia, specifically microglia, to be directly reprogrammed into neurons using factors: neurogenic differentiation 1 (NeuroD1), achaete-scute family BHLH transcription factor 1 (Ascl1), neurogenin 2 (Ngn2), retinal homeobox protein (Rax), cone-rod homeobox protein (Crx) and PR-SET domain zinc-finger transcription factor Blimp1 (Prdm1)(Fig.5.36).

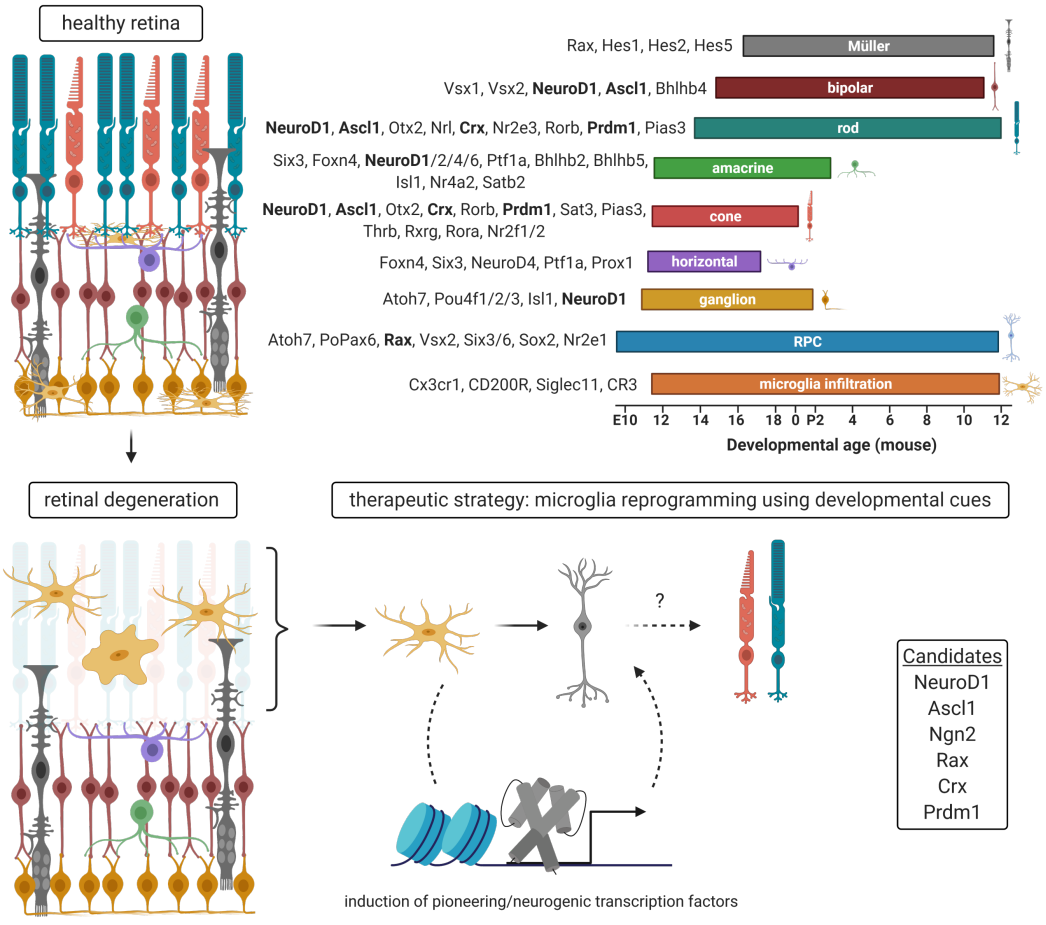

Figure 5.36: Schematic summary of the direct reprogramming concept; retina development timeline adapted from [40, 41, 111, 112]

Primary retinal cultures

In order to test different factors and combinations thereof, it was necessary to establish an appropriate *in vitro* platform. The first attempt was to culture primary retinal cells (4.5) from wildtype C57BL6/J mice and subsequently from *Rd1* mut mice before and after the degeneration peak.

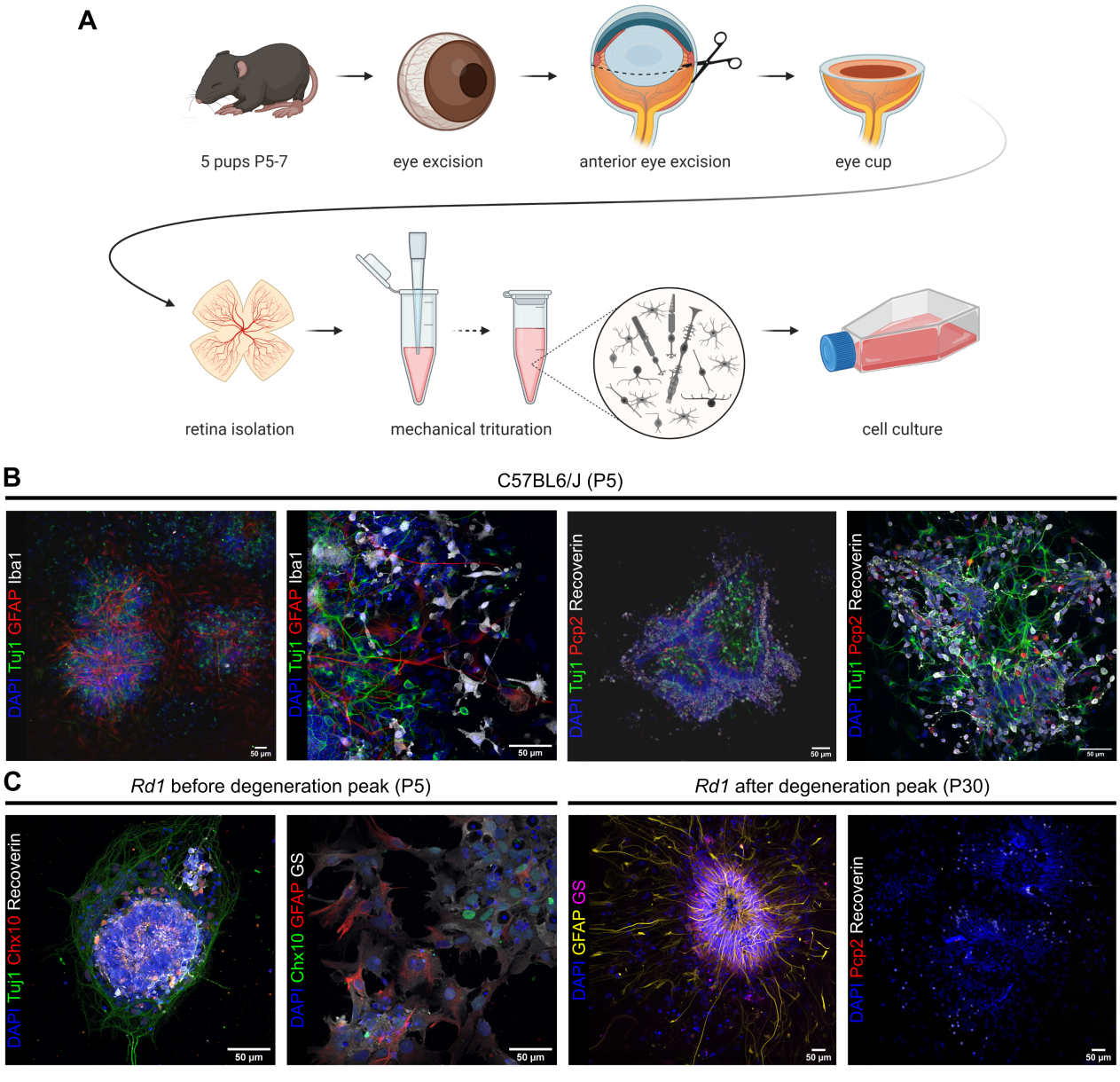

Figure 5.37: Primary mouse retinal cultures: preparation and characterisation

To this end, retinas from young pups aged P5-P7 were used (Fig.5.37.A) and cultured as long as possible, until signs of extensive cell death were observed. Imaging at 7 DIV showed that GFAP$^+$ Müller glia and astrocytes, Iba1$^+$ microglia, Tuj1$^+$ ganglion cells, recoverin$^+$ photoreceptors and Pcp2$^+$ ON bipolar cells were viable in culture (Fig.5.37.B). An interesting

observation was that most neurons were growing on top of glia (astrocytes and Müller) and very few had direct contact with the PDL-coated flask (4.5). To see whether the *Rd1* mut model of retinal degeneration could be used, primary cultures were generated from pups at P5 before the degeneration peak and from adult mice at P30 (Fig.5.37.C). As expected, the *Rd1* mut P5 cultures were made of all major cell types, whereas the P30 cultures had mostly GFAP$^+$, GS$^+$ glia and sporadically some recoverin$^+$ photoreceptors. Primary cultures from adult mice were very poor in proliferation and cell viability, therefore the *Rd1* mut model was deemed redundant.

Reprogramming microglia into neurons: testing factors *in vitro* using lentiviruses

The direct conversion of cells from one cell fate to another requires a strong push, i.e. high levels of factor expression to evoke changes. For the purposes of testing the different factors *in vitro*, each of them was packaged in a lentivirus vector (4.5) together with a reporter (mCherry or eGFP), under the control of a strong ubiquitous promoter (CAG). Using an optimised protocol for culturing primary retinal microglia (4.5, Fig.5.39.A), the aim was to achieve microglia-to-neuron conversion (Fig.5.38).

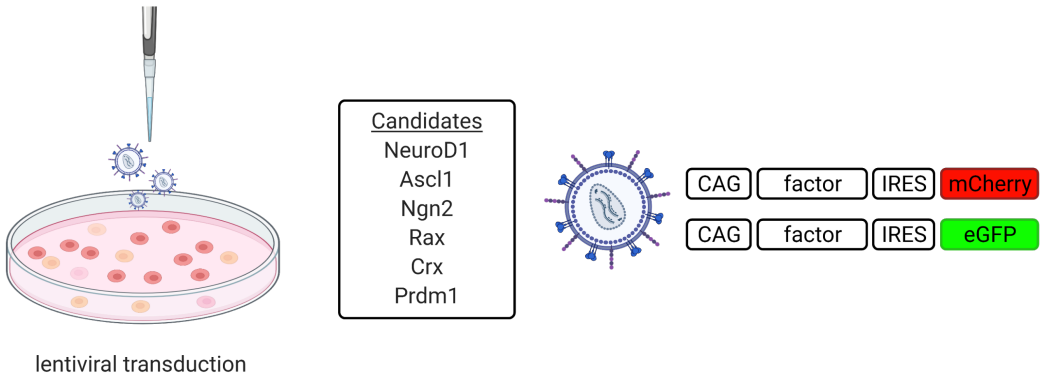

Figure 5.38: Schematic summary of testing factors *in vitro* using lentivirus vectors

Since the reprogramming of cortical microglia into neurons using NeuD1 has been previously described [113], an analogous proof-of-concept experiment was performed, where primary cortical microglia (Fig.5.39.A-B) were infected *in vitro* with LV/CAG-mNeuD1-IRES-mCherry. At 7 DPI newly formed Tuj1$^+$ neurons were detected that appeared immature and not reminiscent of cortical pyramidal neurons (Fig.5.39.C). The reprogramming events were traceable by the expression of the reporter, together with cell-specific markers indicating the original identity of the transduced cell, e.g. a microglia if traces of Iba1 are found (Fig.5.39.D). Following the successful proof-of-concept using cortical microglia, retinal microglia were infected with

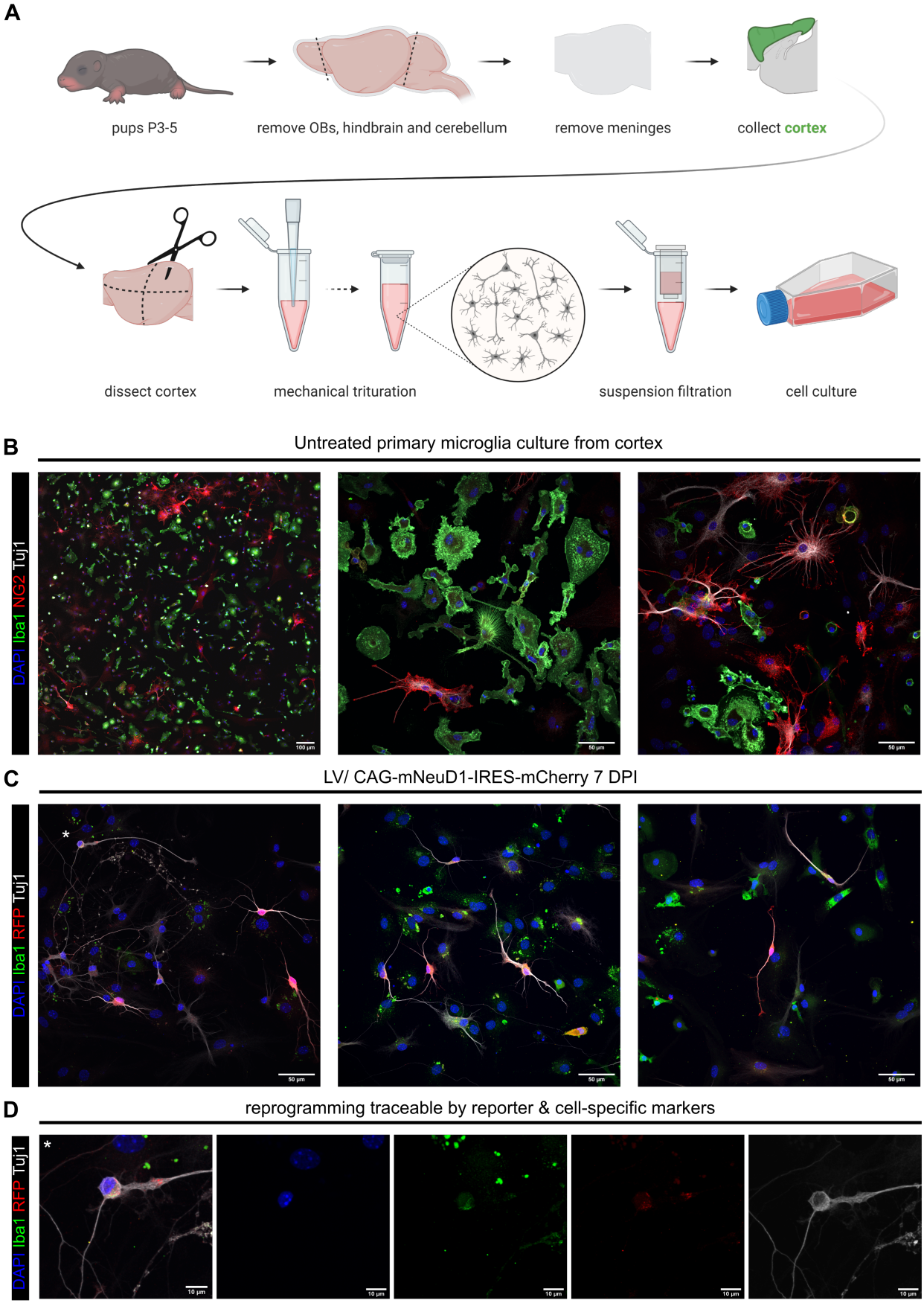

Figure 5.39: Proof-of-concept study: *in vitro* reprogramming of cortical glia into neurons

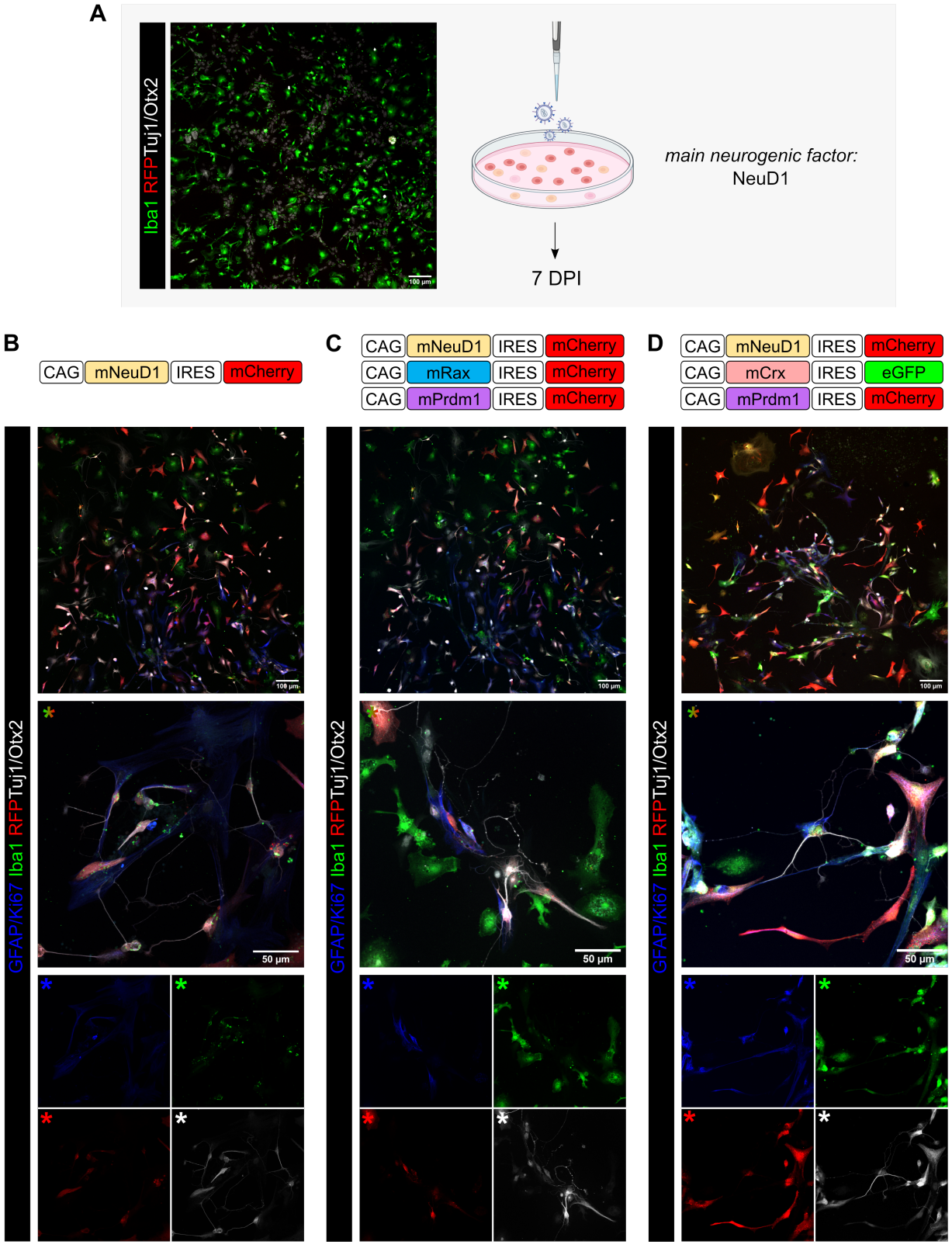

Figure 5.40: *in vitro* reprogramming of retinal glia into neurons with NeuD1 as main factor

lentiviruses carrying different combinations of factors and analysed 7 days later (Fig.5.40.A) NeuD1 alone was successful at converting retinal GFAP$^+$ or Iba1$^+$ glia into Tuj1$^+$ neurons

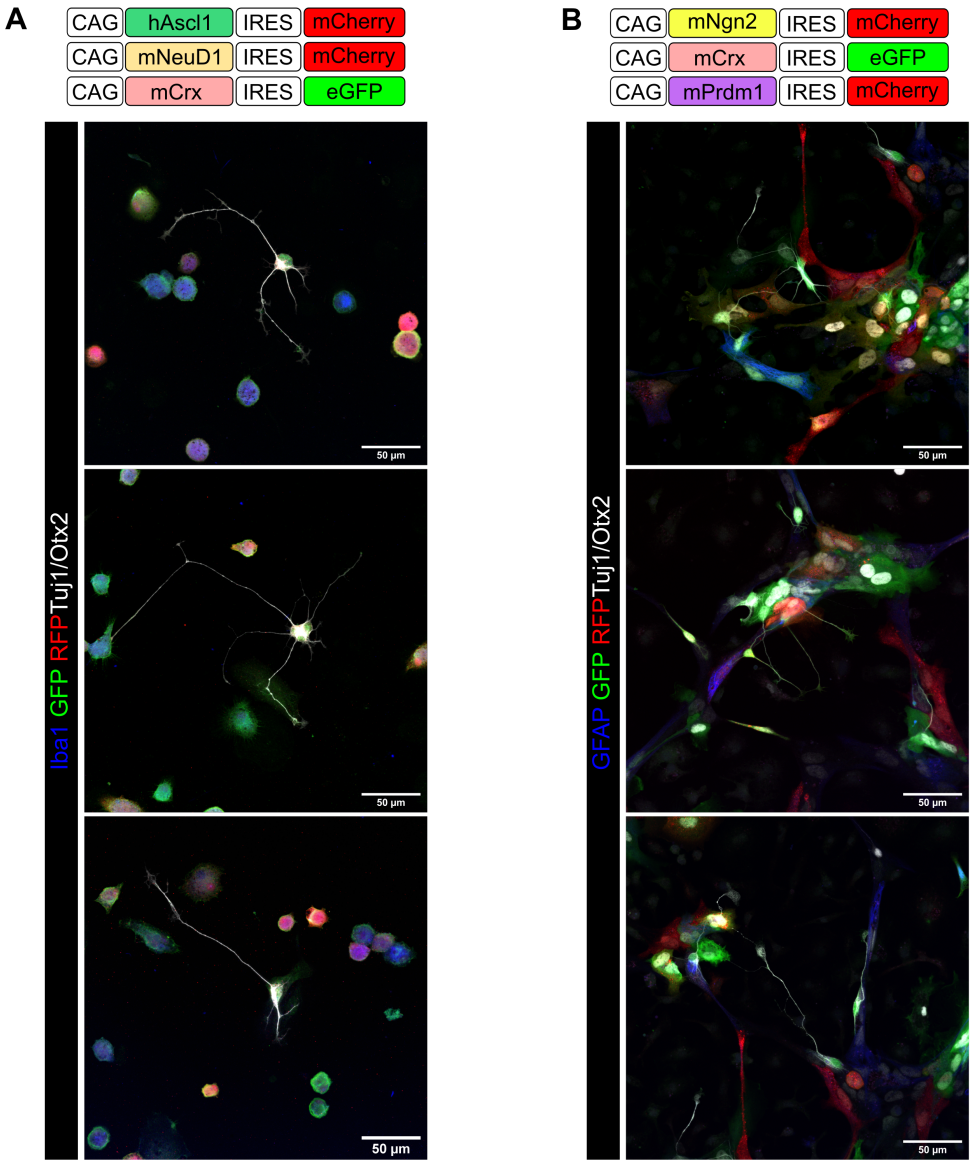

Figure 5.41: *in vitro* reprogramming of retinal glia into neurons with combinations of neurogenic factors NeuD1, Ascl1 and Ngn2

(Fig.5.40.B), as seen for cortical glia (Fig.5.39). The simultaneous combination of NeuD1 with other factors found downstream in retinal differentiation, such as Rax, Crx, or Prdm1, did not have any obvious effects on reprogramming yield compared to NeuD1 alone (Fig.5.40.C-D). Instead, when NeuD1 was combined with a second neurogenic factor Ascl1, the reprogrammed $Tuj1^{+}Otx2^{+}$ neurons had a more mature morphology with two main processes (Fig.5.41.A). It was also observed that with Ngn2 there were more $Tuj1^{+}Otx2^{+}$ cells compared to all other conditions, although those cells had an immature morphology (Fig.5.41.B). This *in vitro* testing platform was not without limitations; specifically it was observed that after lentivirus infection most retinal microglia would become active (amoeboid morphology) and not get transduced (Fig.5.42.A). Furthermore, there was a high rate of incomplete glia-to-neuron reprogramming

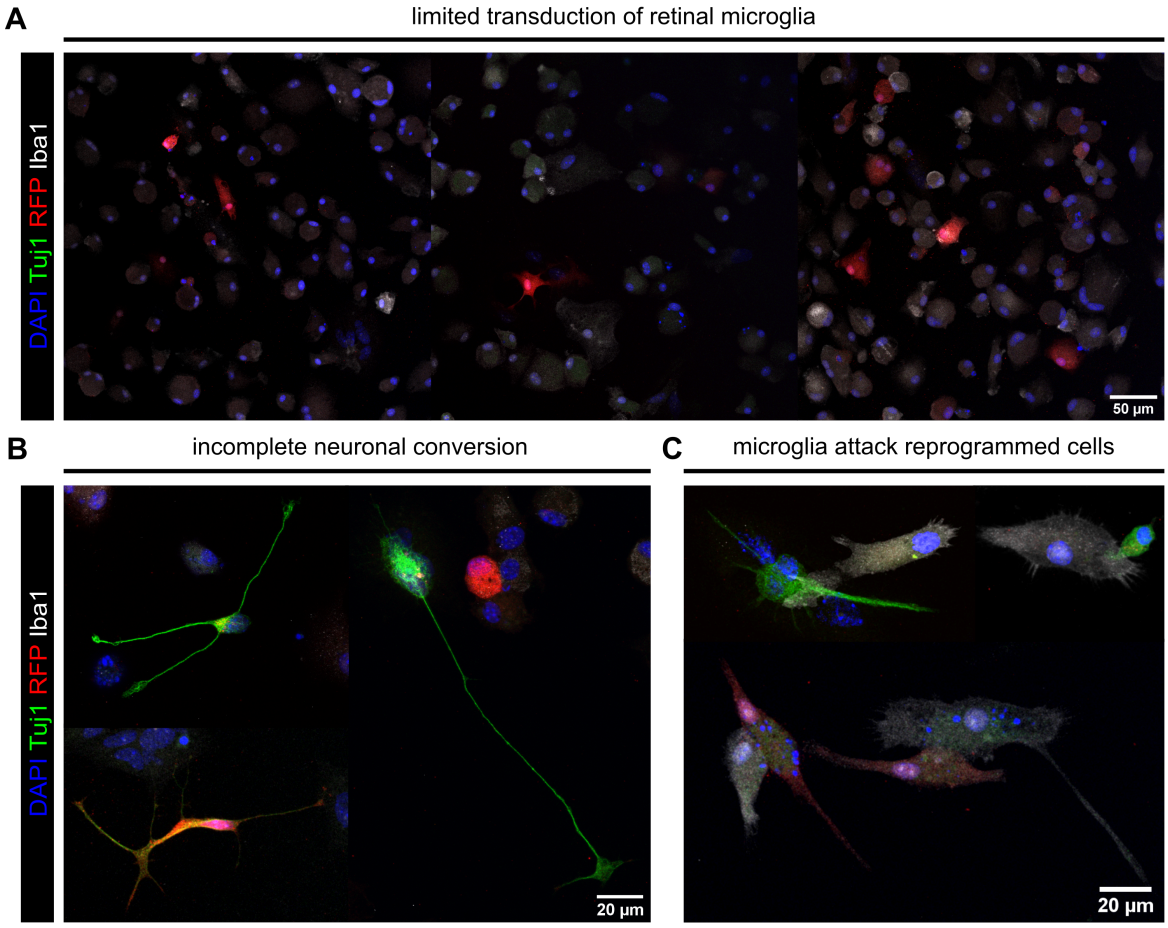

Figure 5.42: Limitations of reprogramming microglia using lentivirus vectors

(Fig.5.42.B) and most importantly, some untransduced microglia would attack the cells that converted or were in the process of converting into neurons (Fig.5.42.C). This could be a phenomenon linked to the *in vitro* culture system, however it emphasises the challenge of targeting microglia for reprogramming.

Discussion

6.1 A binary reporter to assess vector potency *in vitro*

As a matter of principle, before a biological hypothesis or therapeutic intervention is tested in a living organism *in vivo*, it is a prerequisite to first develop and validate key aspects using an *ex vivo* system. The use of *ex vivo* systems as a test bed, e.g. *in vitro* cell culture, generates proof-of-principle data that provide insight ahead of experiments *in vivo*. For the purpose of assessing whether novel AAV vectors are capable of delivering cargo to their target cells, an immortalised cell line with high AAV transduction susceptibility was used, namely HeLa cells [79]. This *in vitro* model was designed to assess vectors with a cargo expressing the α-subunit of CNG channels, which would be used to treat IRDs with mutations in those genes. The primary aim was to confirm the formation of a functional ion-conducting CNG channel after AAV delivery and therefore required constituents that would interact with the channel to form a reporter system. These constituents were cGMP, as CNG channels in the retina are cGMP-dependent [114], and a quantifiable signal that would report ion influx. To this end, the piggyBac transposon system [80] was used to integrate a light-inducible RhGC [83] and a GECI into the cells' genome, under the control of a TetON system [81, 82].

The resulting cells were first validated for their ability to produce cGMP after RhGC illumination (Fig.5.3) and their inducible GECI expression after exposure to doxycycline (Fig.5.2). From the three GECIs tested, i.e. GCaMP6s, jRCaMP1a and jRCaMP1b, the latter was the least reliable, as the emitted signal did not discriminate differences in intracellular Ca^{2+} levels(5.2.C). A positive control study was then performed, by introducing a TetON-inducible *Cnga1* in the engineered HeLa lines, to confirm that the three proteins RhGC, CNG and GECI would be able to interact in a cascade (Fig.5.4). It was sufficient to introduce the α-subunit of CNG, as these can form functional homomeric channels, unlike the corresponding β-subunits [114]. This confirmed the reporter system was behaving as intended (Fig.5.5) and was then followed by testing vectors that carry a *Cnga3*-expressing cassette (Fig.5.6). As this *in vitro* system was not ratiometric, the pattern of increasing GECI signal from low to high extracellular Ca^{2+} was key to determining that the rAAV vector was successful in delivering the *Cnga3* gene. Aspects such as cell density, cell death, doxycycline uptake and AAV distribution could vary among experimental set-ups, which made consistency between GECI detection methods a crucial parameter. Due to the contradicting results between imaging and plate-reader signal quantification for jRCaMP1a (Fig.5.6.B-C), which were likely due to background fluorescence from dead or dying cells, the most reliable *in vitro* system was HeLa cells expressing RhGC

and GCaMP6s. Indeed, GCaMP6s has the highest calcium affinity from the other GCaMP6 family members [84] and has been deemed optimal for high-throughput assays [115]. The engineered cell line was successfully used to discriminate *Cnga3*-carrying vectors with distinct potencies (Fig.5.7), as well as demonstrate the applicability of this system to test vectors with a *Pde6a*-expressing cassette in the presence of CNG (Fig.5.8).

Note that transgene cassettes with photoreceptor-specific promoters were able to drive gene expression in HeLa cells, where such promoters should be inactive. Promoter activation *in trans* has been reported in transfection experiments [116], indicating the possibility that at high MOIs the interaction between the AAV cargo and HeLa genome can trigger gene expression under an otherwise inactive promoter. Another important consideration is that single protein subunits were delivered. Though it is known that CNG α-subunits can form homotetrameric channels [114], it was not clear whether the rod PDE α-subunit would suffice to perform cGMP-hydrolysis. The rod PDE6 enzyme is normally comprised of two catalytic subunits α and β encoded by *Pde6a* and *Pde6b*, and two inhibitory γ-subunits encoded by *Pde6g* [117]. Using this *in vitro* system, the hydrolysis of cGMP was measured indirectly by the decrease in CNG-mediated GCaMP6s signal (Fig.5.8.B-C). The fact that the GCaMP6s signal decreased below the baseline (Fig.5.8.C) was more likely an effect of time rather than the change in extracellular solution. It is possible that the gradually decreasing GCaMP6s signal reflected a slower cGMP hydrolysis as a result of an incomplete PDE protein with limited catalytic capacity. To decipher more intricate details of channel function in such a multiplexed setting, ratiometric calcium indicators could be used [118], although the variable number of AAV-borne CNG channels would skew the readings in each assay. After a series of optimisation steps, it was possible to deliver an *in vitro* model that was able to inform on the potency of vectors ahead of preclinical studies *in vivo*.

6.2 Optimising gene therapy for inherited retinal dystrophies

Multiple gene therapies for monogenic retinal diseases are rapidly advancing to clinical trials, with the first approved drug voretigene neparvovec already being administered in the clinic [119]. For a thorough review on clinical trials in retinal dystrophies see [35]. Whilst an important medical advancement, rAAV vectors currently used in the clinic are based on natural AAV serotypes that pose limitations on efficiency. This has a clinical impact particularly for retinal dystrophies manifesting in rods and RPE cells, such as Lebers congenital amaurosis (LCA2)[120, 121, 122] since photoreceptor degeneration continued even after subretinal gene

therapy with an rAAV2-RPE65 vector [123, 124, 125]. This shortcoming could be apportioned to the LCA2-pathology in RPE cells and/or the subretinal administration route, which can be deleterious and often only achieves local transduction, resulting in limited therapeutic effect. While the option of multiple subretinal injections remains, the risks associated with detaching an already compromised retina at multiple sites overweighs the benefits. Furthermore, the expertise and equipment required for subretinal injections, currently only performed by highly trained vitreoretinal surgeons at specialised centres, may limit the treatment availability. Notably, the accuracy of subretinal injections has been challenged in terms of actual volume delivered versus intended volume delivered [126]. Alternative injection methods have been attempted, such as sub-inner limiting membrane injection [127] or suprachoroidal injection [128, 129], which could overcome risks associated with retinal detachment. Nevertheless, intravitreal delivery of retinal gene therapies could be offered with potentially greater precision by a larger pool of professionals and without the need for specialised equipment. The development of novel AAV capsids, capable of deep penetration of the retina layers after intravitreal administration, as these report here, could considerably improve patient outcome [86].

6.2.1 Directed evolution of AAVs for intravitreal gene delivery

While we continue to advance our understanding of AAV trafficking and how this is facilitated by capsid-host cell interactions [130, 131, 132, 133], bottom-up capsid engineering relies on selective pressures applied to capsid libraries, in order to generate superior vectors for targeting specific cell populations. In this study, a library of peptide-display diversified AAVs based on AAV2 was screened in C57BL6/J mice. The library was subjected to a genotype-phenotype coupling step that enabled the generation of uniform capsids, displaying the 7-mer on the capsid surface by each of the 60 subunits (Fig.5.9.A, 5.11.A,C) for differential cellular contact. Capsid variants with strong or wildtype AAV2-like affinity for HSPG were excluded before *in vivo* screening by counter-selecting the library on a heparin affinity column (Fig.5.9.C). HSPG serves as a natural primary receptor of AAV2 [134, 135], and is responsible for both its broad tropism and limited spreading. Intriguingly, it appears that the ability to bind HSPG, albeit with a lower affinity than AAV2, is critical for retinal transduction through the vitreous, agreeing with previous reports [136], and therefore fostered the selection of variants with respective features from the AAV library. Structural modelling of the novel capsids (Fig.5.11) using Robetta [89, 137] and comparison to the parental AAV2 showed a shift in the geometry of the hypervariable loop 4 on the capsid surface (Fig.5.11.B,D). This loop forms the second highest peak at the three-

fold symmetry axis of the AAV2 capsid (Fig.5.9.A) and is part of the HSPG binding motif, as well as a target of neutralising antibodies. Similar to the novel capsids, the insertion of LALGETTRP peptide in AAV2.7m8 extended this loop and changed its orientation, though recent work indicates that such peptide-extended loops on the capsid surface can be flexible in 3D space [138].

Canonical HSPG binding to R585 and R588 [134] is disturbed by the peptide insertion because it separates the two residues (Fig.5.9.B). However, the arginine residue at position 7 of the inserted peptide in AAV2.GL and AAV2.NN forms a new binding motif together with the two alanine residues of the linker and the R588 of the parental AAV2 sequence [88, 139]. This motif is accessible for receptor binding and the altered loop structure potentially causes the lower heparin affinity compared to AAV2 (Fig.5.12.C). Another possibility is that the deamidation status of N587 has changed as a result of the peptide secondary structure blocking accessibility to the residue. Deamidation of asparagine residues has been associated with reduced transduction of AAV8, which was partially reversed when the +1 position was switched to alanine [140]. Although the backbone for the novel capsids is AAV2, asparagine deamidation has been reported for various serotypes [140], suggesting that this modification is independent of serotype and could play a role in the improved potency of AAV2.GL and AAV2.NN. Irrespective of the structural modifications, there was no impact on the production titres of AAV2.GL and AAV2.NN, as they were similar or higher than AAV2 and AAV2.7m8 (Fig.5.12.A-B); a promising feature for clinical translation. By comparing the *in silico* models of AAV2.GL and AAV2.NN to the structure of AAV2.7m8 [138], it became evident that a capsid diversification strategy with distinct starting libraries and screening approaches can result in structurally different capsid variants, albeit with similar capabilities. As such, library-borne engineered vectors will ultimately reflect the screening criteria used to distil them, even though only a fraction of the theoretical variants in a library were experimentally screened. This phenomenon is starting to be addressed by machine-guided AAV design, so that theoretical libraries are first screened computationally to determine the optimal subset for experimental screening [141, 142].

The AAV library was administered intravenously and thus variants had to pass multiple extracellular barriers to reach the retina within only 24 hours. Specifically, virions had to escape systemic clearance and to penetrate through the blood-vessel endothelial and blood-retina barriers (BRB). Importantly, also intracellular barriers had to be crossed for effective gene expression in photoreceptors. Upon cell entry the vector particles must traffic through and escape the endolysosomal pathway, shuttle through nuclear pores and uncoat their genome to enable

transgene expression [143]. The novel capsid variants were able to cross these intracellular barriers with greater efficiency than AAV2, as shown by the higher levels of nuclear localisation (Fig.5.12.E) and higher efficiency in transgene expression. As the intention was to engineer superior AAV vectors for retinal application, the top five candidates found in cones or rods (Fig.5.10.A) were validated for retinal penetrance after intravitreal injection in mice, which set apart AAV2.GL and AAV2.NN (Fig.5.10.B-C). Both were shown to outperform the parental AAV2 and state-of-art AAV2.7m8 after intravitreal delivery, with regard to both qualitative (Fig.5.13.B-D, Fig.5.14.C) and quantitative reporter expression (Fig.5.13.F, Fig.5.14.B). Given these results, AAV2.GL and AAV2.NN were further evaluated in larger mammals and human retinal explants, as they are more clinically relevant models.

A pertinent issue with screening for novel AAV capsids in C57BL6/J mice is whether the resulting capsids are exclusively potent in specific mouse line only, and whether their efficiency translates across species [144]. Whilst it cannot be excluded that efficiencies may vary in different mouse strains, the data provided herein confirm high retinal potency in the C57BL6/J and mixed C57BL6/J x 129/sv lines. Indeed, AAV capsid potency in the retina varies in larger mammals, potentially as a result of distinct morphological features [145] as well as the presence of neutralising antibodies in dogs [146] and in primates [147]. Both AAV2.GL and AAV2.NN had a similarly improved *in vivo* efficiency in dogs (Fig.5.15) and non-human primates (Fig.5.16). In dogs, reporter expression co-localised with photoreceptor markers (Fig.5.15.D-E) and was not restricted to areas with blood-vessels; a pattern often observed in larger animals as the ILM is less compact near the vasculature. This finding was partially replicated in NHPs as a strong punctate signal was detected in the periphery of their fundus at 8 WPI (Fig.5.16.A-B). However, stronger eGFP signal was observed close to major blood vessels in this species. The macula and *fovea centralis* were also strongly transduced (Fig.5.16.C-E), which is apportioned to the specialised retinal lamination at the fovea, and speaks for the clinical applicability of the novel capsids to target cone-specific dystrophies (Fig.5.17). The final model used to test AAV2.GL and AAV2.NN was human retinal tissue kept *ex vivo* as explant cultures, which is arguably informative about transduction of human cells [148]. Retinal explants are missing relevant *in vivo* barriers, such as the ILM, and can therefore inform on only some aspects of viral transduction in the human retina. Nevertheless, human retinal explants were successfully transduced by AAV2.GL and AAV2.NN, with a particularly high efficacy in human photoreceptors using E11 vg (Fig.5.18.C) and less with E10 vg (Fig.5.19).

For clinical translation, a careful consideration of vector immunogenicity is necessary. To this end, the effects of various vector-specific elements such as the exact vector genome compo-

sition (e.g. CpG content), the immunogenic potential of the encoded transgene or production-related factors need to be considered. Interestingly, although no screening for immune-evasion was performed, both AAV2.GL and AAV2.NN showed no indication of increased immunogenicity in the retina of mouse, dog and NHP (Fig.5.20). In contrast, both variants were less sensitive to pre-existing antibodies (Fig.5.12.F). The inflammation events observed in 2 dogs of the large animal study were independent of the vector capsid injected and likely in response to eGFP. In a previous study of different AAV2 capsid variants delivered intravitreally, inflammation was also detected in some dogs and a subsequent study of peripheral blood mononuclear cells showed a robust response to eGFP but not to the capsid [94]. Immune response to the widely used reporter gene eGFP is a recognised issue [149]. As such, further studies dedicated to vector immunogenicity are needed to fully characterise AAV2.GL and AAV2.NN. In this context, the novel vectors could be further improved via rational design-based modification of immunogenic residues at the capsid surface or optimisation of the AAV genome in order to mitigate any risk of immune response [150, 151].

So far, it is unclear which receptors mediate the specific tropism of the novel variants. While the unique 7-mer peptides of AAV2.GL and AAV2.NN differ in amino-acid sequence, both end with a P-S/T-R motif. This sequence on its own or in combination with the linker sequence (AA) and additional residues of the 7-mer and/or the subsequent AAV2-VP1 sequence (RQ), could participate in specific receptor interactions. Further investigation is required to identify any unknown receptors targeted by the AAV peptide display-selected capsid variants, as previously reported [152], or determine whether the novel capsids interact with known AAV receptors AAVR [130, 153] or GPR108 [133].

6.3 *Cnga3* gene supplementation therapy with AAV2.GL

In order to expand on the eGFP reporter-based studies, the cone-favouring vector AAV2.GL was assessed in a series of preclinical studies for gene supplementation in the *Cnga3*$^{-/-}$ mouse model of achromatopsia [20]. By choosing a mouse model of cone photoreceptor degeneration, the challenge of detecting any rescue effect was greater, as cones are already limited in number in the mouse retina ($\tilde{3}$% of all photoreceptors)[154]. As such, any level of visual restoration would demonstrate that it was possible to target and revive a very scarce cell type.

The therapeutic vector AAV2.GL/mSWS-mCnga3 and a reporter vector AAV2.GL/mSWS-eGFP were delivered subretinally in 2-week-old *Cnga3*$^{-/-}$ mice, in order to investigate the potency of the novel capsid using the conventional administration route. Although ubiquitous

promoters are known to outperform cell-specific promoters [155], the cone-specific promoter SWS was able to drive high levels of cargo expression. After 6 WPI, the entire hemisphere of eyes treated with the reporter vector was eGFP$^+$ (Fig.5.22.B) indicating the vector had spread beyond the margins of the subretinal bleb. This phenomenon was also confirmed in eyes that received the therapeutic vector, as retinal sections from the quadrant (Q3) proximal to the injection site (Q2) had PNA$^+$Cnga3$^+$ cones (Fig.5.23). The functional recovery of photopic ERG responses was maintained throughout the 18-week duration of the study, though the peak of cone activity was reached at 10 WPI and gradually decreased after (Fig.5.22.C-E). As the injections were done in the nasal part of the retina, this could be apportioned to the faster cone degeneration in that locus. Indeed it has been described that naso-ventral cones are completely lost after the third postnatal month in *Cnga3*$^{-/-}$ mice [14].

Gene supplementation with AAV2.GL/mSWS-mCnga3, via the less invasive intravitreal route, was able to rescue cone responses already after 6 WPI (Fig.5.24.B-D), showing that the speed with which the vector targeted cones was not affected by the increase in physical barriers. As a result, a widespread Cnga3 expression was detected in cones across the treated retina (Fig.5.25) with a protein expression pattern and IHC-signal intensity comparable to wildtype (Fig.5.24.E). Interestingly, in this specific context, AAV2.GL was equally efficient to the state-of-art vector AAV2.7m8, as the same level of cone recovery was achieved and maintained over the study period for both vectors (Fig.5.26). Despite effective treatment, the amplitude of rescued photopic responses was an order of magnitude lower than in wildtype animals (Fig.5.24.D). Considering the wildtype-like pattern of Cnga3 protein (Fig.5.24.E) and the recovery of *Cnga3* transcripts back to wildtype levels after treatment (Fig.5.27.C), there appears to be a threshold of cone rescue achievable with gene supplementation alone. To address this possibility, achromatopsia models of larger mammals [156, 157] could be used to expand on current findings.

There are indeed many aspects of photoreceptor and retinal physiology, in the degenerative context of *Cnga3*$^{-/-}$, that are crucial for cone survival. In this form of IRD, cones lose their outer segments [14, 158] and therefore their contact with the RPE and, to some extent, Müller glia. This leads to starvation, nutritional imbalance and accumulation of reactive oxygen species as well as retinoids at toxic levels. As such, it was hypothesised that by restoring the outer segment of cones, it would be possible to re-establish their metabolic homeostasis and improve the outcome of *Cnga3* gene supplementation. To this end, the role of the miRNA cluster 96/182/183 was considered, as it was found crucial for the development and maintenance of cone photoreceptor outer segments [21]. miRNAs are a group of small RNAs that have a

broad yet temporal effect on retinal cells throughout their development and life [112, 159]. The ablation of some or all members of the miRNA-96/182/183 cluster causes severe retinal degeneration [160, 96, 97], whilst their overexpression in retinal organoids induced short outer segments [21] and reprogrammed human RPE cells into neurons [161]. As such, there could be a link between the pathways targeted by miRNA-96/182/183 and those triggered during cone recovery after *Cnga3* supplementation.

To investigate this, a selection of genes targeted by the miRNA cluster [21, 162] were first assessed in the wildtype and *Cnga3*$^{-/-}$ retina of 2-3 month old mice, showing that none were differentially expressed (Fig.5.27.A). At the same time, the baseline levels of miRNA-96/182/183 were determined in adult retinas of C57BL6/J x 129/sv mixed wildtype, *Cnga3*$^{-/-}$ (C57BL6/J x 129/sv mixed) and C57BL6/J (Fig.5.27.B); retinas from C57BL6/J were also assessed to exclude any background-related discrepancies. Of note, the mature miRNA-5p strand for each cluster member was quantified and, although retinal samples were harvested simultaneously, their levels were highly variable in all genotypes tested. This variability is a known phenomenon for miRNA-96/182/183 and other neuronal miRNA species that rapidly turnover in response to light [163].

After 18 WPI, the supplementation of *Cnga3* lead to the anticipated recovery of *Cnga3*, *Cngb3* and *Arr3* back to wildtype-like expression levels. Interestingly, this was accompanied by a significant increase of *Slc6a6*, *Dhcr24*, *Fcho2* and *Tacc1* transcripts (Fig.5.27.C) and a trending increase of miRNA-96/182/183 levels compared to untreated *Cnga3*$^{-/-}$ and wildtype retinas (Fig.5.27.D). This is the first report correlating these genes to the *Cnga3*$^{-/-}$ condition, as a previous gene expression profiling study did not identify them [15]. The accumulation of miRNA-96/182/183 likely resulted from the increase in their target transcripts *Slc6a6* (miRNA-96 and miRNA-183), *Dhcr24* (miRNA-96 and miRNA-182), *Fcho2* (miRNA-183) and *Tacc1* (miRNA-96 and miRNA-182), and suggests that cones trigger multiple pathways in their attempt to recover following *Cnga3* supplementation (Fig.6.1).

Dchr24 encodes for the 24-dehydrocholesterol reductase, an enzyme required for cholesterol biosynthesis [164], and is upregulated in retinal glia when cellular cholesterol levels are reduced [165]. In the process of photoreceptor recovery and tissue remodelling, glia populations such as microglia and Müller glia become activated, thereby increasing their requirement for cholesterol. Microglia can be either a friend or a foe during retinal healing [166, 167], but their presence is essential [41]. Anti-inflammatory strategies using Cx3cl1 [168] or TGF-β [169] have lead to improved cone survival in degenerative contexts; such approaches could be combined with *Cnga3* supplementation in future studies. *Fcho2* encodes for the F-BAR domain only protein 2,

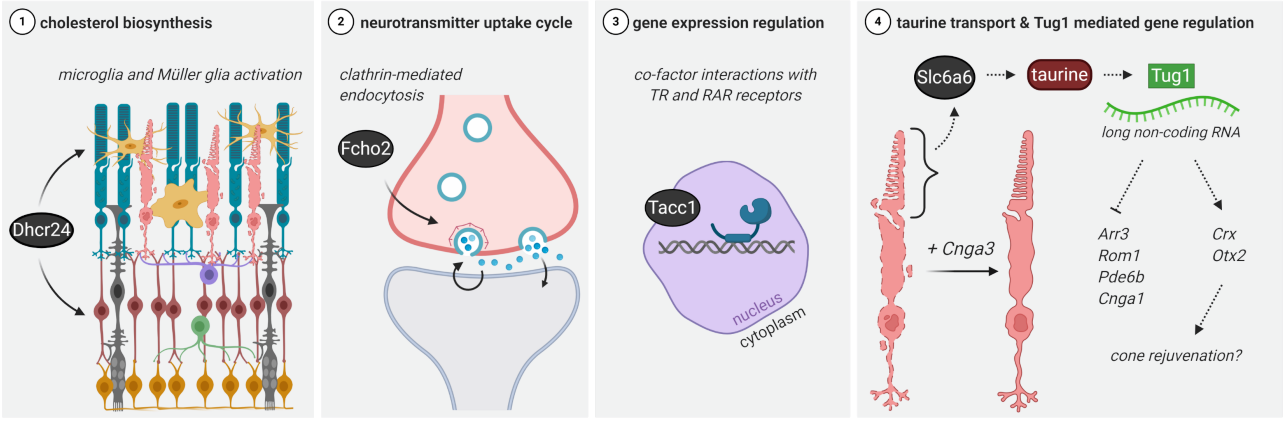

Figure 6.1: Schematic of potential mechanisms triggered during *Cnga3* supplementation to facilitate cone survival

which is required for clathrin-mediated endocytosis [170]. This process is activated during the neurotransmitter re-uptake cycle and is potentially upregulated in recovering cones that have a higher demand for glutamate recycling at their pedicles. A gene with broader effects that was upregulated after *Cnga3* treatment, is the transforming acidic coiled coil protein *Tacc1*, known as a transcriptional co-factor that interacts with several nuclear receptors including thyroid hormone receptors and retinoic-acid receptors [171]. Finally, the taurine transporter gene *Slc6a6* was upregulated in treated eyes. This factor is highly expressed in ciliated cells and is naturally upregulated in degenerating photoreceptors as it has neuroprotective effects [172, 95]. It modulates gene expression via the retinal long nonconding RNA *Tug1*, which is necessary for retinal development and upregulates early photoreceptor transcription factors Crx and Otx2 [172]. As such, recovering cones after *Cnga3* treatment likely upregulate this pathway to trigger an innate rejuvenation program.

6.4 Alternative strategies to restore vision

Inherited retinal dystrophies (IRDs) are a major cause of blindness worldwide. Of all the approaches developed to alleviate these conditions, gene supplementation therapy has so far been the most successful. By delivering the correct copy of a mutated or missing gene in affected photoreceptors, it is possible to rescue their function and/or halt their degeneration [173, 174, 175, 176]. Although gene supplementation therapy is a promising approach, it comes with several limitations that hinder its widespread application for the treatment of all patients suffering from IRDs. More than 300 genes causing various forms of IRD are known (link), and would require the development of equally many customised therapies to treat each of the

affected patient populations.

Furthermore, as gene supplementation therapy relies on the presence of viable and therefore rescuable photoreceptors, only patients with early- and mid-stage retinal degeneration are suitable candidates for treatment. This requires the early diagnosis of patients via genetic testing, which is a process subject to further optimisation that not a large patient pool may have access to. To address this, new avenues are being explored to develop gene-independent and broadly applicable therapies that can treat patients at later disease stages, when no viable photoreceptors are left.

6.4.1 Approach I: turning ON bipolar cells photosensitive

The mammalian CNS is not innately capable of regeneration. This means that irrespective of the underlying cause, photoreceptor depletion is not naturally reversible and leads to various forms of blindness. However, the retinal network that remains structurally intact in the absence of photoreceptors could be repurposed in order to regenerate light-induced responses (Fig.5.28).

Various attempts have been made to to deliver optogenetic tools to ON bipolar cells, with variable outcomes depending on the method. Different variants of the murine Grm6 promoter (mGluR6)[177, 178, 179, 180, 181, 182, 183, 184] and its human homologue [185] have been explored to drive and optimally restrict gene expression to these cells. They were used in applications such as *in vivo* electroporation [177] with adjuvant therapies to enhance transduction [183], or engineered AAV vectors [179, 186] such as AAV2.Y444F [181, 182] and AAV2.7m8 [180, 185]. Initial efforts to engineer AAVs that specifically target ON bipolar cells have been reported [179], though these relied on transgenic animals for screening, making it impossible to transpose this approach on animals evolutionarily closer to humans. The purification of ON bipolar cells for basic research has so far also relied on transgenic mouse lines [103]. Using larger mammals such as dogs and NHPs would be of more relevance to humans, however no transgenic lines or other strategies exist yet to specifically isolate ON bipolar cells from these species. This limitation holds true for other cell types in the retina as well, which has lead to the use of alternative AAV-based strategies [187]. The lack of methods for isolating ON bipolar cells is largely due to the lack of a specific cell surface marker or reliable antibodies against known membrane proteins, e.g. mGluR6. In turn, this prevents the use of methods that strictly rely on the recognition of surface antigens, e.g. magnetic-activated cell sorting.

(I) a universal method to sort ON bipolar cells

To overcome these limitations, a universal FACS protocol was developed, based on intracellular markers Goα and Pcp2, that can isolate ON bipolar cells from healthy or degenerating mouse and NHP retinas. These markers were selected for their specificity and consistency in both healthy and degenerating retinas (Fig.5.30.A). The strategy to first gate the Goα^{+} and then the Pcp2^{+} population was based on the histology profile of the antibodies, as Goα leaked in the IPL (Fig.5.30.A). A broad signal for Pcp2 was detected during FACS, which led to the hypothesis that these could be separate cell populations, i.e. Goα^{+}/Pcp2$^{+\text{high}}$ and Goα^{+}/Pcp2$^{+\text{low}}$. This distinction could reflect variable protein levels or even subtle differences within the ON bipolar cell pool that are not yet investigated. This hypothesis was also supported by the results of a single-cell RNAseq analysis of the entire mouse retina, which showed variable Pcp2 expression levels across ON bipolar subtypes, as well as detectable expression in at least one OFF bipolar subtype [103].

Following sorting of populations Goα^{+}/Pcp2$^{+\text{high}}$, Goα^{+}/Pcp2$^{+\text{low}}$ and Goα^{-}/Pcp2^{-}, RNA and gDNA was extracted from the fixed cells. A potential caveat of fixing the cells is that the quality of nucleic acids could be compromised, even after reverting the cross-links via protease K treatment. It was important therefore to investigate the impact of fixation on sensitive downstream analyses, while characterising the sorted populations. Both RNA and gDNA material were of sufficient quantity and quality to perform RNAseq, qPCR and to detect viral genomes as part of an AAV library screen. Although these methods were not compromised by the fixation step in this method, it cannot be excluded that this process may not be equally compatible with other downstream applications. As such, the identification of a specific surface marker for direct ON bipolar isolation across species remains of interest.

The consistent profile of the ON bipolar markers Goα and Pcp2 across disease states and species was crucial for the translatability of this method. An alternative combination with a generic bipolar marker that does not discriminate between ON and OFF bipolar cells, e.g. Chx10 [188, 189, 190], together with Pcp2 could have been attempted, following the general-to-specific strategy often suggested for sorting. However, the differential expression of generic markers across species could have interfered with the universal applicability of the method. As seen in the data from *Rd1* wt samples (Fig.5.31.C) and NHP (Fig.5.35.C), the purity of a sorted population can be compromised even when cell-specific markers are used. Indeed, *Rho* transcripts were detected in some Goα^{+}/Pcp2$^{+\text{high}}$ and most Goα^{+}/Pcp2$^{+\text{low}}$ populations, due to the much greater number of rod photoreceptors present in the retina compared to any other

cell type [107], which further underlines the importance of the sorting panel.

Acute cell isolation using tissue dissociation followed by cell sorting can result in severely compromised neuronal viability, given the overall mechanical strain and duration of the procedure. While the fixation step between dissociation and sorting helped preserve a high cell viability (96%) for both mouse samples, NHP cells did not survive equally well. This could be apportioned to the time between necropsy and retina isolation from the eye (approximately six hours), the sample handling or the overnight explant culture (Fig.5.34.A). The latter could be avoided by having direct access to the NHP eyes immediately after necropsy and by processing the retinas without interruption. Alternatively, immediate fixation of the dissociated cells and subsequent sorting 24 hours later could potentially minimise cell death without substantially affecting the subsequent sort.

With this method it was possible to successfully and exclusively isolate ON bipolar cells from both mice and NHPs, yet further validation using human retinal tissue remains a future task. Nevertheless, as drug-delivery tools such as viral and non-viral vectors [191] are screened using rodents and NHPs, this method has great translational potential. It is envisioned that this method could facilitate the development of next-generation, cell type-specific gene delivery or genetic engineering tools to treat late-stage retinal degeneration.

6.4.2 Approach II: manipulating cell fates

The concept of a permanent cell fate was first challenged in the 1960's when a differentiated adult cell nucleus was reverted to an undifferentiated state after it was fused with an oocyte; a process called somatic-cell nuclear transfer (SCNT) [192, 193]. Years later, reprogramming was revived by the discovery of 4 master-regulators (Oct3/4, Sox2, c-Myc, and Klf4) capable of reverting differentiated cells into pluripotent stem cells [194]. The field was further revolutionised when cells of one lineage were directly reprogrammed into that of another lineage, without requiring an intermediate stem-cell stage [195]. The direct reprogramming of fibroblasts into neurons using Ascl1, Brn2, and either Myt1l or Zic1 [195], changed the question from "can we manipulate cell fates" to "which factor combination can yield a desired cell population".

It soon became evident that various other cell types could be converted into neurons, such as astrocytes [196, 197, 198, 199], Müller glia [200, 201, 202, 203, 204], T-lymphocytes [205], urine cells [206] and microglia [113]. To achieve this, ingenious strategies have been employed using regenerative cues from other organisms [26] that are absent in mammals or switched off after development [207, 203], cell-fusion with pluripotent stem cells resembling SCNT [202] or

cocktails of small molecules that induce transcriptomic changes [196, 199, 208, 209]. A common theme across these methods is that successful conversion of one cell type into another generally requires a change in the epigenetic landscape of the target cell, i.e. DNA accessibility, histone acetylation and DNA methylation [210, 211, 212, 213, 214]; the absence of such plasticity has been shown to be detrimental for reprogramming [27, 212]. Destabilising the genome has been achieved by chemically removing epigenome blockades using the histone deacetylase inhibitor trichostatin-A [203], or by the pioneering factor alone, e.g. Ascl1 [215] or NeuroD1 [113]. As such, there are multiple recipes to reach the same or similar outcome.

Most of the reprogramming attempts have focused on regenerating neurons in the brain, whereas fewer have targeted the retina with varying results. Indeed one of the greatest challenges remains the generation of mature photoreceptors that are viable, functional and well integrated in the neuronal network. To start addressing this, in this body of work, it was first hypothesised that the ideal targets for direct reprogramming into photoreceptors would be bipolar cells, as both cell types originate from the same Otx2$^+$ precursors and only diverge into separate populations by the transient expression of Prdm1 [216, 217]. Even if successful, this approach would have no therapeutic potential as it would deprive one vital cell population to replenish another. Instead, considering the detrimental effects of rogue microglia in the degenerating retina, it was hypothesised that microglia would be a better target.

(II) reprogramming microglia *in vitro*

A small collection of pioneering neurogenic factors and master-regulators of photoreceptor development were selected for testing in microglia, namely NeuroD1 [113, 218], Ascl1 [219, 203], Ngn2 [220], Rax [221], Crx [222, 223, 224] and Prdm1 [216, 217] (Fig.5.36). These factors were packed into lentiviral vectors under the control of a strong ubiquitous promoter (CAG) and used to infect microglia *in vitro* (Fig.5.38). The first proof-of-concept study was able to reproduce the microglia-to-neuron conversion previously reported [113] by overexpressing NeuroD1 in cortical microglia (Fig.5.39). Converted cells were identified by their co-expression of the lentiviral construct reporter mCherry, together with cell-specific markers indicating what the newly formed Tuj1$^+$ neuron used to be, i.e. microglia when traces of Iba1 were detected (Fig.5.39.D). To unequivocally report reprogramming events, a more suitable *in vitro* system would be to use cells with intrinsic reporters, so that fluorescently labelled microglia could be imaged live as they change fate. This would require a transgenic mouse line, as cell source for the *in vitro* culture, that would express one fluorophore under the control of a microglia-specific

promoter (e.g. Cx3cr1 [225, 226]) and another under a photoreceptor-precursor promoter (e.g. Crx), or an earlier neuronal promoter (e.g. NeuroD1).

Subsequent testing of NeuroD1 overexpression in retinal microglia had encouraging outcomes, with reprogrammed neurons emerging after only 7 DIV, albeit with immature morphological features such as multiple processes and bulky somata (Fig.5.40.B), unlike native mature Tuj1$^+$ neurons (Fig.5.37.B). The co-delivery of NeuroD1 with Rax, Crx and Prdm1 did not change the effects seen by NeuroD1 alone (Fig.5.40.C-D). This could be apportioned to the minimalistic 2D environment and short culturing period, as cells may have needed longer to use photoreceptor-specific transcription factors. Only the combination of multiple neurogenic factors lead to better-formed neurons (Fig.5.41.A), however most reprogramming events were incomplete (Fig.5.42.B) and the converted cells were seemingly attacked by surrounding microglia (Fig.5.42.B), making it impossible to estimate the reprogramming yield.

(II) reprogramming microglia *in vivo* using NeuroD1

To gain some insight into retinal microglia reprogramming *in vivo*, a first pilot study could be performed using the Ai14 transgenic mouse line and the pioneer factor NeuroD1, given its ability to single-handedly reprogram cortical microglia [113]. To this end, lentiviral vectors would be replaced by rAAV, as the latter outperform the former with regard to retinal transduction. The novel vector AAV2.GL could be used based on its broad potency in the retina. To trigger retinal microglia reprogramming, AAV2.GL would be packaged with the coding sequences of NeuroD1 and Cre, under the control of a CD68 promoter [227] and injected subretinally in Ai14 eyes. The retinal detachment during subretinal injection would trigger a desirable glia activation and microglia infiltration, which could be complemented with additional injuries such as retinal puncture wounds to increase the localisation of microglia, thereby increasing the target cell population. It is important to note that activated microglia have a different receptor expression on their surface than dormant cells [228], thereby altering their susceptibility to receptor-mediated viral entry. Transduced cells would be traced *in vivo* as a result of Cre-dependent TdTomato expression (Fig.6.2), with the assumptions that the CD68 promoter would limit expression only in microglia and that Cre expression would be limited only to transduced cells. Although the mouse line provider warns about some Cre-independent TdTomato background (link), the vector-mediated TdTomato signal could be monitored *in vivo* with fundus fluorescence imaging and subsequent histological analyses. Should the promoter and vector combination lead to unspecific expression in non-microglia cells or show only limited

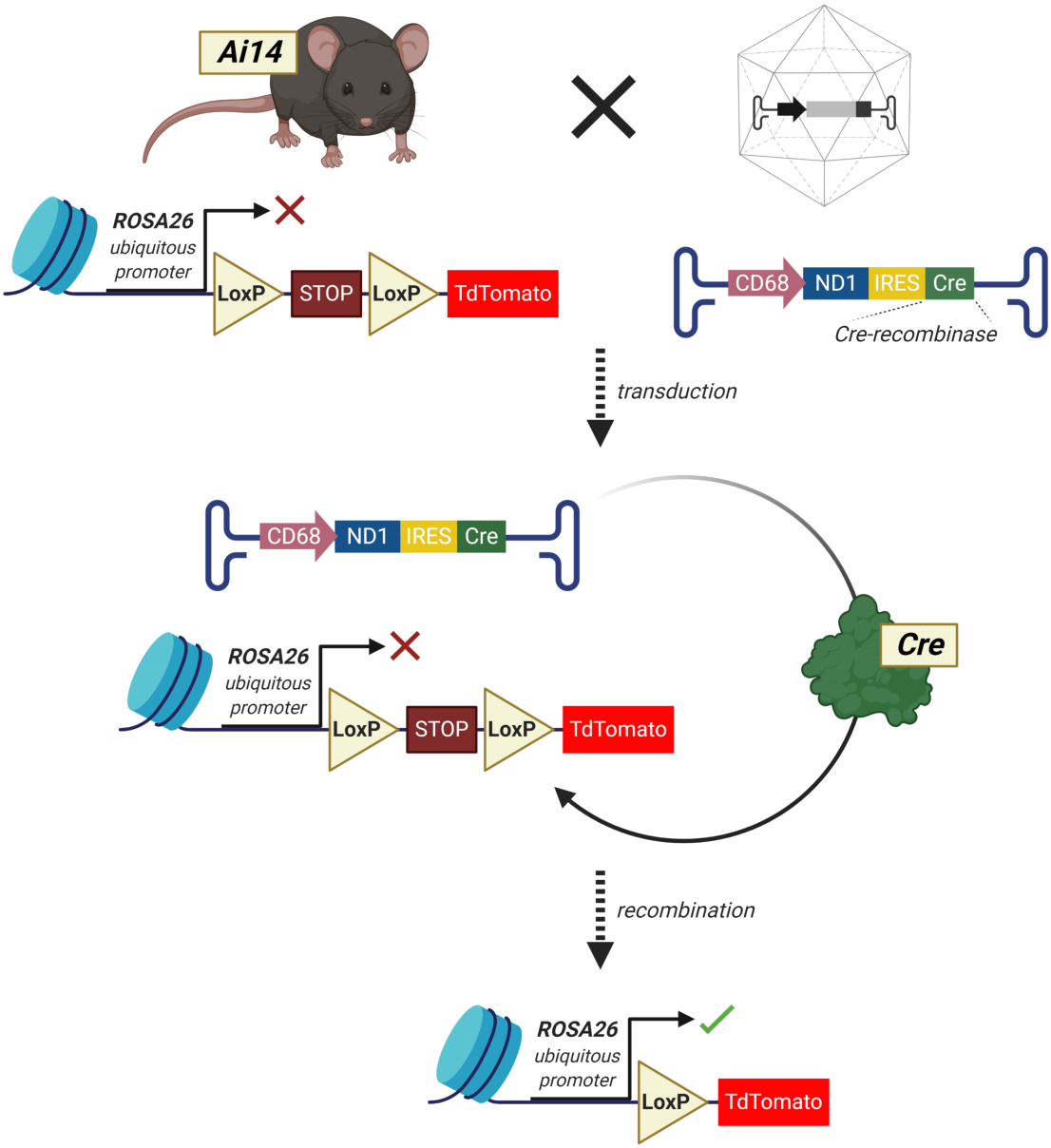

Figure 6.2: *in vivo* system for reprogramming glia into neurons

expression in microglia, alternatives could be investigated, particularly since there is increased scepticism about the interpretation of reprogramming outcomes in the retina [229]. Previous work assessing all natural AAV serotypes showed none were permissive in microglia, except for an engineered AAV6 variant (Y731F/Y705F/T492V) that was able to efficiently and selectively transduce microglia *in vitro* using microglia-specific promoters (F4/80 or CD68)[53]. Indeed the specific targeting of microglia remains a challenge, as $\leq$20% transduction has been reported *in vivo* from studies in the brain [228], where microglia are even more abundant than in the retina. This means there is still need for research on improving the AAV targeting of microglia *in vivo*. For exogenous NeuroD1 expression, a different vector such as AAV6 variant Y731F/Y705F/T492V or a different microglia-specific promoter (F4/80) could be tested for the

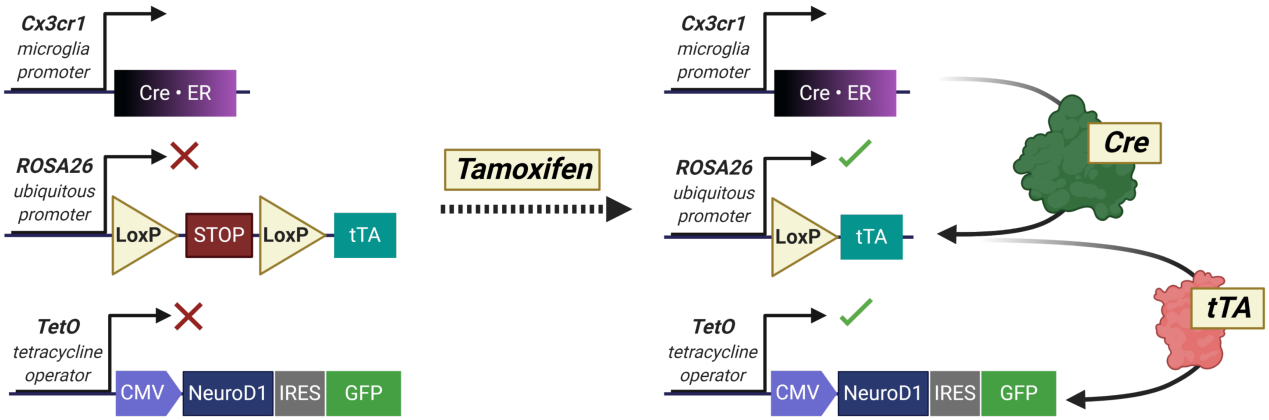

Figure 6.3: Schematic illustration of a transgenic mouse line with dual check-point inducible NeuroD1 expression; Cre • ER: fusion Cre-recombinase with mouse oestrogen receptor 1, tTA: tetracycline-controlled transactivator

restricted expression only in microglia [53]. Each AAV capsid and promoter combination should be tested for exclusive microglia expression, since capsid-promoter interactions can alter the cell-specificity of AAVs in the CNS [230]. For truly robust conclusions, a transgenic mouse line could be used that ensures tight control over transgene expression and restricts issues caused by the Cre/lox system [231]. To this end, a model of tamoxifen-inducible Cre-recombinase expression under a microglia-specific promoter that activates a tetracycline response element [232] driving NeuroD1, would be ideal (Fig.6.3).

Summary

Taken together, this work has delivered a series of optimised therapeutic strategies for the treatment of retinal degeneration at different stages of the disease (Fig.3.7). Two novel potent AAV capsid variants were introduced that expand our current toolbox for gene delivery in research and clinical application. Efficient gene delivery via the intravitreal route has significant clinical implications, as clinical trials could expand patient recruitment to non-specialised centres, making treatment more accessible. In addition to applications for gene therapy of IRDs, the widespread retinal transduction properties of AAV2.GL and AAV2.NN render them optimal vectors for therapies against more common or acquired retinal disorders like age-related macular degeneration, diabetic macular oedema or diabetic retinopathy. Making intravitreal gene delivery a common practice, by using capsids like AAV2.GL and AAV2.NN, could revolutionise the therapeutic impact and accessibility to gene therapy for patients with inherited or acquired retinal dystrophies. To demonstrate this translational potential with a preclinical disease model, it was shown that AAV2.GL successfully delivered the *Cnga3* gene in an established mouse model of achromatopsia (*Cnga3*$^{-/-}$), following intravitreal administration. This lead to both the rescue of cone photoreceptor function and a change in the molecular profile of treated retinas towards a rejuvenated state. With this, it was possible to obtain a first glimpse into the global changes caused during gene supplementation therapy, thus paving the way for further investigation of how best to rescue cones in achromatopsia patients. For patients at the late-stages of retinal degeneration, this work provided insight into two alternative strategies that could overcome the complete loss of photoreceptors. Specifically, a universal protocol for isolating ON bipolar cells was developed that can advance the targeted delivery of optogenetic tools in the retina, in order to equip the remaining ON circuit with photosensing abilities. Moreover, initial efforts were described for directly reprogramming retinal microglia into neurons, which highlighted potential pitfalls and gave promising outcomes due for optimisation.

In sum, this thesis places a stone to the wider edifice of the retina regeneration field.

Declaration of author contributions

Directed evolution of novel vectors for intravitreal gene delivery

Prof. Dr. Hildegard Büning and team (Hannover Medical School) prepared the AAV library, performed NGS and the *in vitro* characterisation of novel capsids. Prof. Dr. Stylianos Michalakis and Dr. Christian Schön (LMU) performed library screens in mice and the initial human explant cultures. The *in vivo* large animal studies (dog, NHP) were performed by Prof. Dr. Simon Petersen-Jones and team (Michigan State University).

A universal protocol for isolating ON bipolar cells

Dr. Lisa Richter and Dr. Neda Tafrishi from the Core Facility Flow Cytometry (Biomedical Centre, LMU) performed the cell sorting. RNA sequencing using RNA from sorted cell populations was performed by Dr. Robert Lucas and team (University of Manchester) and Dr. Rachel Scholey (University of Manchester) performed the subsequent data analysis. The plots comparing RNAseq data of sorted populations to single cell RNAseq databases using the Single Cell Portal of the Broad Institute were prepared by Dr. Elisa Murenu. The NHP injections were performed by Dr. Jasmina Cehajic-Kapetanovic (University of Oxford) at the Covance Preclinical Services test facility in Münster, Germany. The detection of AAV genomes from sorted populations was done by Prof. Dr. Dirk Grimm and team (University of Heidelberg).

Publications

M. Pavlou, C. Schön, L. M. Ocelli, A. Rossi, N. Meumann, R. F. Boyd, J. T. Bartoe, J. Siedlecki, M. J. Gerhardt, S. Babutzka, J. Bogedein, J. E. Wagner, S. G. Priglinger, M. Biel, S. M. Petersen-Jones, H. Büning†, S. Michalakis†, "Novel AAV capsids for intravitreal gene therapy of photoreceptor disorders", *EMBO Molecular Medicine*, pp. e13392, feb 2021

E. Murenu*, **M. Pavlou***, L. Richer, K. Rapti, S. Just, J. Cehajic-Kapetanovic, N. Tafrishi, A. Hayes, R. Scholey, R. Lucas, H. Büning, D. Grimm, S. Michalakis†, "A universal protocol for isolating retinal ON bipolar cells across species via fluorescence-activated cell sorting", *Molecular Therapy - Methods & Clinical Development*, vol. 20, pp. 587-600, jan 2021

M. Völkner, **M. Pavlou**, H. Büning, S. Michalakis†, M. O. Karl†, "Optimized adeno-associated virus vectors for efficient transduction of human retinal organoids", *Human Gene Therapy*, accepted

A. L. Panagiotopoulos, N. Karguth, **M. Pavlou**, S. Böhm, G. Gasparoni, J. Walter, A. Graf, H. Blum, M. Biel, L. M. Riedmayr†, E. Becirovic†, "Antisense Oligonucleotide- and CRISPR-Cas9-Mediated Rescue of mRNA Splicing for a Deep Intronic CLRN1 Mutation", *Molecular Therapy - Nucleic Acids*, vol. 21, pp. 10501061, sep 2020

M. Pavlou, M, Shah, P. Gikas, T. Briggs, S. J. Roberts†, U. Cheema†, "Osteomimetic matrix components alter cell migration and drug response in a 3D tumour-engineered osteosarcoma model", *Acta Biomaterialia*, vol. 96, pp. 247-257, sep 2019

P. A. Redondo, **M. Pavlou**, M. Loizidou, U. Cheema†, "Elements of the niche for adult stem cell expansion", *Journal of Tissue Engineering*, vol. 8, pp. 1-18, aug 2017

* these authors contributed equally

† corresponding authors

Bibliography

[1] R. F. Schmidt, F. Lang, and M. Heckmann, eds., *Physiologie des Menschen*. Springer-Lehrbuch, Berlin, Heidelberg: Springer Berlin Heidelberg, 2011.

[2] S. Veleri, C. H. Lazar, B. Chang, P. A. Sieving, E. Banin, and A. Swaroop, "Biology and therapy of inherited retinal degenerative disease: Insights from mouse models," *DMM Disease Models and Mechanisms*, vol. 8, pp. 109–129, feb 2015.

[3] R. H. Masland, "The Neuronal Organization of the Retina," *Neuron*, vol. 76, pp. 266–280, oct 2012.

[4] T. Baden, T. Euler, and P. Berens, "Understanding the retinal basis of vision across species," *Nature Reviews Neuroscience*, vol. 21, pp. 5–20, jan 2020.

[5] J. R. Sanes and R. H. Masland, "The Types of Retinal Ganglion Cells: Current Status and Implications for Neuronal Classification," *Annual Review of Neuroscience*, vol. 38, pp. 221–246, jul 2015.

[6] A. J. Emanuel and M. T. H. Do, "Melanopsin tristability for sustained and broadband phototransduction," *Neuron*, vol. 85, pp. 1043–1055, mar 2015.

[7] R. H. Masland, "The tasks of amacrine cells," *Visual Neuroscience*, vol. 29, pp. 3–9, jan 2012.

[8] T. Euler, S. Haverkamp, T. Schubert, and T. Baden, "Retinal bipolar cells: Elementary building blocks of vision," *Nature Reviews Neuroscience*, vol. 15, pp. 507–519, jul 2014.

[9] J. Sparrrow, D. Hicks, and C. Hamel, "The Retinal Pigment Epithelium in Health and Disease," *Current Molecular Medicine*, vol. 10, pp. 802–823, dec 2010.

[10] F. Mazzoni, H. Safa, and S. C. Finnemann, "Understanding photoreceptor outer segment phagocytosis: Use and utility of RPE cells in culture," *Experimental Eye Research*, vol. 126, pp. 51–60, 2014.

[11] R. Bachmann-Gagescu and S. C. Neuhauss, "The photoreceptor cilium and its diseases," *Current Opinion in Genetics and Development*, vol. 56, pp. 22–33, jun 2019.

[12] R. H. Masland, "The fundamental plan of the retina," *Nature Neuroscience*, vol. 4, no. 9, pp. 877–886, 2001.

[13] F. M. Nadal-Nicolás, V. P. Kunze, J. M. Ball, B. T. Peng, A. Krisnan, G. Zhou, L. Dong, and W. Li, "True S-cones are concentrated in the ventral mouse retina and wired for color detection in the upper visual field," *eLife*, vol. 9, pp. 1–30, may 2020.

[14] S. Michalakis, H. Geiger, S. Haverkamp, F. Hofmann, A. Gerstner, and M. Biel, "Impaired opsin targeting and cone photoreceptor migration in the retina of mice lacking the cyclic nucleotide-gated channel CNGA3," *Investigative Ophthalmology and Visual Science*, vol. 46, pp. 1516–1524, apr 2005.

[15] H. Ma, A. Thapa, L. M. Morris, S. Michalakis, M. Biel, M. B. Frank, M. Bebak, and X. Q. Ding, "Loss of cone cyclic nucleotide-gated channel leads to alterations in light response modulating system and cellular stress response pathways: A gene expression profiling study," *Human Molecular Genetics*, vol. 22, pp. 3906–3919, oct 2013.

[16] S. Kohl, D. Zobor, W. C. Chiang, N. Weisschuh, J. Staller, I. G. Menendez, S. Chang, S. C. Beck, M. G. Garrido, V. Sothilingam, M. W. Seeliger, F. Stanzial, F. Benedicenti, F. Inzana, E. Héon, A. Vincent, J. Beis, T. M. Strom, G. Rudolph, S. Roosing, A. I. Hollander, F. P. Cremers, I. Lopez, H. Ren, A. T. Moore, A. R. Webster, M. Michaelides, R. K. Koenekoop, E. Zrenner, R. J. Kaufman, S. H. Tsang, B. Wissinger, and J. H. Lin, "Mutations in the unfolded protein response regulator ATF6 cause the cone dysfunction disorder achromatopsia," *Nature Genetics*, vol. 47, pp. 757–765, jun 2015.

[17] M. H. Remmer, N. Rastogi, M. P. Ranka, and E. J. Ceisler, "Achromatopsia," *Current Opinion in Ophthalmology*, vol. 26, pp. 333–340, jul 2015.

[18] S. Michalakis, E. Becirovic, and M. Biel, "Retinal cyclic nucleotide-gated channels: From pathophysiology to therapy," *International Journal of Molecular Sciences*, vol. 19, p. 749, mar 2018.

[19] J. P. Greenberg, J. Sherman, S. A. Zweifel, R. W. Chen, T. Duncker, S. Kohl, B. Baumann, B. Wissinger, L. A. Yannuzzi, and S. H. Tsang, "Spectral-domain optical coherence tomography staging and autofluorescence imaging in achromatopsia," *JAMA Ophthalmology*, vol. 132, no. 4, pp. 437–445, 2014.

[20] M. Biel, M. Seeliger, A. Pfeifer, K. Kohler, A. Gerstner, A. Ludwig, G. Jaissle, S. Fauser, E. Zrenner, and F. Hofmann, "Selective loss of cone function in mice lacking the cyclic nucleotide-gated channel CNG3," *Proceedings of the National Academy of Sciences*, vol. 96, pp. 7553–7557, jun 1999.

[21] V. Busskamp, J. Krol, D. Nelidova, J. Daum, T. Szikra, B. Tsuda, J. Jüttner, K. Farrow, B. G. Scherf, C. P. P. Alvarez, C. Genoud, V. Sothilingam, N. Tanimoto, M. Stadler, M. Seeliger, M. Stoffel, W. Filipowicz, and B. Roska, "MiRNAs 182 and 183 Are Necessary to Maintain Adult Cone Photoreceptor Outer Segments and Visual Function," *Neuron*, vol. 83, pp. 586–600, aug 2014.

[22] S. Michalakis, R. Mühlfriedel, N. Tanimoto, V. Krishnamoorthy, S. Koch, M. D. Fischer, E. Becirovic, L. Bai, G. Huber, S. C. Beck, E. Fahl, H. Büning, F. Paquet-Durand, X. Zong, T. Gollisch, M. Biel, and M. W. Seeliger, "Restoration of cone vision in the CNGA3-/- mouse model of congenital complete lack of cone photoreceptor function," *Molecular Therapy*, vol. 18, no. 12, pp. 2057–2063, 2010.

[23] J. jing Pang, W. T. Deng, X. Dai, B. Lei, D. Everhart, Y. Umino, J. Li, K. Zhang, S. Mao, S. L. Boye, L. Liu, V. A. Chiodo, X. Liu, W. Shi, Y. Tao, B. Chang, and W. W. Hauswirth, "AAV-mediated cone rescue in a naturally occurring mouse model of CNGA3-achromatopsia," *PLoS ONE*, vol. 7, no. 4, 2012.

[24] S. J. Gasparini, S. Llonch, O. Borsch, and M. Ader, "Transplantation of photoreceptors into the degenerative retina: Current state and future perspectives," *Progress in Retinal and Eye Research*, vol. 69, pp. 1–37, mar 2019.

[25] G. J. Chader, "Degenerative Retinopathies," in *Ocular Therapeutics*, ch. 20, pp. 443–472, Elsevier Ltd, jan 2008.

[26] D. Goldman, "Müller glial cell reprogramming and retina regeneration," *Nature Reviews Neuroscience*, vol. 15, pp. 431–442, jun 2014.

[27] Y. Lu, B. Brommer, X. Tian, A. Krishnan, M. Meer, C. Wang, D. L. Vera, Q. Zeng, D. Yu, M. S. Bonkowski, J.-H. Yang, S. Zhou, E. M. Hoffmann, M. M. Karg, M. B. Schultz, A. E. Kane, N. Davidsohn, E. Korobkina, K. Chwalek, L. A. Rajman, G. M. Church, K. Hochedlinger, V. N. Gladyshev, S. Horvath, M. E. Levine, M. S. Gregory-Ksander, B. R. Ksander, Z. He, and D. A. Sinclair, "Reprogramming to recover youthful epigenetic information and restore vision," *Nature*, vol. 588, pp. 124–129, dec 2020.

[28] M. P. Simunovic, W. Shen, J. Y. Lin, D. A. Protti, L. Lisowski, and M. C. Gillies, "Optogenetic approaches to vision restoration," *Experimental Eye Research*, vol. 178, pp. 15–26, jan 2019.

[29] S. Thompson, F. R. Blodi, S. Lee, C. R. Welder, R. F. Mullins, B. A. Tucker, S. F. Stasheff, and E. M. Stone, "Photoreceptor cells with profound structural deficits can support useful vision in mice," *Investigative Ophthalmology and Visual Science*, vol. 55, pp. 1859–1866, feb 2014.

[30] J. A. Brzezinski and T. A. Reh, "Photoreceptor cell fate specification in vertebrates," *Development (Cambridge, England)*, vol. 142, no. 19, pp. 3263–73, 2015.

[31] J. M. Daum, Ö. Keles, S. J. Holwerda, H. Kohler, F. M. Rijli, M. Stadler, and B. Roska, "The formation of the light-sensing compartment of cone photoreceptors coincides with a transcriptional switch," *eLife*, vol. 6, 2017.

[32] A. F. Olena and J. G. Patton, "Genomic organization of microRNAs," *Journal of Cellular Physiology*, vol. 222, pp. 540–545, mar 2010.

[33] G. M. Borchert, W. Lanier, and B. L. Davidson, "RNA polymerase III transcribes human microRNAs," *Nature Structural & Molecular Biology*, vol. 13, no. 12, 2006.

[34] S. Lumayag, C. E. Haldin, N. J. Corbett, K. J. Wahlin, C. Cowan, S. Turturro, P. E. Larsen, B. Kovacs, P. D. Witmer, D. Valle, D. J. Zack, D. A. Nicholson, and S. Xu, "Inactivation of the microRNA-183/96/182 cluster results in syndromic retinal degeneration," *Proceedings of the National Academy of Sciences*, vol. 110, pp. E507–E516, feb 2013.

[35] I. Trapani and A. Auricchio, "Seeing the Light after 25 Years of Retinal Gene Therapy," *Trends in Molecular Medicine*, vol. 24, pp. 669–681, aug 2018.

[36] S. D. Klapper, A. Swiersy, E. Bamberg, and V. Busskamp, "Biophysical properties of optogenetic tools and their application for vision restoration approaches," *Frontiers in Systems Neuroscience*, vol. 10, p. 74, sep 2016.

[37] J. B. Demb and J. H. Singer, "Functional Circuitry of the Retina," *Annual Review of Vision Science*, vol. 1, no. 1, pp. 263–289, 2015.

[38] K. A. Martemyanov and A. P. Sampath, "The Transduction Cascade in Retinal ON-Bipolar Cells: Signal Processing and Disease," *Annual Review of Vision Science*, vol. 3, pp. 25–51, sep 2017.

[39] J. E. Burda and M. V. Sofroniew, "Reactive gliosis and the multicellular response to CNS damage and disease," *Neuron*, vol. 81, pp. 229–248, jan 2014.

[40] F. Li, D. Jiang, and M. A. Samuel, "Microglia in the developing retina," *Neural Development*, vol. 14, pp. 1–13, dec 2019.

[41] K. Rashid, I. Akhtar-Schaefer, and T. Langmann, "Microglia in retinal degeneration," *Frontiers in Immunology*, vol. 10, 2019.

[42] Y. Huang, Z. Xu, S. Xiong, G. Qin, F. Sun, J. Yang, T.-F. Yuan, L. Zhao, K. Wang, Y.-X. Liang, L. Fu, T. Wu, K.-F. So, Y. Rao, and B. Peng, "Dual extra-retinal origins of microglia in the model of retinal microglia repopulation," *Cell Discovery*, vol. 4, p. 9, dec 2018.

[43] E. Hastie and R. J. Samulski, "Adeno-Associated Virus at 50: A Golden Anniversary of Discovery, Research, and Gene Therapy Success - A Personal Perspective," *Human Gene Therapy*, vol. 26, pp. 257–265, may 2015.

[44] R. J. Samulski, K. I. Berns, M. Tan, and N. Muzyczka, "Cloning of adeno-associated virus into pBR322: Rescue of intact virus from the recombinant plasmid in human cells," *Proceedings of the National Academy of Sciences*, vol. 79, no. 6 I, pp. 2077–2081, 1982.

[45] P.-J. Xiao and R. J. Samulski, "Cytoplasmic Trafficking, Endosomal Escape, and Perinuclear Accumulation of Adeno-Associated Virus Type 2 Particles Are Facilitated by Microtubule Network," *Journal of Virology*, vol. 86, pp. 10462–10473, oct 2012.

[46] A.-M. Douar, K. Poulard, D. Stockholm, and O. Danos, "Intracellular Trafficking of Adeno-Associated Virus Vectors: Routing to the Late Endosomal Compartment and Proteasome Degradation," *Journal of Virology*, vol. 75, pp. 1824–1833, feb 2001.

[47] F. Sonntag, S. Bleker, B. Leuchs, R. Fischer, and J. A. Kleinschmidt, "Adeno-Associated Virus Type 2 Capsids with Externalized VP1/VP2 Trafficking Domains Are Generated prior to Passage through the Cytoplasm and Are Maintained until Uncoating Occurs in the Nucleus," *Journal of Virology*, vol. 80, pp. 11040–11054, nov 2006.

[48] F. K. Ferrari, T. Samulski, T. Shenk, and R. J. Samulski, "Second-strand synthesis is a rate-limiting step for efficient transduction by recombinant adeno-associated virus vectors.," *Journal of virology*, vol. 70, no. 5, pp. 3227–3234, 1996.

[49] M. Penaud-Budloo, C. Le Guiner, A. Nowrouzi, A. Toromanoff, Y. Chérel, P. Chenuaud, M. Schmidt, C. von Kalle, F. Rolling, P. Moullier, and R. O. Snyder, "Adeno-Associated

Virus Vector Genomes Persist as Episomal Chromatin in Primate Muscle," *Journal of Virology*, vol. 82, pp. 7875–7885, aug 2008.

[50] A. Westhaus, M. Cabanes-Creus, A. Rybicki, G. Baltazar, R. G. Navarro, E. Zhu, M. Drouyer, M. Knight, R. F. Albu, B. H. Ng, P. Kalajdzic, M. Kwiatek, K. Hsu, G. Santilli, W. Gold, B. Kramer, A. Gonzalez-Cordero, A. J. Thrasher, I. E. Alexander, and L. Lisowski, "High-Throughput in Vitro, Ex Vivo, and in Vivo Screen of Adeno-Associated Virus Vectors Based on Physical and Functional Transduction," *Human Gene Therapy*, vol. 31, pp. 575–589, may 2020.

[51] A. Srivastava, "In vivo tissue-tropism of adeno-associated viral vectors," *Current Opinion in Virology*, vol. 21, pp. 75–80, dec 2016.

[52] D. Grimm and S. Zolotukhin, "E Pluribus Unum: 50 Years of Research, Millions of Viruses, and One Goal-Tailored Acceleration of AAV Evolution," *Molecular Therapy*, vol. 23, no. 12, pp. 1819–1831, 2015.

[53] A. M. Rosario, P. E. Cruz, C. Ceballos-Diaz, M. R. Strickland, Z. Siemienski, M. Pardo, K. L. Schob, A. Li, G. V. Aslanidi, A. Srivastava, T. E. Golde, and P. Chakrabarty, "Microglia-specific targeting by novel capsid-modified AAV6 vectors," *Molecular Therapy - Methods and Clinical Development*, vol. 3, 2016.

[54] F. M. Mowat, K. R. Gornik, A. Dinculescu, S. L. Boye, W. W. Hauswirth, S. M. Petersen-Jones, and J. T. Bartoe, "Tyrosine capsid-mutant AAV vectors for gene delivery to the canine retina from a subretinal or intravitreal approach," *Gene Ther*, vol. 21, no. 1, pp. 96–105, 2014.

[55] D. Dalkara, L. C. Byrne, R. R. Klimczak, M. Visel, L. Yin, W. H. Merigan, J. G. Flannery, and D. V. Schaffer, "In vivo-directed evolution of a new adeno-associated virus for therapeutic outer retinal gene delivery from the vitreous," *Sci Transl Med*, vol. 5, no. 189, p. 189ra76, 2013.

[56] D. Grimm, J. S. Lee, L. Wang, T. Desai, B. Akache, T. A. Storm, and M. A. Kay, "In vitro and in vivo gene therapy vector evolution via multispecies interbreeding and retargeting of adeno-associated viruses.," *Journal of virology*, vol. 82, pp. 5887–911, jun 2008.

[57] M. Jang, S. E. Lee, and I.-H. Cho, "Adeno-Associated Viral Vector Serotype DJ-Mediated Overexpression of N171-82Q-Mutant Huntingtin in the Striatum of Juvenile Mice Is a New

Model for Huntington's Disease," *Frontiers in Cellular Neuroscience*, vol. 12, p. 157, jun 2018.

[58] K. Y. Chan, M. J. Jang, B. B. Yoo, A. Greenbaum, N. Ravi, W. L. Wu, L. Sánchez-Guardado, C. Lois, S. K. Mazmanian, B. E. Deverman, and V. Gradinaru, "Engineered AAVs for efficient noninvasive gene delivery to the central and peripheral nervous systems," *Nature Neuroscience*, vol. 20, pp. 1172–1179, aug 2017.

[59] D. G. R. Tervo, B. Y. Hwang, S. Viswanathan, T. Gaj, M. Lavzin, K. D. Ritola, S. Lindo, S. Michael, E. Kuleshova, D. Ojala, C. C. Huang, C. R. Gerfen, J. Schiller, J. T. Dudman, A. W. Hantman, L. L. Looger, D. V. Schaffer, and A. Y. Karpova, "A Designer AAV Variant Permits Efficient Retrograde Access to Projection Neurons," *Neuron*, vol. 92, pp. 372–382, oct 2016.

[60] S. Russell, J. Bennett, J. A. Wellman, D. C. Chung, Z. F. Yu, A. Tillman, J. Wittes, J. Pappas, O. Elci, S. McCague, D. Cross, K. A. Marshall, J. Walshire, T. L. Kehoe, H. Reichert, M. Davis, L. Raffini, L. A. George, F. P. Hudson, L. Dingfield, X. Zhu, J. A. Haller, E. H. Sohn, V. B. Mahajan, W. Pfeifer, M. Weckmann, C. Johnson, D. Gewaily, A. Drack, E. Stone, K. Wachtel, F. Simonelli, B. P. Leroy, J. F. Wright, K. A. High, and A. M. Maguire, "Efficacy and safety of voretigene neparvovec (AAV2-hRPE65v2) in patients with RPE65-mediated inherited retinal dystrophy: a randomised, controlled, open-label, phase 3 trial," *The Lancet*, vol. 390, no. 10097, pp. 849–860, 2017.

[61] S. L. Boye, S. Choudhury, S. Crosson, G. Di Pasquale, S. Afione, R. Mellen, V. Makal, K. R. Calabro, D. Fajardo, J. Peterson, H. Zhang, M. T. Leahy, C. K. Jennings, J. A. Chiorini, R. F. Boyd, and S. E. Boye, "Novel AAV44.9-Based Vectors Display Exceptional Characteristics for Retinal Gene Therapy," *Mol Ther*, vol. 28, no. 6, pp. 1464–1478, 2020.

[62] H. Khabou, M. Garita-Hernandez, A. Chaffiol, S. Reichman, C. Jaillard, E. Brazhnikova, S. Bertin, V. Forster, M. Desrosiers, C. Winckler, O. Goureau, S. Picaud, J. Duebel, J.-A. Sahel, and D. Dalkara, "Noninvasive gene delivery to foveal cones for vision restoration.," *JCI insight*, vol. 3, jan 2018.

[63] D. G. Gibson, "Enzymatic assembly of overlapping DNA fragments," in *Methods in Enzymology*, vol. 498, pp. 349–361, Academic Press Inc., 2011.

[64] J. Schindelin, I. Arganda-Carreras, E. Frise, V. Kaynig, M. Longair, T. Pietzsch, S. Preibisch, C. Rueden, S. Saalfeld, B. Schmid, J.-Y. Tinevez, D. J. White, V. Harten-

stein, K. Eliceiri, P. Tomancak, and A. Cardona, "Fiji: an open-source platform for biological-image analysis.," *Nature methods*, vol. 9, pp. 676–82, jul 2012.

[65] Y. Fei and T. E. Hughes, "Transgenic expression of the jellyfish green fluorescent protein in the cone photoreceptors of the mouse," *Vis Neurosci*, vol. 18, no. 4, pp. 615–623, 2001.

[66] R. Mühlfriedel, S. Michalakis, M. Garcia Garrido, M. Biel, and M. W. Seeliger, "Optimized technique for subretinal injections in mice," *Methods Mol Biol*, vol. 935, pp. 343–349, 2013.

[67] F. M. Mowat, K. R. Gornik, A. Dinculescu, S. L. Boye, W. W. Hauswirth, S. M. Petersen-Jones, and J. T. Bartoe, "Tyrosine capsid-mutant AAV vectors for gene delivery to the canine retina from a subretinal or intravitreal approach," *Gene Therapy*, vol. 21, pp. 96–105, jan 2014.

[68] C. Schön, S. Asteriti, S. Koch, V. Sothilingam, M. Garcia Garrido, N. Tanimoto, J. Herms, M. W. Seeliger, L. Cangiano, M. Biel, and S. Michalakis, "Loss of HCN1 enhances disease progression in mouse models of CNG channel-linked retinitis pigmentosa and achromatopsia," *Hum Mol Genet*, vol. 25, no. 6, pp. 1165–1175, 2016.

[69] A. Rossi, L. Dupaty, L. Aillot, L. Zhang, C. Gallien, M. Hallek, M. Odenthal, S. Adriouch, A. Salvetti, and H. Büning, "Vector uncoating limits adeno-associated viral vector-mediated transduction of human dendritic cells and vector immunogenicity," *Scientific Reports*, 2019.

[70] A. Girod, M. Ried, C. Wobus, H. Lahm, K. Leike, J. Kleinschmidt, G. Deleage, and M. Hallek, "Genetic capsid modifications allow efficient re-targeting of adeno-associated virus type 2," *Nat Med*, vol. 5, no. 12, p. 1438, 1999.

[71] S. A. Nicklin, H. Büning, K. L. Dishart, M. de Alwis, A. Girod, U. Hacker, A. J. Thrasher, R. R. Ali, M. Hallek, and A. H. Baker, "Efficient and selective AAV2-mediated gene transfer directed to human vascular endothelial cells," *Mol Ther*, vol. 4, no. 3, pp. 174–181, 2001.

[72] E. Becirovic, S. Böhm, O. N. P. Nguyen, L. M. Riedmayr, V. Hammelmann, C. Schön, E. S. Butz, C. Wahl-Schott, M. Biel, and S. Michalakis, "AAV Vectors for FRET-Based Analysis of Protein-Protein Interactions in Photoreceptor Outer Segments," *Frontiers in Neuroscience*, vol. 10, no. July, pp. 1–13, 2016.

[73] U. T. Hacker, L. Wingenfeld, D. M. Kofler, N. K. Schuhmann, S. Lutz, T. Herold, S. B. King, F. M. Gerner, L. Perabo, J. Rabinowitz, D. M. McCarty, R. J. Samulski, M. Hallek, and H. Büning, "Adeno-associated virus serotypes 1 to 5 mediated tumor cell directed gene transfer and improvement of transduction efficiency," *J Gene Med*, vol. 7, no. 11, pp. 1429–1438, 2005.

[74] Y. Feodorova, M. Koch, S. Bultman, S. Michalakis, and I. Solovei, "Quick and reliable method for retina dissociation and separation of rod photoreceptor perikarya from adult mice," *MethodsX*, vol. 2, pp. 39–46, 2015.

[75] D. Eberle, S. Schubert, K. Postel, D. Corbeil, and M. Ader, "Increased integration of transplanted CD73-positive photoreceptor precursors into adult mouse retina," *Invest Ophthalmol Vis Sci*, vol. 52, no. 9, pp. 6462–6471, 2011.

[76] A. Wistuba, A. Kern, S. Weger, D. Grimm, and J. A. Kleinschmidt, "Subcellular compartmentalization of adeno-associated virus type 2 assembly.," *Journal of virology*, vol. 71, no. 2, pp. 1341–1352, 1997.

[77] Y. Feodorova, M. Koch, S. Bultman, S. Michalakis, and I. Solovei, "Quick and reliable method for retina dissociation and separation of rod photoreceptor perikarya from adult mice," *MethodsX*, vol. 2, pp. 39–46, jan 2015.

[78] C. Heinrich, S. Gascón, G. Masserdotti, A. Lepier, R. Sanchez, T. Simon-Ebert, T. Schroeder, M. Gtz, and B. Berninger, "Generation of subtype-specific neurons from postnatal astroglia of the mouse cerebral cortex," *Nature Protocols*, vol. 6, pp. 214–228, feb 2011.

[79] N. W. Keiser, Z. Yan, Y. Zhang, D. C. Lei-Butters, and J. F. Engelhardt, "Unique Characteristics of AAV1, 2, and 5 Viral Entry, Intracellular Trafficking, and Nuclear Import Define Transduction Efficiency in HeLa Cells," *Human Gene Therapy*, vol. 22, pp. 1433–1444, nov 2011.

[80] M. H. Wilson, C. J. Coates, and A. L. George, "PiggyBac transposon-mediated gene transfer in human cells," *Molecular Therapy*, vol. 15, pp. 139–145, jan 2007.

[81] M. Gossen, S. Freundlieb, G. Bender, G. Müller, W. Hillen, and H. Bujard, "Transcriptional activation by tetracyclines in mammalian cells," *Science*, vol. 268, no. 5218, pp. 1766–1769, 1995.

[82] F. Yao, T. Svensjö, T. Winkler, M. Lu, C. Eriksson, and E. Eriksson, "Tetracycline repressor, tetR, rather than the tetR-mammalian cell transcription factor fusion derivatives, regulates inducible gene expression in mammalian cells," *Human Gene Therapy*, vol. 9, pp. 1939–1950, sep 1998.

[83] U. Scheib, K. Stehfest, C. E. Gee, H. G. Körschen, R. Fudim, T. G. Oertner, and P. Hegemann, "The rhodopsin-guanylyl cyclase of the aquatic fungus Blastocladiella emersonii enables fast optical control of cGMP signaling," *Science Signaling*, vol. 8, no. 389, pp. 1–8, 2015.

[84] T. W. Chen, T. J. Wardill, Y. Sun, S. R. Pulver, S. L. Renninger, A. Baohan, E. R. Schreiter, R. A. Kerr, M. B. Orger, V. Jayaraman, L. L. Looger, K. Svoboda, and D. S. Kim, "Ultrasensitive fluorescent proteins for imaging neuronal activity," *Nature*, vol. 499, no. 7458, pp. 295–300, 2013.

[85] H. Dana, B. Mohar, Y. Sun, S. Narayan, A. Gordus, J. P. Hasseman, G. Tsegaye, G. T. Holt, A. Hu, D. Walpita, R. Patel, J. J. Macklin, C. I. Bargmann, M. B. Ahrens, E. R. Schreiter, V. Jayaraman, L. L. Looger, K. Svoboda, and D. S. Kim, "Sensitive red protein calcium indicators for imaging neural activity," *eLife*, vol. 5, pp. 1–24, 2016.

[86] M. Pavlou, C. Schön, L. M. Occelli, A. Rossi, N. Meumann, R. F. Boyd, J. T. Bartoe, J. Siedlecki, M. J. Gerhardt, S. Babutzka, J. Bogedein, J. E. Wagner, S. G. Priglinger, M. Biel, S. M. Petersen-Jones, H. Büning, and S. Michalakis, "Novel AAV capsids for intravitreal gene therapy of photoreceptor disorders," *EMBO Molecular Medicine*, 2021.

[87] L. Perabo, H. Büning, D. M. Kofler, M. U. Ried, A. Girod, C. M. Wendtner, J. Enssle, and M. Hallek, "In vitro selection of viral vectors with modified tropism: The adeno-associated virus display," *Molecular Therapy*, vol. 8, pp. 151–157, jul 2003.

[88] L. Perabo, J. Endell, S. King, K. Lux, D. Goldnau, M. Hallek, and H. Büning, "Combinatorial engineering of a gene therapy vector: directed evolution of adeno-associated virus," *The Journal of Gene Medicine*, vol. 8, pp. 155–162, feb 2006.

[89] S. Raman, R. Vernon, J. Thompson, M. Tyka, R. Sadreyev, J. Pei, D. Kim, E. Kellogg, F. Dimaio, O. Lange, L. Kinch, W. Sheffler, B. H. Kim, R. Das, N. V. Grishin, and D. Baker, "Structure prediction for CASP8 with all-atom refinement using Rosetta," *Proteins: Structure, Function and Bioinformatics*, vol. 77, pp. 89–99, 2009.

[90] Y. Song, F. Dimaio, R. Y. R. Wang, D. Kim, C. Miles, T. Brunette, J. Thompson, and D. Baker, "High-resolution comparative modeling with RosettaCM," *Structure*, vol. 21, pp. 1735–1742, oct 2013.

[91] L. Perabo, D. Goldnau, K. White, J. Endell, J. Boucas, S. Humme, L. M. Work, H. Janicki, M. Hallek, A. H. Baker, and H. Büning, "Heparan sulfate proteoglycan binding properties of adeno-associated virus retargeting mutants and consequences for their in vivo tropism," *J Virol*, vol. 80, no. 14, pp. 7265–7269, 2006.

[92] E. D. Horowitz, K. S. Rahman, B. D. Bower, D. J. Dismuke, M. R. Falvo, J. D. Griffith, S. C. Harvey, and A. Asokan, "Biophysical and Ultrastructural Characterization of Adeno-Associated Virus Capsid Uncoating and Genome Release," *Journal of Virology*, vol. 87, pp. 2994–3002, mar 2013.

[93] D. Dalkara, L. C. Byrne, R. R. Klimczak, M. Visel, L. Yin, W. H. Merigan, J. G. Flannery, and D. V. Schaffer, "In vivo-directed evolution of a new adeno-associated virus for therapeutic outer retinal gene delivery from the vitreous," *Science Translational Medicine*, vol. 5, no. 189, 2013.

[94] R. F. Boyd, D. G. Sledge, S. L. Boye, S. E. Boye, W. W. Hauswirth, A. M. Komáromy, S. M. Petersen-Jones, and J. T. Bartoe, "Photoreceptor-targeted gene delivery using intravitreally administered AAV vectors in dogs," *Gene Therapy*, vol. 23, pp. 223–230, feb 2016.

[95] L. Xiang, X. J. Chen, K. C. Wu, C. J. Zhang, G. H. Zhou, J. N. Lv, L. F. Sun, F. F. Cheng, X. B. Cai, and Z. B. Jin, "MiR-183/96 plays a pivotal regulatory role in mouse photoreceptor maturation and maintenance," *Proceedings of the National Academy of Sciences*, vol. 114, pp. 6376–6381, jun 2017.

[96] K. C. Wu, X. J. Chen, G. H. Jin, X. Y. Wang, D. D. Yang, Y. P. Li, L. Xiang, B. W. Zhang, G. H. Zhou, C. J. Zhang, and Z. B. Jin, "Deletion of miR-182 leads to retinal dysfunction in mice," *Investigative Ophthalmology and Visual Science*, vol. 60, pp. 1265–1274, mar 2019.

[97] C.-J. Zhang, L. Xiang, X.-J. Chen, X.-Y. Wang, K.-C. Wu, B.-W. Zhang, D.-F. Chen, G.-H. Jin, H. Zhang, Y.-C. Chen, W.-Q. Liu, M.-L. Li, Y. Ma, and Z.-B. Jin, "Ablation of Mature miR-183 Leads to Retinal Dysfunction in Mice," *Investigative Opthalmology & Visual Science*, vol. 61, p. 12, mar 2020.

[98] E. Murenu, M. Pavlou, L. Richter, K. Rapti, S. Just, J. Cehajic-Kapetanovic, N. Tafrishi, A. Hayes, R. Scholey, R. Lucas, H. Büning, D. Grimm, and S. Michalakis, "A universal protocol for isolating retinal ON bipolar cells across species via fluorescence-activated cell sorting," *Molecular Therapy - Methods & Clinical Development*, jan 2021.

[99] C. E. Keeler, "The Inheritance of a Retinal Abnormality in White Mice," *Proceedings of the National Academy of Sciences*, vol. 10, pp. 329–333, jul 1924.

[100] C. Bowes, T. Li, M. Danciger, L. C. Baxter, M. L. Applebury, and D. B. Farber, "Retinal degeneration in the rd mouse is caused by a defect in the β subunit of rod cGMP-phosphodiesterase," *Nature*, vol. 347, no. 6294, pp. 677–680, 1990.

[101] S. J. Pittler and W. Baehr, "Identification of a nonsense mutation in the rod photoreceptor cGMP phosphodiesterase β-subunit gene of the rd mouse," *Proceedings of the National Academy of Sciences*, vol. 88, pp. 8322–8326, oct 1991.

[102] N. Hasan, T. A. Ray, and R. G. Gregg, "CACNA1S expression in mouse retina: Novel isoforms and antibody cross-reactivity with GPR179," *Visual neuroscience*, vol. 33, p. E009, jan 2016.

[103] K. Shekhar, S. W. Lapan, I. E. Whitney, N. M. Tran, E. Z. Macosko, M. Kowalczyk, X. Adiconis, J. Z. Levin, J. Nemesh, M. Goldman, S. A. McCarroll, C. L. Cepko, A. Regev, and J. R. Sanes, "Comprehensive Classification of Retinal Bipolar Neurons by Single-Cell Transcriptomics," *Cell*, vol. 166, pp. 1308–1323.e30, aug 2016.

[104] A. Dhingra, A. Lyubarsky, M. Jiang, E. N. Pugh, L. Birnbaumer, P. Sterling, and N. Vardi, "The light response of ON bipolar neurons requires Gαo," *Journal of Neuroscience*, vol. 20, pp. 9053–9058, dec 2000.

[105] Y. Xu, P. Sulaiman, R. M. Feddersen, J. Liu, R. G. Smith, and N. Vardi, "Retinal ON bipolar cells express a new PCP2 splice variant that accelerates the light response," *Journal of Neuroscience*, vol. 28, pp. 8873–8884, sep 2008.

[106] E. N. Star, M. Zhu, Z. Shi, H. Liu, M. Pashmforoush, Y. Sauve, B. G. Bruneau, and R. L. Chow, "Regulation of retinal interneuron subtype identity by the Iroquois homeobox gene irx6," *Development (Cambridge)*, vol. 139, pp. 4644–4655, dec 2012.

[107] C. J. Jeon, E. Strettoi, and R. H. Masland, "The major cell populations of the mouse retina," *Journal of Neuroscience*, vol. 18, pp. 8936–8946, nov 1998.

[108] Y.-R. Peng, K. Shekhar, W. Yan, D. Herrmann, A. Sappington, G. S. Bryman, T. van Zyl, M. T. H. Do, A. Regev, and J. R. Sanes, "Molecular Classification and Comparative Taxonomics of Foveal and Peripheral Cells in Primate Retina," *Cell*, vol. 176, pp. 1–16, jan 2019.

[109] K. Börner, E. Kienle, L.-Y. Huang, J. Weinmann, A. Sacher, P. Bayer, C. Stüllein, J. Fakhiri, L. Zimmermann, A. Westhaus, J. Beneke, N. Beil, E. Wiedtke, C. Schmelas, D. Miltner, A. Rau, H. Erfle, H.-G. Kräusslich, M. Müller, M. Agbandje-Mckenna, and D. Grimm, "Pre-arrayed Pan-AAV Peptide Display Libraries for Rapid Single-Round Screening," *Molecular Therapy*, vol. 28, pp. 1016–1032, 2020.

[110] S. Gascón, G. Masserdotti, G. L. Russo, and M. Götz, "Direct Neuronal Reprogramming: Achievements, Hurdles, and New Roads to Success," *Cell Stem Cell*, 2017.

[111] A. M. Santos, R. Calvente, M. Tassi, M. C. Carrasco, D. Martín-Oliva, J. L. Marín-Teva, J. Navascués, and M. A. Cuadros, "Embryonic and postnatal development of microglial cells in the mouse retina," *Journal of Comparative Neurology*, vol. 506, pp. 224–239, jan 2008.

[112] E. A. Bassett and V. A. Wallace, "Cell fate determination in the vertebrate retina," *Trends in Neurosciences*, vol. 35, pp. 565–573, 2012.

[113] T. Matsuda, T. Irie, S. Katsurabayashi, Y. Hayashi, T. Nagai, N. Hamazaki, A. M. D. Adefuin, F. Miura, T. Ito, H. Kimura, K. Shirahige, T. Takeda, K. Iwasaki, T. Imamura, and K. Nakashima, "Pioneer Factor NeuroD1 Rearranges Transcriptional and Epigenetic Profiles to Execute Microglia-Neuron Conversion," *Neuron*, vol. 101, pp. 472–485.e7, feb 2019.

[114] A. Gerstner, X. Zong, F. Hofmann, and M. Biel, "Molecular cloning and functional characterization of a new modulatory cyclic nucleotide-gated channel subunit from mouse retina," *Journal of Neuroscience*, vol. 20, pp. 1324–1332, feb 2000.

[115] N. Wu, W. K. Nishioka, N. C. Derecki, and M. P. Maher, "High-throughput-compatible assays using a genetically-encoded calcium indicator," *Scientific Reports*, vol. 9, pp. 1–17, dec 2019.

[116] N. A. Smirnov, S. B. Akopov, D. A. Didych, and L. G. Nikolaev, "In trans promoter activation by enhancers in transient transfection," *Gene*, vol. 603, pp. 15–20, mar 2017.

[117] A. Goc, M. Chami, D. T. Lodowski, P. Bosshart, V. Moiseenkova-Bell, W. Baehr, A. Engel, and K. Palczewski, "Structural characterization of the rod cGMP phosphodiesterase 6," *Journal of Molecular Biology*, vol. 401, no. 3, pp. 363–373, 2010.

[118] Y. Zhao, S. Araki, J. Wu, T. Teramoto, Y. F. Chang, M. Nakano, A. S. Abdelfattah, M. Fujiwara, T. Ishihara, T. Nagai, and R. E. Campbell, "An expanded palette of genetically encoded Ca2+ indicators," *Science*, vol. 333, pp. 1888–1891, sep 2011.

[119] J. J. Darrow, "Luxturna: FDA documents reveal the value of a costly gene therapy," *Drug Discovery Today*, vol. 24, pp. 949–954, apr 2019.

[120] J. W. Bainbridge, A. J. Smith, S. S. Barker, S. Robbie, R. Henderson, K. Balaggan, A. Viswanathan, G. E. Holder, A. Stockman, N. Tyler, S. Petersen-Jones, S. S. Bhattacharya, A. J. Thrasher, F. W. Fitzke, B. J. Carter, G. S. Rubin, A. T. Moore, and R. R. Ali, "Effect of Gene Therapy on Visual Function in Leber's Congenital Amaurosis," *New England Journal of Medicine*, vol. 358, pp. 2231–2239, may 2008.

[121] W. W. Hauswirth, T. S. Aleman, S. Kaushal, A. V. Cideciyan, S. B. Schwartz, L. Wang, T. J. Conlon, S. L. Boye, T. R. Flotte, B. J. Byrne, and S. G. Jacobson, "Treatment of Leber congenital amaurosis due to RPE65 mutations by ocular subretinal injection of adeno-associated virus gene vector: Short-term results of a phase I trial," *Human Gene Therapy*, vol. 19, pp. 979–990, oct 2008.

[122] A. M. Maguire, F. Simonelli, E. A. Pierce, E. N. Pugh, F. Mingozzi, J. Bennicelli, S. Banfi, K. A. Marshall, F. Testa, E. M. Surace, S. Rossi, A. Lyubarsky, V. R. Arruda, B. Konkle, E. Stone, J. Sun, J. Jacobs, L. Dell'Osso, R. Hertle, J.-x. Ma, T. M. Redmond, X. Zhu, B. Hauck, O. Zelenaia, K. S. Shindler, M. G. Maguire, J. F. Wright, N. J. Volpe, J. W. McDonnell, A. Auricchio, K. A. High, and J. Bennett, "Safety and Efficacy of Gene Transfer for Leber's Congenital Amaurosis," *New England Journal of Medicine*, vol. 358, pp. 2240–2248, may 2008.

[123] A. V. Cideciyan, S. G. Jacobson, W. A. Beltran, A. Sumaroka, M. Swider, S. Iwabe, A. J. Roman, M. B. Olivares, S. B. Schwartz, A. M. Komáromy, W. W. Hauswirth, and G. D. Aguirre, "Human retinal gene therapy for Leber congenital amaurosis shows advancing retinal degeneration despite enduring visual improvement," *Proceedings of the National Academy of Sciences*, vol. 110, no. 6, p. E517, 2013.

[124] J. W. Bainbridge, M. S. Mehat, V. Sundaram, S. J. Robbie, S. E. Barker, C. Ripamonti, A. Georgiadis, F. M. Mowat, S. G. Beattie, P. J. Gardner, K. L. Feathers, V. A. Luong, S. Yzer, K. Balaggan, A. Viswanathan, T. J. de Ravel, I. Casteels, G. E. Holder, N. Tyler, F. W. Fitzke, R. G. Weleber, M. Nardini, A. T. Moore, D. A. Thompson, S. M. Petersen-Jones, M. Michaelides, L. I. van den Born, A. Stockman, A. J. Smith, G. Rubin, and R. R. Ali, "Long-Term Effect of Gene Therapy on Leber's Congenital Amaurosis," *New England Journal of Medicine*, vol. 372, pp. 1887–1897, may 2015.

[125] S. G. Jacobson, A. V. Cideciyan, A. J. Roman, A. Sumaroka, S. B. Schwartz, E. Heon, and W. W. Hauswirth, "Improvement and Decline in Vision with Gene Therapy in Childhood Blindness," *New England Journal of Medicine*, vol. 372, pp. 1920–1926, may 2015.

[126] S. T. Hsu, H. Gabr, C. Viehland, K. Sleiman, H. T. Ngo, O. M. Carrasco-Zevallos, L. Vajzovic, R. P. McNabb, S. S. Stinnett, J. A. Izatt, A. N. Kuo, and C. A. Toth, "Volumetric Measurement of Subretinal Blebs Using Microscope-Integrated Optical Coherence Tomography," *Transl Vis Sci Technol*, vol. 7, no. 2, p. 19, 2018.

[127] P. D. Gamlin, J. J. Alexander, S. L. Boye, C. D. Witherspoon, and S. E. Boye, "SubILM injection of AAV for gene delivery to the retina," *Methods in Molecular Biology*, vol. 1950, pp. 249–262, 2019.

[128] K. Ding, J. Shen, Z. Hafiz, S. F. Hackett, R. L. e Silva, M. Khan, V. E. Lorenc, D. Chen, R. Chadha, M. Zhang, S. van Everen, N. Buss, M. Fiscella, O. Danos, and P. A. Campochiaro, "AAV8-vectored suprachoroidal gene transfer produces widespread ocular transgene expression," *Journal of Clinical Investigation*, vol. 129, pp. 4901–4911, nov 2019.

[129] G. Yiu, S. H. Chung, I. N. Mollhoff, U. T. Nguyen, S. M. Thomasy, J. Yoo, D. Taraborelli, and G. Noronha, "Suprachoroidal and Subretinal Injections of AAV Using Transscleral Microneedles for Retinal Gene Delivery in Nonhuman Primates," *Molecular Therapy - Methods and Clinical Development*, vol. 16, pp. 179–191, mar 2020.

[130] C. Summerford and R. J. Samulski, "AAVR: A multi-serotype receptor for AAV," *Molecular Therapy*, vol. 24, no. 4, pp. 663–666, 2016.

[131] A. M. Dudek, S. Pillay, A. S. Puschnik, C. M. Nagamine, F. Cheng, J. Qiu, J. E. Carette, and L. H. Vandenberghe, "An Alternate Route for Adeno-associated Virus (AAV) Entry Independent of AAV Receptor.," *Journal of virology*, vol. 92, pp. e02213–17, apr 2018.

[132] B. A. Hamilton, X. Li, A. A. Pezzulo, M. H. Abou Alaiwa, and J. Zabner, "Polarized AAVR expression determines infectivity by AAV gene therapy vectors," *Gene Therapy*, vol. 26, pp. 240–249, jun 2019.

[133] A. M. Dudek, N. Zabaleta, E. Zinn, S. Pillay, J. Zengel, C. Porter, J. S. Franceschini, R. Estelien, J. E. Carette, G. L. Zhou, and L. H. Vandenberghe, "GPR108 Is a Highly Conserved AAV Entry Factor," *Molecular Therapy*, vol. 28, pp. 367–381, feb 2020.

[134] A. Kern, K. Schmidt, C. Leder, O. J. Muller, C. E. Wobus, K. Bettinger, C. W. Von der Lieth, J. A. King, and J. A. Kleinschmidt, "Identification of a heparin-binding motif on adeno-associated virus type 2 capsids," *J Virol*, vol. 77, no. 20, pp. 11072–11081, 2003.

[135] S. R. Opie, K. H. Warrington, M. Agbandje-McKenna, S. Zolotukhin, and N. Muzyczka, "Identification of Amino Acid Residues in the Capsid Proteins of Adeno-Associated Virus Type 2 That Contribute to Heparan Sulfate Proteoglycan Binding," *Journal of Virology*, vol. 77, pp. 6995–7006, jun 2003.

[136] K. T. Woodard, K. J. Liang, W. C. Bennett, and R. J. Samulski, "Heparan Sulfate Binding Promotes Accumulation of Intravitreally Delivered Adeno-associated Viral Vectors at the Retina for Enhanced Transduction but Weakly Influences Tropism," *Journal of Virology*, vol. 90, pp. 9878–9888, nov 2016.

[137] Y. Song, F. DiMaio, R. Y. Wang, D. Kim, C. Miles, T. Brunette, J. Thompson, and D. Baker, "High-resolution comparative modeling with RosettaCM," *Structure*, vol. 21, no. 10, pp. 1735–1742, 2013.

[138] A. Bennett, A. Keravala, V. Makal, J. Kurian, B. Belbellaa, R. Aeran, Y. S. Tseng, D. Sousa, J. Spear, M. Gasmi, and M. Agbandje-McKenna, "Structure comparison of the chimeric AAV2.7m8 vector with parental AAV2," *J Struct Biol*, vol. 209, no. 2, p. 107433, 2020.

[139] S. Uhrig, O. Coutelle, T. Wiehe, L. Perabo, M. Hallek, and H. Büning, "Successful target cell transduction of capsid-engineered rAAV vectors requires clathrin-dependent endocytosis," *Gene Therapy*, vol. 19, pp. 210–218, feb 2012.

[140] A. R. Giles, J. J. Sims, K. B. Turner, L. Govindasamy, M. R. Alvira, M. Lock, and J. M. Wilson, "Deamidation of Amino Acids on the Surface of Adeno-Associated Virus Capsids Leads to Charge Heterogeneity and Altered Vector Function," *Mol Ther*, vol. 26, no. 12, pp. 2848–2862, 2018.

[141] P. J. Ogden, E. D. Kelsic, S. Sinai, and G. M. Church, "Comprehensive AAV capsid fitness landscape reveals a viral gene and enables machine-guided design," *Science*, vol. 366, pp. 1139–1143, nov 2019.

[142] D. H. Bryant, A. Bashir, S. Sinai, N. K. Jain, P. J. Ogden, P. F. Riley, G. M. Church, L. J. Colwell, and E. D. Kelsic, "Deep diversification of an AAV capsid protein by machine learning," *Nature biotechnology*, 2021.

[143] W. Ding, L. Zhang, Z. Yan, and J. F. Engelhardt, "Intracellular trafficking of adeno-associated viral vectors," *Gene Therapy*, vol. 12, pp. 873–880, jun 2005.

[144] J. Hordeaux, Q. Wang, N. Katz, E. L. Buza, P. Bell, and J. M. Wilson, "The Neurotropic Properties of AAV-PHP.B Are Limited to C57BL/6J Mice," 2018.

[145] D. Dalkara, K. D. Kolstad, N. Caporale, M. Visel, R. R. Klimczak, D. V. Schaffer, and J. G. Flannery, "Inner limiting membrane barriers to AAV-mediated retinal transduction from the vitreous," *Mol Ther*, vol. 17, no. 12, pp. 2096–2102, 2009.

[146] R. F. Boyd, S. L. Boye, T. J. Conlon, K. E. Erger, D. G. Sledge, I. M. Langohr, W. W. Hauswirth, A. M. Komaromy, S. E. Boye, S. M. Petersen-Jones, and J. T. Bartoe, "Reduced retinal transduction and enhanced transgene-directed immunogenicity with intravitreal delivery of rAAV following posterior vitrectomy in dogs," *Gene Ther*, vol. 23, no. 6, pp. 548–556, 2016.

[147] M. A. Kotterman, L. Yin, J. M. Strazzeri, J. G. Flannery, W. H. Merigan, and D. V. Schaffer, "Antibody neutralization poses a barrier to intravitreal adeno-associated viral vector gene delivery to non-human primates," *Gene Ther*, vol. 22, no. 2, pp. 116–126, 2015.

[148] A. Murali, C. A. Ramlogan-Steel, S. Andrzejewski, J. C. Steel, and C. J. Layton, "Retinal explant culture: A platform to investigate human neuro-retina," *Clin Exp Ophthalmol*, vol. 47, no. 2, pp. 274–285, 2019.

[149] R. Stripecke, M. Carmen Villacres, D. Skelton, N. Satake, S. Halene, and D. Kohn, "Immune response to green fluorescent protein: implications for gene therapy," *Gene Ther*, vol. 6, no. 7, pp. 1305–1312, 1999.

[150] B. A. Perez, A. Shutterly, Y. K. Chan, B. J. Byrne, and M. Corti, "Management of neuroinflammatory responses to AAV-mediated gene therapies for neurodegenerative diseases," *Brain Sciences*, vol. 10, feb 2020.

[151] Y. K. Chan, S. K. Wang, C. J. Chu, D. A. Copland, A. J. Letizia, H. Costa Verdera, J. J. Chiang, M. Sethi, M. K. Wang, W. J. Neidermyer, Y. Chan, E. T. Lim, A. R. Graveline, M. Sanchez, R. F. Boyd, T. S. Vihtelic, R. G. C. O. Inciong, J. M. Slain, P. J. Alphonse, Y. Xue, L. R. Robinson-McCarthy, J. M. Tam, M. H. Jabbar, B. Sahu, J. F. Adeniran, M. Muhuri, P. W. L. Tai, J. Xie, T. B. Krause, A. Vernet, M. Pezone, R. Xiao, T. Liu, W. Wang, H. J. Kaplan, G. Gao, A. D. Dick, F. Mingozzi, M. A. McCall, C. L. Cepko, and G. M. Church, "Engineering adeno-associated viral vectors to evade innate immune and inflammatory responses," *Science Translational Medicine*, vol. 13, p. eabd3438, feb 2021.

[152] J. Sallach, G. Di Pasquale, F. Larcher, N. Niehoff, M. Rübsam, A. Huber, J. Chiorini, D. Almarza, S. A. Eming, H. Ulus, S. Nishimura, U. T. Hacker, M. Hallek, C. M. Niessen, and H. Büning, "Tropism-modified AAV vectors overcome barriers to successful cutaneous therapy," *Molecular Therapy*, vol. 22, pp. 929–939, may 2014.

[153] S. Pillay, N. L. Meyer, A. S. Puschnik, O. Davulcu, J. Diep, Y. Ishikawa, L. T. Jae, J. E. Wosen, C. M. Nagamine, M. S. Chapman, and J. E. Carette, "An essential receptor for adeno-associated virus infection," *Nature*, vol. 530, no. 7588, pp. 108–112, 2016.

[154] S. N. Peirson, L. A. Brown, C. A. Pothecary, L. A. Benson, and A. S. Fisk, "Light and the laboratory mouse," *J Neurosci Methods*, vol. 300, pp. 26–36, 2018.

[155] M. E. McClements and R. E. MacLaren, "Gene therapy for retinal disease," *Transl Res*, vol. 161, no. 4, pp. 241–254, 2013.

[156] N. Tanaka, E. V. Dutrow, K. Miyadera, L. Delemotte, C. M. MacDermaid, S. L. Reinstein, W. R. Crumley, C. J. Dixon, M. L. Casal, M. L. Klein, G. D. Aguirre, J. C. Tanaka, and K. E. Guziewicz, "Canine CNGA3 Gene Mutations Provide Novel Insights into Human Achromatopsia-Associated Channelopathies and Treatment," *PLOS ONE*, vol. 10, p. e0138943, sep 2015.

[157] A. Moshiri, R. Chen, S. Kim, R. A. Harris, Y. Li, M. Raveendran, S. Davis, Q. Liang, O. Pomerantz, J. Wang, L. Garzel, A. Cameron, G. Yiu, J. T. Stout, Y. Huang, C. J. Murphy, J. Roberts, K. N. Gopalakrishna, K. Boyd, N. O. Artemyev, J. Rogers, and

S. M. Thomasy, "A nonhuman primate model of inherited retinal disease," *Journal of Clinical Investigation*, vol. 129, pp. 863–874, feb 2019.

[158] M. A. Genead, G. A. Fishman, J. Rha, A. M. Dubis, D. M. O. Bonci, A. Dubra, E. M. Stone, M. Neitz, and J. Carroll, "Photoreceptor structure and function in patients with congenital achromatopsia," *Investigative Ophthalmology and Visual Science*, vol. 52, pp. 7298–7308, sep 2011.

[159] S. G. Wohl, N. L. Jorstad, E. M. Levine, and T. A. Reh, "Müller glial microRNAs are required for the maintenance of glial homeostasis and retinal architecture," *Nature Communications*, vol. 8, pp. 1–15, dec 2017.

[160] J. Fan, L. Jia, Y. Li, S. Ebrahim, H. May-Simera, A. Wood, R. J. Morell, P. Liu, J. Lei, B. Kachar, L. Belluscio, H. Qian, T. Li, W. Li, G. Wistow, and L. Dong, "Maturation arrest in early postnatal sensory receptors by deletion of the miR-183/96/182 cluster in mouse," *Proceedings of the National Academy of Sciences*, vol. 114, no. 21, pp. E4271–E4280, 2017.

[161] M. Davari, Z.-S. Soheili, S. Samiei, Z. Sharifi, and E. R. Pirmardan, "Overexpression of miR-183/-96/-182 triggers neuronal cell fate in Human Retinal Pigment Epithelial (hRPE) cells in culture," *Biochemical and Biophysical Research Communications*, vol. 483, pp. 745–751, jan 2017.

[162] M. Zuzic, J. E. R. Arias, S. G. Wohl, and V. Busskamp, "Retinal miRNA functions in health and disease," *Genes*, vol. 10, may 2019.

[163] J. Krol, V. Busskamp, I. Markiewicz, M. B. Stadler, S. Ribi, J. Richter, J. Duebel, S. Bicker, H. J. Fehling, D. Schübeler, T. G. Oertner, G. Schratt, M. Bibel, B. Roska, and W. Filipowicz, "Characterizing Light-Regulated Retinal MicroRNAs Reveals Rapid Turnover as a Common Property of Neuronal MicroRNAs," *Cell*, vol. 141, pp. 618–631, may 2010.

[164] N. El-Darzi, A. Astafev, N. Mast, A. Saadane, M. Lam, and I. A. Pikuleva, "N,N-Dimethyl-3β-hydroxycholenamide Reduces Retinal Cholesterol via Partial Inhibition of Retinal Cholesterol Biosynthesis Rather Than its Liver X Receptor Transcriptional Activity," *Frontiers in Pharmacology*, vol. 9, p. 827, jul 2018.

[165] K. Nieweg, H. Schaller, and F. W. Pfrieger, "Marked differences in cholesterol synthesis between neurons and glial cells from postnatal rats," *Journal of Neurochemistry*, vol. 109, pp. 125–134, apr 2009.

[166] Y. Okunuki, R. Mukai, E. A. Pearsall, G. Klokman, D. Husain, D. H. Park, E. Korobkina, H. L. Weiner, O. Butovsky, B. R. Ksander, J. W. Miller, and K. M. Connor, "Microglia inhibit photoreceptor cell death and regulate immune cell infiltration in response to retinal detachment," *Proceedings of the National Academy of Sciences*, vol. 115, pp. E6264–E6273, jul 2018.

[167] E. B. Miller, P. Zhang, K. Ching, E. N. Pugh, and M. E. Burns, "In vivo imaging reveals transient microglia recruitment and functional recovery of photoreceptor signaling after injury," *Proceedings of the National Academy of Sciences*, vol. 116, pp. 16603–16612, aug 2019.

[168] S. K. Wang, Y. Xue, P. Rana, C. M. Hong, and C. L. Cepko, "Soluble CX3CL1 gene therapy improves cone survival and function in mouse models of retinitis pigmentosa.," *Proceedings of the National Academy of Sciences*, vol. 116, pp. 10140–10149, may 2019.

[169] S. K. Wang, Y. Xue, and C. L. Cepko, "Microglia modulation by TGF-β1 protects cones in mouse models of retinal degeneration," *Journal of Clinical Investigation*, vol. 140, pp. 4360–4369, aug 2020.

[170] W. M. Henne, E. Boucrot, M. Meinecke, E. Evergren, Y. Vallis, R. Mittal, and H. T. McMahon, "FCHo proteins are nucleators of Clathrin-Mediated endocytosis," *Science*, vol. 328, pp. 1281–1284, jun 2010.

[171] R. Guyot, S. Vincent, J. Bertin, J. Samarut, and P. Ravel-Chapuis, "The transforming acidic coiled coil (TACC1) protein modulates the transcriptional activity of the nuclear receptors TR and RAR," *BMC Molecular Biology*, vol. 11, p. 3, jan 2010.

[172] T. L. Young, T. Matsuda, and C. L. Cepko, "The noncoding RNA Taurine Upregulated Gene 1 is required for differentiation of the murine retina," *Current Biology*, vol. 15, pp. 501–512, mar 2005.

[173] D. Dalkara and J. A. Sahel, "Gene therapy for inherited retinal degenerations," *Comptes Rendus - Biologies*, vol. 337, no. 3, pp. 185–192, 2014.

[174] S. Veleri, C. H. Lazar, B. Chang, P. A. Sieving, E. Banin, and A. Swaroop, "Biology and therapy of inherited retinal degenerative disease: insights from mouse models.," *Disease models & mechanisms*, vol. 8, pp. 109–29, feb 2015.

[175] J. H. Stern, Y. Tian, J. Funderburgh, G. Pellegrini, K. Zhang, J. L. Goldberg, R. R. Ali, M. Young, Y. Xie, and S. Temple, "Regenerating Eye Tissues to Preserve and Restore Vision," *Cell Stem Cell*, vol. 22, pp. 834–849, jun 2018.

[176] A. V. Garafalo, A. V. Cideciyan, E. Héon, R. Sheplock, A. Pearson, C. WeiYang Yu, A. Sumaroka, G. D. Aguirre, and S. G. Jacobson, "Progress in treating inherited retinal diseases: Early subretinal gene therapy clinical trials and candidates for future initiatives," *Progress in Retinal and Eye Research*, vol. 77, p. 100827, jul 2020.

[177] P. S. Lagali, D. Balya, G. B. Awatramani, T. A. Münch, D. S. Kim, V. Busskamp, C. L. Cepko, and B. Roska, "Light-activated channels targeted to ON bipolar cells restore visual function in retinal degeneration," *Nature Neuroscience*, vol. 11, pp. 667–675, jun 2008.

[178] M. M. Doroudchi, K. P. Greenberg, J. Liu, K. A. Silka, E. S. Boyden, J. A. Lockridge, A. C. Arman, R. Janani, S. E. Boye, S. L. Boye, G. M. Gordon, B. C. Matteo, A. P. Sampath, W. W. Hauswirth, and A. Horsager, "Virally delivered channelrhodopsin-2 safely and effectively restores visual function in multiple mouse models of blindness," *Molecular Therapy*, vol. 19, pp. 1220–1229, jul 2011.

[179] T. Cronin, L. H. Vandenberghe, P. Hantz, J. Juttner, A. Reimann, Á. Kacsó, R. M. Huckfeldt, V. Busskamp, H. Kohler, P. S. Lagali, B. Roska, and J. Bennett, "Efficient transduction and optogenetic stimulation of retinal bipolar cells by a synthetic adenoassociated virus capsid and promoter," *EMBO Molecular Medicine*, vol. 6, pp. 1175–1190, sep 2014.

[180] E. Macé, R. Caplette, O. Marre, A. Sengupta, A. Chaffiol, P. Barbe, M. Desrosiers, E. Bamberg, J. A. Sahel, S. Picaud, J. Duebel, and D. Dalkara, "Targeting channelrhodopsin-2 to ON-bipolar cells with vitreally administered AAV restores on and off visual responses in blind mice," *Molecular Therapy*, vol. 23, pp. 7–16, jan 2015.

[181] M. van Wyk, J. Pielecka-Fortuna, S. Löwel, and S. Kleinlogel, "Restoring the ON Switch in Blind Retinas: Opto-mGluR6, a Next-Generation, Cell-Tailored Optogenetic Tool," *PLoS Biology*, vol. 13, may 2015.

[182] B. M. Gaub, M. H. Berry, A. E. Holt, E. Y. Isacoff, and J. G. Flannery, "Optogenetic Vision Restoration Using Rhodopsin for Enhanced Sensitivity," *Molecular Therapy*, vol. 23, pp. 1562–1571, oct 2015.

[183] J. Cehajic-Kapetanovic, C. Eleftheriou, A. E. Allen, N. Milosavljevic, A. Pienaar, R. Bedford, K. E. Davis, P. N. Bishop, and R. J. Lucas, "Restoration of vision with ectopic expression of human rod opsin," *Current Biology*, vol. 25, pp. 2111–2122, aug 2015.

[184] Q. Lu, T. H. Ganjawala, E. Ivanova, J. G. Cheng, D. Troilo, and Z. H. Pan, "AAV-mediated transduction and targeting of retinal bipolar cells with improved mGluR6 promoters in rodents and primates," *Gene Therapy*, vol. 23, pp. 680–689, aug 2016.

[185] E. C. Hulliger, S. M. Hostettler, and S. Kleinlogel, "Empowering Retinal Gene Therapy with a Specific Promoter for Human Rod and Cone ON-Bipolar Cells," *Molecular Therapy - Methods and Clinical Development*, vol. 17, pp. 505–519, jun 2020.

[186] S. Batabyal, S. Gajjeraman, S. Pradhan, S. Bhattacharya, W. Wright, and S. Mohanty, "Sensitization of ON-bipolar cells with ambient light activatable multi-characteristic opsin rescues vision in mice," *Gene Therapy*, pp. 1–15, oct 2020.

[187] S. Choudhury, C. E. Strang, J. J. Alexander, M. L. Scalabrino, J. Lynch Hill, D. T. Kasuga, C. D. Witherspoon, S. L. Boye, P. D. Gamlin, and S. E. Boye, "Novel Methodology for Creating Macaque Retinas with Sortable Photoreceptors and Ganglion Cells," *Frontiers in Neuroscience*, vol. 10, p. 551, dec 2016.

[188] I. S. Liu, J. de Chen, L. Ploder, D. Vidgen, D. van der Kooy, V. I. Kalnins, and R. R. Mclnnes, "Developmental expression of a novel murine homeobox gene (Chx10): Evidence for roles in determination of the neuroretina and inner nuclear layer," *Neuron*, vol. 13, no. 2, pp. 377–393, 1994.

[189] M. Burmeister, J. Novak, M. Y. Liang, S. Basu, L. Ploder, N. L. Hawes, D. Vidgen, F. Hoover, D. Goldman, V. I. Kalnins, T. H. Roderick, B. A. Taylor, M. H. Hankin, and R. R. McInnes, "Ocular retardation mouse caused by Chx10 homeobox null allele: Impaired retinal progenitor proliferation and bipolar cell differentiation," *Nature Genetics*, vol. 12, pp. 376–384, apr 1996.

[190] S. Rowan and C. L. Cepko, "Genetic analysis of the homeodomain transcription factor Chx10 in the retina using a novel multifunctional BAC transgenic mouse reporter," *Developmental Biology*, vol. 271, pp. 388–402, jul 2004.

[191] E. Himawan, P. Ekström, M. Buzgo, P. Gaillard, E. Stefánsson, V. Marigo, T. Loftsson, and F. Paquet-Durand, "Drug delivery to retinal photoreceptors," *Drug Discovery Today*, vol. 24, pp. 1637–1643, aug 2019.

[192] J. B. Gurdon and V. Uehlinger, ""Fertile" intestine nuclei," *Nature*, vol. 210, no. 5042, pp. 1240–1241, 1966.

[193] C. R. Nicholas and A. R. Kriegstein, "Regenerative medicine: Cell reprogramming gets direct," *Nature*, vol. 463, pp. 1031–1032, feb 2010.

[194] K. Takahashi and S. Yamanaka, "Induction of Pluripotent Stem Cells from Mouse Embryonic and Adult Fibroblast Cultures by Defined Factors," *Cell*, vol. 126, pp. 663–676, aug 2006.

[195] T. Vierbuchen, A. Ostermeier, Z. P. Pang, Y. Kokubu, T. C. Südhof, and M. Wernig, "Direct conversion of fibroblasts to functional neurons by defined factors," *Nature*, vol. 463, pp. 1035–1041, feb 2010.

[196] Z. Guo, L. Zhang, Z. Wu, Y. Chen, F. Wang, and G. Chen, "In vivo direct reprogramming of reactive glial cells into functional neurons after brain injury and in an Alzheimer's disease model," *Cell Stem Cell*, vol. 14, pp. 188–202, feb 2014.

[197] L. Zhang, J.-C. Yin, H. Yeh, N.-X. Ma, G. Lee, X. A. Chen, Y. Wang, L. Lin, L. Chen, P. Jin, G.-Y. Wu, and G. Chen, "Small Molecules Efficiently Reprogram Human Astroglial Cells into Functional Neurons," *Cell Stem Cell*, vol. 17, pp. 735–747, dec 2015.

[198] S. Gascón, E. Murenu, G. Masserdotti, M. Conrad, and B. Berninger, "Identification and Successful Negotiation of a Metabolic Checkpoint in Direct Neuronal Reprogramming," *Cell Stem Cell*, vol. 18, pp. 396–409, 2016.

[199] L. Gao, W. Guan, M. Wang, H. Wang, J. Yu, Q. Liu, B. Qiu, Y. Yu, Y. Ping, X. Bian, L. Shen, and G. Pei, "Direct Generation of Human Neuronal Cells from Adult Astrocytes by Small Molecules," *Stem Cell Reports*, vol. 8, pp. 538–547, mar 2017.

[200] M. O. Karl, S. Hayes, B. R. Nelson, K. Tan, B. Buckingham, and T. A. Reh, "Stimulation of neural regeneration in the mouse retina," *Proceedings of the National Academy of Sciences*, vol. 105, pp. 19508–19513, dec 2008.

[201] J. Pollak, M. S. Wilken, Y. Ueki, K. E. Cox, J. M. Sullivan, R. J. Taylor, E. M. Levine, and T. A. Reh, "ASCL1 reprograms mouse Müller glia into neurogenic retinal progenitors," *Development (Cambridge)*, vol. 140, pp. 2619–2631, jun 2013.

[202] D. Sanges, G. Simonte, U. Di Vicino, N. Romo, I. Pinilla, M. Nicolás, and M. P. Cosma, "Reprogramming Müller glia via in vivo cell fusion regenerates murine photoreceptors," *Journal of Clinical Investigation*, vol. 126, pp. 3104–3116, aug 2016.

[203] N. L. Jorstad, M. S. Wilken, W. N. Grimes, S. G. Wohl, L. S. Vandenbosch, T. Yoshimatsu, R. O. Wong, F. Rieke, and T. A. Reh, "Stimulation of functional neuronal regeneration from Müller glia in adult mice," *Nature*, vol. 548, pp. 103–107, aug 2017.

[204] R. P. d. M. Guimarães, B. S. Landeira, D. M. Coelho, D. C. F. Golbert, M. S. Silveira, R. Linden, R. A. de Melo Reis, and M. R. Costa, "Evidence of Müller Glia Conversion Into Retina Ganglion Cells Using Neurogenin2," *Frontiers in Cellular Neuroscience*, vol. 12, p. 410, nov 2018.

[205] K. Tanabe, C. E. Ang, S. Chanda, V. H. Olmos, D. Haag, D. F. Levinson, T. C. Südhof, and M. Wernig, "Transdifferentiation of human adult peripheral blood T cells into neurons," *Proceedings of the National Academy of Sciences*, vol. 115, pp. 6470–6475, jun 2018.

[206] G. Xu, F. Wu, X. Gu, J. Zhang, K. You, Y. Chen, A. Getachew, Y. Zhuang, X. Zhong, Z. Lin, D. Guo, F. Yang, T. Pan, H. Wei, and Y.-x. Li, "Direct Conversion of Human Urine Cells to Neurons by Small Molecules," *Scientific Reports*, vol. 9, p. 16707, dec 2019.

[207] O. Torper, U. Pfisterer, D. A. Wolf, M. Pereira, S. Lau, J. Jakobsson, A. Björklund, S. Grealish, and M. Parmar, "Generation of induced neurons via direct conversion in vivo," *Proceedings of the National Academy of Sciences*, vol. 110, pp. 7038–7043, apr 2013.

[208] Y. Yang, R. Chen, X. Wu, Y. Zhao, Y. Fan, Z. Xiao, J. Han, L. Sun, X. Wang, and J. Dai, "Rapid and Efficient Conversion of Human Fibroblasts into Functional Neurons by Small Molecules," *Stem Cell Reports*, vol. 13, pp. 862–876, 2019.

[209] B. Mahato, K. D. Kaya, Y. Fan, N. Sumien, R. A. Shetty, W. Zhang, D. Davis, T. Mock, S. Batabyal, A. Ni, S. Mohanty, Z. Han, R. Farjo, M. J. Forster, A. Swaroop, and S. H. Chavala, "Pharmacologic fibroblast reprogramming into photoreceptors restores vision," *Nature*, vol. 581, pp. 83–88, may 2020.

[210] D. Smith, J. Yang, M.-L. Liu, and C.-L. Zhang, "Small Molecules Modulate Chromatin Accessibility to Promote NEUROG2-Mediated Fibroblast-to-Neuron Reprogramming," *Stem Cell Reports*, vol. 7, pp. 955–969, nov 2016.

[211] A. Hamon, D. García-García, D. Ail, J. Bitard, A. Chesneau, D. Dalkara, M. Locker, J. E. Roger, and M. Perron, "Linking YAP to Müller Glia Quiescence Exit in the Degenerative Retina.," *Cell reports*, vol. 27, pp. 1712–1725.e6, may 2019.

[212] N. L. Jorstad, M. S. Wilken, L. Todd, C. Finkbeiner, P. Nakamura, N. Radulovich, M. J. Hooper, A. Chitsazan, B. A. Wilkerson, F. Rieke, and T. A. Reh, "STAT Signaling Modifies Ascl1 Chromatin Binding and Limits Neural Regeneration from Muller Glia in Adult Mouse Retina," *Cell Reports*, vol. 30, pp. 2195–2208.e5, feb 2020.

[213] L. S. VandenBosch, S. G. Wohl, M. S. Wilken, M. Hooper, C. Finkbeiner, K. Cox, L. Chipman, and T. A. Reh, "Developmental changes in the accessible chromatin, transcriptome and Ascl1-binding correlate with the loss in Müller Glial regenerative potential," *Scientific Reports*, vol. 10, dec 2020.

[214] L. S. VandenBosch and T. A. Reh, "Epigenetics in neuronal regeneration," *Seminars in Cell and Developmental Biology*, vol. 97, pp. 63–73, jan 2020.

[215] S. Chanda, C. E. Ang, J. Davila, C. Pak, M. Mall, Q. Y. Lee, H. Ahlenius, S. W. Jung, T. C. Südhof, and M. Wernig, "Generation of induced neuronal cells by the single reprogramming factor ASCL1," *Stem Cell Reports*, vol. 3, pp. 282–296, aug 2014.

[216] J. A. Brzezinski, D. A. Lamba, and T. A. Reh, "Blimp1 controls photoreceptor versus bipolar cell fate choice during retinal development.," *Development (Cambridge, England)*, vol. 137, pp. 619–29, feb 2010.

[217] J. A. Brzezinski, K. Uoon Park, and T. A. Reh, "Blimp1 (Prdm1) prevents re-specification of photoreceptors into retinal bipolar cells by restricting competence," *Developmental Biology*, vol. 384, pp. 194–204, dec 2013.

[218] T. Aavani, N. Tachibana, V. Wallace, J. Biernaskie, and C. Schuurmans, "Temporal profiling of photoreceptor lineage gene expression during murine retinal development," *Gene Expression Patterns*, vol. 23-24, pp. 32–44, jan 2017.

[219] T. Vierbuchen, A. Ostermeier, Z. P. Pang, Y. Kokubu, T. C. Südhof, and M. Wernig, "Direct conversion of fibroblasts to functional neurons by defined factors," *Nature*, vol. 463, pp. 1035–1041, feb 2010.

[220] B. Aydin, A. Kakumanu, M. Rossillo, M. Moreno-Estellés, G. Garipler, N. Ringstad, N. Flames, S. Mahony, and E. O. Mazzoni, "Proneural factors Ascl1 and Neurog2 contribute to neuronal subtype identities by establishing distinct chromatin landscapes," *Nature Neuroscience*, 2019.

[221] T. Furukawa, C. A. Kozak, C. L. Cepko, L. S. Wright, K. A. Wallace, E. L. McMillan, S.-C. Zhang, and D. M. Gamm, "Rax, a novel paired-type homeobox gene, shows expression in the anterior neural fold and developing retina.," *Proceedings of the National Academy of Sciences*, vol. 94, pp. 3088–93, apr 1997.

[222] T. Furukawa, E. M. Morrow, and C. L. Cepko, "Crx, a Novel otx-like Homeobox Gene, Shows Photoreceptor-Specific Expression and Regulates Photoreceptor Differentiation," *Cell*, vol. 91, pp. 531–541, nov 1997.

[223] D. D. Glubrecht, J.-H. Kim, L. Russell, J. S. Bamforth, and R. Godbout, "Differential CRX and OTX2 expression in human retina and retinoblastoma," *Journal of Neurochemistry*, vol. 111, pp. 250–263, oct 2009.

[224] P. A. Ruzycki, X. Zhang, and S. Chen, "CRX directs photoreceptor differentiation by accelerating chromatin remodeling at specific target sites," *Epigenetics & Chromatin*, vol. 11, p. 42, dec 2018.

[225] S. Jung, J. Aliberti, P. Graemmel, M. J. Sunshine, G. W. Kreutzberg, A. Sher, and D. R. Littman, "Analysis of Fractalkine Receptor CX3CR1 Function by Targeted Deletion and Green Fluorescent Protein Reporter Gene Insertion," *Molecular and Cellular Biology*, vol. 20, pp. 4106–4114, jun 2000.

[226] X. F. Zhao, M. M. Alam, Y. Liao, T. Huang, R. Mathur, X. Zhu, and Y. Huang, "Targeting microglia using Cx3cr1-Cre lines: Revisiting the specificity," *eNeuro*, vol. 6, pp. 1–11, jul 2019.

[227] R. Lang, R. L. Rutschman, D. R. Greaves, and P. J. Murray, "Autocrine Deactivation of Macrophages in Transgenic Mice Constitutively Overexpressing IL-10 Under Control of the Human CD68 Promoter," *The Journal of Immunology*, vol. 168, pp. 3402–3411, apr 2002.

[228] M. E. Maes, G. Colombo, R. Schulz, and S. Siegert, "Targeting microglia with lentivirus and AAV: Recent advances and remaining challenges," *Neuroscience Letters*, vol. 707, aug 2019.

[229] S. Blackshaw and J. R. Sanes, "Turning lead into gold: reprogramming retinal cells to cure blindness," *Journal of Clinical Investigation*, vol. 131, feb 2021.

[230] S. K. Powell, R. J. Samulski, and T. J. McCown, "AAV Capsid-Promoter Interactions Determine CNS Cell-Selective Gene Expression In Vivo," *Molecular Therapy*, vol. 28, pp. 1373–1380, may 2020.

[231] A. J. Song and R. D. Palmiter, "Detecting and Avoiding Problems When Using the Crelox System," *Trends in Genetics*, vol. 34, pp. 333–340, may 2018.

[232] R. S. Donocoff, N. Teteloshvili, H. Chung, R. Shoulson, and R. J. Creusot, "Optimization of tamoxifen-induced Cre activity and its effect on immune cell populations," *Scientific Reports*, vol. 10, pp. 1–12, dec 2020.